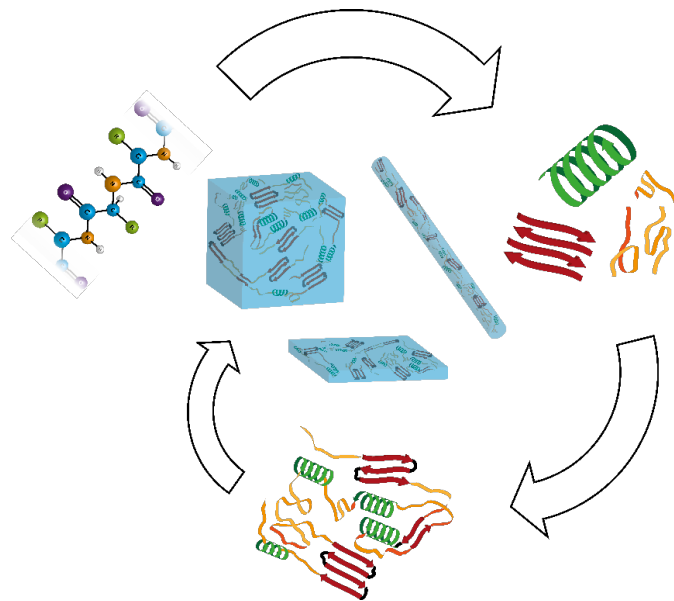


# Structural Control of Synthetic Polypeptides in Biomaterials at Multiple Dimensional Scales



*Nicholas Jun-An Chan*

(ORCID: 0000-0001-7608-144X)

*MEng*

Submitted in total fulfilment for the jointly awarded degree of Doctor of Philosophy at the University of Melbourne and the University of Bayreuth

*and*

In consideration for the academic grade of

**Doctor rerum naturalium (Dr. rer. nat)**

March 2022

Department of Chemical and Biochemical Engineering

The University of Melbourne

*and*

Chair of Biomaterials

The University of Bayreuth





The work reported in this thesis was performed at the Department of Biomaterials within the Bayreuth School of Mathematical and Natural Sciences (BayNAT) at the University of Bayreuth and the Polymer Science Group within the School of Chemical and Biochemical Engineering at the University of Melbourne from July 2017 to March 2022 under the supervision of Prof. Dr. Greg Qiao and Prof. Dr. Thomas Scheibel as a Joint PhD degree within the DAAD Bayreuth-Melbourne Polymer/Colloid Network.

**Thesis submitted:** 31.03.2022

**Date of scientific colloquium:** 13.10.2022

**Director of BayNAT:** Prof. Dr. Hans Keppler

**Doctoral committee:**

Prof. Dr. Thomas Scheibel

Prof. Dr. Mukundan Thelakkat

Prof. Greg Qiao

## *Abstract*

---

Proteins and peptides hold particular interest amongst biopolymers as major structural and functional natural components of many materials. Polypeptides themselves are their molecular structure which are sequences of amino acids with proteins being approximately 100 amino acids or greater in length while peptides are below this length. Once covalently linked, side chains interact with the molecular backbone resulting in spontaneous protein folding and thus resulting in well-defined, sequence-specific secondary structures including  $\alpha$ -helices,  $\beta$ -sheets and random coils. However, such secondary structures can be manipulated through processing to yield materials with unique structures. As secondary structures and their eventual overall conformation results in different physical and chemical properties, this study aims to address the combination of these issues for the development of different materials.

This study investigates a range of novel fabrication methods for manipulating and utilizing the secondary structures of non-sequence specific polypeptides in materials at different dimensional scales. Specifically, strategies to fabricate hydrogels, films and fibers have all been developed to produce materials which either utilize secondary structure-based nanostructures which have been traditionally hard to utilize such as  $\beta$ -sheet nanocrystals or produces materials with secondary structures contradictory to their usual structure. Subsequent properties resulting from this secondary structure control were investigated to discern their impact and subsequent potential in various applications.

For the development of hydrogels, synthetic polypeptides are generally used to form secondary structure-based physical crosslinks.  $\beta$ -sheet crosslinks are especially favourable due to their role in tough natural silks and thus been used to develop tough hydrogels. In this study, chemically crosslinked hydrogels were initially synthesized with pendant amine groups to initiate the polymerization of poly(L-valine) (PVal) and poly(L-valine-*r*-glycine) (PLVG) as  $\beta$ -sheet forming polypeptide. By grafting from the hydrogel, issues of steric hindrance are mitigated and thus hydrogels with high  $\beta$ -sheet content can be produced. The resulting hydrogels displayed greatly improved mechanical strength over their counterparts, lacking  $\beta$ -sheets with improved compressive strength and stiffness of up to 30 MPa (300 times greater than the initial network) and 6 MPa (100 times greater than the initial network), respectively. Furthermore, this technique was found to be applicable to a range of different polymer hydrogels, with demonstrated applicability in 3D printed structures.

For the development of modified surfaces, synthetic polypeptides have previously been applied to deposition- and polymerization-based techniques. Our group has previously utilized a unique surface modification method whereby macrocrosslinkers with multiple polymerizable sidechains are utilized in a process called the continuous assembly of polymers (CAP). To observe the effect of using this specific conformation on polypeptides, poly(L-lysine) (PLLys) based polymers were utilized as a model for CAP utilizing reversible addition–fragmentation chain-transfer (RAFT) polymerization as the polymerization medium. Through manipulation of different RAFT agents and conditions, surface films of up to  $36.1 \pm 1.1$  nm thick which could be increased to  $94.9 \pm 8.2$  nm upon multiple applications of this process. Versatility was found in using poly(L-glutamic acid) (PLGlu) as another model polypeptide. Furthermore, films had high random coil conformation which is especially unusual PLLys films which would favour  $\alpha$ -helical conformations. Enzymatic degradation was found using different digestive and wound healing proteases with different rates of degradation depending on the use of PLLys or PLGlu- based macrocrosslinkers.

Finally, fibers utilising  $\beta$ -sheets have been developed using sequence-specific methods to control aggregation. Other methods utilizing  $\beta$ -sheets require multi-step or complicated processes to yield the precursor polymer required for polymer formation. Thus, this study develops a method of fabricating fibers using a broad range of preexisting polymers by introducing the valine-based monomer into the precursor solution (i.e. the fiber spinning dope) and triggering polymerization during fiber spinning resulting in PVal.  $\beta$ -sheets could be successfully integrated into all polymeric fibers, but with greatly differing impacts on substructures based on intermolecular bonding. Polymers (polycaprolactone (PCL) and cellulose acetate) with low hydrogen bonding potential were found to show increased crystallization. Such polymers displayed increase tensile strength upon  $\beta$ -sheet introduction (2.2 and 4.3 times increase respectively for PCL and cellulose acetate fibers). In contrast, poly(amide) based polymers with high hydrogen-bonding potential (Nylon 6 and poly(benzyl-L-glutamate) (PBLG)) did not show any increased crystallization, though an increase in extensibility at break (2.9 and 1.8 times increase respectively for nylon 6 and PBLG) was observed. Finally, in other polymers without either of these features, intercalation of  $\beta$ -sheets into the usual polymeric assembly of the polymer results in either minimal or reduced mechanical properties.

In summary, fabrication processes for a broad range of different polypeptide based materials have been investigated to control both secondary structure and polymeric substructures. From

this, properties such as mechanical and degradation potential have been studied in relation to these properties and thus revealed a range of novel approaches to polypeptide-based material fabrication.

## ***Zusammenfassung***

---

Proteine und Peptide sind unter den Biopolymeren von besonderem Interesse die Grundlage für wichtige strukturelle und funktionelle natürliche Komponenten. Die molekulare Struktur der Polypeptide besteht aus Aminosäuresequenzen, wobei Proteine eine Länge von etwa 100 Aminosäuren oder mehr aufweisen, während Peptide eine geringere Länge haben. Nach der kovalenten Verknüpfung interagieren die Seitenketten mit dem molekularen Rückgrat, was zu einer spontanen Faltung des Proteins und damit zu wohldefinierten, sequenzspezifischen Sekundärstrukturen wie  $\alpha$ -Helices,  $\beta$ -Faltblättern und Zufallsknäuel führt. Solche Sekundärstrukturen können jedoch durch Verarbeitung manipuliert werden, um Materialien mit einzigartigen Strukturen zu erhalten. Sekundärstrukturen und ihre Gesamtkonformation führt zu unterschiedlichen physikalischen und chemischen Eigenschaften. Diese Arbeit zielt darauf ab, die Kombination dieser Aspekte für die Entwicklung verschiedener Materialien zu untersuchen.

In dieser Studie wird eine Reihe neuartiger Herstellungsmethoden für die Kontrolle der Sekundärstruktur von nicht sequenzspezifischen Polypeptiden in Materialien mit unterschiedlichen Maßstäben untersucht. Insbesondere wurden Strategien zur Herstellung von Hydrogelen, Filmen und Fasern entwickelt, um Materialien zu produzieren, die entweder auf Sekundärstrukturen basierende Nanostrukturen nutzen, die traditionell schwer zu verwenden sind, wie z. B.  $\beta$ -Faltblatt-Nanokristalle, oder sekundärstrukturbildende Materialien, die ihrer üblichen Sekundärstruktur widersprechen. Diese sich aus dieser Kontrolle der Sekundärstruktur ergebenden Eigenschaften wurden untersucht, um ihre Auswirkungen und ihr Potenzial für verschiedene Anwendungen zu erkennen.

Für die Entwicklung von Hydrogelen werden im Allgemeinen synthetische Polypeptide verwendet, um sekundärstrukturbasierte physikalische Vernetzungen zu bilden. In natürlichen Seiden sind  $\beta$ -Faltblätter mitverantwortlich für die hohe mechanische Stabilität und dienen daher als Vorbild zur Entwicklung mechanisch stabiler Hydrogele. In dieser Studie werden zunächst chemisch vernetzte Hydrogele mit anhängenden Amingruppen synthetisiert, um die Polymerisation von Poly(L-Valin) (PVal) und Poly(L-Valin-r-Glycin) (PLVG) als  $\beta$ -Faltblattbildendes Polypeptid zu initiieren. Durch die Verwendung der „grafting from“ Polymerisation, bei der vom Hydrogel ausgehend gepfropft wird, werden die Probleme der sterischen Hinderung reduziert, so dass Hydrogele mit hohem  $\beta$ -Faltblattgehalt hergestellt werden können. Die resultierenden Hydrogele zeigten eine stark verbesserte mechanische Festigkeit

gegenüber den Hydrogelen ohne induzierte  $\beta$ -Faltblätter. Die Druckfestigkeit und Steifigkeit konnte auf bis zu 30 MPa verbessert werden, was ungefähr 300 Mal höher als die des ursprünglich Netzwerks ist, bzw. 6 MPa, was 100 Mal höher als die des ursprünglich Netzwerks ist. Darüber hinaus wurde festgestellt, dass diese Technik auf eine Reihe verschiedener Polymer-Hydrogele übertragbar ist, wobei die Anwendbarkeit in 3D-gedruckten Strukturen nachgewiesen wurde.

Für die Entwicklung modifizierter Oberflächen wurden bisher synthetische Polypeptide basierend auf Abscheidungs- und Polymerisationstechniken eingesetzt. Unsere Gruppe hat eine einzigartige Methode zur Oberflächenmodifizierung etabliert, bei der Makrovernetzer mit mehreren polymerisierbaren Seitenketten verwendet werden. Dies wird als kontinuierliche Assemblierung von Polymeren (CAP) bezeichnet. Um die Auswirkungen der spezifischen Konformation der Polypeptide zu beobachten, wurden Polymere auf der Basis von Poly(L-Lysin) (PLLys) als Modell für CAP unter Verwendung der reversiblen Additions-Fragmentierungs-Kettentransfer (RAFT)-Polymerisation als Polymerisationsmedium verwendet. Durch Manipulation verschiedener RAFT-Agenzien und -Bedingungen konnten Filme mit einer Dicke von bis zu  $36,1 \pm 1,1$  nm erzeugt werden, die Schichtdicke konnte bei mehrfacher Anwendung dieses Prozesses auf  $94,9 \pm 8,2$  nm erhöht werden. Die Vielseitigkeit dieser Methode wurde durch die Verwendung von Poly(L-Glutaminsäure) (PLGlu) als weiteres Modellpolypeptid demonstriert. Darüber hinaus wiesen die Filme eine hohe Zufallsknäuel Konformation auf, was besonders für PLLys-Filme ungewöhnlich ist, da diese die  $\alpha$ -helikale Konformationen bevorzugen. Es wurde ein enzymatischer Abbau mit verschiedenen Verdauungs- und Wundheilungsproteasen durchgeführt, wobei die Abbauraten je nach Verwendung von PLLys- oder PLGlu-basierten Makrovernetzern variierten.

Außerdem wurden Fasern durch sequenzspezifische Methoden entwickelt, die  $\beta$ -Faltblätter enthalten, um die Probleme der Aggregationskontrolle in den Griff zu bekommen. Andere Methoden, die  $\beta$ -Faltblätter verwenden, erfordern mehrstufige oder komplizierte Prozesse, um das für die Polymerbildung erforderliche Vorstufenpolymer zu erhalten. Daher wird in dieser Studie eine Methode zur Herstellung von Fasern unter Verwendung eines breiten Spektrums bereits vorhandener Polymere entwickelt, indem das auf Valin basierende Monomer in die Vorstufenlösung (d. h. die Spinnlösung) eingebracht und die Polymerisation während des Faserspinnens initiiert wird, was zu PVal führt.  $\beta$ -Faltblätter konnten erfolgreich in alle Polymerfasern integriert werden, allerdings mit sehr unterschiedlichen Auswirkungen auf die intermolekularen Bindungen der resultierenden Substrukturen. Es wurde festgestellt, dass die

Polymere Polycaprolacton (PCL) und Celluloseacetat mit einem niedrigem Wasserstoffbrückenbindungspotenzial eine Zunahme des kristallinen Anteils aufweisen. Bei diesen Polymeren wurde festgestellt, dass die Zugfestigkeit nach der Einführung von  $\beta$ -Faltblättern zunimmt (2,2- bzw. 4,3-facher Anstieg für PCL- und Celluloseacetat-Fasern). Im Gegensatz dazu zeigten Polymere auf Poly(amid)-Basis mit einem hohem Wasserstoffbrückenbindungspotenzial (Nylon 6 und Poly(benzyl-L-glutamat) (PBLG)) keine Zunahme des kristallinen Anteils, obwohl ein Anstieg der Dehnbarkeit bei Bruch (2,9- bzw. 1,8-facher Anstieg für Nylon 6 und PBLG) beobachtet wurde. Bei anderen Polymeren, die keines dieser Merkmale aufweisen, führt die Einlagerung von  $\beta$ -Faltblättern in die Polymerstruktur zu minimalen oder reduzierten mechanischen Eigenschaften.

Zusammenfassend lässt sich sagen, dass die präsentierten Herstellungsverfahren für eine Vielzahl verschiedener Materialien untersucht wurde, um sowohl die Sekundärstruktur als auch die polymeren Substrukturen zu untersuchen. Darauf aufbauend wurden die mechanische Stabilität und das Abbaupotenzial in Relation zur Sekundärstruktur untersucht und so eine Reihe neuer Ansätze für die Herstellung von Materialien auf Polypeptidbasis aufgezeigt.

## ***Declaration of Authorship***

---

This declaration certifies the following:

1. This thesis comprises only my original work towards the PhD except where indicated in the Preface;
2. Due acknowledgement has been made in the text to all other material used
3. The thesis is less than 100,000 words in length, exclusive of tables, maps, bibliographies and appendices.

Nicholas Jun-An Chan

2022



## ***Eidesstattliche Versicherungen und Erklärungen***

---

(§ 9 Satz 2 Nr. 3 PromO BayNAT)

Hiermit versichere ich eidesstattlich, dass ich die Arbeit selbstständig verfasst und keine anderen als die von mir angegebenen Quellen und Hilfsmittel benutzt habe (vgl. Art. 64 Abs. 1 Satz 6 BayHSchG).

(§ 9 Satz 2 Nr. 3 PromO BayNAT)

Hiermit erkläre ich, dass ich die Dissertation nicht bereits zur Erlangung eines akademischen Grades eingereicht habe und dass ich nicht bereits diese oder eine gleichartige Doktorprüfung endgültig nicht bestanden habe.

(§ 9 Satz 2 Nr. 4 PromO BayNAT)

Hiermit erkläre ich, dass ich Hilfe von gewerblichen Promotionsberatern bzw. -vermittlern oder ähnlichen Dienstleistern weder bisher in Anspruch genommen habe noch künftig in Anspruch nehmen werde.

(§ 9 Satz 2 Nr. 7 PromO BayNAT)

Hiermit erkläre ich mein Einverständnis, dass die elektronische Fassung meiner Dissertation unter Wahrung meiner Urheberrechte und des Datenschutzes einer gesonderten Überprüfung unterzogen werden kann.

(§ 9 Satz 2 Nr. 8 PromO BayNAT)

Hiermit erkläre ich mein Einverständnis, dass bei Verdacht wissenschaftlichen Fehlverhaltens Ermittlungen durch universitätsinterne Organe der wissenschaftlichen Selbstkontrolle stattfinden können.

## *Preface*

---

1. **Chapter 1** (p 1 – 60) is written by Nicholas Chan
2. The text in **Chapter 2** (p 61-83) is taken from “Spider-silk inspired polymeric networks by harnessing the mechanical potential of  $\beta$ -sheets through network guided assembly” *Nature Communications* **2020**, *11* (1), 1630
  - Nicholas Chan performed the inclusion of glycine into the system
  - Dunyin Gu and Nicholas Chan performed the inclusion of valine into the system
  - Dunyin Gu performed the FTIR measurement for networks without glycine. Nicholas Chan performed the FTIR measurement for networks including glycine
  - Min Liu and He Xie performed the SEM. Subsequent data was analyzed by Nicholas Chan
  - Dunyin Gu performed the XRD and TGA
  - Nicholas Chan performed the degradation studies and mechanical testing
  - Thomas Pattison and Nicholas Chan developed the 3D printing technique. Nicholas Chan performed subsequent analysis
  - The writing of the original draft was performed by Nicholas Chan
  - The review and editing of the manuscript were performed by all authors
  - Conceptualization was performed by Nicholas Chan, Dunyin Gu, Shereen Tan and Greg Qiao
  - Funding was raised by Greg Qiao
3. The text in **Chapter 3** (p 84-110) is taken from ““Crosslinked Polypeptide Films via RAFT-Mediated Continuous Assembly of Polymers” *Angewandte Chemie International Edition* **2022**, *61* (9), e202112842
  - Nicholas Chan performed the synthesis of all macromonomers and modified wafers including optimization of the technique.
  - Sarah Lentz performed the FTIR measurements.
  - Sarah Lentz and Nicholas Chan performed the degradation studies
  - The writing of the original draft was performed by Nicholas Chan
  - The review and editing of the manuscript were performed by all authors

- Conceptualization was performed by Nicholas Chan, Sarah Lentz, Shereen Tan, Thomas Scheibel and Greg Qiao
  - Funding was raised by Greg Qiao
4. The text in **Chapter 4** (p 111-143) is taken from the manuscript titled “Mimicry of silk utilizing synthetic polypeptides” and submitted to *Advance Functional Materials*.
    - Nicholas Chan performed the fabrication of all fiber samples
    - Nicholas Chan performed the FTIR analysis of all samples and DSC of PCL samples
    - Sarah Lentz performed the SEM of all samples
    - Sabine Rosenfeldt performed the SAXS and XRD of all samples including analysis
    - Nicholas Chan was responsible of all tensile mechanical testing
    - The writing of the original draft was performed by Nicholas Chan
    - The review and editing of the manuscript were performed by all authors
    - Conceptualization was performed by Nicholas Chan, Mona Schultebeyring and Thomas Scheibel
    - Funding was raised by Greg Qiao and Thomas Scheibel
  5. **Chapter 5** (p 144 – 147) is written by Nicholas Chan
  6. **Chapter 6** (p 148 – 160) is written by Nicholas Chan

# ***Publications***

---

## **Peer-Reviewed Journal Papers**

### **Chapter 1**

“Mimicry of silk utilizing synthetic polypeptides”

**Nicholas J. Chan**, Sarah Lentz, Paul A. Gurr, Thomas Scheibel, Greg G. Qiao, *Progress in Polymer Science*, *Under Review*

### **Chapter 2**

“Spider-silk inspired polymeric networks by harnessing the mechanical potential of  $\beta$ -sheets through network guided assembly”

**Nicholas J. Chan**, Dunyin Gu, Shereen Tan, Qiang Fu, Thomas Geoffrey Pattison, Andrea J O'Connor, Greg G Qiao, *Nature Communications* **2020**, *11* (1), 1630

### **Chapter 3**

“Crosslinked Polypeptide Films via RAFT-Mediated Continuous Assembly of Polymers”

**Nicholas J. Chan**, Sarah Lentz, Paul A. Gurr, Shereen Tan, Thomas Scheibel, Greg G. Qiao, *Angewandte Chemie International Edition* **2022**, *61* (9), e202112842

### **Chapter 4**

“Robust  $\beta$ -sheet reinforced fibers fabricated from unmodified polymers”

**Nicholas J. Chan**, Sarah Lentz, Paul A. Gurr, Shereen Tan, Mona Schultebeyring, Sabine Rosenfeldt, Anna Schenk, Thomas Scheibel, Greg G. Qiao, *Advanced Functional Materials*, *Submitted*

## Other Publications

### Peer-reviewed

“Ring opening polymerization of  $\alpha$ -amino acids: advances in synthesis, architecture and applications of polypeptides and their hybrids”

Alicia Rasines Mazo, Stephanie Allison-Logan, Fatemeh Karimi, **Nicholas Jun-An Chan**, Wenlian Qiu, Wei Duan, Neil M. O’Brien-Simpson and Greg G. Qiao, *Chemical Society Review*, **2020**, 49 (4), 4737-4834

### Book Chapter

“CHAPTER 13 – New Approaches Towards the Design of Tough Amphiphilic Polymeric Co-networks”

Shereen Tan, **Nicholas J. Chan**, Joe Collins, Qiang Fu, Greg G. Qiao, *Amphiphilic Polymer Co-networks: Synthesis, Properties, Modelling and Applications*; The Royal Society of Chemistry, 2020

## *Scientific Presentations*

---

1. Workshop Series: Building an International Career, 2021, online, 17.11.2021, “Building an International Network”, oral presentation
2. Nano Singapore 2021, online, 23.11.2021, “Crosslinked polypeptide films via RAFT mediated continuous assembly of polymers”, oral presentation

## *Acknowledgements*

---

This section will never be long enough. While a thesis chronicles the works of a single individual, it is the combined support of many others that contribute no matter how direct that support may be. 4.5 years filled with much experimental heartbreak, general mental exhaustion and a tiny global, world-halting pandemic called COVID-19 has all been counterbalanced by intriguing friends, exciting opportunities and, at times, just the hint of luck from the right sources. And none of the latter list could have come without the people behind me during this time and preceding.

First and foremost, I would like to thank Prof. Greg Qiao. It has been no secret that we have argued, gotten annoyed at each other, and been frustrated with each other, but I can confidently say this has been in service of better science. You have taken enormous risks with me whether it be the projects or the organisational relationships you have entrusted to me while providing academic and intellectual support. Perhaps most importantly, you trusted me to start a Joint PhD with the University of Bayreuth which has taken my personal research and career ambitions down a very different path than expected. Further to this, I would like to thank Prof. Andrea O'Connor who, as my committee chair, gave some very interesting perspectives that gave me a more expansive way of looking at my research. I would also like to thank Jodie Salmons and Louise Baker for the administrative help you have provided – it has not gone unnoticed.

I would further like to thank Prof. Thomas Scheibel. I understand that I am a very odd scenario entering your lab as an outsider and the risk you took in taking me in has been greatly noted. Your guidance from a very different perspective has been immeasurably useful. Furthermore, thank you for trusting me with the facilities in your laboratory and providing a lot of morale support when it was hard to find in a geographical place still unfamiliar to me. Thank you to Andrea Bodner and Sabrina Schwägerl for your administrative assistance.

To my Polymer Science Group lab mates past and present, thank you for all the support and mostly listening to me complain at every other hour. To Dr. Paul Gurr, I honestly am not sure I would have made it through this time without your help both experimentally and mentally. I hope you realise that I look up to you a lot as I am sure so many have in the past and still do now. To Dr Shereen Tan, it would have been easy for you to just ditch me as a student the minute you found different work outside our group but even from a far you have provided a lot of support, especially when it comes to presenting my research and communicating – a skill I

have really needed help with. To those who have moved on from the group – Steph, Fatemeh, Hadi, Min, Wenlian, Amin and Bingxin – you have all been hilarious and supportive lab mates to no end. For those still around in some capacity – Vianna, Amrish, Arunjunai, Hoseong, Sadegh, Zahra and John – it saddens me to not get to experience the rest of your PhDs with you all, but also comforting to know the group has good people in it. Special mention to Dr. Joel Scofield and Ross Wylie who have both been close friends and provided me an endless source of escapism through our collective nerdistry (e.g. Pokémon and Dungeons & Dragons).

To my lab mates from the Chair of Biomaterials, you have made a very anxious and unfamiliar person feel at home very fast. Annika, Annika, Vanessa, Vanessa, Charlotte, Charlotte, Julia, Julia (none of these are typos), Merisa, Xuen, Kai, Tim, Christoph, Christina, Ashish, Edgardo and Shakir – all of you have made me and my wife feel at home when we could have very much felt the opposite. The further technical expertise I obtained from you all is something I can hold on to for many years to come.

Special mention must go to Sarah Lentz who also performed a Joint PhD between the same laboratories. Words cannot express how much I owe you in terms of knowledge and hospitality when it comes to adaptation to German culture and the laboratory itself. The effect you have had on my lab skills and thought processes can be directly seen throughout my thesis. You and your husband, Michi, are people we are proud to call close friends. We were honoured to have you at our wedding and be at yours as not only our degrees were so intertwined, but the social relationships we have as well. Thank you so much for everything and one day I can only hope to repay the massive debt.

I would like to thank the Melbourne School of Engineering and to the DAAD Germany International Exchange Service for their financial support through my academic endeavours and overseas travel.

Before the most personal and important acknowledgement, I have one more person to thank – Dr. Roger Slade. You would likely not remember me as you came out of retirement for one semester to teach Chemistry Olympiad (Scotch College's version of advanced Year 11 Chemistry). The first assignment you assigned us was what I thought was too difficult for me, so I effectively just flunked it without trying with the mindset that I tried advanced and was not good enough, so I can just go back to normal. For you, it was unacceptable that I did not even bother to succeed because I was scared of failure. Instead, you pulled me aside and went question by question, explaining which may have actually been out of my reach and which



questions I should have actually given a proper go. So, I kept trying. Tried for more than ten years since that day. And I guess, by the time this goes through, I will have completed a doctorate focused on Chemistry. And I am sure that if you brought this much of an impact on me in one semester, there are many more who you had such a great impact on. This stuck out to me more than many other lessons I learnt despite being blessed with so many great teachers. It deeply saddens me that I could not finish this in time to show you how your firm, yet encouraging teachings impacted someone in a tangible way. But I hope you knew that you had a legacy. I am glad I maybe got to be a small crumb of it.

Finally, to my friends and family, thank you for everything. My wife, Chaohui (Ada), you have had to put up with a lot from me with highs and lows, and through it all you have stuck by my side. I am grateful to have someone who not only sympathises with my annoyances and celebrates my successes but puts me in my place when I am being unreasonable. A lifetime of thanks is owed; this was impossible without you. To my friends, you have been there to listen to many a rambling, so thanks for putting up with me. Owain and (Dr.) Quillan, thanks for listening to me ramble and catering to my long rants. Someone said that you two think of me as the smart brother, but I hope you guys realise one day that it is you two that I look up to. Quillan, you are the smartest person I know; I hope you stop trying to hide that one day. Owain, you got your life together so much faster than I did; you will have a world of choices with your unnaturally broad and high skillset. To my parents – A/Prof. Phyllis Lau and Dr. Raymond Chan – I put your titles here because most people have parental support from a distance, but I had the support of a father who has been through it before and a mother who literally sees the changes as they are going right beside me. I feel like I got a cheat code through this having you two as parents both during this doctorate and through life.

# ***Table of Contents***

---

<b><i>Abstract</i></b> .....	i
<b><i>Zusammenfassung</i></b> .....	iv
<b><i>Declaration of Authorship</i></b> .....	vii
<b><i>Eidesstattliche Vericherungen und Erklärungen</i></b> .....	viii
<b><i>Preface</i></b> .....	ix
<b><i>Publications</i></b> .....	xi
<b><i>Scientific Presentations</i></b> .....	xiii
<b><i>Acknowledgements</i></b> .....	xiv
<b><i>Table of Contents</i></b> .....	xvii
<b><i>List of Figures</i></b> .....	xxi
<b><i>List of Tables</i></b> .....	xxx
<b><i>List of Abbreviations</i></b> .....	xxxix
1.1 An Overview of Polymeric Materials .....	1
1.2 Synthetic Polymerization Methods .....	3
1.2.1 Synthetic polypeptide synthesis.....	3
1.2.1.1 N-carboxyanhydride Ring Opening Polymerization (NCA ROP) .....	3
1.2.2 Chemoenzymatic Polymerization.....	6
1.2.3 Free radical polymerization (FRP) .....	7
1.2.3.1 Reversible addition-fragmentation (RAFT) polymerization.....	8
1.3 Synthetic Polypeptide Structures .....	9
1.3.1 Secondary Structure.....	9
1.3.1.1 Physiological Conditions.....	9
1.3.1.2 Non-physiological conditions .....	11
1.3.2 Molecular Architectures .....	13
1.3.3 Graft Polypeptides .....	15
1.4 Multidimensional Material Fabrication .....	17

1.4.1	Three Dimensional Materials – Gels .....	18
1.4.1.1	Chemically Crosslinked Hydrogels.....	19
1.4.1.2	Physically Crosslinked Hydrogels .....	20
1.4.1.3	Cryogels .....	22
1.4.1.4	3D Printing Gels.....	22
1.4.2	Two Dimensional Materials – Films and Modified Surfaces.....	23
1.4.2.1	Polymer Deposition.....	24
1.4.2.2	Polymer Grafting.....	27
1.4.3	One Dimensional Materials – Fibers .....	29
1.4.3.1	Microfiber Spinning .....	<b>Error! Bookmark not defined.</b>
1.5	Material Properties.....	30
1.5.1	Mechanical.....	30
1.5.2	Degradation .....	33
1.5.3	Biologically relevant properties.....	35
1.5.3.1	Cell Support and proliferation.....	36
1.6	Objectives .....	37
1.7	Thesis Overview .....	38
1.7.1	Manipulation of $\beta$ -sheets Within Networks .....	39
1.7.2	Crosslinked Films <i>via</i> Continuous Assembly of Polymers .....	40
1.7.3	Mechanical Enhancement of Synthetic Fibers through $\beta$ -sheets.....	40
1.8	References.....	42
2.1.	Chapter Perspectives.....	54
2.2.	Main Text.....	55
2.3.	Supporting Information.....	69
3.1.	Chapter Perspectives.....	77
3.2.	Main Text.....	78
3.3.	Supporting Information.....	87

4.1.	Chapter Perspectives .....	104
4.2.	Main Text.....	105
4.3.	Supporting Information.....	131
5.1	Conclusion .....	137
5.2	Future Perspectives .....	138
5.3	References.....	142
6.1.	Methods for Chapter 2 .....	144
6.1.1.	Materials .....	144
6.1.2.	Synthesis of <i>L</i> -valine <i>N</i> -carboxyanhydride (Val NCA).....	145
6.1.3.	Synthesis of glycine <i>N</i> -carboxyanhydride (Gly NCA).....	145
6.1.4.	Synthesis of initial OEGMA hydrogel network .....	145
6.1.5.	Synthesis of initial OEGMA cryogel networks.....	146
6.1.6.	Synthesis of $\beta$ -sheets-incorporated networks .....	146
6.1.7.	Synthesis of PMMA-grated networks .....	146
6.1.8.	Synthesis of 3D-printed initial networks.....	147
6.1.9.	Synthesis of $\beta$ -sheets-incorporated 3D-printed networks.....	147
6.2.	Methods for Chapter 3 .....	147
6.2.1.	Materials .....	147
6.2.2.	Synthesis of <i>Z</i> -protected lysine <i>N</i> -carboxyanhydride (Lys( <i>Z</i> ) NCA) and Benzyl-protected Glutamic Acid <i>N</i> -carboxyanhydride (Glu(OBzl) NCA).....	148
6.2.3.	Synthesis of Poly(L-glutamic acid(OBzl)- <i>r</i> -L-lysine( <i>Z</i> )).....	149
6.2.4.	Deprotection of Poly(L-glutamic acid(OBzl)- <i>r</i> -L-lysine( <i>Z</i> )) .....	149
6.2.5.	Deprotection of Poly(L-glutamic acid(OBzl)- <i>r</i> -L-lysine( <i>Z</i> )) .....	149
6.2.6.	Methacrylation of poly(L-lysine) to form PLLMA.....	150
6.2.7.	Methacrylation of poly(L-lysine- <i>r</i> -L-glutamic acid) to form PLGMA.....	150
6.2.8.	Silanization of silica wafers.....	150
6.2.9.	PLLMA reversible addition fragmentation chain transfer-mediated continuous assembly of polymers (CAP-RAFT) on pretreated silica substrates .....	151

6.2.10.	PLGMA CAP-RAFT on pretreated silica substrates .....	151
6.3.	Methods for Chapter 4 .....	152
6.3.1.	Materials .....	152
6.3.2.	Synthesis of Valine NCA (Val NCA) and Benzyl-protected Glutamic Acid (Glu(OBzl) NCA) .....	152
6.3.3.	Synthesis of Poly(benzyl-L-glutamic acid) (PBLG) .....	153
6.3.4.	Wet Spinning of Polymeric Fibers .....	153
6.3.5.	Deacetylation of Cellulose Acetate Fibers .....	153
6.4.	Instrumentation and Characterization .....	154
6.4.1.	Nuclear magnetic resonance (NMR) .....	154
6.4.1.1.	Conversion within $\beta$ -sheet laden networks .....	154
6.4.2.	Attenuated total reflection – Fourier transform infrared spectroscopy (ATR-FTIR)	154
6.4.3.	Fluorescent imaging of Thioflavin T (ThT) stained networks .....	155
6.4.4.	Scanning electron microscopy (SEM) .....	155
6.4.5.	Differential scanning calorimetry (DSC) .....	155
6.4.6.	Swelling ratio measurement .....	155
6.4.7.	Compressive mechanical testing .....	155
6.4.8.	Tensile mechanical testing .....	155
6.5.	References .....	156
	<b><i>Appendix A: Mimicry of silk utilizing synthetic polypeptides</i></b> .....	157

# List of Figures

---

## Chapter 1

Figure 1. Schematic of different hierarchical levels of proteins beginning from the monomeric state to the primary, secondary, tertiary and finally (in some case.) quaternary structure.

Figure 2. Schematic of NCA ROP synthesis. a) *N*-carboxyanhydride (NCA) synthesis *via* phosgenation. b) Ring opening polymerization (ROP) *via* i) the normal amine mechanism, ii) the activated monomer mechanism and iii) transition metal catalysis.

Figure 3. Schematic of chemoenzymatic polymerization of polypeptides. Notably, protease is preserved along the reaction pathway and only a catalytic amount is required.

Figure 4. General schematic of Mechanism for free radical polymerization with a vinyl monomer. All four steps of chain growth polymerizations are present (initiation, propagation, transfer and termination). Note that radical transfer is a side reaction rather than a growth step.

Figure 5. Mediating equilibrium reactions for chain transfer agents with the polymer for reversible addition-fragmentation chain transfer (RAFT) polymerization. Reprinted (adapted) with permission from <sup>31</sup>. Copyright 2017 American Chemical Society

Figure 6. Secondary structure propensities of all canonical amino acids based on their presence in a)  $\beta$ -sheets and b)  $\alpha$ -helices. This is from an Open Access article distributed under the terms of the Creative Commons Attribution License, which permits unrestricted use, distribution, and reproduction in any medium, provided the original work is properly cited.<sup>34</sup>

Figure 7. a) Molecular structure of linear polymers of i) end group functionalized polypeptides and ii) block copolymers. b) Synthesis pathways to such molecules *via* i) a functional initiator/macromolecule with an initiating end group, ii) a bifunctional initiator or ii) coupling of end groups from both blocks.

Figure 8. Synthesis of graft polypeptides *via* a) grafting-to with polypeptide branches, b) grafting-from using side chain initiating sites or c) grafting-through of polypeptides with polymerizable end groups.

Figure 9. Different morphologies of 3D gel structures. a) Methods of crosslinking polypeptide gels through i) chemical crosslinking with multifunctional crosslinkers or ii) physical crosslinking (usually secondary structure formation) through environmental change such as

heat, pH or light. b) Different morphologies available through fabrication conditions including i) regular gelation and ii) cryogelation, allowing the gel to crosslink at temperatures below solvent freezing point result is solvent crystal formation, growth and then removal by thawing, yielding a microporous structure with more concentrate polymer walls. c) 3D printing gel structures. i) Fuse deposition modelling (FDM) involves layer-by-layer extrusion of the preformed gel. ii) Stereolithography (SLA) involves forming the gel using a pointed layer which cures each layer separately with a moving pointed laser. iii) Digital light processing (DLP) is similar to SLA, except a projection unit irradiates each layer all at once.

Figure 10. Different methods of forming polypeptide films or modified surfaces. a) Common deposition methods for forming films. i) Dip coating involves immersing a substrate entirely into a polymer solution the deposited polymer remaining on the substrate upon withdrawal. ii) Drop casting instead applies the polymer solution on the substrate surface and allows the solvent to evaporate, leaving behind the desired film. iii) Spin coating is similar to drop casting except after the polymer solution is on the surface, the substrate is spun which bot causes spreading of the polymer solution and evaporation of solvent. b) Fabrication of layer-by-layer films through the sequential deposition of polyions. Each layer has an opposing charge to the previous layer. c) Polymerization methods for modifying surfaces *via* i) grafting polymers to the surface with a functional terminal end group, ii) grafting polymers from the surfaces by using initiating sites on the substrate surface to cause polymerization upon monomer deposition, iii) grafting through end-functionalized polymers which polymerize at the substrate surface, iv) bottlebrush polymer formation by utilizing initiating sites on the substrate surface to graft through end-functionalized polymers, or v) chemically crosslinked films manufactured through continuous assembly polymerization (CAP) which utilizes initiating sites on the substrate surface to graft through side chain-functionalized polymers.

Figure 11. a) Melt spinning, where a molten polymer is drawn through a nozzle and cooled below melting temperature while drawing, b) Dry spinning, where a polymer solution is drawn through a nozzle, while solvent is evaporated from the resulting fiber, c) Wet spinning, where a polymer solution is extruded into a nonsolvent coagulation bath and drawn through or d) Dry-jet spinning, which is similar to wet spinning except a small air gap is present before the polymer solution enters the coagulation bath.

Figure 12. a) Sample stress-strain curve with correlated parameters for strength, strain at break, toughness and Young's modulus. b) Breakdown of individual secondary structures under load:

i) the stepwise uncoiling of  $\alpha$ -helices and ii) the simultaneous rupturing of hydrogen bonds between  $\beta$ -strands in  $\beta$ -sheets.

Figure 13. Different degradation mechanisms a) Enzyme catalysed degradation of polypeptides *via* hydrolysis of the polyamide backbone. b) Redox reactions as they pertain to thiol chemistry as it relates to i) disulphide bridges and ii) thioether bonds

Figure 14. Research theme of the thesis stemming from the implementation of synthetic polypeptides is three-, two- and one-dimensional materials

Figure 15. a) Schematic of  $\beta$ -sheet laden networks b) Thioflavin T staining shows binding of an amorphous network upon inclusion of glycine c) notable  $\beta$ -sheet shift was observed with a high signal at  $1633\text{ cm}^{-1}$  shifting with the inclusion of glycine. d) Mechanically, gels were found to be tough and tunable with glycine e) example of a 3D printed,  $\beta$ -sheet laden network.

Figure 16. a) Schematic of general CAP-RAFT process b) Kinetics using a model dithiobenzoate initiator in and absent from the reaction solution c) result after performing CAP on wafers d) FTIR spectra indicates a different material and secondary conformation as would be exerted.

Figure 17. ai) Schematic of wet spinning fibers with  $\beta$ -sheet laden networks ii) based on the matrix, d) FTIR indicating a lack of hydrogen bonding. This leads to c) tensile mechanical testing of samples which was found to increase in strength.



## Chapter 2

Figure 1. Fabrication of peptide  $\beta$ -sheets loaded composite networks.

Figure 2. Characteristics of networks in deionised water (glass vial diameter  $\sim$ 25 mm) at pH 6.7.

Figure 3. SEM cross-sectional images of  $\beta$ -sheets-incorporated hydrogel.

Figure 4. Confocal images of  $\beta$ -sheets-incorporated networks stained via ThT assay.

Figure 5. Structural characterizations of initial and  $\beta$ -sheets-incorporated networks.

Figure 6. Mechanical properties summary of  $\beta$ -sheets-incorporated networks.

Figure 7. TGA analysis of the initial and  $\beta$ -sheet incorporated networks.

Figure 8. Degradation profiles of  $\beta$ -sheets-incorporated networks in harsh environments.

Figure 9. 3D-printed networks with similar chemical composition to previous hydrogels.

Supplementary Figure 1. SEM cross-sectional images of initial networks at various magnifications (from left to right, scale bars are 50  $\mu$ m, 5  $\mu$ m with increasing magnification) with different morphologies showing (a) hydrogel and (b) cryogels.

Supplementary Figure 2. SEM cross-sectional images of  $\beta$ -sheets incorporated hydrogel networks at various magnifications (from left to right, scale bars are 50  $\mu$ m, 5  $\mu$ m with increasing magnification): (a) 50:50 valine to glycine monomer at 0.8M ( $\sim$ 120 mg/mL of val NCA); (b) glycine 100% 0.8M.

Supplementary Figure 3. ATR-FTIR Spectra showing characterizations of initial network and  $\beta$ -sheet (400 – 4000  $\text{cm}^{-1}$ ) incorporated final networks obtained using different glycine concentrations at a constant monomer molar concentration (0.8M).

Supplementary Figure 4. Preparation of PMMA-grafted networks (hydrogels & cryogels) through functionalization of initial network with trithiocarbonate iniferters (TTC); ii) insertion of PMMA chains via UV-initiated RAFT polymerization based on the attached TTC iniferters, in the presence of MMA monomers at three different concentrations (30, 120, and 360 mg/mL).

Supplementary Figure 5 (a) & (c) Compression strain-stress curves of PMMA grafted networks, hydrogels and cryogels respectively, prepared with different MMA concentrations (30, 120, and 360 mg/mL); (b) & (d) compression moduli (stiffness) of PMMA grafted

networks vs. those of  $\beta$ -sheets incorporated counterparts, hydrogels and cryogels respectively, as a function of corresponding monomer concentrations. Error bars determined by experimental error.

Supplementary Figure 6:  $^1\text{H}$  NMR spectra for (a) 15, (b) 30, (c) 60, (d) 120 and (e) 180 mg/mL of Val NCA in DMF with integral of the Val NCA doublet at 0.92 ppm analysed using the two singlets at 2.88 ppm and 2.96 ppm of the two methyl groups from DMF being used to normalize these integrals. (f) Val NCA concentration plotted against value of the integral at 0.92 ppm.

Supplementary Figure 7:  $^1\text{H}$  NMR spectrum of GH10 reaction solution and calculation of conversion of Val NCA in GH10

Supplementary Figure 8:  $^1\text{H}$  NMR spectrum of GH10 reaction solution and calculation of conversion of Gly NCA in GH10

## Chapter 3

Figure 1. Schematic for CAP-RAFT using a polypeptide macroinitiator onto a surface functionalized with RAFT agent. a) Graphical schematic of CAP-RAFT of PLLMA macrocrosslinker through the use of blue light ( $4 \text{ mW cm}^{-2}$ ,  $\lambda_{\text{max}}=460 \text{ nm}$ ). b) Chemical schematic representing the use of model dithiobenzoate and trithiocarbonate RAFT agents.

Figure 2. AFM imaging and analysis of CAP-RAFT films using a PLLMA macrocrosslinker utilizing different model RAFT agents. ai, aii) Analysis of film growth utilizing a dithiobenzoate RAFT agent observing kinetics of film growth (ai) and film roughness (aii) both with and without RAFT agent in solution. aiii, aiv) Analysis of film growth utilizing a trithiocarbonate RAFT agent observing kinetics of film growth (aiii) and film roughness (aiv) both with and without RAFT agent in solution. b) Surface morphology after 48 h of CAP-RAFT utilizing systems imaged using AFM with bi) a dithiobenzoate RAFT agent anchored to the surface as well as in RAFT agent in solution; bii) a dithiobenzoate RAFT agent anchored to the surface but not in the reaction solution; biii) a trithiocarbonate RAFT agent anchored to the surface as well as in RAFT agent in solution; and biv) a trithiocarbonate anchored to the surface but not in the reaction solution (scale bars= $1 \mu\text{m}$ ).

Figure 3. Multiple layers synthesized using CAP-RAFT. a) Schematic for reinitiation and execution of multiple layers of CAP-RAFT. b) Film thickness for multiple layers with PLLMA macrocrosslinker determined using AFM. c) FTIR spectra of the Amide I band of each layer. d) Surface morphology as revealed by AFM imaging of the di) 2nd, dii) 3rd and diii) 4th layers. (scale bars= $1 \mu\text{m}$ ). EDC is 1-ethyl-3-(3-dimethylaminopropyl) carbodiimide.

Figure 4. a) Comparative film thickness and roughness upon introduction of PLGlu as the initial layer and the second layer; b) FTIR spectra of top PLGlu layer; c) surface morphology of PLGlu layer as the ci) initial layer and cii) the second layer (scale bars= $1 \mu\text{m}$ ).

Figure 5. a) Schematic of enzymatic degradation of polypeptide films via hydrolysis of amide bonds in the polypeptide backbone (in red). Notably, the RAFT polymer remains intact (in black). b–e) AFM images of films treated with enzyme. b) PLLMA-based films before (bi, bii) and after incubation (biii, biv) with  $1 \text{ mg mL}^{-1}$   $\alpha$ -chymotrypsin at  $25 \text{ }^\circ\text{C}$ . c) PLGMA-based films before (ci, cii) and after incubation (ciii, civ) with  $1 \text{ mg mL}^{-1}$   $\alpha$ -chymotrypsin at  $25 \text{ }^\circ\text{C}$ . d) PLLMA-based films before (di, dii) and after incubation (diii, div) with  $1 \text{ mg mL}^{-1}$  Protease XIV at  $37 \text{ }^\circ\text{C}$ . e) PLGMA-based films before (ei, eii) and after incubation (eiii, eiv) with  $1 \text{ mg mL}^{-1}$  Protease XIV at  $37 \text{ }^\circ\text{C}$ . For b–e): 2D (i, iii) and 3D (ii, iv) image maps were utilized.

Protease solutions used were 1 mg mL<sup>-1</sup>  $\alpha$ -chymotrypsin at 25 °C (b, c) and 1 mg mL<sup>-1</sup> Protease XIV at 37 °C (d, e) (scale bars=200 nm).

Figure S1: Scheme for synthesis of N-carboxyanhydrides

Figure S2: Synthesis of poly(L-lysine-*r*-L-lysine-*g*-methacrylamide) (PLLMA) (a) NCA ROP of Lys(Z) NCA using hexylamine as an initiator; (b) Deprotection of Z-protecting group using HBr, (c) Methacrylation of exposed amine groups with methacrylic anhydride.

Figure S3: Synthesis of poly(L-glutamic acid-*r*-L-lysine-*g*-methacrylamide) (PLGMA) (a) NCA ROP of Lys(Z) and Glu(Bzl) NCA using hexylamine as an initiator; (b) Deprotection of Z-protecting group using HBr, (c) Methacrylation of exposed amine groups with methacrylic anhydride.

Figure S4: Anchoring of initiator to silicon wafers.

Figure S5: Mechanism of LAP RAFT system.

Figure S6: DLS of supernatant with CTA present in 0.5 mg/mL solutions of DMSO.

Figure S7: DLS of supernatant without CTA present in 0.5 mg/mL solutions of DMSO.

Figure S8: <sup>1</sup>H NMR (in DMSO) between 7.0 and 7.6 ppm of PLLMA a) before reaction and b) after reaction without CTA in solution and c) after reaction with CTA in solution. Reaction supernatant was dialysed against DMSO, revealing splitting patterns consistent with aromatic rings which would only be present after degradation of RAFT agent by free amines on the PLLMA

Figure S9: <sup>1</sup>H NMR of PLLMA including calculation for methacrylation percentage

Figure S10: <sup>1</sup>H NMR of PLGMA including calculation for methacrylation percentage

## Chapter 4

Figure 1. a) Schematic of experimental apparatus in i) horizontal and ii) vertical configurations. Vertical configurations were employed when the solvent was significantly denser than the nonsolvent. bi) Block flow diagram of stages of fiber fabrication and ii) the corresponding chemical schematic within each fiber during each stage. c) Chemical structure of all spun polymers.

Figure 2. Fourier transform infrared (FTIR) spectroscopy of Amide I band ( $1600\text{-}1700\text{ cm}^{-1}$ ) for fiber samples with and without PVal for a) nylon 6, b) poly(caprolactone) (PCL), c) cellulose acetate, d) cellulose, e) poly(benzyl-L-glutamate) and f) eADF4(C16).

Figure 3. Scanning electron microscopy (SEM) of fiber surface at i, iii) low magnification and ii, iv) high magnification for fiber samples i, ii) with and iii, iv) without PVal for a) nylon 6, b) poly(caprolactone) (PCL), c) cellulose acetate, d) cellulose, e) poly(benzyl-L-glutamate) and f) eADF4(C16).

Figure 4. Scanning electron microscopy (SEM) of fiber cross-section at i, iii) low magnification and ii, iv) high magnification for fiber samples i, ii) with and iii, iv) without PVal for a) nylon 6, b) poly(caprolactone) (PCL), c) cellulose acetate, d) cellulose, e) poly(benzyl-L-glutamate) and f) eADF4(C16). Features mentioned in text highlighted in yellow.

Figure 5. X-ray diffraction (XRD) spectra for fiber samples with and without PVal for nylon 6, poly(caprolactone) (PCL), cellulose acetate, cellulose, poly(benzyl-L-glutamate) (PBLG) and eADF4(C16).

Figure 6. Example tensile mechanical testing curves for fibers without polypeptide and with Pval and PGly for a) nylon 6, b) poly(caprolactone) (PCL), c) cellulose acetate, d) cellulose, e) poly(benzyl-L-glutamate) and f) eADF4(C16). g) Summary of relative impact of PVal on strength, extension at break, Young's modulus and toughness for all polymers. Samples which experience a strength increase outlined in red, samples which experience an increase in strain at break outlined in dashed blue and samples which experience no significant difference or reduced mechanical properties outlined in green.

Figure S1: Full Fourier transform infrared (FTIR) spectra for fiber samples without polypeptide and with Pval and PGly for a) nylon 6, b) poly(caprolactone) (PCL), c) cellulose acetate, d) cellulose, e) poly(benzyl-L-glutamate) and f) eADF4(C16).

Figure S2: Scanning electron microscopy (SEM) fiber cross-section at high magnification for fiber samples of nylon 6 with PVal with highlighted  $\beta$ -sheet region.

Figure S3: Differential scanning calorimetry (DSC) thermogram of PCL fibers with and without PCL with crystallinity quoted

Figure S4: Small angle X-ray scattering (SAXS) spectra for fiber samples with and without PVal for a) nylon 6, b) poly(caprolactone) (PCL), c) cellulose acetate, d) cellulose, e) poly(benzyl-L-glutamate) and f) eADF4(C16).

## ***List of Tables***

---

### **Chapter 2**

Table 1. Estimated polymerization degree of Val/Gly NCA in the initial networks.

### **Chapter 3**

Table 1. Secondary structure elements of multi-layered PLLMA and PLGMA films (determined using ATR-FTIR).

Table S1: Summary of PLLMA macromonomer.

Table S2: Thickness of films in the absence of specific elements used in the CAP-RAFT procedure.

Table S3: Summary of PLGMA macromonomer.

### **Chapter 4**

Table 1: Summary of processing conditions for wet-spinning of polymers both with and without Val NCA

Table 2: Summary of the mass fractal dimensions of all polymers with and without PVal.

Table S1: Chemical Information on Poly(benzyl-L-glutamate)

Table S2: Summary of relative intensity of  $\beta$ -sheet peak relative to key non  $\beta$ -sheet peak within polymer.

## *List of Abbreviations*

---

ATRP	Atom transfer radical polymerization
CAP	Continuous assembly of polymers
CGC	Critical gelation concentration
CTA	Chain transfer agent
DCM	Dichloromethane
DMF	Dimethylformamide
DNA	Deoxyribonucleic acid
DP	Degree of polymerization
DSC	Differential scanning calorimetry
FRP	Free radical polymerization
NCA	<i>N</i> -carboxyanhydride
NMR	Nuclear magnetic resonance
PADLG	Poly(allyl- <sub>DL</sub> -glycine)
PBLA	Poly(benzyl- <sub>L</sub> -aspartate)
PBLG	Poly(benzyl- <sub>L</sub> -glutamate)
PCL	Polycaprolactone
PEG	Poly(ethylene glycol)
PLAla	Poly( <sub>L</sub> -alanine)
PLGEG	Poly( <sub>L</sub> -glutamic acid- <i>g</i> -oligo(ethylene glycol))
PLGlu	Poly( <sub>L</sub> -glutamic acid)
PLLys	Poly( <sub>L</sub> -lysine)
PLPTyr	Poly( <sub>L</sub> -phosphotyrosine)
PLVG	Poly( <sub>L</sub> -valine- <i>r</i> -glycine)
PMLG	Poly(methyl- <sub>L</sub> -glutamate)
PNLC	Poly( <i>S</i> -( <i>o</i> -nitrobenzyl)- <sub>L</sub> -cysteine)
PVal	Poly( <sub>L</sub> -valine)
PZLL	Poly(carbobenzyloxy- <sub>L</sub> -lysine)
RAFT	Reversible addition–fragmentation chain-transfer
RNA	Ribonucleic acid
ROP	Ring opening polymerization
SCOP	Structural Classification of Protein
SEM	Scanning electron microscopy
ThT	Thioflavin T
UV	Ultraviolet



## ***Chapter 1:***

### **Introduction**

---

#### 1.1 An Overview of Polymeric Materials

Before their formal codification as a class of molecules, polymers had already naturally been embedded into material science.<sup>1</sup> While natural polymers such as natural rubbers, silks and regenerated cellulose can be plotted throughout history, it would not be until 1907 when the first synthetic plastic polymer, polyoxybenzylmethyleneglycolanhydride – more commonly known as Bakelite - would be invented by Bakeland.<sup>2</sup> Furthermore, the production of synthetic substitutes such as nylon and synthetic rubber leading into World War II progressed significantly due to decreasing natural resources, leading to the polymers becoming a cornerstone of material science at multiple dimensional scales.<sup>3</sup>

In general, polymers can be classified into two different categories - synthetic polymers and biopolymers.<sup>4,5</sup> As the name suggests, synthetic polymers are synthesized *via* synthetic routes, being built from well-defined monomers using different polymerization techniques such as uncontrolled radical polymerization, atom transfer radical polymerization (ATRP) and reversible addition-fragmentation transfer (RAFT) polymerization.<sup>6,7</sup> On the other hand, biopolymers are from a cellular origin and, with the exception of a few polymers including natural rubbers, can be further classified into three classes based on their monomeric structure and subsequent natural function.<sup>8-10</sup> Polysaccharides are, at their simplest, derived from monomers with two or more hydroxyl groups and a carboxyl group (known as monosaccharides) though the most common examples are colloquially known as sugars, where the monosaccharides are a ring structure. Polynucleotides consist of monomers based on a five-membered sugar ring structure, nucleobase and a phosphate group and includes deoxyribonucleic acid (DNA) and ribonucleic acid (RNA) which both act as the “genetic script” for the design of perhaps the most diverse class of biopolymers - proteins.

The specific function of a protein is based on their overall structure which in and of itself is derived from the hierarchical structure based on the folding of their primary structure – namely the polypeptide chain.<sup>11,12</sup> Natural polypeptides comprise from a sequence of 21 canonical amino acids with all amino acids consisting of four groups extending from a carbon center – a hydrogen atom, a carboxylic acid functional group, an amino functional group, and a unique side chain different for each amino acid.<sup>13</sup> It is the size of this polypeptide chain which defines

the final folded product as a proteins (100 or more amino acid residues in length) or a peptides (less than 100 amino acid residues in length). This carbon is classified as the chiral carbon for almost all amino acids (the exception being glycine which has a second hydrogen atom as its unique side chain), giving these amino acids two stereoisomers. The *L*-isomer are generally the natural form of an amino acid though the *D*-isomer does sometimes occur, usually due to posttranslational modifications (controlled modifications after synthesis). Conjugation of carboxyl and amino groups result in peptide bonds which, when sequenced, results in the protein primary structure known as a polypeptide chain. These polypeptide chains will then fold through intramolecular bonding into secondary, tertiary and, in some cases, quaternary structures (Figure 1), though the first of these will be discussed later in more detail as it is the most relevant of these hierarchical levels.

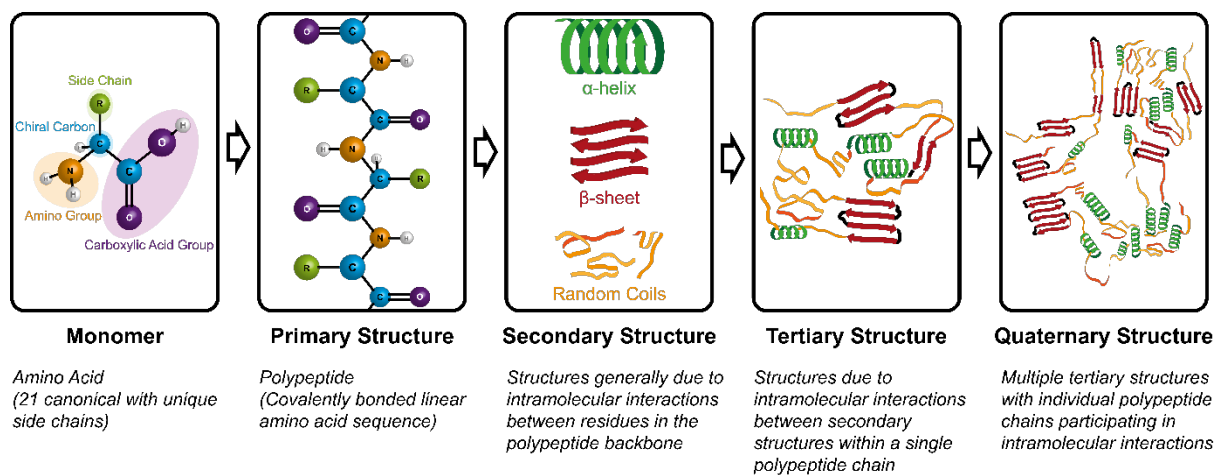


Figure 1: Schematic of different hierarchical levels of proteins beginning from the monomeric state to the primary, secondary, tertiary and finally (in some case.) quaternary structure.

The diversity of synthetic techniques towards achieving the desired polypeptide chain reflects the popularity of such biopolymers. In modern day science, four techniques stand out as notable; solid state peptide synthesis,<sup>14</sup> recombinant protein production,<sup>15,16</sup> *N*-carboxyanhydride ring opening polymerization (NCA ROP)<sup>17</sup> and chemoenzymatic polymerization.<sup>18</sup> These four techniques can be separated into sequence specific techniques and non-sequence specific. The two sequence specific techniques – solid state peptide synthesis and recombinant protein production – are extremely useful for designing polypeptides with specific and controlled folding patterns. Solid state peptide synthesis, however, tends to be limited to peptides (chains smaller than 100 residues in length) and becomes incredibly expensive upon reaching approximately 10 residues in length. Recombinant proteins can overcome this issue easily, but this technique can become complicated when designing chimeric and fusion proteins (i.e. combining two proteins together) along with a low

throughput. The two non-sequence specific synthetic methods – NCA ROP and chemoenzymatic polymerization – are intriguingly both polymerization techniques and thus these polypeptides share similarities more typical of synthetic polymers and be characterized using such qualifiers.

## 1.2 Synthetic Polymerization Methods

Synthetic polymerization methods can be divided into two broad families – step-growth and chain-growth polymerizations.<sup>19</sup> In step-growth polymerization, multifunctional monomers are polymerized through end-to-end coupling.<sup>20</sup> This also means that short chain polymers (oligomers) may also couple together to form the polymer. In contrast, chain-growth polymerization encompasses any polymerization technique where a monomer reacts with a terminal end of the polymer to grow the polymer chain monomer-by-monomer.<sup>21</sup> Fundamentally, chain-growth polymerization has four potential stages – initiation, propagation, transfer, and termination. Chain initiation begins the chain by generating a functional group, radical or some other reactive component. Chain propagation is the sequential addition of monomer to the polymer chain resulting in an intermediate reactive component which is continuously regenerated at the terminus of the polymer. Chain transfer occurs when the reactive component is transferred from one chain to another chain or another molecule. Chain termination is the final stage of a polymer where the regenerative center is no longer present in the chain. The number of monomers per polymer chain (otherwise known as the degree of polymerization, DP) and the distribution of these chain lengths (the dispersity,  $\mathcal{D}$ ) may be either controlled or uncontrolled in both cases.

### 1.2.1 Synthetic polypeptide synthesis

As stated before, NCA ROP and chemoenzymatic polymerization can be utilized to design homopolypeptides and non-sequence specific polypeptides. Each of these, coincidentally, also represent each of the two broad categories of polymerization as NCA ROP and chemoenzymatic polymerization are chain-growth and step-wise polymerizations respectively.

#### 1.2.1.1 *N*-carboxyanhydride Ring Opening Polymerization (NCA ROP)

NCA ROP marks a well-established methodology towards the synthesis of synthetic polypeptides (Figure 2).<sup>22,23</sup> In 1906, Leuchs reported the first synthesis of an NCA, heating *N*-carbethoxyglycine chloride to form glycine NCA,<sup>24</sup> and later, in 1908, found that they would decompose in the presence of water to what is now known to be homopolypeptides.<sup>25</sup> Nowadays, the most common method of synthesizing  $\alpha$ -amino acid NCAs is *via* phosgenation

which forms a five-member ring by conjugating to both the amino and carboxylic acid group stemming from the  $\alpha$ -carbon (Figure 2a).<sup>22,23</sup> From this, the most common polymerization route is *via* the normal amine mechanism, where an initiating nucleophile (often a primary amine) causes the ring opening of a single monomer (Figure 2bi). This results in a primary amine, which then can perform a nucleophilic attack on another monomer and resulting in propagation and thus chain-growth ring opening polymerization. As this initiator remains appended to the resulting polypeptide, end group functionalization is facile. Generally using this method, the degree of polymerization (DP) can be controlled by defining the monomer-to-initiator ratio. However, issues of control arise due to deprotonation of the monomer, which then leads to the monomer itself becoming an initiator and triggering the activated monomer mechanism. While usually this is an unwanted side reaction, which results in reduced control, this can instead be triggered by intentionally deprotonating the monomer using a base (such as a tertiary amine) (Figure 2bii). While this does yield uncontrolled polymerization, the net result is a long chain polypeptide, which can still be rendered useful depending on application. Comparatively, initiation *via* metal complexes reduces this side reaction through oxidative addition and amide proton migration (Figure 2biii). Although it lacks the same facile nature of the other two mechanisms, this results in a high level of control. While each of these mechanisms have their own unique pitfalls and benefits, they share a common issue, which can be restrictive.

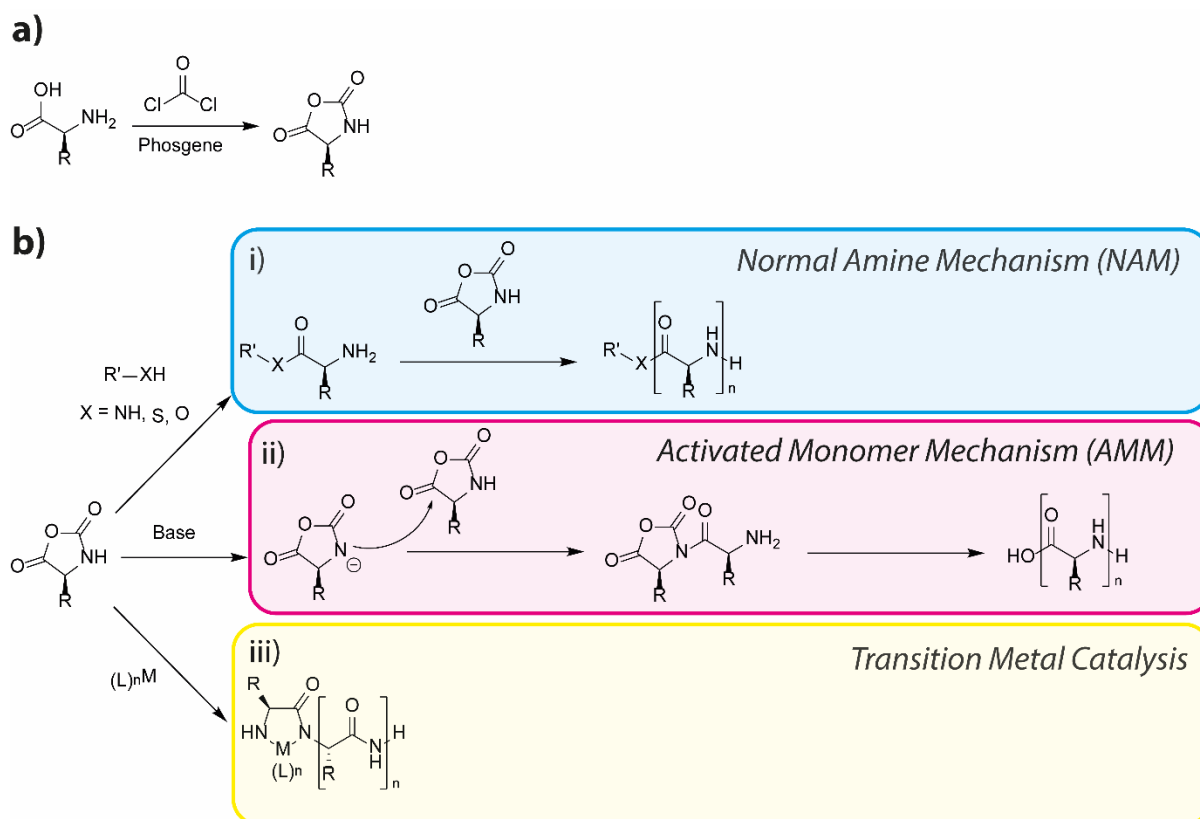


Figure 2: Schematic of NCA ROP synthesis. a) *N*-carboxyanhydride (NCA) synthesis *via* phosgenation. b) Ring opening polymerization (ROP) *via* i) the normal amine mechanism, ii) the activated monomer mechanism and iii) transition metal catalysis.

As NCAs are susceptible to nucleophilic attack, they require stringent nucleophile-free conditions during synthesis.<sup>22,23</sup> This firstly means that all conditions must be anhydrous as water is a nucleophile, which, while complexifying synthesis, is a technical issue rather than a design issue. Secondly, this means that canonical amino acids with nucleophilic side chains cannot be used directly. This encompasses the majority of intrinsically functional residues such as lysine and serine. Additionally, due to the process of NCA synthesis itself attacking the carboxylic acid functional group, residues with this functional side chain also cannot be used directly. As such, protecting groups coupled to the side chain functional groups (such as benzyl-protected groups or *tert*-butyl protecting groups) are often used to prevent such reactions from occurring and then removed post-polymerization, adding an extra synthetic step.<sup>26</sup> It should be noted, however, that these protected amino acids - along with other modified amino acids - will adopt their own secondary structures and may be utilized in their protected form.

## 1.2.2 Chemoenzymatic Polymerization

Chemoenzymatic synthesis revolves around the conjugation of molecular units through enzyme catalysis and thus the spontaneous repetition of this conjugation leads to step-wise polymerization.<sup>27,28</sup> While chemoenzymatic polymerization has been utilized to synthesize oligosaccharides, its application has naturally expanded into polypeptide synthesis (Figure 3).<sup>18</sup> Under normal circumstances, the enzyme employed is naturally responsible for the coupling of the specific molecules in question. However, chemoenzymatic polymerization actually works on the concept of thermodynamic equilibrium and reversing the usual functionality of proteases, which hydrolyze peptide bonds to instead push equilibrium towards polypeptide synthesis. Generally, this can be accelerated through the use of amino acid esters. Present at the active site of the protease is a catalytic cysteine or serine residue, which cleaves the ester bond, resulting in an unstable acyl-protease intermediate. This intermediate is highly susceptible to aminolysis *via* another monomer (or even polypeptide) and leading to the desired conjugation. As stated above, this is repeated to yield the step-wise growth of polypeptides. As with NCA ROP, chemoenzymatic polymerization comes with its own set of issues.

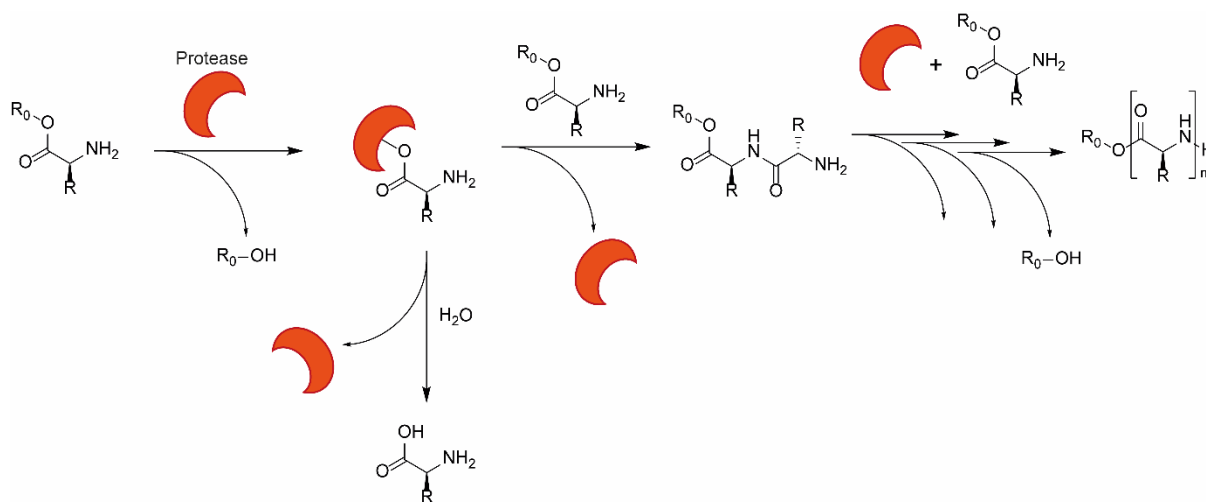


Figure 3: Schematic of chemoenzymatic polymerization of polypeptides. Notably, protease is preserved along the reaction pathway and only a catalytic amount is required.

Chemoenzymatic polymerization is based on an enzyme catalysis and thermodynamic equilibrium, and thus reaction conditions must cater to both components.<sup>18</sup> Enzymes are sensitive to their environment, thus, the solvent system is highly important. To preserve natural and predictable functionality, water or aqueous solvents are thus favored. While this is synthetically more stringent than NCA ROP, this does mean that the overall synthesis does not necessitate harsh or toxic substances (as such substances are likely to denature the enzyme anyway). Furthermore, the lack of toxic starting materials (*i.e.* phosgene) makes this a far more

benign reaction overall and easily industrially applicable. However, this reaction is fundamentally based on forcing a usually unfavorable reaction. Furthermore, the acyl-protease intermediate can undergo hydrolysis leading to premature termination of the polymerization. These issues severely limit the DP of the subsequent polypeptides with lengths remaining below 20 residues.

### 1.2.3 Free radical polymerization (FRP)

While the majority of materials to be discussed are purely polypeptide-based, many will utilize a combination of different starting polymers resulting in a composite material. Thus, a brief overview of a few notable polymerization methods is useful.

The vast majority of polymerization techniques are a subset of free radical polymerization where the regenerative component is a radical.<sup>7,29</sup> Carbon-carbon double-bonds at the end of a monomer are generally the most susceptible to this method of polymerization (with the example used in Figure 4 being a vinyl monomer). Other side chains such as acrylate, methacrylate and methacrylamides can be used to control the rate of polymerization. In terms of initiation, a molecule which can generate radicals through some stimuli including light, heat or redox is employed. Due to the high reactivity and instability of radicals, many subsets of radical polymerizations aim to mediate this polymerization by introducing an equilibrium reaction to render the polymer reversibly dormant (called reversible-deactivation polymerization) and generally control of the radical transfer step. This then leads to a controlled polymerization scheme, which means that both DP and  $\bar{D}$  can be well defined.

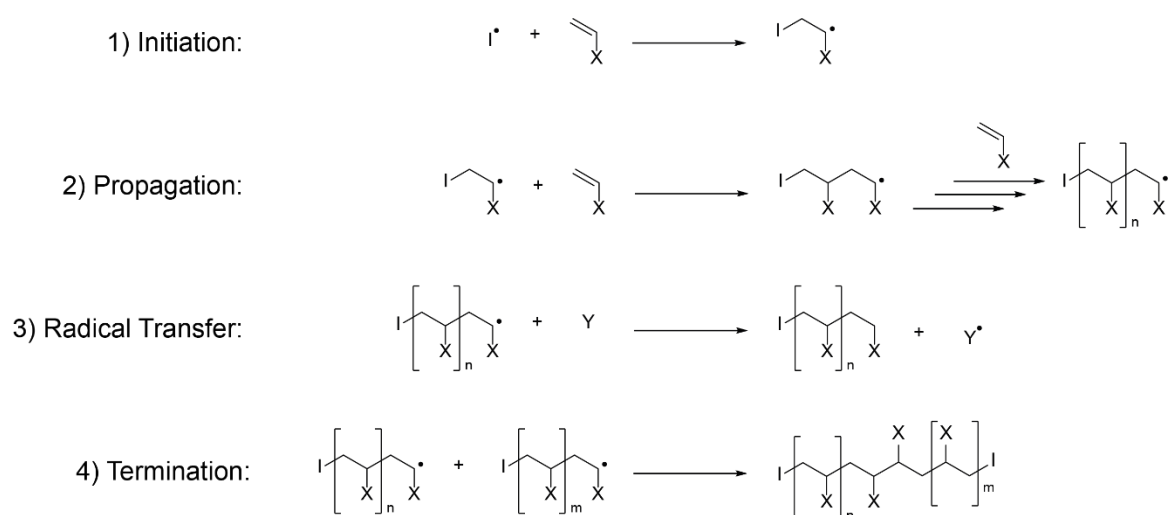


Figure 4: General schematic of Mechanism for free radical polymerization with a vinyl monomer. All four steps of chain growth polymerizations are present (initiation, propagation, transfer and termination). Note that radical transfer is a side reaction rather than a growth step.

### 1.2.3.1 Reversible addition-fragmentation (RAFT) polymerization

Reversible addition-fragmentation chain transfer (RAFT) polymerization controls the polymerization through the use of a chain transfer agent (CTA, also referred to as RAFT agent) to introduce the equilibrium reaction for control (Figure 5).<sup>30</sup> Radicals are transferred to a thiocarbonylthio group (Z-(C=S)S-R) from the initiator, which forces propagation primarily through this chain. Monomer groups are inserted between the Z and (C=S)S-R, thus becoming part of the Z group for the continued propagation. Generally, DP can be designed to be based on a specific monomer-to-CTA ratio, but these values are not completely equivalent as numerous polymers may be formed.

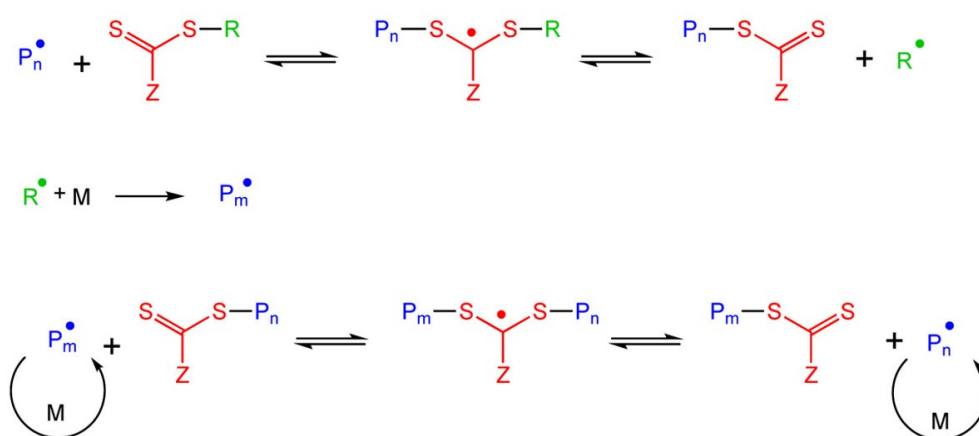


Figure 5: Mediating equilibrium reactions for chain transfer agents with the polymer for reversible addition-fragmentation chain transfer (RAFT) polymerization. Reprinted (adapted) with permission from <sup>30</sup>. Copyright 2017 American Chemical Society

Ultimately, this results in four possible polymers existing within the reaction based on the terminal ends.<sup>30</sup> On the propagating terminal, chains will either exist with or without the thiocarbonylthio end-group. On the other terminal end, alongside those chains initiated by the active CTA, others will be initiated directly by the radical initiator. The relative quantity of chains with each terminal end can actually be predicted, thus, allowing for accurate control. While this level of control is ultimately based on numerous factors (radical initiator, solvent, monomer reactivity, etc.), the one most unique to RAFT polymerization is the choice of CTA. While the R-group has an impact, it is far subtler than the impact of the Z-group with dithiobenzoates and trithiocarbonates both being popular choices. Both offer excellent control, though dithiobenzoates are comparatively less stable over time and prone to potential hydrolysis.



## 1.3 Synthetic Polypeptide Structures

As NCA ROP and chemoenzymatic polymerization both yield polypeptides, it is useful to consider them in these terms instead of the sequence specificity usually associated with proteins. While they are both non-sequence specific, they both can implement multiple monomers in random or block conformations and both have a dispersity curve instead of a specific molecular weight as would be associated with sequence specific proteins. As such, a more general view of polypeptide folding has to be taken as opposed to the usual sequence specific approach.

### 1.3.1 Secondary Structure

As stated previously, secondary structure formation is the result of primary structure folding via intramolecular supramolecular interactions, such as hydrophobic interactions,  $\pi$ - $\pi$  stacking, Van der Waals forces, and ionic bonding.<sup>31</sup> While numerous secondary structures exist, the most common are  $\beta$ -sheets,  $\alpha$ -helices and random coils. Both  $\beta$ -sheets and  $\alpha$ -helices are well-defined structures with unique packing characteristics while random coils represent the absence of well-defined packing and thus are more amorphous. Subsequent functions can then potentially be translated by emulating these secondary structures, and their unique packing structure further dictates different material properties. As such, the prediction of secondary structures based on a defined polypeptide sequence is a mandatory necessity in polypeptide material design.<sup>32</sup> As manipulation of conditions and molecular architecture is important in secondary structure design, details involving such manipulation are further detailed in Appendix A, Section 4-5.

#### 1.3.1.1 Polypeptide Structure Under Physiological Conditions

For polymerization-based techniques in particular, a broad approach dictated by individual amino acid propensities and interactions based on amino acid chemical structure is sufficient. In 2012, Fujiwara et al. used a statistical approach to catalogue individual amino acid  $\alpha$ -helix and  $\beta$ -sheet forming propensities based on the frequency that each given amino acid is found to be present in the corresponding secondary structure extracted from the associated library of the SCOP classification (Structural Classification of Protein) (Figure 6).<sup>33</sup>  $\beta$ -sheets have a somewhat straightforward design paradigm, with amino acids, which possess either aromatic or branching chains from the  $\beta$ -carbon favoring this structure. This was a refinement on the long-standing belief that  $\beta$ -sheet formation is the consequence of hydrophobic residues as this requirement now excludes hydrophobic residues, which typically prefer  $\alpha$ -helical

conformations (e.g. alanine) while including threonine, which is the only hydrophilic residue to show a high  $\beta$ -sheet propensity.  $\alpha$ -helices are more complicated, with no clear class trend of individual amino acids standing out as a common trend. Alanine, methionine, glutamic acid and glutamine all possess a slightly greater propensity towards  $\alpha$ -helices compared to other amino acids, yet all vary in terms of hydrophobicity, functionality and charge. Instead of taking each amino acid as an individual entity, Engel *et al.* considered sequences with  $\alpha$  helical conformations, determining that most  $\alpha$ -helices are formed from amphiphilic sequence (*i.e.* sequences containing both hydrophobic and hydrophilic amino acids).<sup>34</sup> While the absence of  $\beta$ -sheets and  $\alpha$ -helices does not preclude the immediate inference of random coils, the two notable residues with low propensities for both secondary structures, glycine and proline, can be used to induce such amorphous structures.<sup>35,36</sup> While proline is responsible for unique secondary structures - namely polyproline helices and triple helices - the ring structure of its side chain creates a molecular kink, which otherwise forces neighboring residues out of otherwise favorable conformations.<sup>37</sup> On the other hand, glycine has a hydrogen as its side chain, limiting the side chain interactions. Therefore, it can participate in for secondary structure formation.<sup>38</sup> While proline can be considered a secondary structure breaker, glycine is not so as its presence in a chain does not force amino acids out of position and, in some cases, can actually assist with  $\alpha$ -helical folding due to its compact nature. Thus, this gives a strong basis to determine which amino acids may be required to achieve specific structures.

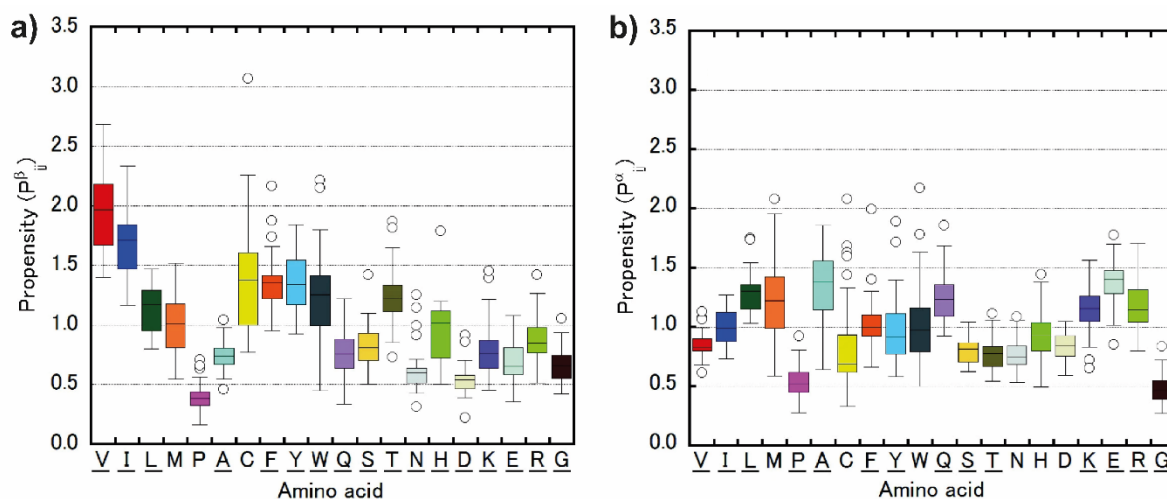


Figure 6: Secondary structure propensities of all canonical amino acids based on their presence in a)  $\beta$ -sheets and b)  $\alpha$ -helices. This is from an Open Access article distributed under the terms of the Creative Commons Attribution License, which permits unrestricted use, distribution, and reproduction in any medium, provided the original work is properly cited.<sup>33</sup>

It should be noted that the above paradigms pertain to the canonical amino acids, and such trends are not completely transferrable when utilizing side-chain modified amino acids. While

canonical aromatic amino acids trend towards  $\beta$ -sheet formation, homopolypeptides with aromatic protected residues such as poly(benzyl-L-aspartate) (PBLA),<sup>39</sup> poly(benzyl-L-glutamate) (PBLG),<sup>40</sup> and poly(carbobenzyloxy-L-lysine) (PZLL)<sup>41</sup> generally have a DP dependent secondary structure with block lengths less than around 10 residues yielding  $\beta$ -sheet conformations while any larger blocks form  $\alpha$ -helices. Interestingly, this is not true for all aromatic side chain modified amino acids as poly(*S*-(*o*-nitrobenzyl)-L-cysteine) (PNLC) actually favours  $\beta$ -sheet formation.<sup>42</sup> Poly(tert butyl-L-lysine) also maintains a DP dependent secondary structure similar to the aromatic protected residues.<sup>43</sup> This range of examples should show that, while there may be broad trends which can be used to predict the secondary structure conformations of modified amino acids (e.g. DP dependence), experimental evidence is more telling of the potential secondary structure changes.

Modulation of stereoisomerism has a far more universal effect as mixtures of stereoisomers tend to disrupt secondary structure. As would be expected, homopolypeptides of racemic residues (i.e. 1:1 ratio of L- and D-stereoisomers) generally lack structure and thereby provide the possibility of affecting reducing secondary structure formation by moving from a pure enantiomer toward a racemic polypeptide.<sup>44-46</sup> An exception is the body of work performed by the Wooley group, which has observed the  $\beta$ -sheet formation of poly(allyl DL-glycine) (PADLG).<sup>47-49</sup> Notably, these structures were found in DMF instead of water and as such,  $\beta$ -sheet structure formation would also be driven by solvent influence (discussed later). Interestingly, complete substitution of the residues specifically also changes the coiling direction of  $\alpha$ -helices regardless of whether the polypeptide is a homopolypeptide or a defined sequence.<sup>50,51</sup> It should be noted that to develop polypeptides with multiple stereoisomers using the aforementioned methodologies can be difficult as both methods are slightly stereoselective.<sup>52,53</sup>

It is important to note, however, that these structural paradigms primarily refer physiological conditions.

### 1.3.1.2 Polypeptide Structure Under Non-physiological conditions

pH sensitivity can be seen most prominently due to the effects of charged side chains, where protonation or deprotonation of these groups (particularly the primary amine and carboxylic acid side chains of lysine and glutamic acid respectively) dictates intermolecular interactions. By converting such residues to their nonionic forms, the subsequent residue becomes more hydrophobic and results in abnormal secondary structure formation. PLGlu and PLLys have

pKa of 6.5 and 9.85 respectively, which gives a guide to their pH-sensitivity when not applied to a homopolypeptidic state.<sup>54</sup> Furthermore, both have been shown to form  $\beta$ -sheet fibrils in their non-charged state whether it be due to acidity or salinity.<sup>55,56</sup> Furthermore, the presence of both polypeptides in their ionic state results in polyionic complexation, which nets  $\beta$ -sheet structures despite both residues possessing an average propensity towards  $\beta$ -sheet formation.<sup>51</sup> Interestingly as the two residues directly oppose each other in terms of charged state, they can be used in conjunction to form a zwitterionic polypeptide with multiple stages of structural change over a wide pH range.<sup>57</sup>

Thermal shifts can also cause amino acids to deviate from expected secondary structure conformations.<sup>58,59</sup> For example, PLLys undergoes an  $\alpha$ -helix to  $\beta$ -sheet secondary structure change upon heating in aqueous basic conditions.<sup>60</sup> Interestingly, this transition temperature lowers with an increased molecular weight from  $\sim 35^\circ\text{C}$  at 10 kD to  $\sim 15^\circ\text{C}$  at 300 kD with the emergence of insoluble aggregates,  $\beta$ -sheets and  $\beta$ -strands, which directly contradicts theoretical stabilizing effects of water on  $\alpha$ -helical conformations. It is postulated that the secondary structure transition is due to the formation of unstable helical intermediates, which would form more stable  $\beta$ -strands. This effect is not limited to only charged residues, as poly(L-alanine) (PLAla) has been found to undergo an  $\alpha$ -helix to  $\beta$ -sheet transition upon heating above  $210^\circ\text{C}$ .<sup>61</sup> These strands would already be spatially restricted within a single molecule for longer polypeptide chains. Polypeptides with modified side chain residues may also be susceptible to temperature-sensitivity. PHLG was found to undergo no apparent thermosensitivity. However, PSLG, with its long alkyl side chain, saw a shift from  $\alpha$ -helix to  $\beta$ -sheet structures.

Many of the aforementioned intermolecular interactions are also heavily assisted by solvent interactions in water, and as such transitioning polypeptides into different solvents can yield unexpected secondary structure formation.<sup>62</sup> While it is difficult to properly characterize every single solvent-amino-acid relationship, generalised relationships can be deduced by considering the polarity of solvents. Water itself is more polar solvent than the vast majority of solvents, and thus introducing polypeptides into organic solvents already demonstrates a decreased solvent polarity. Hydrogen bonding in water is found to be both highly reversible and easily formed, while in less polar solvents hydrogen bonds are less likely to break, implying irreversibility to secondary structures in such solvents including  $\alpha$ -helices and  $\beta$ -sheets.<sup>63</sup> Multiple sources have shown that both polar and nonpolar solvents lead to an increase in  $\alpha$ -helicity specifically.<sup>64-67</sup> Furthermore, a reduced polarity correlates to a trend towards increased

$\alpha$ -helicity (demonstrated with an increase alkyl chain length of alcohols) to the point where  $\beta$ -sheet formation may occur.

### 1.3.2 Molecular Architectures

At their most simple, synthetic components can be integrated into polypeptides. The range of such molecules is expansive, including bifunctional initiators, aromatic initiators and macroinitiators (the latter of which results in a block copolymer) (Figure 7a).

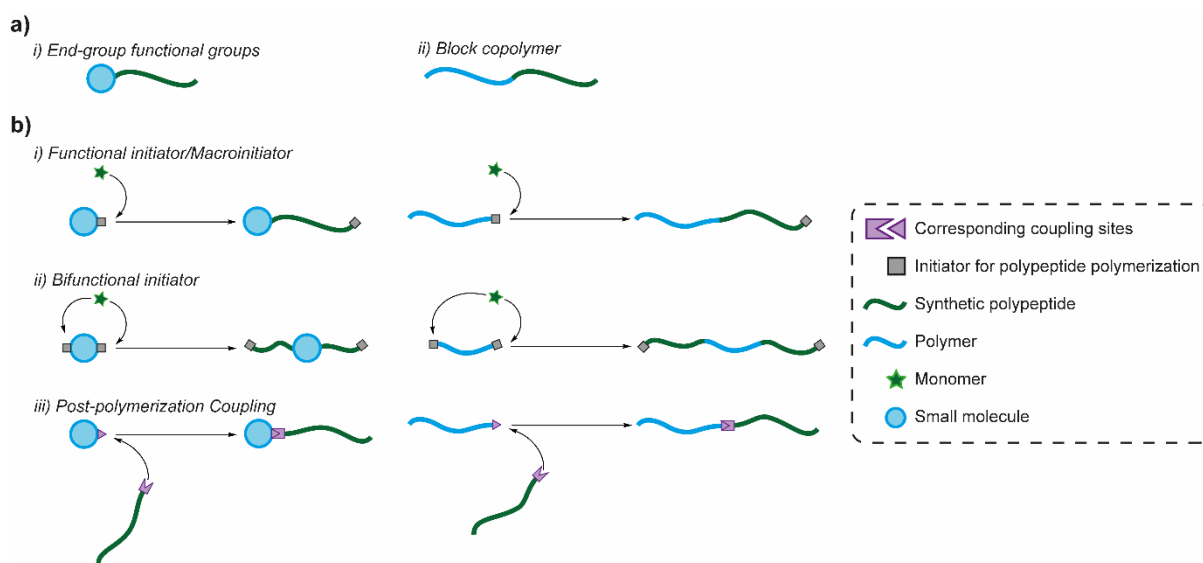


Figure 7: a) Molecular structure of linear polymers of i) end group functionalized polypeptides and ii) block copolymers. b) Synthesis pathways to such molecules *via* i) a functional initiator/macroinitiator with an initiating end group, ii) a bifunctional initiator or iii) coupling of end groups from both blocks.

Through introduction of these different groups, packing structures can be controlled and manipulated as desired. By relying on the intermolecular interactions and subsequent self-assembly of non-peptidic components, polypeptides can be designed with altered functionality and secondary structure. The simplest methodology is through the use of a functional initiator, which may have its own unique packing structure (Figure 7bi). The Li group has studied this impact on the packing of PLGlu-based polymers with oligo(ethylene glycol) (PLGEG) chains stemming from the residues by utilizing alkyl-based initiators with varying lengths.<sup>68,69</sup> By increasing alkyl-chain length, hydrophobic interaction can be increased thus forcing packing and alignment of PLGEG into nanoribbons. This altered packing with increasing alkyl-chain length was reflected in  $\alpha$ -helical and  $\beta$ -sheet content changing from 66% to 7% and 4 to 39%, respectively.<sup>69</sup> This structural increase in  $\beta$ -sheets associated with increased alkyl chain length is maintained if the alkyl chain is coupled post-polymerization in other systems as well.<sup>70</sup> This component can also be located within the polypeptide itself by utilizing a molecule with two initiating sites – dubbed a bifunctional initiator – resulting in a ABA triblock copolymer (Figure

7bii).<sup>71,72</sup> For example, Numata and coworkers utilized a bifunctional with L-leucine ethyl esters as the initiating sites, which could be identified by the enzyme papain for chemoenzymatic polymerization, resulting in PLAla and PGly.<sup>73</sup> Subsequent PLAla polypeptides were found to have reduced crystallinity compared to those synthesized using a monofunctional L-leucine ethyl ester (from 63.6% to 47.9%). The reduced crystallinity can be attributed to the bulky L-leucine units located within the polypeptide disrupting the usual packing. Notably, such packing structures can be manipulated to introduce environmental sensitivity absent from the usual polymer, such as performed by Jeong *et al.*<sup>74</sup> A modified azobenzene was utilized as a bifunctional initiator to yield poly(ethylene glycol) (PEG)-PLAla-PEG polymers with the azobenzene group located within the PLAla block. As azobenzene groups undergo “trans” to “cis” from upon irradiation from visual to UV light. Due to the molecular kink caused by this transition, the resulting micelles were found to decrease from 147 to 82 nm due to the tighter packing structure, and also resulted in decreased  $\beta$ -sheet content. It should be noted that, while the PLAla block was polymerized from the modified azobenzene bifunctional initiator, PEG was coupled afterwards. This technique to yield block (or multiblock) copolymers, however, is an anomaly.

A macroinitiator is the most common methodology of yielding multiblock copolymers with a polypeptide block which can similarly affect packing structure.<sup>75-77</sup> From a synthetic standpoint, very little distinguishes the use of polymers as initiators from small molecules unless the block in question is also synthesized, for which three main strategies exist to accommodate both sets of polymerization; direct polymerization of the second block, post-polymerization coupling and utilization of bifunctional initiators. Direct polymerization of a second block is not a common strategy as it requires the two polymerization techniques to have some congruency such as ROP of poly(caprolactone) (PCL) or poly(trimethylene carbonate) yielding a terminal hydroxyl for NCA ROP.<sup>78</sup> Post-polymerization coupling to yield the desired functional group is much more common, as initiating groups for other polymerization methods are commonly susceptible to coupling reactions themselves allowing the post-polymerization coupling of molecules in general to be generally straightforward (Figure 7biii).<sup>79,80</sup> Xu *et al.* performed ROP to yield PEG-poly(lactic-co-glycolic acid), but instead of utilizing the hydroxyl functional group for polymerization, utilized Steglich esterification with a carboxylic acid group.<sup>81</sup> A common issue for introducing a second molecule with an initiating site for NCA ROP in particular is that the most common initiating group – primary amines – is highly reactive and often susceptible to these coupling techniques. Thus, in this case, a Boc protecting

group was required, which was deprotected after coupling. This issue is also present when utilizing asymmetric bifunctional initiators. RAFT agents, for example, are susceptible to aminolysis,<sup>82-84</sup> thus a primary amine for NCA ROP cannot be present for synthesis. Similarly, a protecting group can be utilized to prevent this amino group from reacting before NCA ROP can be triggered.<sup>85</sup> Notably, with the latter two strategies this may potentially leave a molecules located between the two groups, which may result in undesired intermolecular interactions.

To this point, linear architectures have been the focus of discussion, though branched polymers offer their own properties and packing.<sup>86</sup> Branched polymers are generally more compact due to the restricted mobility of their branched chains, leading to unique rheological properties. While the definition of branched polymers makes this a very broad class of polymer, subclasses with unique, well-defined architectures have been identified of which two have commonly been utilized for the design of polypeptide-based structures - graft polymers and star polymers.

### 1.3.3 Graft Polypeptides

In general, graft polymers consist of a linear polymeric backbone and polymers stemming from this backbone and are synthesized using one of three different strategies: grafting-to, grafting-from and grafting-through (Figure 8).<sup>87</sup> Grafting-to approaches involve the coupling of the branching polymers to functional side-chains of the linear backbone (Figure 8a). This strategy is ideal for utilizing the polypeptide as a graft polymer backbone as exemplified by He *et al.* through the grafting of poly(*N*-isopropylacrylamide) to a PLGlu backbone.<sup>88</sup> Grafting-from approaches involve polymerizing the branching polymer directly from the backbone (Figure 8b). From a synthetic standpoint, Cheng and coworkers interestingly demonstrated that secondary structure formation could be utilized to accelerate polymerization using grafting-from techniques with PBLG.<sup>89</sup> By performing grafting from a backbone with primary amines in DCM (due to its low dielectric constant), near-complete conversion (98%) was found within two hours, while conversion was found to be less than 40% after 24 h for the linear counterpart. They postulated that this was due to the assistance of neighboring  $\alpha$ -helix formation during polymerization. While the former approach yields brush polypeptides with well-defined polymer branches, they are limited by coupling efficiency due to steric hindrance. Conversely, the latter approach is not limited by steric hindrance though the branches may be ill-defined in terms of length and, if performed using random polymerization, distribution of monomers. Nottelet *et al.* demonstrates this difference upon synthesizing PCL-g-PLLys using both strategies, with those synthesized *via* the grafting from approach demonstrating a higher dispersity from this effect.<sup>90</sup> Grafting through aims to mitigate the issues in both cases by

utilizing a polymerizable end group on the branch polypeptides and polymerizing through these to yield the polymer backbone (Figure 8c). PLGEG blocks would be one example already presented above, where an  $\alpha$ -helical forming PLGlu acts as the polypeptide backbone and short chain oligo(ethylene glycol) chains are the branches.<sup>68,69</sup> The resulting packing of such graft polymers is a product of both backbone and branch intermolecular interactions.

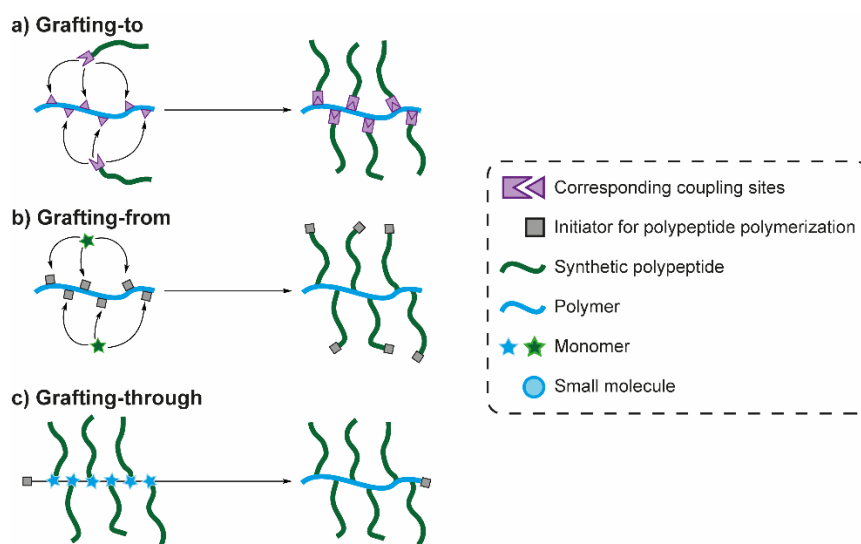


Figure 8: Synthesis of graft polypeptides *via* a) grafting-to with polypeptide branches, b) grafting-from using side chain initiating sites or c) grafting-through of polypeptides with polymerizable end groups.

Uniquely, this validates the use of polypeptides as the graft polymer backbone to yield unique structures. Generally,  $\alpha$ -helical forming polypeptides have been favored as the polypeptide backbone for grafting-to and grafting-from strategies, as their folding allows side chains to remain exposed for reaction.<sup>31,91,92</sup> The work performed by Engler *et al.* presented a grafting-to method of utilizing alkyne side chains of poly(propargyl-L-glutamate) to attach azide-terminated PEG, achieving close to 100% grafting efficiency.<sup>93</sup> An  $\alpha$ -helical structure was maintained within the backbone despite increasing the molecular weight of the PEG branches from 750 to 5000 g/mol. While a molecule like PEG does not inherently change the secondary structure content of the polypeptide backbone itself (at least under benign conditions), this is not universal as demonstrated by Bounduelle and coworkers upon the grafting of a DNA sequence to a PLGlu-based backbone and, thus, transitioning the backbone's favored conformation from  $\alpha$ -helix to  $\beta$ -sheets.<sup>94</sup> For grafting through methodologies, this is no longer an issue, thus,  $\beta$ -sheet forming polypeptides can be utilized in addition to the aforementioned  $\alpha$ -helix formers by developing a NCA-based macromonomer.<sup>95-97</sup> Crucially, the polypeptide backbone maintains its environmental sensitivity with the Li group demonstrating PEG-grafted



PLCys, which would undergo  $\beta$ -sheet to random coil transition upon oxidation of the thioester bond associated to the L-cysteine residues.<sup>98</sup>

In the converse case (*i.e.* utilizing the polypeptide as the grafting branch instead of the backbone), the polypeptide branches generally maintain similar secondary structure characteristics to their linear counterparts though this depends on the backbone environmental sensitivity.<sup>99</sup> Higuchi and coworkers demonstrated the importance of an environmentally sensitive backbone with a poly(allylamine) backbone, bearing pendant amines along with poly(methyl-L-glutamate) (PMLG) branches.<sup>100</sup> Generally PMLG favors  $\alpha$ -helical conformations, which was found to remain unchanged when the graft polypeptide was prepared. However, upon acidification, a conformation transition from  $\alpha$ -helices to  $\beta$ -sheet was observed. Furthermore, this transition could be reduced or muted completely upon introduction of sodium chloride (*i.e.* salt). This can be attributed to the ionic state of the pendant amines on the poly(allylamine) backbone which would be protonated under these circumstances resulting in electrostatic repulsion within the backbone and forcing fibril formation. A similar strategy to introduce environmental (specifically pH) sensitivity has been employed by the Jeong group through the utilization of chitosan as the graft polypeptide backbone with free pendant amines located on the saccharide monomeric units.<sup>101,102</sup>

## 1.4 Multidimensional Material Fabrication

At each dimensional level, while a variety of different fabrication techniques can lead to the same class of material, their structure and properties will be intrinsically different based on their fabrication method. Each fabrication technique has its own set of variables associated with it, though as structural control and morphology is an important consideration for all fabrication techniques, solvent system and concentration are universally important variables, defining the secondary structure, morphology and potentially even processibility of a polypeptide. A further detailed outlook on such fabrication methods is provided in Appendix A, Section 4-5.

### 1.4.1 Three Dimensional Materials – Gels

Polymeric networks crosslinked together, which are highly swellable in organic solvents or water, are called organogels and hydrogels, respectively. In general, these fall into two classes based on the method of crosslinking - chemically and physically crosslinked hydrogels (Figure 9a).<sup>103-105</sup>

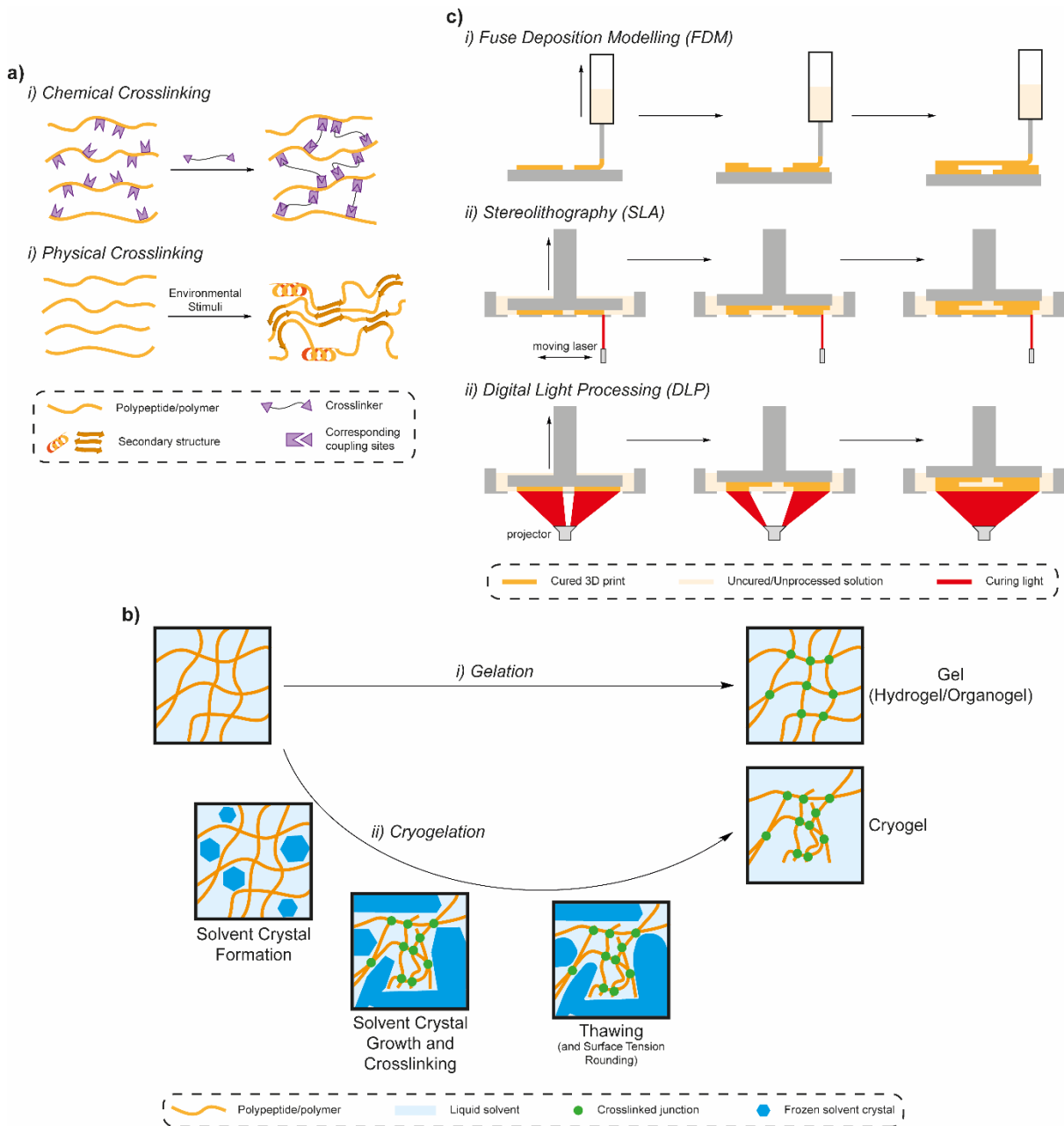


Figure 9: Different morphologies of 3D gel structures. a) Methods of crosslinking polypeptide gels through i) chemical crosslinking with multifunctional crosslinkers or ii) physical crosslinking (usually secondary structure formation) through environmental change such as heat, pH or light. b) Different morphologies available through fabrication conditions including i) regular gelation and ii) cryogelation, allowing the gel to crosslink at temperatures below solvent freezing point, resulting in solvent crystal formation, growth and then removal by thawing, yielding a microporous structure with a higher concentration of polymer in the cryogel walls. c) 3D printing gel structures. i) Fuse deposition modelling (FDM) involves layer-by-layer extrusion of the preformed gel. ii) Stereolithography (SLA) involves forming the gel using a pointed layer which cures each layer separately with a moving pointed laser, iii) Digital light processing (DLP) is similar to SLA, except a projection unit irradiates each layer all at once.

#### 1.4.1.1 Chemically Crosslinked Hydrogels

Chemically crosslinked gels are the result of polymer chains covalently bonded together (Figure 9ai).<sup>106,107</sup> As covalent bonds are cleaved under specific conditions, such gels are generally resistant to environmental degradation. Furthermore, bond cleavage is generally irreversible. The net result is a stable network that may be limited in application. Chemical crosslinking may occur either during polymerization or post-polymerization.

Polymer chains can be chemically crosslinked during polymerization by introducing a monomer with multiple polymerizable groups. When utilizing amino acid monomers, cystine naturally fulfills this criterion through its disulphide bond.<sup>108</sup> Deming and coworkers expanded on this, developing a series of sulphur-based di-amino acids, which were cyclized into di-NCAs and subsequent copolymerized with tert butyl-L-glutamate NCA to form gels.<sup>109</sup> Both increasing the length of these di-NCA crosslinkers, and removal of the disulphide bond (*i.e.* only introducing a single sulphur in the crosslinker between chiral carbons) yielded stiffer hydrogels (to be discussed in Section 1.5.1). Another option is to utilize polypeptides that have been modified with multiple polymerizable groups to act as the crosslinker and, thus, allow the polypeptide to function as a macrocrosslinker. The Rypáček group has previously utilized this strategy utilizing a poly(hydroxy ethyl-L-glutamate)-*r*-PLAAla-*r*-poly(methacrylamide-L-lysine) in this manner.<sup>110,111</sup> Treatment of lysine with methacrylic anhydride allowed for uncontrolled free radical polymerization utilizing an AIBN as an initiator along with 2-hydroxyl ethyl methacrylate as a spacing monomer.

The alternative is far more common where a polypeptide is crosslinked with molecules with multiple reactive groups for coupling or crosslinked with other functional groups on other polypeptide chains. The amine side chain on lysine residues make them a particularly popular choice for coupling of functional groups such as genipin,<sup>112</sup> *N*-hydroxysuccinimide,<sup>113</sup> and glutaraldehyde.<sup>114</sup> Jan and co-workers performed an exhaustive study on PLLys, PLLys-*b*-PLAAla and PLLys-*b*-PGly hydrogels crosslinked with genipin.<sup>115</sup> Overall length was found to drastically reduce gelation time due to the increased chance of chain-to-chain crosslinking occurring. However, all these methods tend to introduce non-native molecules, which may be unfavorable for certain applications, particularly as these molecules would be highly reactive with amines on molecules within mammalian organisms. Thus, forming covalent bonds directly between polypeptide chains without a linker molecule may be favored. The disulphide bonds from cysteine residues in proximity still remains a valid approach in this case as demonstrated by Murphy *et al.* utilizing 32 arm PLLys-*b*-PLCys.<sup>116</sup> As would be expected, the

location of the PLCys within the star affected the packing structure with a significant reduction in  $\beta$ -strands (the structures that constitute  $\beta$ -sheets) found upon relocating the PLCys block from the inner core to the outer arm. It was postulated that these  $\beta$ -strands were not formed from the usual PLCys blocks but rather from the restricted mobility of PLLys blocks in this conformation. Another bonding mechanism found naturally is through the formation of dityrosine bonds.<sup>117,118</sup> The phenolic side chains of two tyrosine residues can be conjugated *via* enzyme-catalyzed radical rearrangement. While horseradish peroxidase is usually used as a model enzyme, enzymes native to mammalian organisms have also been shown to catalyze this reaction. The result is a polypeptide which can form a chemically crosslinked hydrogel *in vivo* rather than solely *in situ*. Lu and coworkers demonstrated this phenolic crosslinking with their poly(L-phosphotyrosine)(PLPTyr)-*b*-PEG-*b*-PLPTyr hydrogels.<sup>119</sup> Uniquely, this provides an interesting basis compared to physical hydrogels, as physical hydrogels before treatment with horseradish peroxidase ended up crosslinking the phenol-based side chains. This technique, however, does not assure chemical crosslinking as the Li group managed to demonstrate a switch from hydrogel to nanogel upon triggering dityrosine coupling.<sup>120</sup>

The impact of chemical crosslinking on morphology and secondary structure varies system to system. By covalently bonding polypeptide chains, their mobility within the system is intrinsically restricted compared to in solution and thus greatly alters their packing. However, the exhaustive study on genipin crosslinked PLLys, PLLys-*b*-PLAla and PLLys-*b*-PGly mentioned previously found primarily expected secondary structures.<sup>115</sup> Generally, PLLys hydrogels were found to primarily form random coil conformations, as would be expected, while introduction of the PLAla block resulted in significant  $\alpha$ -helical structures.

#### 1.4.1.2 Physically Crosslinked Hydrogels

Physically crosslinked gels, in contrast, rely on intermolecular forces such as van der Waals forces, physical entanglements or, in the case of protein and polypeptide-based gels, secondary structure formation to link polymer chains together (Figure 9a<sub>ii</sub>). As explained in Section 1.3.1, secondary structure is environmentally sensitive, which consequently results in gelation characteristics which are stimuli sensitive and often reversible.<sup>121,122</sup> Polypeptides often need to be at a high enough concentration trigger a change from a solution to a gel structure (noted as a sol-gel transition). This concentration is the critical gelation concentration (CGC) and can provide a rough guide to the stability of a gel system (a lower CGC indicates a more stable gel).

Depending on the system, thermal increase can either cause a sol-gel or gel-sol transition, with this transition ideally occurring between 10 - 40 °C for biological applications. Sol-gel transition upon cooling can be observed in numerous PBLG organogels (specifically in solvents favouring  $\alpha$ -helical conformations such as toluene) due to a coil to helix transition.<sup>123,124</sup> Kuo *et al.* demonstrated this coil-to-helix transition upon cooling with their poly(2-ethyl-2-oxazoline)-*b*-PBLG in toluene. Upon cooling to 46 °C, nanoribbons formed due to the natural alignment of helices perpendicular to the ribbon axis, resulting in a fibrillar hydrogel structure. For a heating triggered sol-gel transition, multiblock hybrids with PEG and poloxamer are popular owing to the dehydration effect that PEG undergoes upon heating combined with an increase in rigid secondary structure (often  $\beta$ -sheets). The Jeong group showed particularly extensive work with poly(alanine) with combinations of both L and D isomers in this area.<sup>70,125,126</sup> Wooley and coworkers have shown this thermal sensitivity with their PDLAG-*b*-PEG-*b*-PDLAG hydrogels, which would reorganize into  $\beta$ -sheet-based nanoribbons upon heating.<sup>47</sup>

pH sensitivity in polypeptide-based hydrogels is generally induced through the use of ionic components. All ionic components have a hydrophilic charged state and a more hydrophobic uncharged state. Protonation upon acidification results in cationic functional groups, such as amines becoming charged, and anionic functional groups, such as carboxylic acids, losing their charge, while the reverse occurs upon deprotonation due to basification. By transitioning components to their uncharged, hydrophobic state, this can induce packing in water *via* hydrophobic association.<sup>127</sup> In the case of charged residues such as lysine and glutamic acid, this induces a coil-to- $\beta$ -sheet or coil-to- $\alpha$ -helix transition and, thus, induces hydrogelation.<sup>71,128,129</sup> The introduction of ionic components outside the polypeptide block also similarly affects the packing of the polypeptide chains as shown by Jeong and coworkers through the use of chitosan-*g*-(PLAAla-*b*-PEG) based graft copolymers where the chitosan backbone has pendant amine groups. This results in pH sensitivity as the PLAAla chains are forced closer together with decreasing pH to 3.0 as the chitosan backbone is protonated.<sup>101,102</sup>

Gelation can be triggered instead by combining polypeptide solutions to trigger physical crosslinking. Designing solutions to incur polyionic complexation (PIC) is straightforward as it is triggered by the combination of a polycationic block (*e.g.* PLLys) and a polyanionic block (*e.g.* PLGlu), making design centered around manipulation of electrostatic forces rather than secondary structure formation. The Deming group has developed and characterized a large library of PLLys and PLGlu block based polyionic complexing hydrogels.<sup>109,130,131</sup> The

application of PIC is not restricted to gel formation but can be used to improve gel stability, as demonstrated by Wan *et al.*<sup>132</sup> By introducing sodium alginate as a polyanion to a preformed nanofibrous hydrogel of PHLG-*b*-PLLys, mechanical stability was improved (further explained in Section 1.5.1).

While secondary structure is the primary requirement for physical crosslinking, it is not the only factor to consider. Star polypeptide-based hydrogels accentuate this point well, as despite secondary structure not being affected by the number of arms, CGC is still significantly lower.<sup>133</sup> Phan *et al.*<sup>134</sup> developed a series of stars with diblock copolypeptide arms and PLLys blocks located closest to the core. They could compare the CGC of stars with different residues as the second block (PVal, PLLeu and PLPhe blocks). In all, secondary structures were found to have minor changes, yet there was a drastic decrease in CGC upon increasing the number of arms from three to six, which can be associated to the higher branching and subsequent increase in crosslinking density.

#### 1.4.1.3 Cryogels

Further manipulation of gel structures can be performed by introducing an interconnected network of macropores into a hydrogel through cryogelation (Figure 9b). Cryogelation relies on developing an interconnected polymer-free network, which can be removed and leave a macroporous network structure.<sup>135,136</sup> By crosslinking at temperatures below the solvent freezing point, solvent crystals form and grow until they come into contact with other crystals, leading to an interconnected network, which is then removed by thawing. Shirbin *et al.* has previously studied a series of polypeptide cryogels, utilizing PLLys-*b*-PDLVal and PLLys-*r*-PLGlu in separate studies.<sup>137,138</sup> With increased crosslinking density, both increased wall thickness and pore size were obtained (as a point of reference, pore sizes and wall thicknesses were found within the range of 100-200  $\mu\text{m}$  and 1-10  $\mu\text{m}$  respectively).

#### 1.4.1.4 3D Printing Gels

Within the past decade, 3D polymer printing technology has undergone extensive advancements, with multiple different techniques emerging (Figure 9c). Majority of techniques follow the same general principle; a 3D model is divided into a series of 2D layers which are then fabricated layer-by-layer with the fabrication methodology being technique dependent. As it pertains to crosslinked polymeric networks, fuse deposition modelling (FDM), stereolithography (SLA) and digital light processing (DLP) are all possible avenues for producing 3D printed models.

FDM is the most common methodology, which involves extruding the polymeric network to fabricate each layer with crosslinks maintaining layer-to-layer strength (Figure 9ci).<sup>139</sup> The majority of cases related to gelation systems utilize a shear-thinning hydrogel network.<sup>140</sup> Murphy *et al.* in particular have looked at two 3D printed systems using polypeptides stars.<sup>32,141</sup> In the second of these works, Murphy *et al.* utilized PNLC-*r*-PLGlu-*b*-PLIle hydrogels, employing a combination of physical and chemical crosslinking.<sup>141</sup> Interestingly, this was compared to PNLC-*r*-PLGlu-*b*-PDLIle hydrogels, which lacked the physical interactions necessary to form a stable secondary structure and, thus, a stable 3D print due to the racemic nature of the PDLIle block. The hydrogels could be easily printed due to the physical crosslinking yielded by the PDLIle block and the hydrophobic nature of the *o*-nitrobenzyl-L-cysteine residues. Expanding on this, the polypeptide was also extruded with an alkyne-terminated 4-arm PEG to eventually use as a chemical crosslinker. To utilize this, the photosensitive *o*-nitrobenzyl protecting groups were cleaved from the cysteine residues upon irradiation with UV light, exposing side chain thiol groups, which were subsequently used for thiol-yne click to the alkyne groups of the 4-arm PEG. While this did stabilize the structure, the nanofibrillar nature of the print was lost. In other circumstances, this network is formed upon deposition through some environmental change (*e.g.* light or heat). Li *et al.* took a unique approach, utilizing a two solution system and PLGlu as a backbone instead of as the crosslinking component.<sup>142</sup> DNA strands were conjugated to the PLGlu backbone with the corresponding sticky end extruded in the same location through a separate syringe. As the gelation occurred within seconds of extrusion, stable layers could be formed. Thus, FDM represents one straightforward methodology for yielding 3D printed structures.

SLA and DLP both involve irradiating a prepolymer solution to photocure each layer, though the method in which the layer is irradiated differentiates the two techniques.<sup>143,144</sup> SLA involves using a single point laser, which moves around to cure each layer point-by-point (Figure 9cii). In contrast, DLP irradiates the entire layer at once to cure the polymer (Figure 9ciii). To use either of these techniques, either a photopolymerization or a photocrosslinker must be utilized. Unfortunately, despite the advancements in photochemistry as they relate to synthetic polypeptides, no reports exist to date utilizing polypeptides in SLA or DLP printing.

#### 1.4.2 Two Dimensional Materials – Films and Modified Surfaces

Films have also been developed using synthetic polypeptides (Figure 10). A universal variable to be aware of is the substrate that the film is being developed on, as its surface characteristics will also interact with the film's microstructures at the bottom surface.<sup>145</sup>

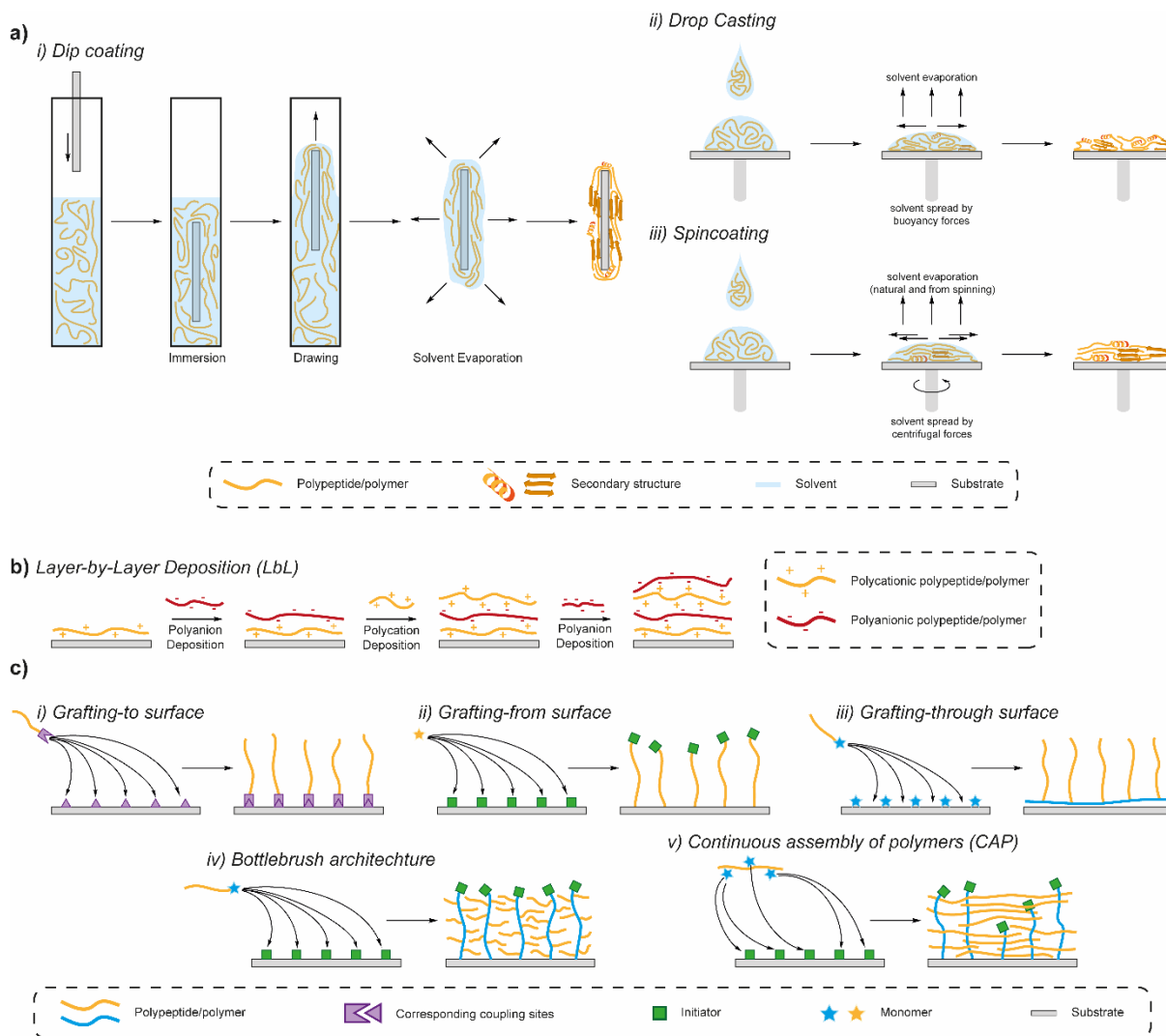


Figure 10: Different methods of forming polypeptide films or modified surfaces. a) Common deposition methods for forming films. i) Dip coating involves immersing a substrate entirely into a polymer solution the deposited polymer remaining on the substrate upon withdrawal. ii) Drop casting instead applies the polymer solution on the substrate surface and allows the solvent to evaporate, leaving behind the desired film. iii) Spin coating is similar to drop casting except after the polymer solution is on the surface, the substrate is spun which both causes spreading of the polymer solution and evaporation of solvent. b) Fabrication of layer-by-layer films through the sequential deposition of polyions. Each layer has an opposing charge to the previous layer. c) Polymerization methods for modifying surfaces *via* i) grafting polymers to the surface with a functional terminal end group, ii) grafting polymers from the surfaces by using initiating sites on the substrate surface to cause polymerization upon monomer deposition, iii) grafting through end-functionalized polymers, which polymerize at the substrate surface, iv) bottlebrush polymer formation by utilizing initiating sites on the substrate surface to graft through end-functionalized polymers, or v) chemically crosslinked films manufactured through continuous assembly polymerization (CAP), which utilizes initiating sites on the substrate surface to graft through side chain-functionalized polymers.

### 1.4.2.1 Polymer Deposition

Majority of polymer deposition methods rely on depositing the polymer onto a substrate and then allowing the development of crosslinks similar to hydrogels as the solvent evaporates (Figure 10a).<sup>146</sup> Briefly, dip coating involves dipping a substrate into polymer solution, removal of substrate from the solution (where the actual amount of polymer deposited can be controlled by controlling the rate of removal), and solvent is then allowed to evaporate (Figure 10ai).<sup>147</sup> Drop casting entails the deposition of polymer onto the substrate followed by spreading of the



solution by diffusion and subsequent evaporation of solvent (Figure 10aai).<sup>148</sup> Spin coating is very similar to drop casting, but the spreading of solution over the substrate is instead primarily controlled by centrifugal forces through the mechanical spinning of the substrate, which also assists in rapidly increasing solvent evaporation (Figure 10aaiii).<sup>147</sup> It should be noted that mass deposition, while related, is not directly correlated to film thickness.

Numerous studies have investigated the structure after using these three techniques.<sup>149</sup> Wasilewski *et al.* has performed a comprehensive study comparing these three techniques with a model cationic peptide onto gold substrates (*i.e.* QCM chips).<sup>150</sup> Dip coating and drop casting both yielded a high degree of aggregation on the substrate, especially when compared to the spin coated counterparts which were more homogeneous. However, spin coating also yielded the thinnest films despite having the highest mass deposition, while dip coating yielded the lowest mass deposition but highest film thickness. Borkner *et al.* has further investigated the secondary structures at different points within films of varying thickness (by multilayering) based on silk-mimicking proteins.<sup>151</sup> During deposition *via* spin coating, films were found to adopt a fractionally unstable metastable state. Thus, upon increasing thickness through multiple depositions, inter- and intra-molecular bonds were more likely in the axis perpendicular to the substrate plane and, thus, leading to an increase in  $\beta$ -sheet structure throughout the films. However, upon treatment with methanol vapor,  $\beta$ -sheet content was found to increase to approximately the same amount in both thin and thicker films, except at the surface where thicker films were found to have a drastically increased  $\beta$ -sheet content comparatively. It was surmised that this was due to the hydrophobicity of the  $\beta$ -sheet content formed at the film surface reducing diffusion of the methanol into the film. While this knowledge dictates useful knowledge about the relationship between thickness and secondary structure, films derived from synthetic polypeptides have primarily focused on the use of the drop casting method to yield films with a defined 2D structure depending on function and desired characterization.<sup>152,153</sup>

Further crosslinking by introducing a crosslinking agent during deposition may further affect film properties similar to crosslinking in gels. Theoretically, by extending a polymer such that it still remains linear should increase the number of physical interactions per molecule upon evaporation, though resulting in a more stable film. The Korley group has produced a large body of work utilizing this concept with ABA triblock copolymers, which are chemically coupled upon deposition *via* both terminal amines.<sup>154-158</sup> In all cases, the middle block acted as a difunctional macroinitiator (either PEG or PDMS) for NCA ROP of a modified benzyl side

chain polypeptide (PZLL, PBLA or PBLG) specifically chosen due to their DP dependent secondary structure, while the crosslinker was a multifunctional isocyanate. The work performed by Matolyak *et al.*, using PBLA-PDMS-PBLA in DMSO and specifically compared the impact of this crosslinking using di- and trifunctional crosslinkers. Conventionally, antiparallel  $\beta$ -sheet structures would be favored using the difunctional crosslinker due to their higher stability. Using the triisocyanate linker reduced this chain mobility, thus forcing parallel  $\beta$ -sheet formation instead while reducing fibril formation. This, in turn, did lead to less favorable mechanical properties, though did improve hysteresis. Thus, the introduction of multifunction crosslinkers does need to be performed with thoughtful design in mind to ensure that films retain specific desired properties.

Drop casting in particular allows for patterning through the use of a mold, but recent advances have allowed other more reproducible and precise methods. Instead of conventional drop casting methods, Wooley and coworkers employed precise spatial control of crosslinking using heat and light from a focused laser to crosslink and, thereby, design a patterned gel.<sup>159</sup> PEG-PADLG, while in a suspension of single-walled carbon nanotubes, was crosslinked into complex 2D patterns using this method, forming an organogel with THF as the solvent, which was left behind after removal of the rest of the uncured solution. The subsequent crosslinked network was evaporated as with other polymer deposition methods leaving behind a stable, patterned film. Notably, as these films are still physically crosslinked, the films could be redissolved after sonication and, moreover, crosslinked again using the same method to yield films. Thus, controlling crosslinking with spatial control can allow for patterning.

Layer-by-layer (LbL) deposition is a unique strategy for developing multilayered films (Figure 10b). While usual methods for developing multilayered films rely on the same intermolecular bonds acting within a single layer, LbL specifically refers to the sequential alternating deposition of polymers with opposite charges and thus relying on electrostatic forces for layer-to-layer bonding resulting in films either purely derived of polypeptide<sup>160,161</sup> or composites including non-peptidic layers<sup>161-163</sup>. Boulmedais *et al.* investigated a wide range of different polypeptide polyanions (PLGlu, PLAsp) and polycations (PLLys, PDLys, poly(L-orthinine) (PLOrt)) multilayered in aqueous solution.<sup>161</sup> Interestingly, film thickness was found to increase when the polyion in solution is not fully charged, as it will form loops due to interaction with the opposite charged surface. As would be expected, reducing the side chain's size appear to also reduce film thickness (PLLys/PLGlu compared to PLOrt/PLGlu and PLLys/PLAsp). This film thickness was reduced even further upon use of PDLys. Interestingly

all of this occurs despite all having similar secondary structure content. While this may seem strange, it does give some small amount of independence between the two variables (thickness and secondary structure content).

#### 1.4.2.2 Polymer Surface Grafting

The techniques applicable to graft polymers can further be applied to surface modification by treating the surface in a similar fashion to a polymer backbone (Figure 10c).<sup>164</sup> Majority of surfaces require functionalization using one of the aforementioned techniques with a trimethoxy-/triethoxysilyl functional molecule, dopamine or PEI for coupling or polymerization to thus employ either grafting-to or grafting-from (otherwise known as surface-initiated polymerization) techniques (Figure 10ci, ii).<sup>165,166</sup> Often this is performed by immersion in a reactant solution. However, Weiringa *et al.* attempted to apply spin coating melted methyl-L-glutamate NCA to form poly(methyl-L-glutamate) (PMLG) onto an amino-functionalized surface for the grafting-from approach, achieving 20 nm thick films.<sup>167</sup> One notable exception is gold, which can be reacted with thiol functional groups to produce a grafting-to surface. The result is a surface with polymer brushes stemming perpendicular to the surface plane (if completely rigid) with unique surface morphologies. While this gives broad direction for the design of grafting-to and grafting-from surfaces, grafting-through surfaces operate on slightly different parameters.

Grafting-through approaches are scarce as the substrate must accommodate the polymerization of the macromonomer end groups parallel to the surface plane itself (Figure 10ciii). One method is to immobilize the same monomeric group on the surface, as the macromonomer yielding a grafting-through film.<sup>168</sup> Another is to employ a polymerization technique, which specifically results in polymer deposition with electrochemical polymerization being a prime candidate. Electrochemical polymerization is triggered after running a current through an electrode, where the resultant polymer is deposited at the electrode surface. Yagci and coworkers have developed numerous works utilizing thiophene terminated polypeptides (synthesized *via* NCA ROP with a thiophene functionalized initiator), which are then susceptible to electrochemical polymerization.<sup>169,170</sup> Interesting, in one work utilizing PLAla polypeptides, PLAla was found to adopt  $\beta$ -sheet conformations despite their usual preference towards  $\alpha$ -helical tendency at the DP used.<sup>171</sup> In another work, they have also shown successful copolymerization with a non-peptide comonomer, implying a degree of potential control of thickness and roughness utilizing this method.<sup>172</sup>

Importantly, the approach taken can intrinsically affect the structure and thickness of the film. In all cases, film thickness can be controlled with the concentration of the reactant solution as the interactions are largely diffusion-based. However, in congruence with graft polymers, grafting-to approaches tend to yield thinner films, which are more homogeneous compared to their grafting-from counterpart. Weiringa *et al.* further investigated the grafting from of PBLG and PMLG from an amino-functionalized surface in DMF solution.<sup>173</sup> While both PBLG and PMLG tend to adopt only (or at least a high majority of)  $\alpha$ -helical structures in solution,<sup>174,175</sup> PMLG surfaces were found to have significant  $\beta$ -sheet content before washing. While PMLG has demonstrated a degree of propensity towards  $\beta$ -sheet formation, the surface confinement of the polypeptides does appear to have an effect on the secondary structures.

As would be expected with polymerization-based fabrication, molecular architecture can be manipulated with bottlebrush structures being a popular candidate (Figure 10civ).<sup>176,177</sup> The general approach is to prepare a surface for radical polymerization to enable the use of a surface grafting-from approach to graft-through methacrylate-ended polypeptides. The Ma group developed a system using a methacrylate terminated polypeptide (PLPhe-*r*-PLLys) and polypeptoid (poly(sarcosine)), both developed from NCA ROP initiated by a methacrylate ended amine initiator.<sup>178</sup> The methacrylate groups could be grafted from the polydopamine coating, which acts as a radical photoinitiator. Secondary structure appeared to be maintained, as measurements showed random coil structures as would be expected from the PLPhe-*r*-PLLys polypeptide. Surface roughness was high at 44.1 nm, though with an average thickness of 310 nm after 1 h of irradiation. Furthermore, as the polymerization is UV light based, photopatterning could be performed with a dot pattern of  $\sim 8$   $\mu\text{m}$  showing a degree of control (though fidelity was low).

Our group has developed a technique for developing a robust, chemically crosslinked surface modification dubbed for continuous assembly of polymers (CAP) (Figure 10cv). Similar to bottlebrush constructions, the substrate surface is prepared for grafting-from approaches for grafting-through polymers, but polymers are side-chain multi-functionalized instead of terminal mono-functionalized leading to chemical crosslinking similar to hydrogels. Thickness and surface morphology are both highly dependent on the type of polymerization that is utilized as well as the macromonomer used. To this point, this technique has not been used to develop protein or polypeptide-based films.

### 1.4.3 One Dimensional Materials – Fibers

Fibers are by far the least well-studied material in relation to synthetic polypeptide materials despite being extensively studied in relation to recombinant and natural proteins and materials (Figure 11). As intermolecular interactions are especially important in the transverse plane, a high number of such interactions is required per polymer chain. Thus, extremely high molecular weight polymers are favored over dispersity. In all cases, variables such as extrusion speed and nozzle diameter are important in determining morphology and diameter respectively.

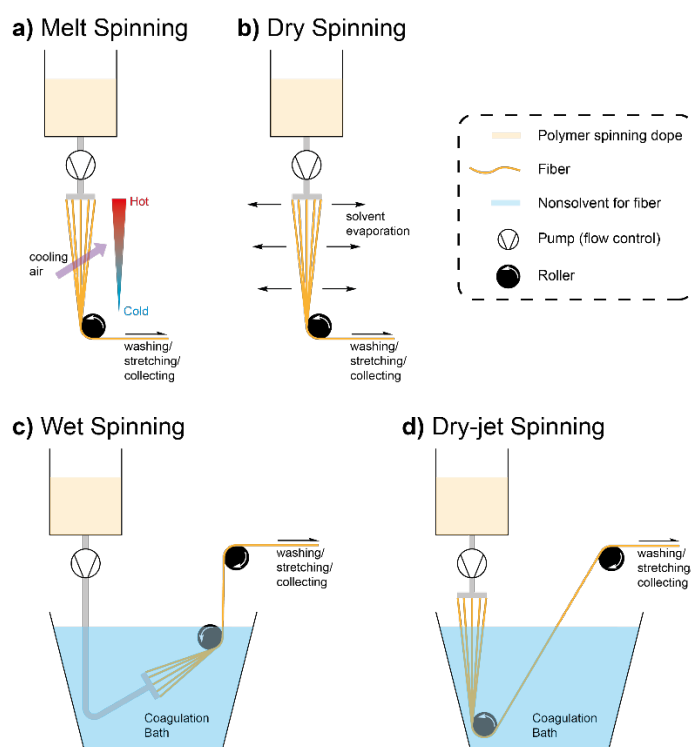


Figure 11: Fabrication of microfibers through a) Melt spinning, where a molten polymer is drawn through a nozzle and cooled below melting temperature while drawing, b) Dry spinning, where a polymer solution is drawn through a nozzle, while solvent is evaporated from the resulting fiber, c) Wet spinning, where a polymer solution is extruded into a nonsolvent coagulation bath and drawn through or d) Dry-jet spinning, which is similar to wet spinning except a small air gap is present before the polymer solution enters the coagulation bath.

Polymeric microfibers are fabricated through the extrusion and drawing of an ejected polymer either in viscous solution or in its liquid state called a spinning dope (Figure 11). Different methods are defined by the different method of drawing out this fiber. Melt spinning is the only technique, where the spinning dope consists of a polymer in its (often heated) melted liquid form with extrusion through a nozzle, drawing through a gaseous environment and subsequent cooling resulting in formation of the fiber (Figure 11a). Dry spinning starts with a solution spinning dope, but in terms of processing is similar, where solvent evaporation instead of cooling occurs while drawing (Figure 11b). Wet spinning instead involves extruding and drawing into a solvent solution (called a coagulation bath), which acts as a nonsolvent to the

polymer (Figure 11c). Dry-jet spinning is similar except that extrusion from the nozzle occurs within an air gap before reaching the coagulation bath (Figure 11d). This provides a wide variety of techniques to potentially process polymers into the desired fiber. Furthermore, fibers in all cases can be strengthened, while made more brittle by stretching the fiber between two collecting rollers at different speeds after drawing (a process called post-stretching). Despite this, very few examples of synthetic polypeptide-based fibers exist.

While secondary structure in the case of dry spinning is primarily dictated by the spinning dope characteristics alone, the introduction of the coagulation bath into the wet spinning and dry-jet spinning systems further complicates this as the nonsolvent also factors into morphology. Sogah and coworkers wet spun from multiblock polymers synthesized by the end-to-end coupling of PLAla-*b*-PEG-*b*-PLAla triblocks. Hexafluoroisopropanol (HFIP) was utilized as a solvent as it helps to solubilize many proteins and forces  $\alpha$ -helicity in many usual  $\beta$ -sheet forming chains including short chain PLAla such as used in this case. However, after extrusion into a 1:1 methanol:acetone coagulation bath, aligned  $\beta$ -sheets were found.

## 1.5 Material Properties

Subsequent material properties are the net result of both the starting polymer and the fabrication technique. Of these, some are universally important while others pertain more to the specific application of the material. To narrow scope, these properties will largely be spoken of in the context of potential biologically relevant applications.

### 1.5.1 Mechanical Properties

For the development of mechanically superior materials, natural structural proteins such as collagen and spider silk form the basis of bioinspired tough materials from polypeptide precursors. Such mechanical properties can come in the form of increased strength (mechanical stress at yield point), strain at break, toughness (capacity to store energy before yield) or Young's modulus (force required to deform per unit of displacement) (Figure 12a). In the case of soft materials, their viscoelastic behavior based on how they flow can yield similarly useful information, where the storage and loss moduli directly refer to the amount of energy that a material can store, which represents the elastic component and the energy dissipation, which represents the viscous component, respectively. These components can often be a function of shear force with shear thickening materials referring to materials which have an increased storage modulus with increased shear rate and shear thinning being the converse. In terms of processability, shear thinning is important for extrusion of materials through a nozzle,

specifically for 3D printing. Storage modulus is also important for determining cell fate. For the integration of polypeptides into any material class, design paradigms from natural structural proteins such as spider and *Bombyx mori* (silkworm) silks, collagen and keratin can all be employed.

In terms of rupturing of the secondary structure itself,  $\beta$ -sheets require the simultaneous rupture of hydrogen bonds between  $\beta$ -strands, while  $\alpha$ -helices can undergo stepwise uncoiling (*i.e.* deformation) before yield (Figure 12b). Coiled-coil structures similar to those of collagen would share a similar stepwise uncoiling to  $\alpha$ -helices, but there would also be the progressive of uncoiling of the superstructure before uncoiling of the individual coils. Within larger structures, this can be implemented either as a continuous network of superstructures or within an amorphous matrix like silks. Both spider and *Bombyx mori* silks utilize  $\beta$ -sheet nanocrystals within an amorphous matrix made up of less ordered protein structures due to nanophase separation during spinning allowing them to operate as a natural nanocomposite. These examples can assist with the design of materials with specific mechanical properties, with similar impact over multiple different dimensional materials.

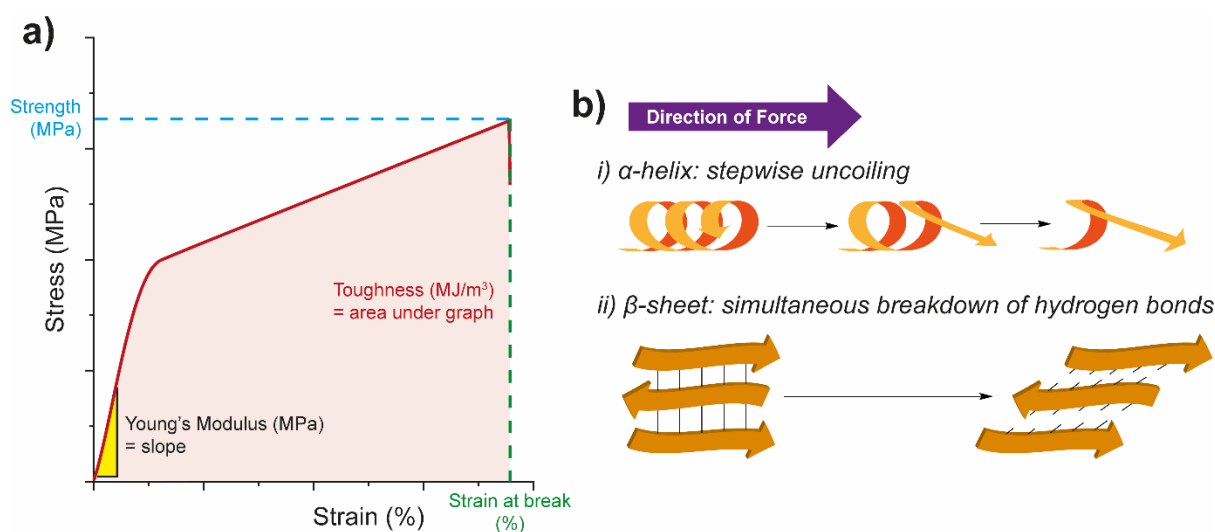


Figure 12: a) Sample stress-strain curve with correlated parameters for strength, strain at break, toughness and Young's modulus. b) Breakdown of individual secondary structures under load: i) the stepwise uncoiling of  $\alpha$ -helices and ii) the simultaneous rupturing of hydrogen bonds between  $\beta$ -strands in  $\beta$ -sheets.

Ultimately, ordered secondary structures tend to assist the increase in mechanical strength compared to random coil counterparts. Deming and coworkers demonstrated this, comparing block copolypeptides containing one long PLLys chain and a short hydrophobic block.<sup>179</sup> Using DP 40 blocks, PVal and PLLeu ( $\beta$ -sheet and  $\alpha$ -helix forming respectively) were found to have CGC around 0.25 wt%, while PDLLeu (random coil conformation) had a CGC around 1 wt%. Furthermore, PVal, PLLeu and PDLLeu blocks had maximum tested storage moduli of  $\sim 500$

Pa (1 wt%), ~2000 (2 wt%) and ~200 Pa (2 wt%) respectively. This mechanical enhancement is translated into chemically crosslinked structures containing secondary structures. Modified PLGlu (for  $\alpha$ -helix formation) and PDLGlu (for random coil formation) has been used as macrocrosslinkers by Chen *et al.* to illustrate this by covalently crosslinking the polypeptide into their hydrogel.<sup>180</sup> Comparatively, the poly(sodium acrylate)-based gels observed an increase in tensile strength from ~40 kPa to ~115 kPa when random coil structures were replaced by  $\alpha$ -helical structures (though this corresponded with an decrease in extension at break from ~1800 % to 1400 %). Thus, the presence of higher ordered secondary structures is a vital component for fabricating structures of superior mechanical qualities.

Even if the secondary structure remains the same, there is an inherent importance embedded into which amino acid residue are selected to construct such structures. In films developed by the Korley group utilizing ABA triblocks with a peptide-PDMS-peptide structure the use of PBLA and PZLL peptides with variations in length (5 DP and 20 DP) with consequentially different secondary structures illustrates this dependency on residue selection when comparing those developed with a 5 wt% peptide content.<sup>155</sup> Using 5 DP PBLA as the peptide sequence resulted in predominantly  $\beta$ -sheet formation with a tensile modulus, strength and strain-at-break of 14.5 MPa, 2.5 MPa and 669.5 %, respectively. Modifying this with a 20 DP PBLA peptide sequence (and the same peptide content controlled with homopolymeric PDMS) resulted in 13%  $\alpha$ -helical content and a drop in all of these qualities (9.26 MPa, 0.8 MPa and 217.2% for modulus, strength and strain-at-break respectively), despite there theoretically being more physical interactions per polymer chain with increased chain length. The converse was actually observed when utilizing PZLL, despite vaguely similar secondary structure-to-peptide length trends. Despite also having a majority of  $\beta$ -sheet structures at DP 5, PZLL-based films yielded mechanically inferior film to the ones developed from the 5 DP PBLA counterpart (modulus, strength and strain-at-break of 5.6 MPa, 1.6 MPa and 399.8 %, respectively). Increasing the  $\alpha$ -helical content to 25% (with a corresponding decrease in  $\beta$ -sheet) through increasing DP to 20 resulted in an increase in all qualities with 8.7 MPa, 5.2 MPa and 821.9 % for modulus, strength and strain-at-break, respectively. While secondary structure content was predicted to be partially responsible, ultimately factors such as the differing fibrillar conformations and quantity of hydrogen bonds also have a significant impact and cannot be ignored.

While there is little sequence control in polymerization techniques, the use of multiblocks can also lends a change in mechanical properties. Deming and coworkers also developed a series



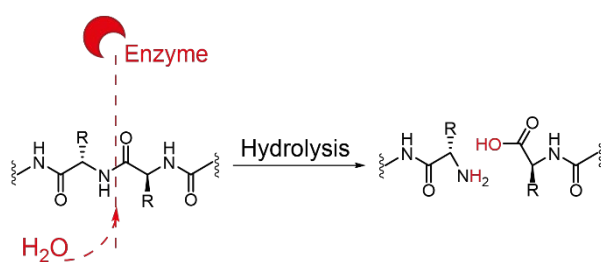
of multiblock copolypeptides within this study utilizing poly(L-methionine sulfoxide) (PLMS)-*r*-PLAla block with PLLys or PLGlu as PIC forming blocks (in this description, PLMS-*r*-PLAla will be block A and PLLys or PLGlu will be block B, noting that PIC gels use a combination of copolypeptides with both B blocks). Their results from hydrogels formed at 10 wt% illustrate the impact of multiblock-based polypeptide hydrogels as ABA hydrogels attained a storage modulus of ~250 Pa compared to the AB hydrogels with a storage modulus of ~50 Pa despite both having the same amount of each residue – in other words, this effect is not purely due to molecular weight, but the resulting assistance in formation of stiffer fibrillar assemblies.

### 1.5.2 Polypeptide Degradation

Over a material's lifespan, it is likely to undergo degradation due to the cleavage of covalent bonds. Naturally, this will affect the mechanical properties over time, which can shorten the usefulness of a material even further to the point of detriment. Furthermore, it is possible to release degradation products over this timeframe, which, if harmful, renders them useless for many biological applications. This does not mean that preventing degradation of materials is always desired, as soft tissue engineering scaffolds should be degraded for the cell's natural extracellular matrix. Furthermore, this degradation may be triggered by specific molecules for targeted drug delivery.

For polypeptides, this degradation is often due to enzyme-catalyzed hydrolysis of amide bonds on the polypeptide backbone (Figure 13a). A class of enzymes known as proteases generally identifies a specific peptide sequence to cleave and trigger hydrolysis at this site. While often this site specificity targets sequences more than three residues in length (such as matrix metalloproteinases) and, thereby, unlikely to reliably cleave the synthetic polypeptides listed above, broad spectrum proteases exist, which are less sequence specific and instead target a class of residues.

### a) Enzymatic Degradation



### b) Thiol-based Redox Chemistry

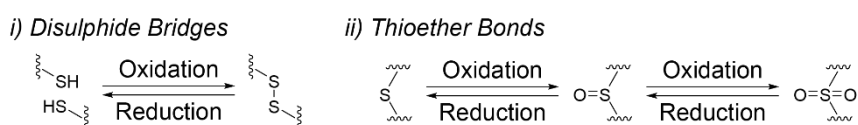


Figure 13: Different degradation mechanisms a) Enzyme catalysed degradation of polypeptides *via* hydrolysis of the polyamide backbone. b) Redox reactions as they pertain to thiol chemistry as it relates to i) disulphide bridges and ii) thioether bonds

Heise and co-worker illustrates this enzymatic selectivity in different works in a range of different polypeptides with a range of different enzymes.<sup>181-183</sup> In one of these works, PEG-poly(L-tyrosine) (PLTyr) hydrogels were treated with both chymotrypsin and trypsin.<sup>183</sup> As a result, treatment with chymotrypsin resulted in complete hydrogel degradation after 7 days due to their preferential identification of aromatic residues for cleavage.<sup>184</sup> On the other hand, trypsin preferentially cleaves upon identification of lysine or arginine and, thus, did not show any significant degradation over the same time period.<sup>185</sup>

Enzymatic degradation can be further tuned through the use of *D*-isomers as they have reduced enzymatic specificity compared to their *L*-isomer counterpart.<sup>186,187</sup> While an effective method of reducing enzymatic degradation, its tunability is somewhat questionable as shown by Chen and coworkers.<sup>188</sup> Using model glycopolypeptides (PLGlu with galactose coupled to the side chain), polypeptides with only the *L*-isomer were found to have reduced *D* and DP upon culturing with proteinase K over 72 h. As can be inferred, polypeptides with only the *D*-isomer exhibited no visible degradation. However, while the racemic polypeptides did appear to have some degradation, it was minor and not a theoretical “midpoint” of degradation between the two extremes, implying that the relationship between ratio of *D*-/*L*-isomers and rate of degradation is nonlinear. This was reflected *in vivo* in a later work from the same group in a series of poly(propargyl-glutamate) based hydrogels with increasing introduction of the *D*-isomer.<sup>189</sup> After injection into model rats, pure *L*-isomer hydrogels were cleared within 28 days. With just 25% of the *D*-isomer, hydrogels were still present in this time frame and cleared before 42 days. The time of clearance showed a general increase of time with increasing

inclusion of the D-isomer until polypeptides with pure D-isomers were still present after 56 days.

Natural sulphur-containing residues such as cysteine and methionine have led to the development of redox-sensitive materials, where degradation occurs on the side chains rather than the polyamide backbone (Figure 13b). In these cases, reduction *via* a peroxide or other reactive oxygen species that may result from natural enzyme cascades yields the breaking down of thiol-based bonds. The reduction of disulphide bonds can lead to the direct disruption of a chemical crosslink, while the oxidation of thioether bonds results in an intrinsic secondary structure change and, thus, the breakdown of physical crosslinks, which can lead to the degradation of materials. Liu *et al.* demonstrated the potential physical crosslink degradation using a heavily modified PLGlu-based polypeptide hydrogel with two branching thioether chains stemming from the end of each side chain.<sup>190</sup> The resulting hydrogel was found to degrade by ~20 % over 30 days naturally in phosphate buffered saline (pH 7.4), but significantly more in the presence of hydrogen peroxide with ~95 % of mass lost over the same time period. As physical crosslinks are not necessarily broken, but altered upon redox-stimuli, it is possible that while a loss of mass may not occur, nanostructure (pore structure in particular) will still be altered and, thus, change other notable physical properties.<sup>98</sup> Interestingly, reactive oxygen species may react with other molecules present within the material. Thus, such bonds can act sacrificially and not only be employed for degradation purposes, but protectively as well.<sup>191</sup>

### 1.5.3 Biologically relevant properties

While biocompatibility of polypeptides with mammalian cells for biological applications may be generally assumed, one notable issue is the introduction of the non-native D-isomers. While it may assist with manipulation of other properties, the inflammatory response revealed by histological staining is notable. Jeong and coworkers demonstrated this comparing PEG-*b*-(PLPhe-*r*-PLAla) and PEG-*b*-(PDPhe-*r*-PDAIa) hydrogels.<sup>192</sup> By changing stereoisomers, besides from a change in coiling of  $\alpha$ -helical structures, this leaves the subsequent implanted hydrogels as close to identical as possible. Hydrogels based on the D-isomers were found to have a stronger histological response with an increase in collagen capsule thickness compared to those with the L-isomer after 5 days of culture within model rats. This increased inflammatory response paired with their aforementioned resistance to enzymatic degradation can make them potentially unfavorable for specific applications. While Chen and coworkers observed similar trends when utilizing PEG-*b*-PLAla and PEG-*b*-PDAIa, they determined a

mixture of stereoisomers could mitigate this.<sup>193</sup> While similar immunoresponse was observed (including a drastic increase in inflammatory cytokines upon utilizing the D-isomer), an equal mixture of the two block copolymers resulted in mild inflammatory response based on histological staining though nowhere near the degree of pure D-isomer. Furthermore, two out of three of the observed inflammatory markers were found to be similar in quantity compared to the L-isomer. Thus, if so desired, the work does use a potential strategy for mitigating inflammatory response.

#### 1.5.3.1 Cell Support and proliferation

As a pseudo-biopolymer, polypeptides generally are biocompatible and can assist with aspects of cell proliferation and cell fate through natural assemblies. Matrigel has often been used as a control by Jeong and coworkers based on natural extracted proteins and shown comparably similar cell growth using variations of PEG-*b*-PLA<sub>1</sub> hydrogels. While maintaining a similar storage modulus, Matrigel and the polypeptide-based hydrogels were both found to show similar cell proliferation of fibroblasts after 21 days, while also showing a notable increase in collagen type I mRNA expression and comparable collagen type III mRNA expression.<sup>194</sup> This is owed to the fibrous nature of the hydrogels. Furthermore, it was found that despite secondary structure, increasing the length of the polypeptide component could assist with the expression of such differentiating markers for cell fate, while somewhat independent of secondary structure. In this specific system, this may partially be due to the reduction of impact of the PEG block with growing PLA<sub>1</sub> size, as PEG is known to have an adverse impact on cell adhesion.

## 1.6 Objectives

The core theme of this thesis is to develop unique fabrication methods for the integration of polypeptides synthesized *via* *N*-carboxyanhydride ring opening polymerization (NCA ROP) in materials at multiple dimensional scales. A major focus is the analysis and control of secondary structure in the resulting materials and investigating the subsequent relationship with properties with a range of different fabrication strategies and techniques utilized.

The first study focused on the development and tuning of the mechanical properties of three-dimensional hydrogels through different fabrication techniques. Specific focus is given to modifying both polypeptide length and sequence, characterizing the resultant secondary structure and correlating this to mechanical properties. Furthermore, the versatility of this technique is explored through use in multiple different morphologies.

The second study aims to develop a unique polymerization method for modifying surfaces with a chemically crosslinked network. The fabrication technique itself was optimized by adjusting polymerization variables. Kinetics, maximum film thickness, morphology and the impact of multiple reapplications of the film were used to characterize and evaluate the techniques.

The aim of the third study is to develop a platform to integrate polypeptides with specific secondary structure forming propensities which is applicable to a range of different fiber-forming polymers and subsequent properties. Elucidating the relationship between polymer and the resulting secondary structure and then correlating this to mechanical changes compared to the polymer fiber on its own are a key point within this. Additionally, its potential as a cell growth scaffold should be further defined.

## 1.7 Thesis Overview

This thesis covers two publications and two manuscript in preparation outlining the fabrication and characterization of materials implementing polypeptides synthesized using NCA ROP. The first manuscript specifically observes NCA ROP as a medium for developing bioinspired polymers and their applications in materials This has been used as the basis for Chapter 1 (manuscript, which is currently under second round revisions for the journal *Progress in Polymer Science*, can be found in Appendix A). The three following chapters investigate the fabrication of materials with different levels of dimensionality. The first of these studies the introduction of polypeptides into three-dimensional materials for mechanical enhancement. The second covers the development of chemically crosslinked surface modification technique using polypeptides. The third manuscript covers the expansion of the first study into a multitude of different fibers.

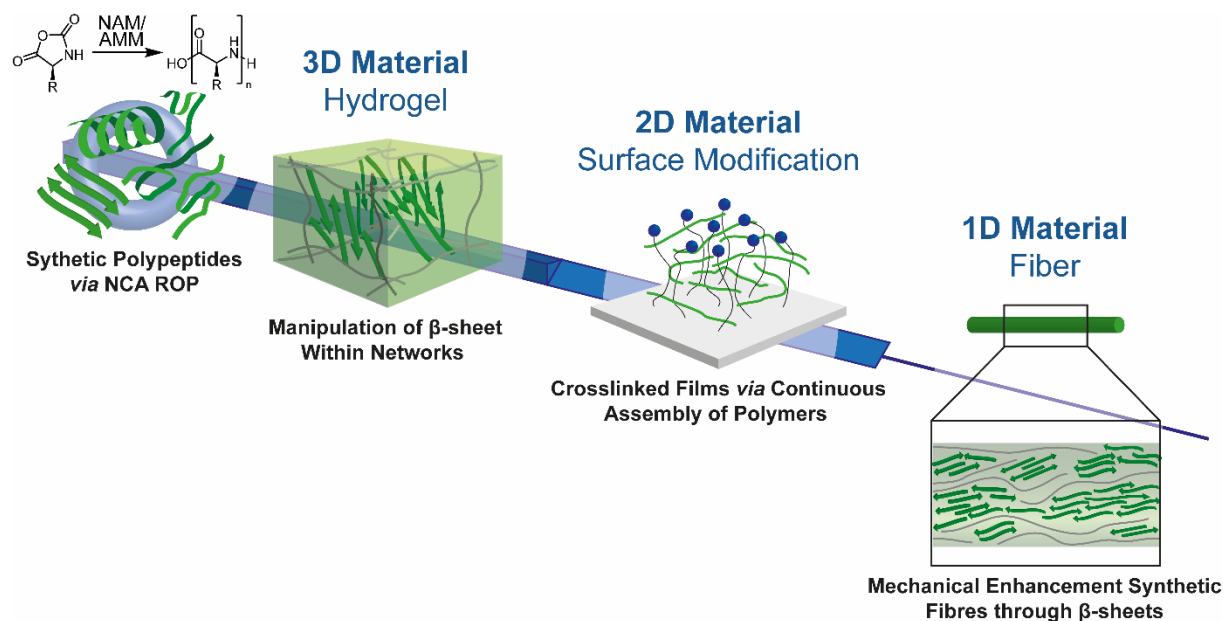


Figure 14: Research theme of the thesis stemming from the implementation of synthetic polypeptides in three-, two- and one-dimensional materials. For the implementation of synthetic polypeptides in three-dimensional materials,  $\beta$ -sheet forming polypeptides have been introduced at a high mass content into hydrogels to produce mechanically tough hydrogels. In two-dimensional materials, chemically crosslinked films were formed using modified synthetic polypeptides resulting in films with unusually high random coil conformations. To fabricate one-dimensional materials, fibers were wet spun from a separate polymer with  $\beta$ -sheet forming polypeptides resulting in structural changes in the bulk fiber which subsequently manifest as changes in mechanical properties.

### 1.7.1 Manipulation of $\beta$ -sheets Within Networks

For the study of three-dimensional materials (**Chapter 2**), the macroscopic structure of spider silk inspired the utilization of  $\beta$ -sheets for the enhancement of hydrogel mechanical properties. Drawing inspiration from the control of  $\beta$ -sheet nanocrystals within an amorphous matrix within spider-silk, highly swellable poly(ethylene glycol) (PEG) hydrogels were synthesized possessing pendant amine groups to graft  $\beta$ -sheet forming polypeptides through NCA ROP (*via* immersion in an NCA solution). L-valine NCA (Val NCA) polymerized into poly(L-valine) (PLV), resulting in  $\beta$ -sheets successfully integrated into the network with the introduction of glycine NCA (Gly NCA) resulting in poly(L-valine-*r*-glycine) (PLVG) changing both the molecular folding of the  $\beta$ -sheets (as identified using FTIR) and the overall microstructure (as identified using SEM). Compressive strength could be increased from 2 kPa without polypeptide to 9.4 MPa upon PVal introduction. By introducing PLVG at different ratios of Val NCA to Gly NCA, mechanical toughness was maintained ( $\sim 2$  MJ/m<sup>3</sup>) while strain at break increased from 40.4 % to 63.2 %. Furthermore, the strategy was found to be applicable in other networks including 3D printed structures.

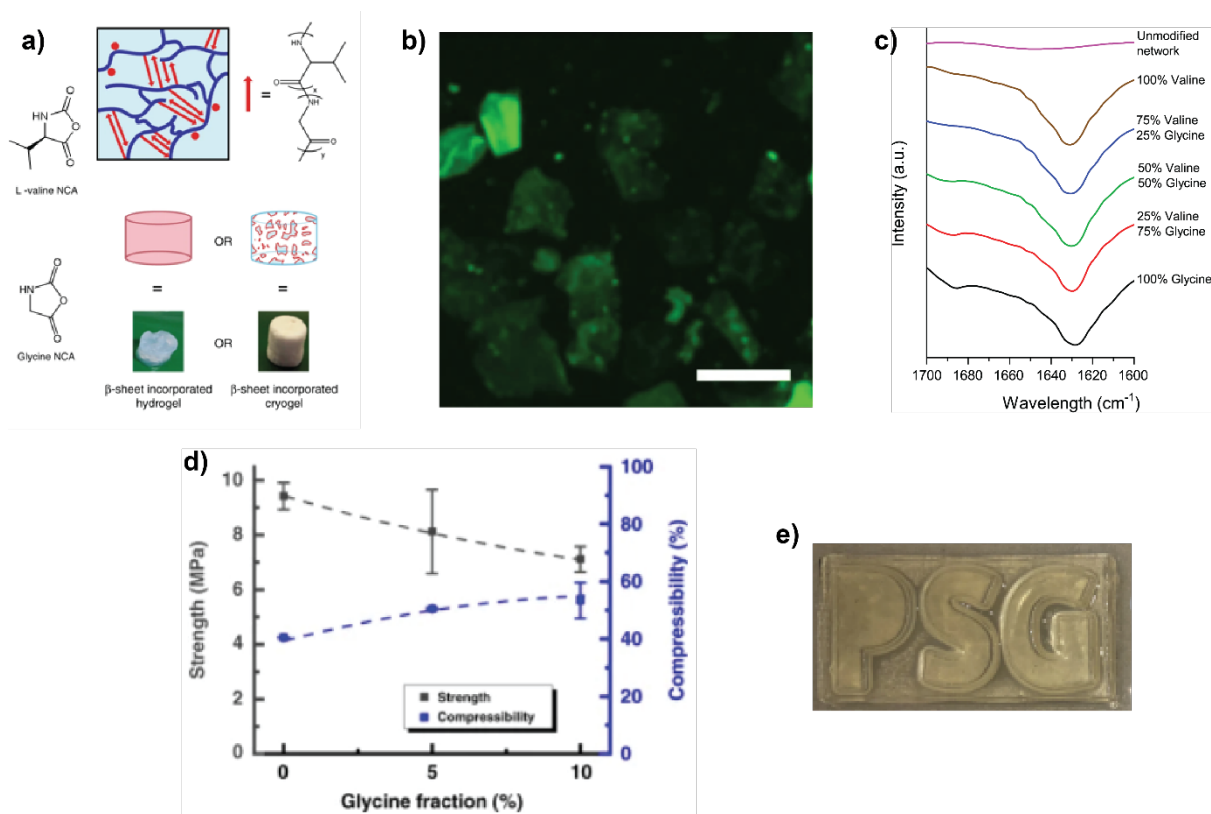


Figure 15: a) Schematic of  $\beta$ -sheet laden networks. b) Thioflavin T staining shows binding of an amorphous network upon inclusion of glycine. c) A notable shift in signal corresponding to the introduction of glycine observed at a high signal at 1633 cm<sup>-1</sup> which corresponds to  $\beta$ -sheets. d) Mechanically, gels were found to be tough a tunable with glycine e) example of a 3D printed,  $\beta$ -sheet laden network.

### 1.7.2 Crosslinked Films *via* Continuous Assembly of Polymers

To utilize polypeptides for two dimensional materials (**Chapter 3**), a unique technique was developed to fabricate chemically crosslinked films with synthetic polypeptides acting as the macrocrosslinker. While many methods exist, the robust methodology developed by our group called the continuous assembly of polymers (CAP) has a unique molecular structure, and, thus, the impact on secondary structure needed to be investigated. Poly(L-lysine) modified with methacrylated side chains (PLLMA) films were formed using CAP by utilizing reversible addition-fragmentation (RAFT) polymerization through the methacrylate side chains. Films with a thickness of  $94.9 \pm 8.2$  nm were found with nanoaggregates as a byproduct of the structure. Furthermore, secondary structure analysis found increased random coil content compared to others poly(L-lysine) films. This was reflected in the poly(L-glutamate) (PLGMA)-based films, which also produced an increased random coil content.

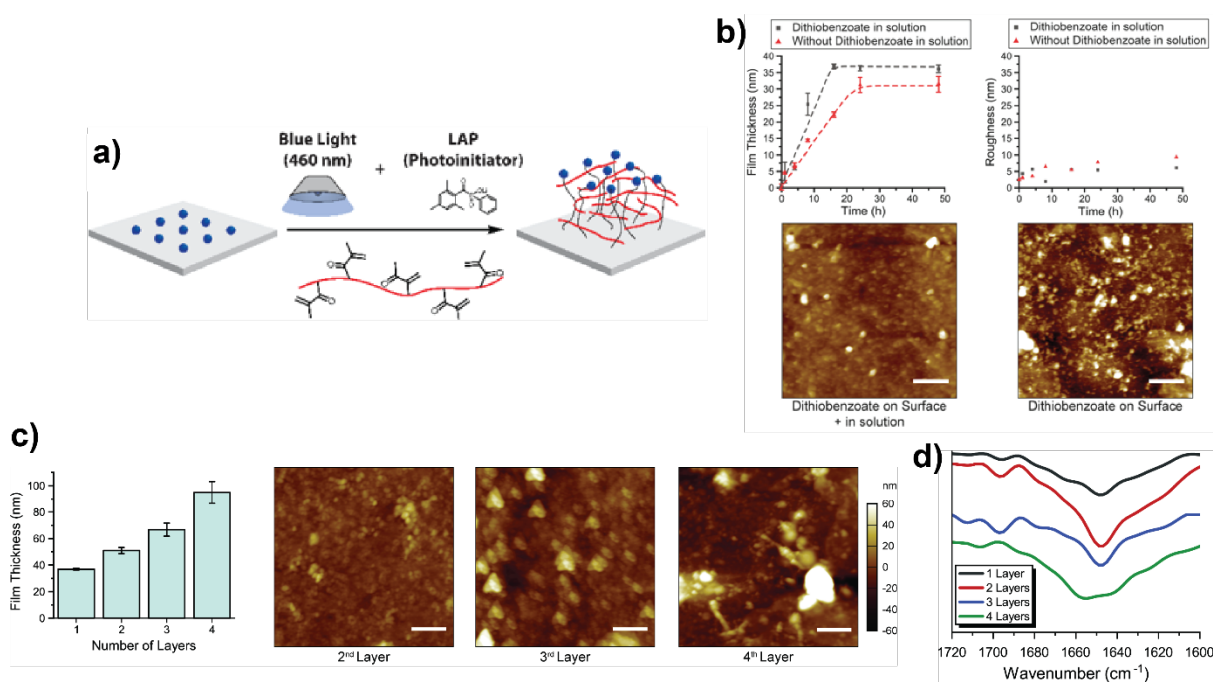


Figure 16: a) Schematic of general CAP-RAFT process. b) Kinetics using a model dithiobenzoate initiator in and absent from the reaction solution. c) Result after performing CAP on wafers. d) FTIR spectra indicates a different material and secondary conformation as would be exerted.

### 1.7.3 Mechanical Enhancement of Synthetic Fibers through $\beta$ -sheets

This study on one-dimensional materials (**Chapter 4**) focused on developing a wide-use platform for introducing  $\beta$ -sheets to impart favorable properties into fibers. As the overall lack of control of  $\beta$ -sheet aggregates still remains an issue in microfiber systems, the concept of introducing the organic solvent Val NCA precursor instead of its insoluble polymerized form



was derived from the work in Chapter 2. By introducing Val NCA into the spinning dope of different polymer fibers, the subsequent growth of PVal and subsequent  $\beta$ -sheet aggregates can be controlled, though the morphology in which these aggregates form is largely dependent on the polymer structure. While  $\beta$ -sheet formation was confirmed, the impact on mechanical properties was largely based on changes to the bulk polymer structure. Polymers with low hydrogen bonding potential (polycaprolactone (PCL) and cellulose acetate) were found to undergo polymer crystallization, leading to an increase in mechanical strength of up to 4.3 times the unmodified control. Other fibers without significant polymer crystal disruption (nylon 6 and poly(benzyl-L-glutamate)) were found to have an increased strain at break of up to 2.9 times the unmodified control. Conversely, disruption to natural occurring polymer structures did result in either minor or reduced mechanical properties in the case of cellulose and the recombinant spider silk, respectively.

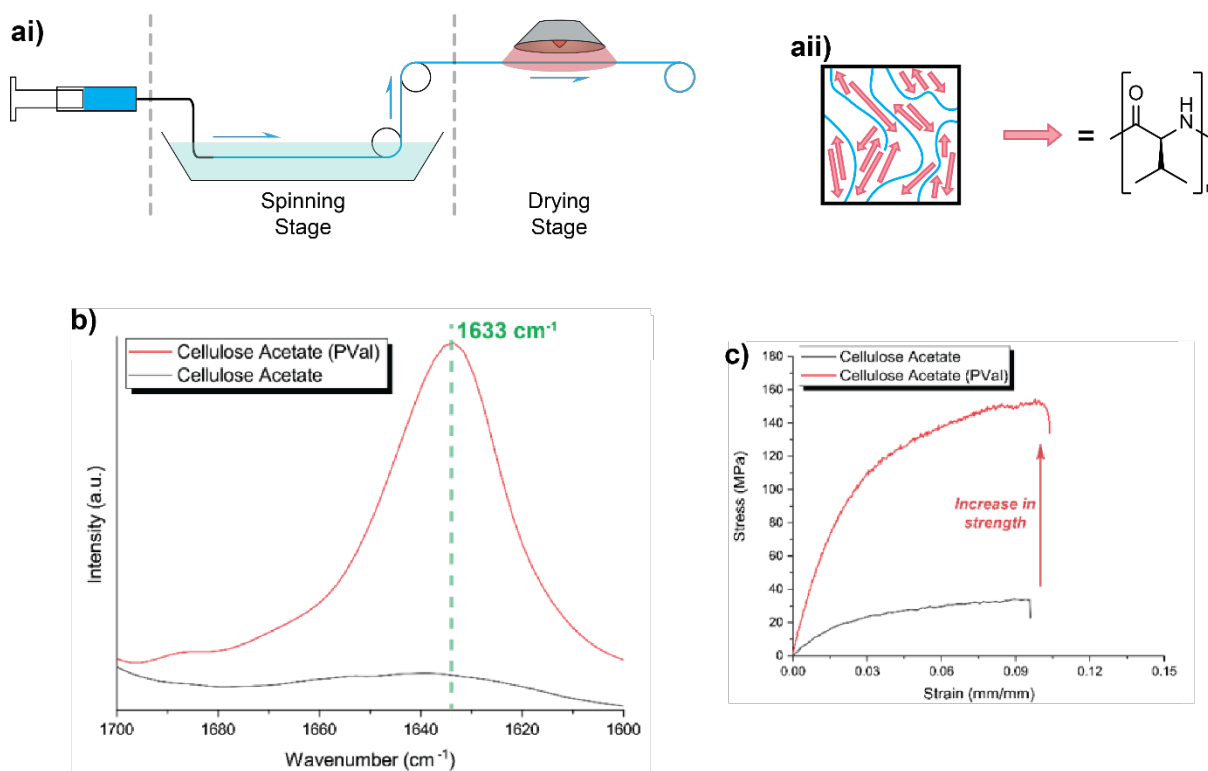


Figure 17: ai) Schematic of wet spinning fibers with  $\beta$ - sheet laden networks ii) based on the matrix, b) FTIR indicating a lack of hydrogen bonding. This leads to c) tensile mechanical testing of samples, which was found to increase in strength.

## 1.8 References

- (1) Cowie, J. M. K. G. *Polymers: Chemistry and Physics of Modern Materials*; Blackie, 1991.
- (2) Bowden, M. E. *Chemical Achievers: The Human Face of the Chemical Sciences*; Chemical Heritage Foundation, 1997.
- (3) Freinkel, S. *Plastic: A Toxic Love Story*; Text Publishing Company, 2011.
- (4) Endres, H.-J.; Siebert-Raths, A. Engineering biopolymers. *Engineering biopolymers* **2011**, *71148*, 3.
- (5) Rasmussen, S. C. Revisiting the Early History of Synthetic Polymers: Critiques and New Insights. *Ambix* **2018**, *65* (4), 356.
- (6) Destarac, M. Controlled radical polymerization: industrial stakes, obstacles and achievements. *Macromolecular Reaction Engineering* **2010**, *4* (3-4), 165.
- (7) Parkatzidis, K.; Wang, H. S.; Truong, N. P.; Anastasaki, A. Recent developments and future challenges in controlled radical polymerization: a 2020 update. *Chem* **2020**.
- (8) George, A.; Sanjay, M.; Srisuk, R.; Parameswaranpillai, J.; Siengchin, S. A comprehensive review on chemical properties and applications of biopolymers and their composites. *International journal of biological macromolecules* **2020**, *154*, 329.
- (9) Tsai, C. S. *Biomacromolecules: Introduction to Structure, Function and Informatics*; Wiley, 2007.
- (10) Alberts, B. *Molecular Biology of the Cell*; W.W. Norton, 2017.
- (11) Branden, C. I.; Tooze, J. *Introduction to Protein Structure*; CRC Press, 2012.
- (12) Kessel, A.; Ben-Tal, N. *Introduction to Proteins: Structure, Function, and Motion, Second Edition*; CRC Press, 2018.
- (13) Banik, S. D.; Nandi, N. In *Biochirality: Origins, Evolution and Molecular Recognition*; Cintas, P., Ed.; Springer Berlin Heidelberg: Berlin, Heidelberg, 2013, DOI:10.1007/128\_2012\_369 10.1007/128\_2012\_369.
- (14) Amblard, M.; Fehrentz, J.-A.; Martinez, J.; Subra, G. Methods and protocols of modern solid phase peptide synthesis. *Molecular Biotechnology* **2006**, *33* (3), 239.
- (15) Gnoth, S.; Jenzsch, M.; Simutis, R.; Lübbert, A. Control of cultivation processes for recombinant protein production: a review. *Bioprocess biosystems engineering* **2008**, *31* (1), 21.
- (16) Porro, D.; Sauer, M.; Branduardi, P.; Mattanovich, D. Recombinant protein production in yeasts. *Molecular biotechnology* **2005**, *31* (3), 245.
- (17) Liu, Y.; Li, D.; Ding, J.; Chen, X. Controlled synthesis of polypeptides. *Chinese Chemical Letters* **2020**, *31* (12), 3001.
- (18) Tsuchiya, K.; Numata, K. Chemoenzymatic Synthesis of Polypeptides for Use as Functional and Structural Materials. *Macromolecular Bioscience* **2017**, *17* (11), 1700177.
- (19) Young, R. J.; Lovell, P. A. *Introduction to Polymers*; CRC Press, 2011.
- (20) Schamboeck, V.; Iedema, P. D.; Kryven, I. Dynamic Networks that Drive the Process of Irreversible Step-Growth Polymerization. *Sci Rep* **2019**, *9* (1), 2276.
- (21) Aplan, M. P.; Gomez, E. D. Recent Developments in Chain-Growth Polymerizations of Conjugated Polymers. *Industrial & Engineering Chemistry Research* **2017**, *56* (28), 7888.
- (22) Kramer, J. R.; Deming, T. J. In *Soft Matter and Biomaterials on the Nanoscale*, 2020, DOI:10.1142/9789811218002\_0006 10.1142/9789811218002\_0006.
- (23) Kricheldorf, H. R. Polypeptides and 100 Years of Chemistry of  $\alpha$ -Amino Acid N-Carboxyanhydrides. *Angewandte Chemie International Edition* **2006**, *45* (35), 5752.

- (24) Leuchs, H. Ueber die Glycin-carbonsäure. *Berichte der Deutschen Chemischen Gesellschaft* **1906**, 39 (1), 857.
- (25) Leuchs, H.; Geiger, W. Über die Anhydride von  $\alpha$ -Amino-N-carbonsäuren und die von  $\alpha$ -Aminosäuren. *European Journal of Inorganic Chemistry* **1908**, 41 (2), 1721.
- (26) Jarowicki, K.; Kocienski, P. Protecting groups. *Journal of the Chemical Society, Perkin Transactions 1* **2000**, DOI:10.1039/B003410J 10.1039/B003410J(16), 2495.
- (27) Ahmed, S. T.; Leferink, N. G. H.; Scrutton, N. S. Chemo-enzymatic routes towards the synthesis of bio-based monomers and polymers. *Molecular Catalysis* **2019**, 467, 95.
- (28) Liu, Y.; Song, L.; Feng, N.; Jiang, W.; Jin, Y.; Li, X. Recent advances in the synthesis of biodegradable polyesters by sustainable polymerization: lipase-catalyzed polymerization. *RSC Advances* **2020**, 10 (59), 36230.
- (29) Ouchi, M.; Sawamoto, M. Sequence-controlled polymers via reversible-deactivation radical polymerization. *Polymer Journal* **2018**, 50 (1), 83.
- (30) Perrier, S. 50th Anniversary Perspective: RAFT Polymerization—A User Guide. *Macromolecules* **2017**, 50 (19), 7433.
- (31) Bonduelle, C. Secondary structures of synthetic polypeptide polymers. *Polymer Chemistry* **2018**, 9 (13), 1517.
- (32) Murphy, R.; Walsh, D. P.; Hamilton, C. A.; Cryan, S.-A.; in het Panhuis, M.; Heise, A. Degradable 3D-Printed Hydrogels Based on Star-Shaped Copolypeptides. *Biomacromolecules* **2018**, 19 (7), 2691.
- (33) Fujiwara, K.; Toda, H.; Ikeguchi, M. Dependence of  $\alpha$ -helical and  $\beta$ -sheet amino acid propensities on the overall protein fold type. *BMC Structural Biology* **2012**, 12 (1), 18.
- (34) Engel, D. E.; DeGrado, W. F. Amino Acid Propensities are Position-dependent Throughout the Length of  $\alpha$ -Helices. *Journal of Molecular Biology* **2004**, 337 (5), 1195.
- (35) Imai, K.; Mitaku, S. Mechanisms of secondary structure breakers in soluble proteins. *Biophysics (Nagoya-shi)* **2005**, 1, 55.
- (36) Krieger, F.; Möglich, A.; Kiefhaber, T. Effect of Proline and Glycine Residues on Dynamics and Barriers of Loop Formation in Polypeptide Chains. *Journal of the American Chemical Society* **2005**, 127 (10), 3346.
- (37) Adzhubei, A. A.; Sternberg, M. J. E.; Makarov, A. A. Polyproline-II Helix in Proteins: Structure and Function. *Journal of Molecular Biology* **2013**, 425 (12), 2100.
- (38) Javadpour, M. M.; Eilers, M.; Groesbeek, M.; Smith, S. O. Helix Packing in Polytopic Membrane Proteins: Role of Glycine in Transmembrane Helix Association. *Biophysical Journal* **1999**, 77 (3), 1609.
- (39) Nakanishi, A.; Shoji, A.; Takegoshi, K. Thermodynamics in Conformational Transition of Poly( $\beta$ -benzyl l-aspartate) As Studied by High-Resolution Solid-State  $^{13}\text{C}$  NMR Spectroscopy. *Macromolecules* **2009**, 42 (23), 9307.
- (40) Levine, B. F.; Bethea, C. G. Second order hyperpolarizability of a polypeptide  $\alpha$ -helix: Poly- $\gamma$ -benzyl-L glutamate. *The Journal of Chemical Physics* **1976**, 65 (5), 1989.
- (41) Matsuoka, M.; Norisuye, T.; Teramoto, A.; Fujita, H. Solution properties of synthetic polypeptides. XV. Helix-coil transition in poly ( $\epsilon$ -carbobenzyloxy L-lysine). *Biopolymers* **1973**, 12 (7), 1515.
- (42) Liu, G.; Dong, C.-M. Photoresponsive Poly(S-(o-nitrobenzyl)-l-cysteine)-b-PEO from a l-Cysteine N-Carboxyanhydride Monomer: Synthesis, Self-Assembly, and Phototriggered Drug Release. *Biomacromolecules* **2012**, 13 (5), 1573.
- (43) Toniolo, C.; Bonora, G. M.; Lüscher, I. F.; Schneider, C. H. Chain-length dependence for secondary structure formation of homo-oligopeptides from  $\epsilon$ -tert-butylloxycarbonyl-L-lysine with a lipophilic C-terminal group. *International Journal of Peptide and Protein Research* **1984**, 23 (1), 47.

- (44) Chen, C.; Wang, Z.; Li, Z. Thermoresponsive polypeptides from pegylated poly-L-glutamates. *Biomacromolecules* **2011**, *12* (8), 2859.
- (45) Choi, Y. Y.; Joo, M. K.; Sohn, Y. S.; Jeong, B. Significance of secondary structure in nanostructure formation and thermosensitivity of polypeptide block copolymers. *Soft Matter* **2008**, *4* (12), 2383.
- (46) Pati, D.; Shaikh, A. Y.; Das, S.; Nareddy, P. K.; Swamy, M. J.; Hotha, S.; Gupta, S. S. Controlled synthesis of O-glycopolypeptide polymers and their molecular recognition by lectins. *Biomacromolecules* **2012**, *13* (5), 1287.
- (47) He, X.; Fan, J.; Zhang, F.; Li, R.; Pollack, K. A.; Raymond, J. E.; Zou, J.; Wooley, K. L. Multi-responsive hydrogels derived from the self-assembly of tethered allyl-functionalized racemic oligopeptides. *Journal of Materials Chemistry B* **2014**, *2* (46), 8123.
- (48) Zou, J.; He, X.; Fan, J.; Raymond, J. E.; Wooley, K. L. Supramolecularly Knitted Tethered Oligopeptide/Single-Walled Carbon Nanotube Organogels. *Chemistry – A European Journal* **2014**, *20* (29), 8842.
- (49) Zou, J.; Zhang, F.; Chen, Y.; Raymond, J. E.; Zhang, S.; Fan, J.; Zhu, J.; Li, A.; Seetho, K.; He, X. et al. Responsive organogels formed by supramolecular self assembly of PEG-block-allyl-functionalized racemic polypeptides into  $\beta$ -sheet-driven polymeric ribbons. *Soft Matter* **2013**, *9* (25), 5951.
- (50) Hong, S. Y.; Oh, J. E.; Lee, K.-H. Effect of d-amino acid substitution on the stability, the secondary structure, and the activity of membrane-active peptide. *Biochemical Pharmacology* **1999**, *58* (11), 1775.
- (51) Perry, S. L.; Leon, L.; Hoffmann, K. Q.; Kade, M. J.; Priftis, D.; Black, K. A.; Wong, D.; Klein, R. A.; Pierce, C. F.; Margossian, K. O. et al. Chirality-selected phase behaviour in ionic polypeptide complexes. *Nature Communications* **2015**, *6* (1), 6052.
- (52) Hashimoto, Y.; Aoyama, A.; Imanishi, Y.; Higashimura, T. Polymerization of optical isomers of phenylalanine N-carboxyanhydride by various secondary amines. *Biopolymers* **1976**, *15* (12), 2407.
- (53) Grazon, C.; Salas-Ambrosio, P.; Antoine, S.; Ibarboure, E.; Sandre, O.; Clulow, A. J.; Boyd, B. J.; Grinstaff, M. W.; Lecommandoux, S.; Bonduelle, C. Aqueous ROPISA of  $\alpha$ -amino acid N-carboxyanhydrides: polypeptide block secondary structure controls nanoparticle shape anisotropy. *Polymer Chemistry* **2021**, DOI:10.1039/D1PY00995H 10.1039/D1PY00995H.
- (54) Batys, P.; Morga, M.; Bonarek, P.; Sammalkorpi, M. pH-Induced Changes in Polypeptide Conformation: Force-Field Comparison with Experimental Validation. *The Journal of Physical Chemistry B* **2020**, *124* (14), 2961.
- (55) Fändrich, M.; Dobson, C. M. The behaviour of polyamino acids reveals an inverse side chain effect in amyloid structure formation. *The EMBO journal* **2002**, *21* (21), 5682.
- (56) Fulara, A.; Dzwolak, W. Bifurcated Hydrogen Bonds Stabilize Fibrils of Poly(L-glutamic) Acid. *The Journal of Physical Chemistry B* **2010**, *114* (24), 8278.
- (57) Li, J.; Wang, T.; Wu, D.; Zhang, X.; Yan, J.; Du, S.; Guo, Y.; Wang, J.; Zhang, A. Stimuli-Responsive Zwitterionic Block Copolypeptides: Poly(N-isopropylacrylamide)-block-poly(lysine-co-glutamic acid). *Biomacromolecules* **2008**, *9* (10), 2670.
- (58) Levy, R. M.; Perahia, D.; Karplus, M. Molecular dynamics of an  $\alpha$ -helical polypeptide: Temperature dependence and deviation from harmonic behavior. *Proceedings of the National Academy of Sciences* **1982**, *79* (4), 1346.
- (59) Bajaj, V. S.; van der Wel, P. C. A.; Griffin, R. G. Observation of a Low-Temperature, Dynamically Driven Structural Transition in a Polypeptide by Solid-State NMR Spectroscopy. *Journal of the American Chemical Society* **2009**, *131* (1), 118.

- (60) Dzwolak, W.; Muraki, T.; Kato, M.; Taniguchi, Y. Chain-length dependence of  $\alpha$ -helix to  $\beta$ -sheet transition in polylysine: Model of protein aggregation studied by temperature-tuned FTIR spectroscopy. *Biopolymers* **2004**, *73* (4), 463.
- (61) Vanhalle, M.; Corneillie, S.; Smet, M.; Van Puyvelde, P.; Goderis, B. Poly(alanine): Structure and Stability of the d and l-Enantiomers. *Biomacromolecules* **2016**, *17* (1), 183.
- (62) Gregory, R. *Protein-Solvent Interactions*; Taylor & Francis, 1995.
- (63) Sneddon, S. F.; Tobias, D. J.; Brooks, C. L. Thermodynamics of amide hydrogen bond formation in polar and apolar solvents. *Journal of Molecular Biology* **1989**, *209* (4), 817.
- (64) Pengo, P.; Pasquato, L.; Moro, S.; Brigo, A.; Fogolari, F.; Broxterman, Q. B.; Kaptein, B.; Scrimin, P. Quantitative correlation of solvent polarity with the  $\alpha$ -3(10)-helix equilibrium: a heptapeptide behaves as a solvent-driven molecular spring. *Angewandte Chemie (International ed. in English)* **2003**, *42* (29), 3388.
- (65) Hirota-Nakaoka, N.; Goto, Y. Alcohol-induced denaturation of  $\beta$ -lactoglobulin: a close correlation to the alcohol-induced  $\alpha$ -helix formation of melittin. *Bioorganic medicinal chemistry* **1999**, *7* (1), 67.
- (66) Baden, N.; Hirota, S.; Takabe, T.; Funasaki, N.; Terazima, M. Thermodynamical properties of reaction intermediates during apoplastocyanin folding in time domain. *The Journal of Chemical Physics* **2007**, *127* (17), 175103.
- (67) Yasuda, S.; Oshima, H.; Kinoshita, M. Structural stability of proteins in aqueous and nonpolar environments. *The Journal of Chemical Physics* **2012**, *137* (13), 135103.
- (68) Chen, C.; Wu, D.; Fu, W.; Li, Z. Tunable Organogelator from Alkyl-Polypeptide Diblock Prepared by Ring-Opening Polymerization. *Australian Journal of Chemistry* **2014**, *67* (1), 59.
- (69) Chen, C.; Wu, D.; Fu, W.; Li, Z. Peptide Hydrogels Assembled from Nonionic Alkyl-polypeptide Amphiphiles Prepared by Ring-Opening Polymerization. *Biomacromolecules* **2013**, *14* (8), 2494.
- (70) Kim, J. Y.; Park, M. H.; Joo, M. K.; Lee, S. Y.; Jeong, B. End Groups Adjusting the Molecular Nano-Assembly Pattern and Thermal Gelation of Polypeptide Block Copolymer Aqueous Solution. *Macromolecules* **2009**, *42* (8), 3147.
- (71) Popescu, M.-T.; Lontos, G.; Avgeropoulos, A.; Tsitsilianis, C. Stimuli responsive fibrous hydrogels from hierarchical self-assembly of a triblock copolypeptide. *Soft Matter* **2015**, *11* (2), 331.
- (72) Popescu, M.-T.; Lontos, G.; Avgeropoulos, A.; Voulgari, E.; Avgoustakis, K.; Tsitsilianis, C. Injectable Hydrogel: Amplifying the pH Sensitivity of a Triblock Copolypeptide by Conjugating the N-Termini via Dynamic Covalent Bonding. *ACS Applied Materials & Interfaces* **2016**, *8* (27), 17539.
- (73) Tsuchiya, K.; Numata, K. Papain-Catalyzed Chemoenzymatic Synthesis of Telechelic Polypeptides Using Bis(Leucine Ethyl Ester) Initiator. *Macromolecular Bioscience* **2016**, *16* (7), 1001.
- (74) Jeong, S. Y.; Moon, H. J.; Park, M. H.; Joo, M. K.; Jeong, B. Molecular captain: A light-sensitive linker molecule in poly(ethylene glycol)-poly(L-alanine)-poly(ethylene glycol) triblock copolymer directs molecular nano-assembly, conformation, and sol-gel transition. *Journal of Polymer Science Part A: Polymer Chemistry* **2012**, *50* (15), 3184.
- (75) Choi, Y. Y.; Jang, J. H.; Park, M. H.; Choi, B. G.; Chi, B.; Jeong, B. Block length affects secondary structure, nanoassembly and thermosensitivity of poly(ethylene glycol)-poly(l-alanine) block copolymers. *Journal of Materials Chemistry* **2010**, *20* (17), 3416.

- (76) Wang, X.; Song, Z.; Tan, Z.; Zhu, L.; Xue, T.; Lv, S.; Fu, Z.; Zheng, X.; Ren, J.; Cheng, J. Facile Synthesis of Helical Multiblock Copolypeptides: Minimal Side Reactions with Accelerated Polymerization of N-Carboxyanhydrides. *ACS Macro Letters* **2019**, *8* (11), 1517.
- (77) Karatzas, A.; Haataja, J. S.; Skoulas, D.; Bilalis, P.; Varlas, S.; Apostolidi, P.; Sofianopoulou, S.; Stratikos, E.; Houbenov, N.; Ikkala, O. et al. Macromolecular Architecture and Encapsulation of the Anticancer Drug Everolimus Control the Self-Assembly of Amphiphilic Polypeptide-Containing Hybrids. *Biomacromolecules* **2019**, *20* (12), 4546.
- (78) Gradišar, Š.; Žagar, E.; Pahovnik, D. Hybrid block copolymers of polyesters/polycarbonates and polypeptides synthesized via one-pot sequential ring-opening polymerization. *Polymer Chemistry* **2018**, *9* (38), 4764.
- (79) Wang, Y.; Ling, J. Synthetic protocols toward polypeptide conjugates via chain end functionalization after RAFT polymerization. *RSC Advances* **2015**, *5* (24), 18546.
- (80) Levit, M.; Zashikhina, N.; Dobrodumov, A.; Kashina, A.; Tarasenko, I.; Panarin, E.; Fiorucci, S.; Korzhikova-Vlakh, E.; Tennikova, T. Synthesis and characterization of well-defined poly(2-deoxy-2-methacrylamido-d-glucose) and its biopotential block copolymers via RAFT and ROP polymerization. *European Polymer Journal* **2018**, *105*, 26.
- (81) Xu, H.; Yang, D.; Cai, C.; Gou, J.; Zhang, Y.; Wang, L.; Zhong, H.; Tang, X. Dual-responsive mPEG-PLGA-PGlu hybrid-core nanoparticles with a high drug loading to reverse the multidrug resistance of breast cancer: An in vitro and in vivo evaluation. *Acta Biomaterialia* **2015**, *16*, 156.
- (82) Xu, J.; He, J.; Fan, D.; Wang, X.; Yang, Y. Aminolysis of polymers with thiocarbonylthio termini prepared by RAFT polymerization: the difference between polystyrene and polymethacrylates. *Macromolecules* **2006**, *39* (25), 8616.
- (83) Boyer, C.; Granville, A.; Davis, T. P.; Bulmus, V. Modification of RAFT-polymers via thiol-ene reactions: A general route to functional polymers and new architectures. *Journal of Polymer Science Part A: Polymer Chemistry* **2009**, *47* (15), 3773.
- (84) Desmet, G. B.; D'hooge, D. R.; Sabbe, M. K.; Reyniers, M.-F.; Marin, G. B. Computational Investigation of the Aminolysis of RAFT Macromolecules. *The Journal of Organic Chemistry* **2016**, *81* (23), 11626.
- (85) Jacobs, J.; Byrne, A.; Gathergood, N.; Keyes, T. E.; Heuts, J. P. A.; Heise, A. Facile Synthesis of Fluorescent Latex Nanoparticles with Selective Binding Properties Using Amphiphilic Glycosylated Polypeptide Surfactants. *Macromolecules* **2014**, *47* (21), 7303.
- (86) Flory, P. J. Molecular size distribution in three dimensional polymers. VI. Branched polymers containing A—R—Bf-1 type units. *Journal of the American Chemical Society* **1952**, *74* (11), 2718.
- (87) Zhang, S.; Li, Z. Stimuli-responsive polypeptide materials prepared by ring-opening polymerization of  $\alpha$ -amino acid N-carboxyanhydrides. *Journal of Polymer Science Part B: Polymer Physics* **2013**, *51* (7), 546.
- (88) He, C.; Zhao, C.; Guo, X.; Guo, Z.; Chen, X.; Zhuang, X.; Liu, S.; Jing, X. Novel temperature- and pH-responsive graft copolymers composed of poly(L-glutamic acid) and poly(N-isopropylacrylamide). *Journal of Polymer Science Part A: Polymer Chemistry* **2008**, *46* (12), 4140.
- (89) Baumgartner, R.; Fu, H.; Song, Z.; Lin, Y.; Cheng, J. Cooperative polymerization of  $\alpha$ -helices induced by macromolecular architecture. *Nature Chemistry* **2017**, *9* (7), 614.

- (90) Nottelet, B.; El Ghzaoui, A.; Coudane, J.; Vert, M. Novel Amphiphilic Poly( $\epsilon$ -caprolactone)-g-poly(L-lysine) Degradable Copolymers. *Biomacromolecules* **2007**, *8* (8), 2594.
- (91) Cheng, Y.; He, C.; Xiao, C.; Ding, J.; Zhuang, X.; Chen, X. Versatile synthesis of temperature-sensitive polypeptides by click grafting of oligo(ethylene glycol). *Polymer Chemistry* **2011**, *2* (11), 2627.
- (92) Jiang, Y.; Wang, S.; Zhang, X.; Tao, Y.; Wang, X. Controlled metal-free polymerization toward well-defined thermoresponsive polypeptides by polymerization at low temperature. *Journal of Polymer Science Part A: Polymer Chemistry* **2016**, *54* (16), 2618.
- (93) Engler, A. C.; Lee, H.-i.; Hammond, P. T. Highly Efficient “Grafting onto” a Polypeptide Backbone Using Click Chemistry. *Angewandte Chemie International Edition* **2009**, *48* (49), 9334.
- (94) Nguyen, M.; Stigliani, J.-L.; Pratviel, G.; Bonduelle, C. Nucleopolypeptides with DNA-triggered  $\alpha$  helix-to- $\beta$  sheet transition. *Chemical Communications* **2017**, *53* (54), 7501.
- (95) Fu, X.; Shen, Y.; Fu, W.; Li, Z. Thermoresponsive Oligo(ethylene glycol) Functionalized Poly-L-cysteine. *Macromolecules* **2013**, *46* (10), 3753.
- (96) Kramer, J. R.; Deming, T. J. Multimodal Switching of Conformation and Solubility in Homocysteine Derived Polypeptides. *Journal of the American Chemical Society* **2014**, *136* (15), 5547.
- (97) Xiong, W.; Fu, X.; Wan, Y.; Sun, Y.; Li, Z.; Lu, H. Synthesis and multimodal responsiveness of poly( $\alpha$ -amino acid)s bearing OEGylated azobenzene side-chains. *Polymer Chemistry* **2016**, *7* (41), 6375.
- (98) Fu, X.; Ma, Y.; Shen, Y.; Fu, W.; Li, Z. Oxidation-Responsive OEGylated Poly-L-cysteine and Solution Properties Studies. *Biomacromolecules* **2014**, *15* (3), 1055.
- (99) Cai, C.; Zhu, W.; Chen, T.; Lin, J.; Tian, X. Synthesis and self-assembly behavior of amphiphilic polypeptide-based brush-coil block copolymers. *Macromolecules* **2009**, *47* (22), 5967.
- (100) Koga, T.; Taguchi, K.; Kobuke, Y.; Kinoshita, T.; Higuchi, M. Structural Regulation of a Peptide-Conjugated Graft Copolymer: A Simple Model for Amyloid Formation. *Chemistry – A European Journal* **2003**, *9* (5), 1146.
- (101) Jang, J. H.; Choi, Y. M.; Choi, Y. Y.; Joo, M. K.; Park, M. H.; Choi, B. G.; Kang, E. Y.; Jeong, B. pH/temperature sensitive chitosan-g-(PA-PEG) aqueous solutions as new thermogelling systems. *Journal of Materials Chemistry* **2011**, *21* (14), 5484.
- (102) Kang, E. Y.; Moon, H. J.; Joo, M. K.; Jeong, B. Thermogelling Chitosan-g-(PAF-PEG) Aqueous Solution As an Injectable Scaffold. *Biomacromolecules* **2012**, *13* (6), 1750.
- (103) Ahmed, E. M. Hydrogel: Preparation, characterization, and applications: A review. *Journal of Advanced Research* **2015**, *6* (2), 105.
- (104) Sangale, P. T.; Manoj, G. Organogel: A novel approach for transdermal drug delivery system. *World Journal of Pharmaceutical Research* **2015**, *4* (3), 423.
- (105) Sharma, S.; Tiwari, S. A review on biomacromolecular hydrogel classification and its applications. *International Journal of Biological Macromolecules* **2020**, *162*, 737.
- (106) Maitra, J.; Shukla, V. K. Cross-linking in hydrogels-a review. *American Journal of Polymer Science* **2014**, *4* (2), 25.
- (107) Parhi, R. Cross-Linked Hydrogel for Pharmaceutical Applications: A Review. *Adv Pharm Bull* **2017**, *7* (4), 515.
- (108) Onder, O. C.; Utroša, P.; Caserman, S.; Podobnik, M.; Žagar, E.; Pahovnik, D. Preparation of Synthetic Polypeptide–PolyHIPE Hydrogels with Stimuli-Responsive Behavior. *Macromolecules* **2021**, *54* (18), 8321.

- (109) Raftery, E. D.; Gharkhanian, E. G.; Ricapito, N. G.; McNamara, J.; Deming, T. J. Influence of Sulfur-Containing Diamino Acid Structure on Covalently Crosslinked Copolypeptide Hydrogels. *Chemistry – An Asian Journal* **2018**, *13* (22), 3547.
- (110) Sedlačík, T.; Studenovská, H.; Rypáček, F. Enzymatic degradation of the hydrogels based on synthetic poly( $\alpha$ -amino acid)s. *Journal of Materials Science: Materials in Medicine* **2011**, *22* (4), 781.
- (111) Studenovská, H.; Vodička, P.; Proks, V.; Hlučilová, J.; Motlík, J.; Rypáček, F. Synthetic poly(amino acid) hydrogels with incorporated cell-adhesion peptides for tissue engineering. *Journal of Tissue Engineering and Regenerative Medicine* **2010**, *4* (6), 454.
- (112) Jan, J.-S.; Chen, P.-S.; Hsieh, P.-L.; Chen, B.-Y. Silicification of Genipin-Cross-Linked Polypeptide Hydrogels Toward Biohybrid Materials and Mesoporous Oxides. *ACS Applied Materials & Interfaces* **2012**, *4* (12), 6865.
- (113) Song, A.; Rane, A. A.; Christman, K. L. Antibacterial and cell-adhesive polypeptide and poly(ethylene glycol) hydrogel as a potential scaffold for wound healing. *Acta Biomater* **2012**, *8* (1), 41.
- (114) Kokufuta, M. K.; Sato, S.; Kokufuta, E. Swelling–shrinking behavior of chemically cross-linked polypeptide gels from poly( $\alpha$ -l-lysine), poly( $\alpha$ -dl-lysine), poly( $\epsilon$ -l-lysine) and thermally prepared poly(lysine): Effects of pH, temperature and additives in the solution. *Colloids and Surfaces B: Biointerfaces* **2011**, *87* (2), 299.
- (115) Wang, S. S. S.; Hsieh, P.-L.; Chen, P.-S.; Chen, Y.-T.; Jan, J.-S. Genipin-cross-linked poly(l-lysine)-based hydrogels: Synthesis, characterization, and drug encapsulation. *Colloids and Surfaces B: Biointerfaces* **2013**, *111*, 423.
- (116) Murphy, R. D.; in het Panhuis, M.; Cryan, S.-A.; Heise, A. Disulphide crosslinked star block copolypeptide hydrogels: influence of block sequence order on hydrogel properties. *Polymer Chemistry* **2018**, *9* (28), 3908.
- (117) Partlow, B. P.; Applegate, M. B.; Omenetto, F. G.; Kaplan, D. L. Dityrosine Cross-Linking in Designing Biomaterials. *ACS Biomaterials Science & Engineering* **2016**, *2* (12), 2108.
- (118) Park, K. M.; Shin, Y. M.; Joung, Y. K.; Shin, H.; Park, K. D. In Situ Forming Hydrogels Based on Tyramine Conjugated 4-Arm-PPO-PEO via Enzymatic Oxidative Reaction. *Biomacromolecules* **2010**, *11* (3), 706.
- (119) Sun, Y.; Hou, Y.; Zhou, X.; Yuan, J.; Wang, J.; Lu, H. Controlled Synthesis and Enzyme-Induced Hydrogelation of Poly(l-phosphotyrosine)s via Ring-Opening Polymerization of  $\alpha$ -Amino Acid N-Carboxyanhydride. *ACS Macro Letters* **2015**, *4* (9), 1000.
- (120) Liu, R.; Shi, Z.; Sun, J.; Li, Z. Enzyme responsive supramolecular hydrogels assembled from nonionic peptide amphiphiles. *Science China Chemistry* **2018**, *61* (10), 1314.
- (121) He, X.; Fan, J.; Wooley, K. L. Stimuli-Triggered Sol–Gel Transitions of Polypeptides Derived from  $\alpha$ -Amino Acid N-Carboxyanhydride (NCA) Polymerizations. *Chemistry – An Asian Journal* **2016**, *11* (4), 437.
- (122) Huang, J.; Heise, A. Stimuli responsive synthetic polypeptides derived from N-carboxyanhydride (NCA) polymerisation. *Chemical Society Reviews* **2013**, *42* (17), 7373.
- (123) Kotharangannagari, V. K.; Sánchez-Ferrer, A.; Ruokolainen, J.; Mezzenga, R. Thermoreversible Gel–Sol Behavior of Rod–Coil–Rod Peptide-Based Triblock Copolymers. *Macromolecules* **2012**, *45* (4), 1982.
- (124) Tohyama, K.; Miller, W. G. Network structure in gels of rod-like polypeptides. *Nature* **1981**, *289* (5800), 813.



- (125) Choi, B. G.; Park, M. H.; Cho, S.-H.; Joo, M. K.; Oh, H. J.; Kim, E. H.; Park, K.; Han, D. K.; Jeong, B. Thermal gelling polyalanine-poloxamine-polyalanine aqueous solution for chondrocytes 3D culture: Initial concentration effect. *Soft Matter* **2011**, *7* (2), 456.
- (126) Park, M. H.; Choi, B. G.; Jeong, B. Complexation-Induced Biomimetic Long Range Fibrous Orientation in a Rigid-Flexible Block Copolymer Thermogel. *Advanced Functional Materials* **2012**, *22* (24), 5118.
- (127) Swann, J. M. G.; Bras, W.; Topham, P. D.; Howse, J. R.; Ryan, A. J. Effect of the Hofmeister Anions upon the Swelling of a Self-Assembled pH-Responsive Hydrogel. *Langmuir* **2010**, *26* (12), 10191.
- (128) Matsumoto, K.; Kawamura, A.; Miyata, T. Conformationally Regulated Molecular Binding and Release of Molecularly Imprinted Polypeptide Hydrogels That Undergo Helix–Coil Transition. *Macromolecules* **2017**, *50* (5), 2136.
- (129) Zhao, S.; Zhu, H.; Chen, Z.; Shuai, S.; Zhang, N.; Liu, Y.; Rao, Z.; Li, Y.; Zhao, C.; Zhou, K. et al. Preparation and properties of a temperature- and pH- responsive polypeptide hydrogel. *Materials Research Express* **2019**, *6* (8), 085711.
- (130) Sun, Y.; Bentolila, L. A.; Deming, T. J. Self-Sorting Microscale Compartmentalized Block Copolypeptide Hydrogels. *ACS Macro Letters* **2019**, *8* (10), 1275.
- (131) Sun, Y.; Wollenberg, A. L.; O’Shea, T. M.; Cui, Y.; Zhou, Z. H.; Sofroniew, M. V.; Deming, T. J. Conformation-Directed Formation of Self-Healing Diblock Copolypeptide Hydrogels via Polyion Complexation. *Journal of the American Chemical Society* **2017**, *139* (42), 15114.
- (132) Wan, Y.; Liu, L.; Yuan, S.; Sun, J.; Li, Z. pH-Responsive Peptide Supramolecular Hydrogels with Antibacterial Activity. *Langmuir* **2017**, *33* (13), 3234.
- (133) Shen, Y.; Zhang, S.; Wan, Y.; Fu, W.; Li, Z. Hydrogels assembled from star-shaped polypeptides with a dendrimer as the core. *Soft Matter* **2015**, *11* (15), 2945.
- (134) Phan, T. H. M.; Huang, C.-C.; Tsai, Y.-J.; Hu, J.-J.; Jan, J.-S. Polypeptide Composition and Topology Affect Hydrogelation of Star-Shaped Poly(L-lysine)-Based Amphiphilic Copolypeptides. *Gels* **2021**, *7* (3), 131.
- (135) Henderson, T.; Ladewig, K.; Haylock, D.; McLean, K.; O’Connor, A. J. Cryogels for biomedical applications. *Journals of Materials Chemistry B* **2013**, *1* (21), 2682.
- (136) Jones, R.; Wilks, E.; Metanomski, W.; Kahovec, J.; Hess, M.; Stepto, R.; Kitayama, T. *Compendium of Polymer Terminology and Nomenclature : IUPAC Recommendations 2008*; 2nd ed.; The Royal Society of Chemistry: Cambridge, 2009.
- (137) Shirbin, S. J.; Lam, S. J.; Chan, N. J.-A.; Ozmen, M. M.; Fu, Q.; O’Brien-Simpson, N.; Reynolds, E. C.; Qiao, G. G. Polypeptide-Based Macroporous Cryogels with Inherent Antimicrobial Properties: The Importance of a Macroporous Structure. *ACS Macro Letters* **2016**, *5* (5), 552.
- (138) Shirbin, S. J.; Karimi, F.; Chan, N. J.-A.; Heath, D. E.; Qiao, G. G. Macroporous Hydrogels Composed Entirely of Synthetic Polypeptides: Biocompatible and Enzyme Biodegradable 3D Cellular Scaffolds. *Biomacromolecules* **2016**, *17* (9), 2981.
- (139) Anitha, R.; Arunachalam, S.; Radhakrishnan, P. J. J. o. M. P. T. Critical parameters influencing the quality of prototypes in fused deposition modelling. *Journal of Materials Processing Technology* **2001**, *118* (1-3), 385.
- (140) Highley, C. B.; Rodell, C. B.; Burdick, J. A. Direct 3D Printing of Shear-Thinning Hydrogels into Self-Healing Hydrogels. *Advanced Materials* **2015**, *27* (34), 5075.
- (141) Murphy, R. D.; Kimmins, S.; Hibbitts, A. J.; Heise, A. 3D-extrusion printing of stable constructs composed of photoresponsive polypeptide hydrogels. *Polymer Chemistry* **2019**, *10* (34), 4675.
- (142) Li, C.; Faulkner-Jones, A.; Dun, A. R.; Jin, J.; Chen, P.; Xing, Y.; Yang, Z.; Li, Z.; Shu, W.; Liu, D. et al. Rapid Formation of a Supramolecular Polypeptide–DNA Hydrogel for

- In Situ Three-Dimensional Multilayer Bioprinting. *Angewandte Chemie International Edition* **2015**, *54* (13), 3957.
- (143) Lee, M. P.; Cooper, G. J. T.; Hinkley, T.; Gibson, G. M.; Padgett, M. J.; Cronin, L. Development of a 3D printer using scanning projection stereolithography. *Sci Rep* **2015**, *5* (1), 9875.
- (144) Zhang, J.; Hu, Q.; Wang, S.; Tao, J.; Gou, M. Digital Light Processing Based Three-dimensional Printing for Medical Applications. *Int J Bioprint* **2019**, *6* (1), 242.
- (145) Felton, L. A. Mechanisms of polymeric film formation. *International Journal of Pharmaceutics* **2013**, *457* (2), 423.
- (146) Cummings, J.; Lowengrub, J. S.; Sumpter, B. G.; Wise, S. M.; Kumar, R. Modeling solvent evaporation during thin film formation in phase separating polymer mixtures. *Soft Matter* **2018**, *14* (10), 1833.
- (147) Scriven, L. E. Physics and Applications of DIP Coating and Spin Coating. *MRS Proceedings* **1988**, *121*, 717.
- (148) Kaliyaraj Selva Kumar, A.; Zhang, Y.; Li, D.; Compton, R. G. A mini-review: How reliable is the drop casting technique? *Electrochemistry Communications* **2020**, *121*, 106867.
- (149) Binazadeh, M.; Zeng, H.; Unsworth, L. D. Effect of peptide secondary structure on adsorption and adsorbed film properties. *Acta Biomaterialia* **2013**, *9* (5), 6403.
- (150) Wasilewski, T.; Szulczyński, B.; Kamysz, W.; Gębicki, J.; Namieśnik, J. Evaluation of Three Peptide Immobilization Techniques on a QCM Surface Related to Acetaldehyde Responses in the Gas Phase. *Sensors* **2018**, *18* (11), 3942.
- (151) Borkner, C. B.; Lentz, S.; Müller, M.; Fery, A.; Scheibel, T. Ultrathin Spider Silk Films: Insights into Spider Silk Assembly on Surfaces. *ACS Applied Polymer Materials* **2019**, *1* (12), 3366.
- (152) Rathore, O.; Sogah, D. Y. Self-Assembly of  $\beta$ -Sheets into Nanostructures by Poly(alanine) Segments Incorporated in Multiblock Copolymers Inspired by Spider Silk. *Journal of the American Chemical Society* **2001**, *123* (22), 5231.
- (153) Huang, H.; Hu, J.; Zhu, Y. Shape-Memory Biopolymers Based on  $\beta$ -Sheet Structures of Polyalanine Segments Inspired by Spider Silks. *Macromolecular Bioscience* **2013**, *13* (2), 161.
- (154) Johnson, J. C.; Wanasekara, N. D.; Korley, L. T. J. Utilizing Peptidic Ordering in the Design of Hierarchical Polyurethane/Ureas. *Biomacromolecules* **2012**, *13* (5), 1279.
- (155) Johnson, J. C.; Wanasekara, N. D.; Korley, L. T. J. Influence of secondary structure and hydrogen-bonding arrangement on the mechanical properties of peptidic-polyurea hybrids. *Journal of Materials Chemistry B* **2014**, *2* (17), 2554.
- (156) Matolyak, L.; Keum, J.; Korley, L. T. J. Molecular Design: Network Architecture and Its Impact on the Organization and Mechanics of Peptide-Polyurea Hybrids. *Biomacromolecules* **2016**, *17* (12), 3931.
- (157) Matolyak, L. E.; Keum, J. K.; Van de Voorde, K. M.; Korley, L. T. J. Synthetic approach to tailored physical associations in peptide-polyurea/polyurethane hybrids. *Organic & Biomolecular Chemistry* **2017**, *15* (36), 7607.
- (158) Matolyak, L. E.; Thompson, C. B.; Li, B.; Keum, J. K.; Cowen, J. E.; Tomazin, R. S.; Korley, L. T. J. Secondary-Structure-Mediated Hierarchy and Mechanics in Polyurea-Peptide Hybrids. *Biomacromolecules* **2018**, *19* (8), 3445.
- (159) He, X.; Fan, J.; Zou, J.; Wooley, K. L. Reversible photo-patterning of soft conductive materials via spatially-defined supramolecular assembly. *Chemical Communications* **2016**, *52* (54), 8455.

- (160) Zhi, Z.-l.; Haynie, D. T. Direct Evidence of Controlled Structure Reorganization in a Nanoorganized Polypeptide Multilayer Thin Film. *Macromolecules* **2004**, *37* (23), 8668.
- (161) Boulmedais, F.; Bozonnet, M.; Schwinté, P.; Voegel, J. C.; Schaaf, P. Multilayered Polypeptide Films: Secondary Structures and Effect of Various Stresses. *Langmuir* **2003**, *19* (23), 9873.
- (162) Rmaile, H. H.; Schlenoff, J. B. Optically Active Polyelectrolyte Multilayers as Membranes for Chiral Separations. *Journal of the American Chemical Society* **2003**, *125* (22), 6602.
- (163) Li, C.; Wang, K.; Gong, Y.-H.; Li, Z.-Y.; Zhang, J.; Luo, G.-F.; Zhuo, R.-X.; Zhang, X.-Z. Fabrication of photosensitive multilayered films vialayer-by-layer assembly with well controlled porous structure. *Journal of Materials Chemistry* **2012**, *22* (5), 2045.
- (164) Wibowo, S. H.; Sulistio, A.; Wong, E. H. H.; Blencowe, A.; Qiao, G. G. Polypeptide films via N-carboxyanhydride ring-opening polymerization (NCA-ROP): past, present and future. *Chemical Communications* **2014**, *50* (39), 4971.
- (165) Majoul, N.; Aouida, S.; Bessaïs, B. Progress of porous silicon APTES-functionalization by FTIR investigations. *Applied Surface Science* **2015**, *331*, 388.
- (166) Mészáros, R.; Thompson, L.; Bos, M.; de Groot, P. Adsorption and Electrokinetic Properties of Polyethylenimine on Silica Surfaces. *Langmuir* **2002**, *18* (16), 6164.
- (167) Wieringa, R. H.; Schouten, A. J. Oriented Thin Film Formation by Surface Graft Polymerization of  $\gamma$ -Methyl L-Glutamate N-Carboxyanhydride in the Melt. *Macromolecules* **1996**, *29* (8), 3032.
- (168) Henze, M.; Mädge, D.; Prucker, O.; Rühle, J. “Grafting Through”: Mechanistic Aspects of Radical Polymerization Reactions with Surface-Attached Monomers. *Macromolecules* **2014**, *47* (9), 2929.
- (169) Bozokalfa, G.; Akbulut, H.; Demir, B.; Guler, E.; Gumus, Z. P.; Odaci Demirkol, D.; Aldemir, E.; Yamada, S.; Endo, T.; Coskunol, H. et al. Polypeptide Functional Surface for the Aptamer Immobilization: Electrochemical Cocaine Biosensing. *Analytical Chemistry* **2016**, *88* (7), 4161.
- (170) Yilmaz, T.; Guler, E.; Gumus, Z. P.; Akbulut, H.; Aldemir, E.; Coskunol, H.; Goen Colak, D.; Cianga, I.; Yamada, S.; Timur, S. et al. Synthesis and application of a novel poly-L-phenylalanine electroactive macromonomer as matrix for the biosensing of ‘Abused Drug’ model. *Polymer Chemistry* **2016**, *7* (47), 7304.
- (171) Akbulut, H.; Yavuz, M.; Guler, E.; Demirkol, D. O.; Endo, T.; Yamada, S.; Timur, S.; Yagci, Y. Electrochemical deposition of polypeptides: bio-based covering materials for surface design. *Polymer Chemistry* **2014**, *5* (12), 3929.
- (172) Kesik, M.; Akbulut, H.; Söylemez, S.; Cevher, Ş. C.; Hızalan, G.; Arslan Udum, Y.; Endo, T.; Yamada, S.; Çırpan, A.; Yağcı, Y. et al. Synthesis and characterization of conducting polymers containing polypeptide and ferrocene side chains as ethanol biosensors. *Polymer Chemistry* **2014**, *5* (21), 6295.
- (173) Wieringa, R. H.; Siesling, E. A.; Geurts, P. F. M.; Werkman, P. J.; Vorenkamp, E. J.; Erb, V.; Stamm, M.; Schouten, A. J. Surface Grafting of Poly(L-glutamates). 1. Synthesis and Characterization. *Langmuir* **2001**, *17* (21), 6477.
- (174) Kugo, K.; Okuno, M.; Kitayama, K.; Kitaura, T.; Nishino, J.; Ikuta, N.; Nishio, E.; Iwatsuki, M. Fourier transform IR attenuated total reflectance study on the secondary structure of poly ( $\gamma$ -methyl L-glutamate) surfaces treated with formic acid. *Biopolymers: Original Research on Biomolecules* **1992**, *32* (3), 197.
- (175) Thoelen, C.; De bruyn, M.; Theunissen, E.; Kondo, Y.; Vankelecom, I. F. J.; Grobet, P.; Yoshikawa, M.; Jacobs, P. A. Membranes based on poly( $\gamma$ -methyl-L-glutamate):

- synthesis, characterization and use in chiral separations. *Journal of Membrane Science* **2001**, *186* (2), 153.
- (176) Zhang, Y.; Kang, K.; Zhu, N.; Li, G.; Zhou, X.; Zhang, A.; Yi, Q.; Wu, Y. Bottlebrush-like highly efficient antibacterial coating constructed using  $\alpha$ -helical peptide dendritic polymers on the poly(styrene-*b*-(ethylene-co-butylene)-*b*-styrene) surface. *Journal of Materials Chemistry B* **2020**, *8* (33), 7428.
- (177) Gao, Q.; Yu, M.; Su, Y.; Xie, M.; Zhao, X.; Li, P.; Ma, P. X. Rationally designed dual functional block copolymers for bottlebrush-like coatings: In vitro and in vivo antimicrobial, antibiofilm, and antifouling properties. *Acta Biomaterialia* **2017**, *51*, 112.
- (178) Gao, Q.; Li, P.; Zhao, H.; Chen, Y.; Jiang, L.; Ma, P. X. Methacrylate-ended polypeptides and polypeptoids for antimicrobial and antifouling coatings. *Polymer Chemistry* **2017**, *8* (41), 6386.
- (179) Nowak, A. P.; Breedveld, V.; Pakstis, L.; Ozbas, B.; Pine, D. J.; Pochan, D.; Deming, T. J. Rapidly recovering hydrogel scaffolds from self-assembling diblock copolypeptide amphiphiles. *Nature* **2002**, *417* (6887), 424.
- (180) Chen, C.; Lan, J.; Li, Y.; Liang, D.; Ni, X.; Liu, Q. Secondary Structure-Governed Polypeptide Cross-Linked Polymeric Hydrogels. *Chemistry of Materials* **2020**, *32* (3), 1153.
- (181) Habraken, G. J. M.; Peeters, M.; Thornton, P. D.; Koning, C. E.; Heise, A. Selective Enzymatic Degradation of Self-Assembled Particles from Amphiphilic Block Copolymers Obtained by the Combination of N-Carboxyanhydride and Nitroxide-Mediated Polymerization. *Biomacromolecules* **2011**, *12* (10), 3761.
- (182) Byrne, M.; Thornton, P. D.; Cryan, S.-A.; Heise, A. Star polypeptides by NCA polymerisation from dendritic initiators: synthesis and enzyme controlled payload release. *Polymer Chemistry* **2012**, *3* (10), 2825.
- (183) Huang, J.; Hastings, C. L.; Duffy, G. P.; Kelly, H. M.; Raeburn, J.; Adams, D. J.; Heise, A. Supramolecular Hydrogels with Reverse Thermal Gelation Properties from (Oligo)tyrosine Containing Block Copolymers. *Biomacromolecules* **2013**, *14* (1), 200.
- (184) Plunkett, K. N.; Berkowski, K. L.; Moore, J. S. Chymotrypsin responsive hydrogel: application of a disulfide exchange protocol for the preparation of methacrylamide containing peptides. *Biomacromolecules* **2005**, *6* (2), 632.
- (185) Thornton, P. D.; McConnell, G.; Ulijn, R. V. Enzyme responsive polymer hydrogel beads. *Chemical communications* **2005**, (47), 5913.
- (186) Weinstock, M. T.; Jacobsen, M. T.; Kay, M. S. Synthesis and folding of a mirror-image enzyme reveals ambidextrous chaperone activity. *Proceedings of the National Academy of Sciences* **2014**, *111* (32), 11679.
- (187) Eckert, D. M.; Malashkevich, V. N.; Hong, L. H.; Carr, P. A.; Kim, P. S. Inhibiting HIV-1 entry: discovery of D-peptide inhibitors that target the gp41 coiled-coil pocket. *Cell* **1999**, *99* (1), 103.
- (188) Shi, S.; Wang, J.; Wang, T.; Ren, H.; Zhou, Y.; Li, G.; He, C.; Chen, X. Influence of residual chirality on the conformation and enzymatic degradation of glycopolypeptide based biomaterials. *Science China Technological Sciences* **2021**, *64* (3), 641.
- (189) Li, D.; Zhao, D.; He, C.; Chen, X. Crucial Impact of Residue Chirality on the Gelation Process and Biodegradability of Thermoresponsive Polypeptide Hydrogels. *Biomacromolecules* **2021**, *22* (9), 3992.
- (190) Liu, L.; Pei, Y.; He, C.; Chen, L. Synthesis of novel thermo- and redox-sensitive polypeptide hydrogels. *Polymer International* **2017**, *66* (5), 712.

- (191) Xu, Q.; He, C.; Ren, K.; Xiao, C.; Chen, X. Thermosensitive Polypeptide Hydrogels as a Platform for ROS-Triggered Cargo Release with Innate Cytoprotective Ability under Oxidative Stress. *Advanced Healthcare Materials* **2016**, *5* (15), 1979.
- (192) Kang, E. Y.; Yeon, B.; Moon, H. J.; Jeong, B. PEG-l-PAF and PEG-d-PAF: Comparative Study on Thermogellation and Biodegradation. *Macromolecules* **2012**, *45* (4), 2007.
- (193) Wang, Y.; Jiang, Z.; Xu, W.; Yang, Y.; Zhuang, X.; Ding, J.; Chen, X. Chiral Polypeptide Thermogels Induce Controlled Inflammatory Response as Potential Immunoadjuvants. *ACS Applied Materials & Interfaces* **2019**, *11* (9), 8725.
- (194) Yun, E. J.; Yon, B.; Joo, M. K.; Jeong, B. Cell Therapy for Skin Wound Using Fibroblast Encapsulated Poly(ethylene glycol)-poly(l-alanine) Thermogel. *Biomacromolecules* **2012**, *13* (4), 1106.

## **Chapter 2:**

# **Spider-silk inspired polymeric networks by harnessing the mechanical potential of $\beta$ -sheets through network guided assembly**

---

---

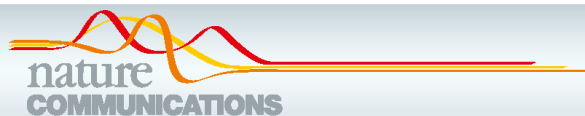
### 2.1. Chapter Perspectives

Spider-silk has inspired research into the utilization of  $\beta$ -sheet forming synthetic polypeptides in hydrogels due to their natural toughness. However,  $\beta$ -sheet aggregation is often uncontrolled, making it difficult to utilize such molecules effectively. To address this issue, the general approach involves synthesizing the polypeptide such that it remains unfolded or well dispersed enough that it does not uncontrollably aggregate and then controlling  $\beta$ -sheet formation to trigger hydrogelation. However, this strategy results in soft materials, which, while tough compared to other soft materials, do not reach the same mechanical potential offered by spider-silk. As a polymerization method towards polypeptide synthesis, NCA ROP offers unique approaches unavailable to other approaches – namely the use of a grafting-from approach.

In this chapter, we report the synthesis of tough  $\beta$ -sheet laden networks. Networks were developed with pendant amine side chains, which could act as the initiator for NCA ROP. By doing so, the formation of  $\beta$ -sheet from poly(L-valine-*r*-glycine) could be spatially controlled. By tuning the amount of glycine present in the network, the conformation of  $\beta$ -sheets could be controlled from strictly antiparallel  $\beta$ -sheet conformations in a continuous network without glycine to a mixture of parallel and antiparallel  $\beta$ -sheet conformations in an amorphous and microporous network upon introduction of glycine. While strength was reduced by the introduction of glycine, mechanical toughness was maintained ( $\sim 2 \text{ MJ/m}^3$ ) accompanied by an increase of strain at break from 40.4 % to 63.2 %. The versatility of the methodology was shown by 3D printing the initial network and then introducing poly(L-valine), resulting in 3D printed  $\beta$ -sheet laden structures. Thus, a methodology for fabricating hydrogels with a high  $\beta$ -sheet content and subsequently superior mechanical properties was developed.

This chapter has produced a research article in *Nature Communications*, published on 2.4.2020 (<https://doi.org/10.1038/s41467-020-15312-x>). In this paper, I was responsible for introducing glycine into the system and subsequent FTIR analysis of these networks, all mechanical testing and degradation studies and investigating the capabilities pertaining to 3D printing.

## 2.2. Main Text



ARTICLE



<https://doi.org/10.1038/s41467-020-15312-x>

OPEN

# Spider-silk inspired polymeric networks by harnessing the mechanical potential of $\beta$ -sheets through network guided assembly

Nicholas Jun-An Chan<sup>1,3</sup>, Dunyin Gu<sup>1,3</sup>, Shereen Tan<sup>1</sup>, Qiang Fu<sup>1</sup>, Thomas Geoffrey Pattison<sup>1</sup>, Andrea J. O'Connor<sup>2</sup> & Greg G. Qiao<sup>1</sup>✉

The high toughness of natural spider-silk is attributed to their unique  $\beta$ -sheet secondary structures. However, the preparation of mechanically strong  $\beta$ -sheet rich materials remains a significant challenge due to challenges involved in processing the polymers/proteins, and managing the assembly of the hydrophobic residues. Inspired by spider-silk, our approach effectively utilizes the superior mechanical toughness and stability afforded by localised  $\beta$ -sheet domains within an amorphous network. Using a grafting-from polymerisation approach within an amorphous hydrophilic network allows for spatially controlled growth of poly(valine) and poly(valine-*r*-glycine) as  $\beta$ -sheet forming polypeptides via N-carboxyanhydride ring opening polymerisation. The resulting continuous  $\beta$ -sheet nanocrystal network exhibits improved compressive strength and stiffness over the initial network lacking  $\beta$ -sheets of up to 30 MPa (300 times greater than the initial network) and 6 MPa (100 times greater than the initial network) respectively. The network demonstrates improved resistance to strong acid, base and protein denaturants over 28 days.

<sup>1</sup>Polymer Science Group, Department of Chemical Engineering, University of Melbourne, Parkville, Melbourne, VIC 3010, Australia. <sup>2</sup>Department of Biomedical Engineering, University of Melbourne, Parkville, Melbourne, VIC 3010, Australia. <sup>3</sup>These authors contributed equally: Nicholas Jun-An Chan, Dunyin Gu. ✉email: [gregghq@unimelb.edu.au](mailto:gregghq@unimelb.edu.au)

Polypeptides are the fundamental building blocks of many naturally occurring materials due to their ability to fold into specific yet complex molecular architectures, including  $\alpha$ -helices and  $\beta$ -sheets<sup>1–4</sup>. The ability to form these secondary structures in response to various environmental cues (e.g. protein concentration<sup>5,6</sup>, metallic ion concentration<sup>7,8</sup> and pH<sup>9</sup>), as well as their diverse functionality, has made them a cornerstone of biochemical research. The importance of how these secondary structures affect material properties is exemplified in naturally occurring dragline spider-silk; a natural polypeptide-based structure which displays a high tensile strength comparable to high tensile steel<sup>10</sup>. Specifically, its excellent mechanical properties are attributed to the spatial arrangement of the amino acids within the polypeptide, which arrange to form higher-order  $\beta$ -sheet architectures through hydrogen bonding primarily from the hydrophobic amino acid residues (i.e. alanine)<sup>11–14</sup>. Surrounding these  $\beta$ -sheet architectures is an arrangement of semi-amorphous, highly extendable glycine-rich regions. This specific arrangement (i.e. composition and spatial) leads to spider silk displaying incredible toughness—a tensile strength between 0.88–1.5 GPa coupled with an extension at break of 21–27 %<sup>10,13</sup>. This incredible mechanical potential garners significant interest towards the utilisation of polypeptides in synthetic materials, such as hydrogels, films and fibres<sup>15–19</sup> for a wide range of applications, including tissue engineering and drug delivery<sup>20–22</sup>.

When synthesising  $\beta$ -sheet forming peptides, both the synthetic technique and the molecular components need to be carefully considered. Synthesis via genetically modified microbes and solid-state synthesis are both common methods for producing peptides, but can require acute knowledge of the peptide sequences that the genes are derived from in the case of the former, and in the case of the latter, solid-state synthesis is limited to the fabrication short chain peptides due to decreasing reaction yield with increased coupling cycles for each amino acid<sup>23–29</sup>. *N*-Carboxyanhydride ring-opening polymerization (NCA ROP) is comparatively a cheaper and a more simple method towards the synthesis of large quantities of polypeptides with a greater potential to create long chain polypeptides, although the method lacks the same level of sequence control observed in solid-state synthesis and genetic engineering<sup>30–35</sup>. Despite this lack of control, we have recently shown the star-shaped polymers synthesised from NCA ROP ‘arms’ are able to observe equivalent, if not better anti-microbial activity when compared to sequence-controlled polypeptides (anti-microbial peptides (AMPs))<sup>36</sup>. Specifically, when designing polypeptides for  $\beta$ -sheet formation, the control of hydrophobic association is fundamental, yet difficult to achieve in the laboratory. This generally leads to ill-defined, uncontrolled and poorly soluble aggregates<sup>14,37</sup>, which greatly impacts the mechanical potential of the formed structures (e.g. bulk hydrogels)<sup>14,37</sup>.

Generally, attempts commonly used to allay the uncontrolled association of hydrophobic residues and subsequent unusable aggregates introduce a high ratio of hydrophilic components to form polypeptides<sup>22</sup>. A grafting-to approach may then be used to subsequently incorporate peptides into a hydrogel<sup>38,39</sup>. For example, Clarke, Pashuck<sup>40</sup> have reported the use of grafted  $\beta$ -sheet forming peptide sequences to the polymeric backbone of hydrogels to induce self-healing properties, however because the peptides remained short with a high hydrophilic residue content, mechanical performance was limited. When employing NCA ROP to synthesise linear polypeptides, hydrophilic blocks such as poly(ethylene glycol)<sup>34,35</sup> or hydrophilic polypeptides<sup>31–33</sup> have often been used to prevent this uncontrolled association from occurring, but their inclusion is highly detrimental to the polypeptides mechanical potential due to the disruption of the hydrophobic association<sup>31–35</sup>. Natural spider-silk uses blocks of alanine to form  $\beta$ -sheets during

the natural silk fiber production process which involves specific environmental changes to encourage the formation of the  $\beta$ -sheets<sup>10</sup>. However, it should be noted that although it is well known that alanine forms  $\beta$ -sheets at low molecular weight (small blocks), high molecular weight (larger blocks) alanine has been shown to form  $\alpha$ -helices<sup>11–43</sup>. Our group has had previous success using valine NCA ROP to form  $\beta$ -sheets, making valine a viable option for constructing spider-silk inspired materials<sup>44</sup>.

Herein, we report a simple method to mimic spider-silk by creating localised  $\beta$ -sheet domains, which endow the formed bulk hydrogels with superior mechanical performance. A grafting-from approach is used to incorporate  $\beta$ -sheet forming polypeptides into a pre-fabricated three-dimensional hydrophilic network, which acts as a template to guide  $\beta$ -sheet assembly to mimic the amorphous matrix found in spider-silk. Free amine groups embedded in the networks are subsequently used as a site for NCA ROP of valine and glycine resulting in the spatial and controlled formation of crystalline  $\beta$ -sheet nanocrystals. The physical characteristics of the  $\beta$ -sheet reinforced networks are reported in terms of compressive characteristics, revealing a three-orders of magnitude increase in toughness attributed to the overall  $\beta$ -sheet network rather than the general effect of increased hydrophobicity. Given the natural ease and versatility of polypeptide synthesis via NCA ROP, this synthetic approach can facilitate the incorporation of  $\beta$ -sheets in a far broader range of materials moving into the foreseeable future.

## Results

### $\beta$ -sheet rich networks synthesis via a grafting-from approach.

To demonstrate a proof of concept, an initial network was synthesised by free radical polymerization with pendant amine groups followed by directed  $\beta$ -sheet incorporation via NCA ROP (Fig. 1). The initial network was designed with pendant amine groups randomly located on the network backbone spaced out with a PEG-based spacer monomer, thus controlling the spatial arrangement of the  $\beta$ -sheet forming polypeptides. The amine groups acted as initiating sites for NCA ROP of  $\beta$ -sheet forming polypeptides, resulting in a polymeric network incorporating non-covalent  $\beta$ -sheet crosslinks. Both hydrogels and cryogels were formed to compare the differences between a conventional (non-porous) and macroporous network. Poly(L-valine) (pVal) chains are known to result in  $\beta$ -sheet formation, resulting in crystalline and rigid  $\beta$ -sheet regions being observed<sup>45</sup>. Thus, glycine was introduced to act as a  $\beta$ -sheet destabilizing residue<sup>12</sup> and being responsible for amorphous  $\beta$ -sheet regions in spider-silk<sup>10</sup>. Thus, L-valine NCA (Val NCA) and glycine NCA (Gly NCA) were synthesised and then used to form crystalline and amorphous  $\beta$ -sheet regions respectively.

The polymerization of  $\beta$ -sheet forming polypeptides via NCA ROP is grown from the available amine groups of the polymer backbone as initiating sites. Hence, Val NCA monomer concentration was varied from 30 to 360 mg/mL to yield increasing pVal chain lengths (Table 1). As expected, the chain length of the valine increased with increasing monomer concentration along with a decrease in conversion. The latter is likely due to the following two reasons. Over the course of  $\beta$ -sheet incorporation, the hydrogels and cryogels noticeably shrink in volume, indicating a reduction in overall pore size which would reduce the diffusion of NCAs into the gels over the course of the reaction. Furthermore, due to the increasing hydrophobicity of networks, the amine groups are hydrophobically shielded from solvent in the late stages of polymerization.

In addition to the valine homopolypeptides formed, hydrogel networks with random copolypeptides were also synthesised with Gly NCA. As glycine is a strong  $\beta$ -sheet breaker<sup>12</sup>, it is used to



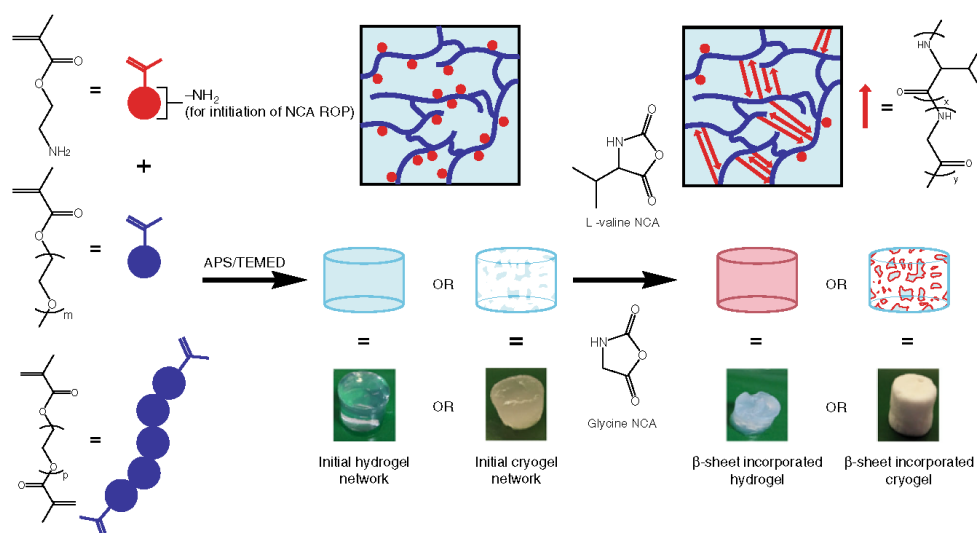


**Fig. 1 Fabrication of peptide  $\beta$ -sheets loaded composite networks.** Networks synthesised via (i) production of two initial networks (a hydrogel and a cryogel) with pendant primary amine groups by free radical polymerization; and (ii) subsequent ROP of Val NCA initiated by the amine groups on the polymer backbone, resulting in the formation of  $\beta$ -sheet secondary structure within the network.

replace small quantities of Val NCA at 5 and 10 mol % within a constant total molar concentration at 2.51 mmol/mL (equivalent molar monomer concentration to HB360 and CB360) in a solution (Table 1). The glycine allowed for slightly longer polypeptides to be formed due to the reduced hydrophobicity associated with the less hydrophobic glycine residue. The conversion of glycine was close to completion while valine conversion was increased to ~82–84%. The amine groups remain hydrophobically shielded from solvent with the low glycine fraction.

**Impact of  $\beta$ -sheet incorporation on network swellability.** The swelling characteristics of the hybrid networks further supports the hydrophobic shielding effect and reduced pore size in  $\beta$ -sheet formation. As expected, the equilibrium swell ratio decreases with increase in the polymerization degree of Val NCA for both hydrogels and cryogels (Fig. 2a). The decreased swelling capacities and subsequent porosity stem from the introduction of hydrophobic pVal grafts and  $\beta$ -sheet conformations. If porosity was the only factor affecting the overall conversion, then polypeptide chain growth would be halted when the decrease of swell ratio stopped. However as evidenced by the cryogels beyond a certain Val NCA concentration (120 mg/mL), the  $\beta$ -sheets-rich cryogels became non-swellable while the conversion continued to drop. The flotation of the cryogels due to a combination of low densities (<750 mg/mL<sup>3</sup>) and insufficient swellability to take on enough overall mass in water (Fig. 2b, c) further shows evidence of hydrophobicity the non-swellable cryogels remains more buoyant than the surrounding water.

**Morphological analysis of continuous  $\beta$ -sheet linked network.** The morphological impact of  $\beta$ -sheet formation was visualised to ascertain the nature of  $\beta$ -sheet crosslinking and the resulting network. Morphological examination via scanning electron microscopy (SEM) was performed for both hydrogels and cryogels. Examination of the initial networks showed smooth surfaces for

both hydrogels and cryogels as expected with highly swellable polymeric networks (Supplementary Fig. 1). At low levels of  $\beta$ -sheet introduction,  $\beta$ -sheet aggregates could be observed, with the gel surfaces being relatively rough (Fig. 3a, c). When  $\beta$ -sheet content was increased, the aggregates in the hydrogels associated with each other to become a continuous network (Fig. 3b). It was found that  $\beta$ -sheets aggregation was reduced with the introduction of glycine compared to samples soaked in the same molar concentration of NCA and samples soaked in the same amount of valine (Supplementary Fig. 2). The slightly porous structure does indicate the attempted aggregation of  $\beta$ -sheets is occurring, but being interrupted by the glycine, with spherical like bumps appearing on the gel surface, suggesting the presence of more amorphous  $\beta$ -sheet regions. Compared to the network with glycine but no valine, no aggregation is present. The characteristic interconnected pore network of the cryogels (Fig. 3d) is preserved, with  $\beta$ -sheets acting as a hydrophobic layer. The  $\beta$ -sheet aggregates bundle with increasing  $\beta$ -sheet content, though aggregates remain more spherical than the continuous network found in the hydrogels.

The morphology of the  $\beta$ -sheet structure was further assessed using a Thioflavin T (ThT) binding assay under fluorescence microscopy<sup>46,47</sup>. As shown in the confocal image (Fig. 4a), the labelled amyloid clusters are scattered further illustrating the lack of amorphous regions and the local aggregation of the  $\beta$ -sheets being responsible for the aggregates observed in the SEM imaging. Increasing pVal content allowed expansion of  $\beta$ -sheets with lateral aggregation extending (Fig. 4b), resulting in the more continuous network observed in the SEM imaging. The introduction of glycine at low concentrations does still result in crystalline  $\beta$ -sheet structures (Fig. 4c). However, the morphology within these crystalline regions is slightly more amorphous, with less defined structures being visible compared to those with homopoly(L-valine) (Fig. 4d). In the case of  $\beta$ -sheets-rich cryogel, the  $\beta$ -sheet regions are spread out across the porous network walls (Fig. 4e). At closer magnification (Fig. 4f), the  $\beta$ -sheet regions being far more densely packed than the hydrogel.

**Table 1** Estimated polymerization degree of Val/Gly NCA in the initial networks.

Experimental Code	Percentage of glycine (mol %)	Val NCA Conc. (mg/mL, mmol/mL)	Gly NCA Conc. (mg/mL, mmol/mL)	Types of initial network	Val Conv. <sup>a</sup> (%)	Gly Conv. <sup>a</sup> (%)	Average DP (Val) <sup>b</sup>	Average DP (Gly) <sup>b</sup>
HB30	0	30, 0.21	N/A	Hydrogel	90.4 ± 4.8	N/A	7.3 ± 0.03	N/A
CB30	0	30, 0.21	N/A	Cryogel	88.8 ± 4.5	N/A	7.2 ± 0.03	N/A
HB60	0	60, 0.42	N/A	Hydrogel	86.4 ± 2.3	N/A	13.9 ± 0.06	N/A
CB60	0	60, 0.42	N/A	Cryogel	83.2 ± 4.8	N/A	13.4 ± 0.06	N/A
HB120	0	120, 0.83	N/A	Hydrogel	85.6 ± 5.5	N/A	27.6 ± 0.14	N/A
CB120	0	120, 0.83	N/A	Cryogel	77.8 ± 8.7	N/A	25.1 ± 0.22	N/A
HB240	0	240, 1.67	N/A	Hydrogel	80.5 ± 2.5	N/A	51.9 ± 0.12	N/A
CB240	0	240, 1.67	N/A	Cryogel	77.8 ± 7.2	N/A	50.2 ± 0.36	N/A
HB360	0	360, 2.51	N/A	Hydrogel	75.2 ± 2.0	N/A	72.7 ± 0.15	N/A
CB360	0	360, 2.51	N/A	Cryogel	76.8 ± 0.4	N/A	74.3 ± 0.03	N/A
GH5	5	342, 2.39	12.7, 0.12	Hydrogel	83.6 ± 10.7	94.8 ± 3.8	76.8 ± 0.77	4.6 ± 0.01
GH10	10	324, 2.26	25.4, 0.25	Hydrogel	82.6 ± 13.9	97.9 ± 0.8	71.9 ± 0.94	9.5 ± 0.01

<sup>a</sup>The NCA monomer conversion rate was determined by <sup>1</sup>H NMR using a calibration curve, according to the integral ratio between remaining NCA monomer and solvent characteristic peaks stipulated in Methods. <sup>b</sup>errors based on standard deviation (*n* = 3). <sup>c</sup>Average DP is the average number of grafted Val repeat units per -NH<sub>2</sub> group along the network backbone, estimated by the molar ratio between converted Val NCA and -NH<sub>2</sub> groups in the initial networks (assuming the initiating efficiency and polymerization rate are the same throughout the networks).

**Crystallinity and parallel/antiparallel nature of  $\beta$ -sheets.** The specific structures and crystallinity were analysed via Attenuated Total Reflectance Fourier Transform Infrared (ATR-FTIR) spectroscopy and X-ray Diffraction (XRD). The FTIR spectra (Fig. 5a) shows a representative range of the networks in this study, with analysis focusing on the numerous peaks assigned to the amide bond. As NCA ROP polymerisation proceeds, the formation of amide functionality is observed with sharp amide A and B bands emerging at around 3280 and 3085 cm<sup>-1</sup> (due to N-H vibrational stretching), indicating successful polymerization<sup>48</sup>. The amide A band is shown to have a small shoulder at 3300 cm<sup>-1</sup> once glycine is introduced, which is more evident in samples containing greater amounts of glycine (Supplementary Fig. 3)<sup>48</sup>. As the amide A band is largely sensitive to hydrogen bonding strength, this can be associated to the change in bond strength. The primary amine assigned to a broad peak between 3300 and 3500 cm<sup>-1</sup> is clearly seen in the initial network and remains as a shoulder overlapping with the amide A peak in subsequent networks. The presence of this signal is to be expected as the terminal primary amine of polypeptides remains after NCA ROP, though its relative strength is drastically reduced with increasing  $\beta$ -sheet induction due to the increase of amide bonds. The amide I band (C=O stretch vibration) has been identified as the most sensitive spectral region corresponding to different polypeptide secondary structures and used to determine their conformations<sup>49</sup>. Hereby, the strong amide peak around 1627 cm<sup>-1</sup> with a weak shoulder at 1690 cm<sup>-1</sup> suggests the formation of  $\beta$ -sheet secondary structure adopted in the mixture of antiparallel and parallel conformations, respectively<sup>49</sup>. The shoulder assigned to the parallel conformations slightly increases with increasing glycine content (most evident in Supplementary Fig. 3), which is known to be less stable than the antiparallel conformation, thus affecting both mechanical and degradation properties<sup>49</sup>. This increase in parallel  $\beta$ -sheets can also be attributed to the lower degree of crystalline  $\beta$ -sheet aggregation observed in the SEM imaging and ThT staining. The amide V band provides more evidence of  $\beta$ -sheet conformations being located around 710 cm<sup>-1</sup> instead of 610–620 cm<sup>-1</sup> assigned to  $\alpha$ -helices<sup>50</sup>. It should be noted that a broad band with a peak at around 590 cm<sup>-1</sup> becomes present in the hydrogels containing glycine but is identified instead as an amide VI (C=O out-of-plane bending) as the amide V band is not diminished in the glycine containing gels<sup>51</sup>. Other distinguishing features of the  $\beta$ -sheet incorporated networks include amide II band (N-H in-plane bending) near 1530 cm<sup>-1</sup>, amide V band (N-H out-of-plane bending) around 710 cm<sup>-1</sup>, and the pVal aliphatic side-chain C-H stretch peaks around 2965 cm<sup>-1</sup> (which is diminished slightly one glycine is introduced)<sup>48–50</sup>. Also, the characteristic peaks of the initial network are still clearly present in the spectra of  $\beta$ -sheets-incorporated networks, including C-H stretch on the polymer backbone, C=O stretch of ester group and C-O-C stretch in the side chain. The increase in  $\beta$ -sheet content with increasing Val NCA concentrations in the ROP process was also highlighted with the intensity of the  $\beta$ -sheet band (amide I) relative to the polymer backbone stretch in the initial network (C-O-C stretch) (Table S1). The higher intensity ratio (referring to a higher  $\beta$ -sheet content) for the cryogel compared with its hydrogel counterpart is presumably caused by the higher propensity of pVal chains for  $\beta$ -sheets formation in a much more confined space (i.e. highly concentrated pore walls). The formation of  $\beta$ -sheet secondary structure was further verified by X-ray diffraction (XRD) (Fig. 5b). XRD patterns only show a broad peak for the initial network, indicating its amorphous nature, whereas two evident diffraction peaks at  $2\theta = 9^\circ$  and  $19^\circ$  can be seen for  $\beta$ -sheets-incorporated networks, attributed to the  $\beta$ -sheet crystalline plane with a typical *d* spacing of 10.1 and

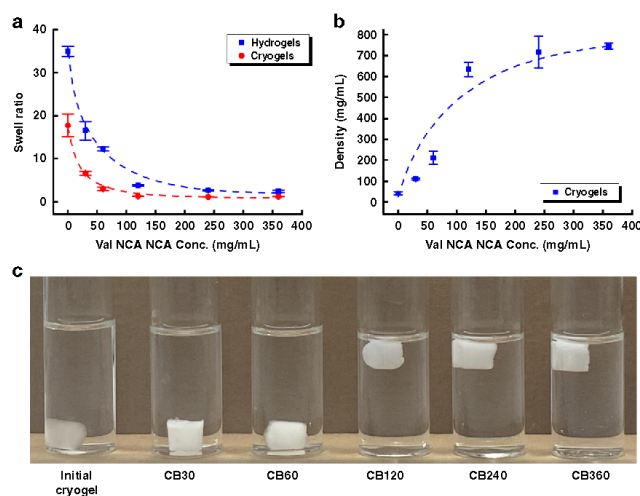


**Fig. 2** Characteristics of networks in deionised water (glass vial diameter -25 mm) at pH 6.7. **a** Equilibrium swell ratios of  $\beta$ -sheets-incorporated hydrogels and cryogels prepared with different Val NCA monomer concentrations (0–360 mg/mL); **b** Summary of bulk density of dry  $\beta$ -sheets-incorporated cryogels as a function of Val NCA concentrations (noting at higher than 120 mg/mL of Val NCA, the cryogels are non-swellable); **c** Photos showing the cryogels with different content of  $\beta$ -sheets. All error bars based on standard deviation ( $n = 3$ ).

4.6 Å, respectively<sup>34,52</sup>. Like the trend observed for FTIR spectra, the two peaks intensify upon elevating the Val NCA concentrations. The transition from broad to sharp peaks suggests the embedment of crystalline  $\beta$ -sheet domains in a semi-amorphous matrix.

**Mechanical toughening impact of  $\beta$ -sheets.** The mechanical toughening via  $\beta$ -sheet incorporation into the networks was characterised by uniaxial compressive testing, observing network behaviour until complete pore disintegration. The easy handling of these gels for compressive mechanical testing sets them distinct from many weak hydrogels physically cross-linked through  $\beta$ -sheets assembly, for which oscillatory rheology was the only applicable mechanical test<sup>31–35</sup>. The stress-strain curves obtained indicate hydrogel stiffening and strength consistently increased with increasing pVal formed  $\beta$ -sheet content with the Young's Modulus increasing by three orders of magnitude (from 2 kPa to 9.4 MPa) (Fig. 6a, b). These features can be attributed to the crystalline  $\beta$ -sheet aggregates identified before, providing a similar property to the double network effect, which is attributed to stiff a second cross-linked network in a soft chemically cross-linked first network. It should be noted that while the effect is similar, the covalent bonding of the  $\beta$ -sheets disqualifies it from being a true double network despite carrying similar properties. The increase in strength and toughness (Fig. 6e) provides further evidence of increased mechanical properties via this methodology. The  $\beta$ -sheet nanocrystals observed in these composite networks by ThT staining and SEM imaging typically feature catastrophic fracture subject to mechanical perturbation, triggered by rupturing of hydrogen bonds that bind  $\beta$ -strands in clusters, as previously reported.

The introduction of glycine was designed to disrupt these  $\beta$ -sheet nanocrystals and help to introduce more amorphous  $\beta$ -sheet regions allowing for a reduction in the brittle nature of the material while minimising strength loss. Toughness remains around 2 MJ/m<sup>3</sup>, implying that the overall integrity of the gel remains intact despite the introduction of  $\beta$ -sheet forming

residues. However, a loss in strength and subsequent increase in compressibility defines the tunable nature of these materials (Fig. 6f), maintaining a similar characteristic curve to the hydrogels with the highest density of  $\beta$ -sheets.

The composite cryogels managed to yield less stiff gels, but with superior strength and compressibility. Cryogels are known to have an intrinsic advantage of being more compressible and mechanically stable over conventional non-porous hydrogels and the weak porous networks prepared otherwise, owing to the densification of polymers in the pore walls. As observed in the ThT staining and SEM imaging, the  $\beta$ -sheets reinforce the existing network pore walls rather than creating completely new walls across pores. The effect of this different morphological reinforcement can be observed when comparing the trends in stiffness in the hydrogel and cryogel morphologies (Fig. 6b, d) with the Young's Modulus of the cryogels only increasing by 2 orders of magnitude (28 kPa to 8 MPa) compared to the 3 orders of magnitude of the hydrogels. Furthermore, the lack of change in the porous network itself is also reflected in the comparative lack of drastic changes in ultimate strain (Fig. 6c), with the initial cryogel having a compressibility of 80%, the most compressible cryogel (due to soaking in 60 mg/mL Val NCA solution) having a compressibility of 88% and the cryogel with the highest  $\beta$ -sheet content having a compressibility of 81%. As expected, the mechanical strength significantly rose by approximately 300 times (from 0.1 to 300 MPa) with 12-fold increase in the Val NCA concentration (from 30 to 360 mg/mL). Further confirmation of the maintenance of the porous network is the distinctive compressive patterns of cellular monoliths (e.g. foams and cork), with three regimes of deformation (inset of Fig. 6c): nearly linear elastic regime, corresponding to bending of pore walls; followed by a near-plateau regime of flat stress, reflecting the easy deformation due to the cell collapse under pressure; and finally an abrupt increase in the stress in the third regime, because of densification of cellular walls.

To ensure that the mechanical enhancement was primarily due  $\beta$ -sheet formation and not simply hydrophobic modification by

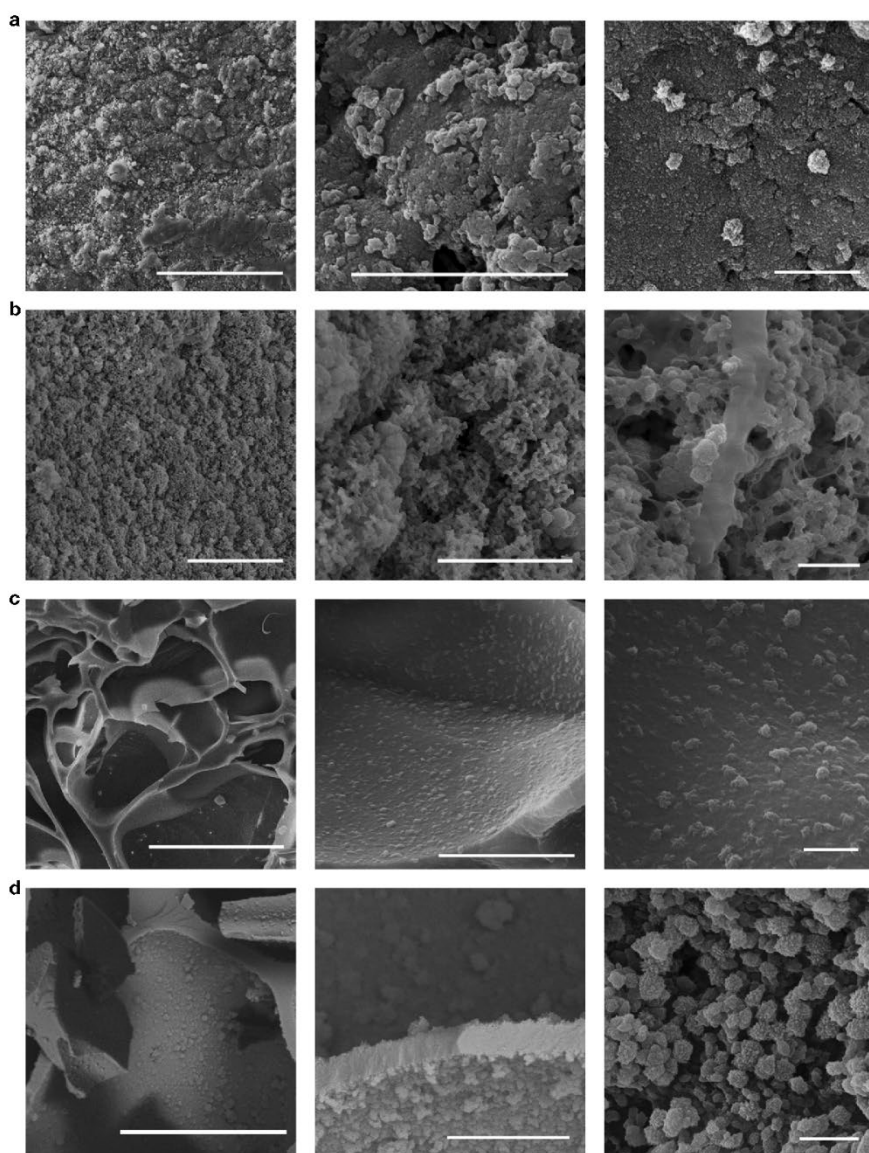


**Fig. 3 SEM cross-sectional images of  $\beta$ -sheets-incorporated hydrogel. a, b** Hydrogels and **c, d** cryogels with different content of  $\beta$ -sheets, CB60 (**a, c**) and CB360 (**b, d**). From left to right, scale bars are 50  $\mu\text{m}$ , 5  $\mu\text{m}$  and 1  $\mu\text{m}$  with increasing magnification.

L-valine and glycine as has been seen in other hydrogels, a network grafted with poly(methyl methacrylate) (PMMA), a typical hydrophobic polymer that is hard to crystallize, was synthesised using RAFT (Supplementary Fig. 4)<sup>53–55</sup>. With insertion of more PMMA grafts in the networks, the hydrogels and cryogels became harder and, in the case of the hydrogels, more brittle (Supplementary Fig. 5), which is in agreement with the observations of

hydrophobically modified hydrogels reported in the literature. The stiffness of the  $\beta$ -sheet incorporated gels was approximately 1 order of magnitude higher than the PMMA at the same monomer concentrations in both the hydrogels and the cryogels, where the difference in stiffness become more pronounced with greater monomer concentrations (Supplementary Fig. 5b, d). This result provides a clear indication that the extraordinary mechanical



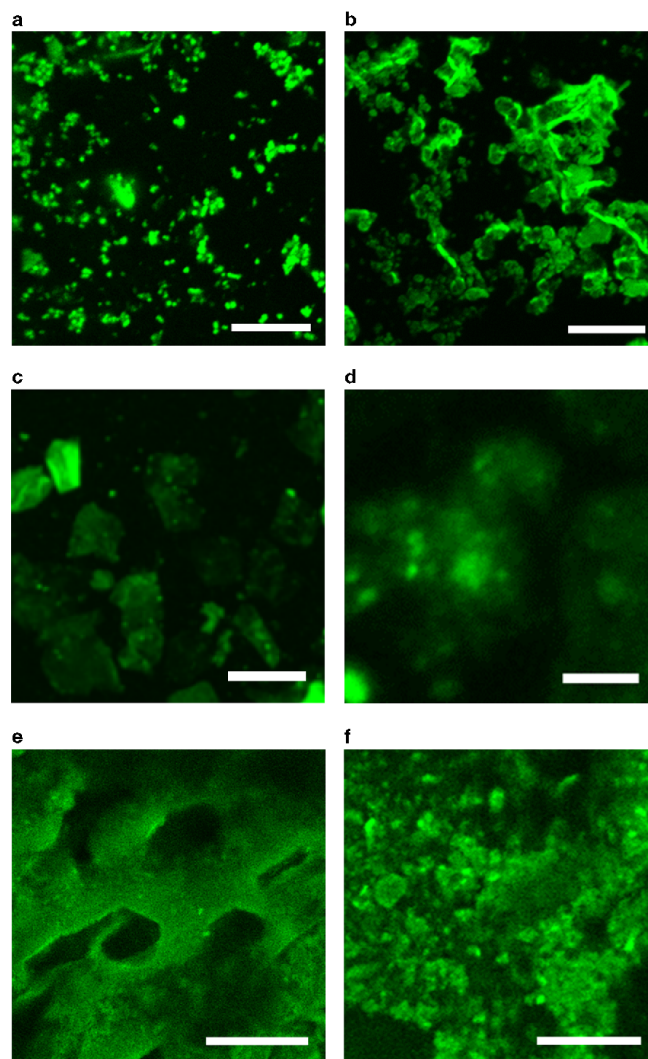


**Fig. 4** Confocal images of  $\beta$ -sheets-incorporated networks stained via ThT assay. **a, b** Hydrogels with different content of  $\beta$ -sheets from HB60 and HB360, respectively (scale bars are 5  $\mu\text{m}$ ); **c** Hydrogel with disrupted  $\beta$ -sheets within GH10 (scale bar is 50  $\mu\text{m}$ ); **d** Magnified  $\beta$ -sheets from GH10 (scale bar is 5  $\mu\text{m}$ ); **e** Cryogel with  $\beta$ -sheet from CB360 (scale bar is 50  $\mu\text{m}$ ); **f** Magnified  $\beta$ -sheets from CB360 (scale bar is 10  $\mu\text{m}$ ).

properties, particularly enhanced stiffness, are primarily driven by the rigid self-assembled  $\beta$ -sheet conformations, rather than the hydrophobicity of polypeptide grafts.

**Increased stability of networks under extreme conditions.** In addition to the improved structural integrity, the incorporation of  $\beta$ -sheets confers greater thermal stability to these networks. Thermogravimetric analysis (TGA) (Fig. 7) shows that with more intense  $\beta$ -sheet conformations, the networks (both hydrogels and cryogels) are more thermally stable, as characterised by higher

remaining fraction between 200 and 300  $^{\circ}\text{C}$ . Opposing energetic effects of enthalpically driven hydrogen bonding of  $\beta$ -sheets and entropically driven hydrophobic interactions of the isopropyl side-chain of Val residues are believed to contribute to such superb resistance to elevated thermal treatment<sup>4,56</sup>. All the networks have an onset temperature of mass loss between 150 and 200  $^{\circ}\text{C}$ , corresponding to the disintegration of initial networks. In general, the networks with more  $\beta$ -sheets start to degrade at a higher temperature, with the hydrogels synthesised from 360 mg/mL Val NCA solution displaying significant degradation at 160  $^{\circ}\text{C}$  greater than the initial network and cryogels synthesised

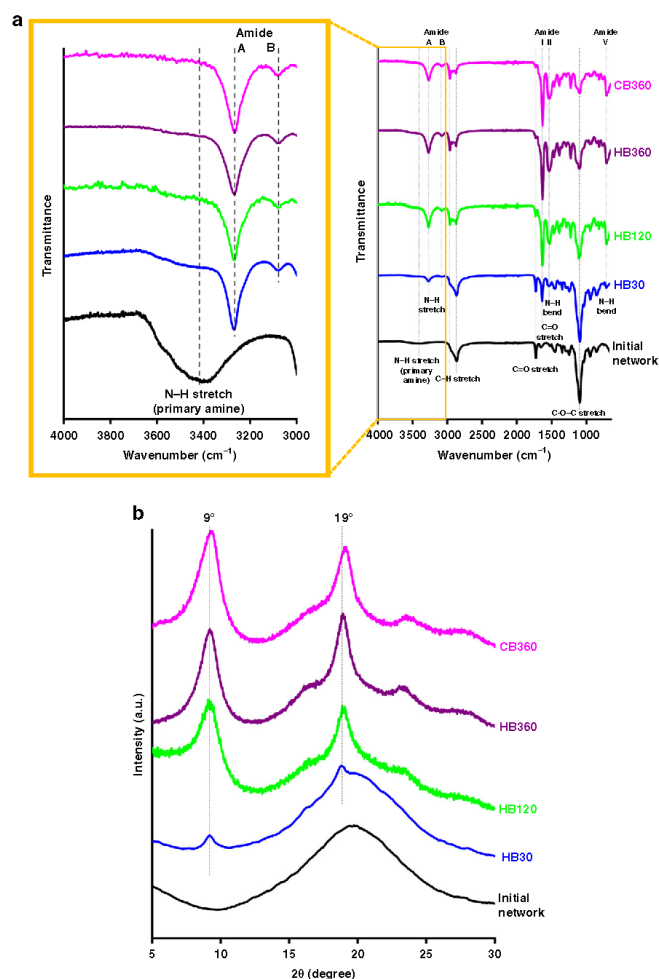


**Fig. 5** Structural characterizations of initial and  $\beta$ -sheets-incorporated networks. Networks obtained using different Val NCA monomer concentrations (HB30, HB60, HB360, CB360) indicated as the suffix of each legend. **a** ATR-FTIR with a focus on the spectrum between the  $3000\text{ cm}^{-1}$  and  $4000\text{ cm}^{-1}$ ; **b** XRD spectra.

from  $360\text{ mg/mL}$  Val NCA solution displaying significant degradation at  $40^\circ\text{C}$  greater than the initial network. A thermal degradation process atypical for hydrophobically modified networks was observed with two distinct stages, implying the hybrid structure with different phases<sup>57</sup>. In the wake of a slow mass drop, a much steeper mass loss occurred to  $\beta$ -sheet-incorporated networks from  $300$  to  $400^\circ\text{C}$ , due to the progressive decomposition of  $\beta$ -sheet crystals in this temperature range<sup>58</sup>. Once the  $\beta$ -sheet network is completely degraded, the  $\beta$ -sheet-incorporated networks follow a similar degradation profile to the respective initial networks. It is noteworthy that the multi-stage mass loss can also be ascribed to the random scission of vinylic ends, head-to-head linkages and polymer backbones in the non-uniform co-

polymeric initial network prepared by conventional free radical polymerization<sup>59</sup>.

The  $\beta$ -sheets-incorporated networks also exhibited remarkable stability at harsh pH conditions ( $2\text{ M HCl}$  and  $2\text{ M NaOH}$  solution) and in the presence of protein denaturants ( $6\text{ M GdnCl}$ ) (Fig. 8). After 4 weeks, the initial networks (hydrogels or cryogels) shrank or fell apart in strongly acidic or basic solutions whereas the  $\beta$ -sheets-rich networks remained intact. As revealed by mass loss study, a much more rapid loss was seen for the initial networks at harsh pH, due to the accelerated hydrolysis of ester groups of acrylate structures, while only a slight loss found for the  $\beta$ -sheets-rich networks under all these severe conditions, since the network architecture was stabilised by the non-covalent interactions of

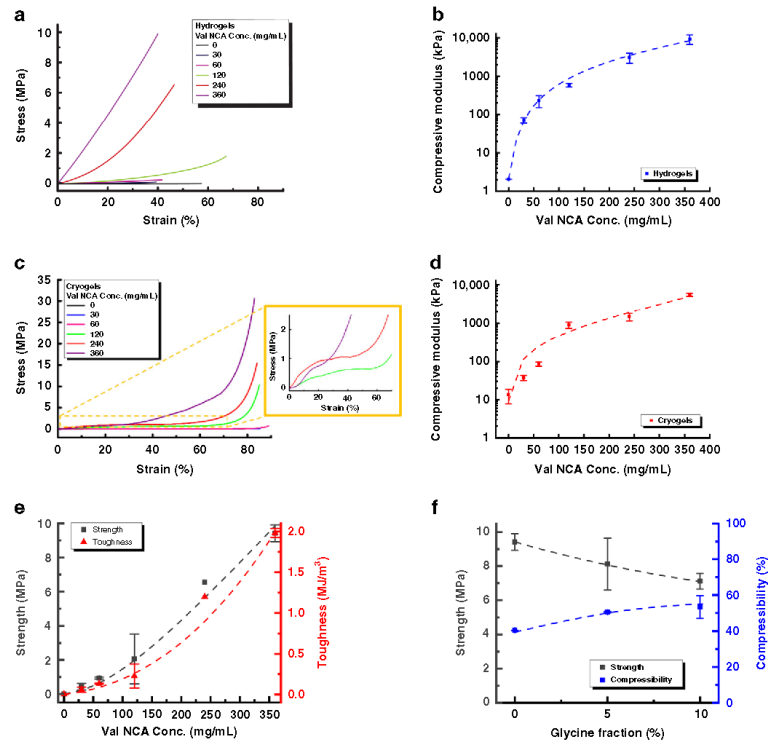


**Fig. 6 Mechanical properties summary of  $\beta$ -sheets-incorporated networks.** Networks obtained using different Val NCA monomer concentrations (0–360 mg/mL): **a, c** Compression strain-stress curves of hydrogels and cryogels respectively; **b, d** Compression moduli (stiffness) of hydrogels and cryogels respectively, as a function of Val NCA monomer concentrations; **e** Strength and toughness of hydrogels; **f** Strength and compression at break (compressibility) of hydrogels with glycine inclusion. All error bars represent standard deviation ( $n = 3$ ).

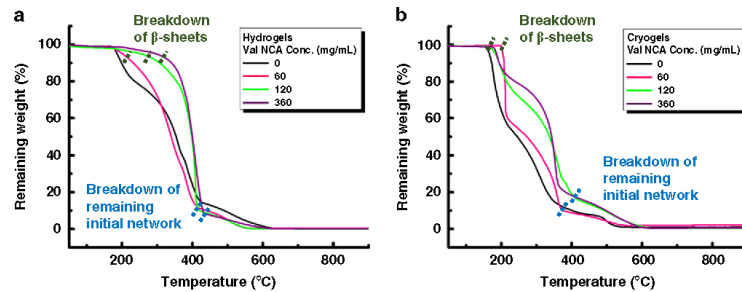


**Fig. 7 TGA analysis of the initial and  $\beta$ -sheet incorporated networks.** Networks made using different Val NCA concentrations (60, 120, 360 mg/mL): **a** hydrogels; **b** cryogels.

interpenetrated  $\beta$ -sheet clusters and the absence of ionisable groups also prevents dissociation of this secondary structure.

**Application within 3D-printed structures.** Recently, polypeptides synthesised via NCA ROP have been used as integral components of 3D-printed scaffolds<sup>60–62</sup>. Using our grafting-

from strategy,  $\beta$ -sheet regions can be loaded into 3D-printed networks, endowing them with the enhanced physical properties defined above (Fig. 9). The initial 3D-printed structure was formed using a similar formulation to the initial networks stated before with an increased solids concentration and crosslinker-to-overall monomer ratio to form a stable enough 3D-printed initial network to handle (Fig. 9c, d). As pendant

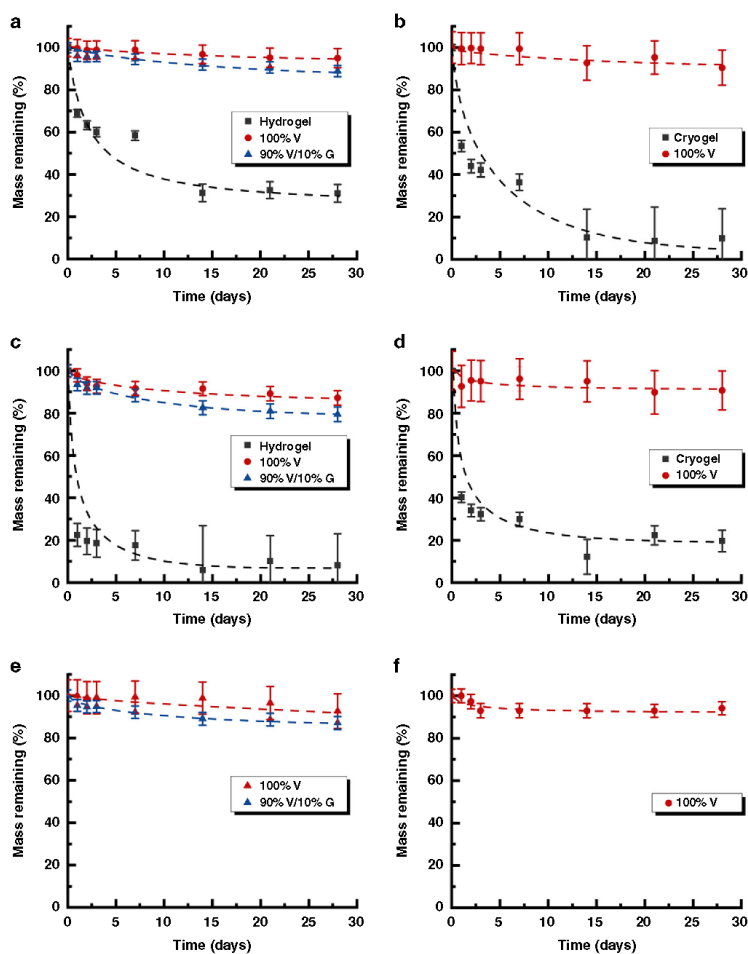


**Fig. 8** Degradation profiles of  $\beta$ -sheets-incorporated networks in harsh environments. **a, c, e** Represent hydrogel degradation while **b, d, f** represents cryogels degradation. **a, b** Were obtained in 2 M HCl; **c, d** were obtained in 2 M NaOH and (**e, f**) were obtained in 6 M GdnCl. Error bars determined by experimental error.

amines are still present in the backbone of the scaffold, the network can be easily impregnated, albeit without the noticeable change in opacity observed in the other networks (Fig. 9c, f). While the networks did not show the same obvious visual change, the networks were noticeable stiffer and stronger when handling. To confirm that NCA ROP had occurred, FTIR spectroscopy was used to compare the network before and after NCA ROP (Fig. 9g). The amide A and B bands assigned to sharp peaks at around  $3280$  and  $3085\text{ cm}^{-1}$  are only present in the networks after NCA ROP has occurred as similarly observed in the networks that were not 3D-printed (shown in Fig. 5a). The presence of these amide stretches is only possible if NCA ROP has been successfully performed with this result showing the versatility of this technique and its potential in the 3D printing space.

## Discussion

In conclusion, a strategy was developed to spatially control the growth of  $\beta$ -sheet forming polypeptides by using a soft polymeric network as an amorphous matrix to embed  $\beta$ -sheet nanocrystals within. The introduction of pendant amines into the polymer backbone of both hydrogels and cryogels to initiate guided NCA ROP allows for these  $\beta$ -sheets domains to adopt a conformation which enables these nanocrystals to be utilised effectively. This approach resulted in long chain poly(valine) grafts of up to 79 repeat units on average which would proceed to form a continuous  $\beta$ -sheet nanocrystal network. Subsequently, compressive strength was found to increase by 3 orders of magnitude up to 9.9 MPa for the hydrogels and 2 orders of magnitude up to 30 MPa for the cryogels. Furthermore, the properties of these networks can be easily tuned using glycine, with poly(valine-r-glycine)



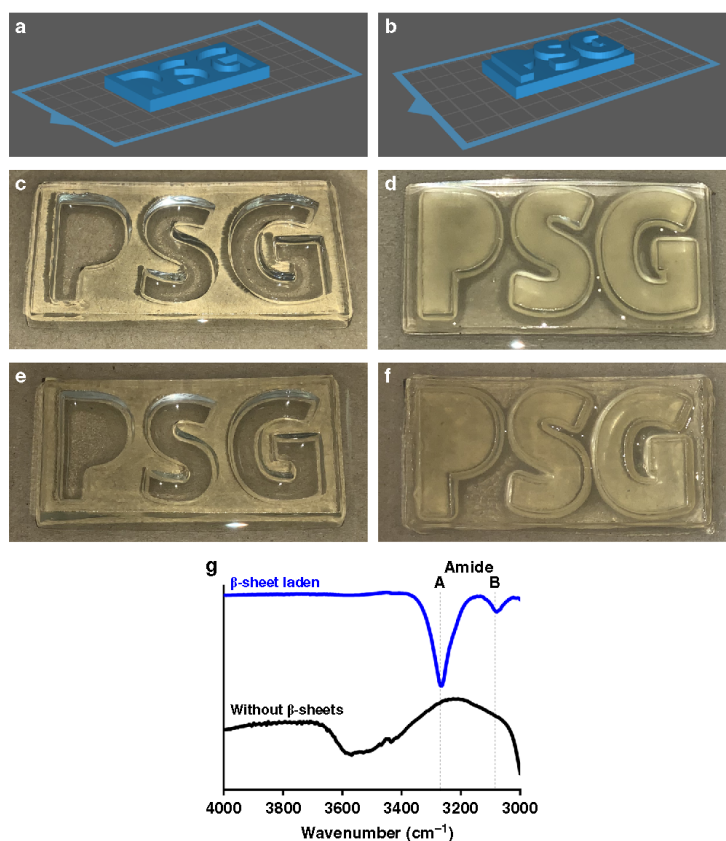


**Fig. 9** 3D-printed networks with similar chemical composition to previous hydrogels. **a, c, e** Are all based off a model printed with letters imprinted into a rectangular plate while **b, d, f** are all based off a model printed with letters protruding from a rectangular plate. **a, b** Are the original 3D models that were printed, **c, d** are the 3D-printed networks immediately after printing and **e, f** are the 3D-printed networks after NCA ROP had been performed on them. **g** ATR-FTIR of a 3D-printed network before and after NCA printing between 3000 and 4000 cm<sup>-1</sup>.

grafts introducing an increased compressibility from 40 to 60% without a significant loss in toughness. This easily employable approach provides a powerful tool in the preparation of unique hybrid networks furnished with  $\beta$ -sheets and can be further used to tune the mechanical and degradation properties in other hydrogels for biomedical functionality and materials science.

## Methods

**Materials.** L-valine ( $\geq 98\%$ ) and glycine ( $\geq 98\%$ ) were purchased from Merck and used as received. Triphosgene (98%), (+)- $\alpha$ -pinene (99%), anhydrous n-pentane ( $>99\%$ ), anhydrous N,N-Dimethylformamide (DMF) ( $>99.8\%$ ), 2-aminoethyl methacrylate hydrochloride (97%), triethylamine ( $\geq 99.5\%$ , TEA), oligo(ethylene glycol) methylether methacrylate ( $M_n = 1100$ , OEGMEMA), oligo(ethylene glycol) dimethacrylate ( $M_n = 750$ , OEGDMA), ammonium persulfate (APS,  $>98\%$ ), N, N, N', N'-Tetramethyl ethylenediamine (TEMED,  $\geq 99.5\%$ ), Diphenyl(2,4,6-trimethylbenzoyl)phosphine oxide (TPO, 97%) Thioflavin T (ThT), Guanidine hydrochloride (GdnCl,  $\geq 99\%$ ), phosphate buffered saline (PBS) tablets, protease from streptomyces griseus (Type XIV), N-(3-Dimethylaminopropyl)-N'-ethyl carbodiimide (EDCI), 4-(Dimethylamino)pyridine (DMAP,  $\geq 99\%$ ) and N, N, N', N''-pentamethyl diethylenetriamine (PMDETA, 99%) were all purchased from Sigma Aldrich and used as received. Anhydrous and deoxygenated Tetrahydrofuran (THF) (Honeywell, 99.9%, HPLC grade) was obtained by distillation from benzophenone and sodium metal under argon. AR grade hydrochloric acid

(HCl), sodium hydroxide (NaOH) and other solvents were purchased from Chem-Supply Pty. Ltd. and used without further purification. L-valine ( $\geq 98\%$ ) was purchased from Merck and used as received. Anhydrous and deoxygenated Tetrahydrofuran (THF) (Honeywell, 99.9%, HPLC grade) was obtained by distillation from benzophenone and sodium metal under argon. Deuterated chloroform ( $CDCl_3$ ) was purchased from Cambridge Isotope Laboratories and used as received. 2-((butylthio)carbonothioyl)thio)propanoic acid (TTC-1) was received from Dulux Group Australia and used as received. Methyl methacrylate (MMA, 99%, Sigma Aldrich) was de-inhibited by basic alumina prior to use.

**Synthesis of L-valine NCA (Val NCA).** L-valine NCA was synthesised using a modified procedure from previously reported literature<sup>44</sup>. Briefly, L-valine (43 mmol, 5 g) was suspended within 80 mL of anhydrous THF in a two-necked round bottom flask under argon. Triphosgene (1.2 $\times$  excess: 17 mmol, 5.1 g) was added and the mixture was continuously stirred 60 °C for 2 h or until all valine had dissolved. The reaction mixture was sparged with argon into a saturated NaOH solution for 1 h after which solvent was removed in vacuo (20 mbar, 40 °C) until equilibrium. The reduced mixture was redissolved in anhydrous 50 mL ethyl acetate which was chilled in 5 °C and then washed with saturated brine at 5 °C and 0.5 w/v % sodium bicarbonate aqueous solution at 5 °C with the organic phase being washed after separation each time. The resulting organic phase was dried using magnesium sulphate with the filtrate being reduced in vacuo (20 mbar, 50 °C) until equilibrium. The residue was recrystallised using n-pentane overnight. The resulting crystals were filtered and reprecipitated to afford a white powder (~60%

Yield),  $^1\text{H NMR}$  (400 MHz,  $\text{CDCl}_3$ ):  $\delta_{\text{H}}$  0.92 (dd, 6 H,  $\text{CH}_3$ ), 2.00–2.18 (m, 1 H, CH), 4.08 (dd, 1 H, cyclic CH), 8.84 (s, 1 H, cyclic NH).

**Synthesis of glycine NCA (Gly NCA).** Glycine NCA was synthesised using a modified procedure from previously reported literature<sup>63</sup>. Glycine (67 mmol, 5 g) was suspended within a mixture of 250 mL of anhydrous THF and 21.2 mL (+)- $\alpha$ -pinene (133 mmol) in a two-necked round bottom flask under argon. Triphosgene (1.2 $\times$  excess; 27 mmol, 7.9 g) was dissolved and added dropwise over 1.5 h while mixture was continuously stirred 70 °C and stirred for a further 1 h. The reaction mixture was sparged with argon into a saturated NaOH solution for 1 h after which the suspension was filtered and the filtrate was reduced in vacuo (20 mbar, 60 °C) until equilibrium. The resulting suspension was redissolved in THF and recrystallized using *n*-pentane overnight. The supernatant was removed and recrystallization was repeated two more times. The resulting white solid was filtered and washed with *n*-pentane (Yield 1.83 g, 27.2%).  $^1\text{H NMR}$  (400 MHz, DMSO):  $\delta_{\text{H}}$  4.33 (s, 2 H, cyclic  $\text{CH}_2$ ), 8.84 (s, 1 H, cyclic NH).

**Synthesis of initial hydrogel network.** 2-aminoethyl methacrylate hydrochloride (1.56 mmol, 258 mg) was first deprotonated with TEA (1.88 mmol, ~300  $\mu\text{L}$ ) in 20 mL of DI water overnight. The mixture was mixed with co-monomer OEGMEMA (1.04 mmol, 1.14 g) and crosslinker OEGDMA (0.87 mmol, 650 mg) and degassed with  $\text{N}_2$  for a few minutes. After addition of APS (20 mg) and TEMED (25  $\mu\text{L}$ ) (solids content ~10 w/w %, APS and TEMED 1–1.2 w/w% of solids), the solution was sonicated and separated into 1 mL batches in 3 mL syringes and allowed to stand at room temperature for 3 days. The resulting gels were swelled in DI water and washed six times to remove unreacted reactant. They were dehydrated in vacuo (20 mbar, 30 °C) for 2 days and stored in vacuo at room temperature for further use.

**Synthesis of initial cryogel networks.** The gel precursor solution was prepared and transferred to the syringes in the same procedures as described above. Then the solution in the mould was frozen at  $-18\text{ }^\circ\text{C}$  and kept at this temperature for 3 days. After thawing and being washed with water, the cryogel sample was dried and stored in vacuo for further use.

**Synthesis of  $\beta$ -sheets-incorporated networks.** The following synthesis of HB360 is used as an example of the formation of  $\beta$ -sheet incorporated networks (refer to Table 1 for full experimental conditions). Dehydrated initial hydrogel network was immersed in the anhydrous DMF (3 mL) for 2 days to achieve swelling equilibrium. The swollen network was transferred to a monomer solution (in 3 mL anhydrous DMF) containing 360 mg/mL of Val NCA. The reaction vials were sealed at room temperature under vacuum for 3 days, the network was washed with DMF (3  $\times$  3 mL) and sonicated in DMF (3 mL) for 30 min. To further remove potential non-grafted monomers/polymers, the network was then washed with THF (6  $\times$  3 mL).

**Synthesis of PMMA-grated networks.** The initial network hydrogel or cryogel was swollen in 3 mL of TTC-1 (RAFT agent) (~40 mg/mL, 0.503 mmol, 6.5 equiv. of amine groups in networks) dissolved in anhydrous DMF. EDCI (90 mg, 0.468 mmol, 6 equiv.) and DMAP (1 mg, 0.0078 mmol, 0.1 equiv.) was then added in the mixture with the reaction sealed at room temperature with occasional agitation under vacuum for 2 days to the RAFT agent. Afterwards, the network was washed with anhydrous DMF for several times to remove the free RAFT agent and remaining catalyst until the network colour did not fade. The network attached with RAFT agent was then transferred to the MMA monomer solutions (in 3 mL anhydrous DMF) at different concentrations (60, 120, 360 mg/mL) in presence of PMDETA (~5  $\mu\text{L}$ , 0.024 mmol, 0.33 equiv.). The reaction mixture was sealed and degassed using nitrogen for approximately 1 h. The UV light source ("Beaufluy-nail lamp", 220 V,  $\lambda_{\text{max}}$  ~ 365 nm, 4  $\times$  9 W) was then switched on, and the reaction mixture was left at room temperature with occasional agitation under positive N2 pressure for 3 days. A small aliquot (~100  $\mu\text{L}$ ) of the supernatant was taken for  $^1\text{H NMR}$  analysis to check monomer conversion rate, according to an established calibration curve as described below. After the reaction, the supernatant was removed, and the network was washed with DMF (3  $\times$  3 mL) and sonicated in DMF (3 mL) for 30 min. To further remove potential non-grafted monomers/polymers, the network was then washed with THF (6  $\times$  3 mL). Finally, the network was dried and stored under vacuum.

**Synthesis of 3D-printed initial networks.** 2-Aminoethyl methacrylate hydrochloride (6.00 mmol, 994 mg), co-monomer OEGMEMA (4.00 mmol, 4.40 g) and crosslinker OEGDMA (10.0 mmol, 7500 mg) were dissolved in 25.8 mL of DMF: deionised water (7:3), with TPO photoinitiator (129 mg, 1 w/w% of solids) dissolved into the solution just prior to printing. The 3D printing was performed on an ANYCUBIC Photon 3D Printer with a  $\lambda_{\text{max}}$  ~ 405 nm and a layer height of 0.5 mm, bottom layer exposure time of 120 s, bottom layer count of 8 and layer exposure time of 80 s. 3D Models were designed using Autodesk® Tinkercad and

slided using ChITuBox 3D Slicer software. The subsequent networks were then soaked in a solution of DMF (10 mL) and TEA (600  $\mu\text{L}$ ) overnight and then washed with anhydrous DMF (6  $\times$  10 mL).

**Synthesis of  $\beta$ -sheets-incorporated 3D-printed networks.** The swollen networks were transferred to vials containing 50 mL of valine NCA in anh. DMF (120 mg/mL). The vials were then sealed and agitated at room temperature under vacuum for 3 days. The resulting networks were then washed with six aliquots of DI water, followed by subsequent washing with DMF (3  $\times$  3 mL) before being sonicated in DMF (3 mL) for 30 min.

**Instrumentation.** Proton ( $^1\text{H}$ ) Nuclear Magnetic Resonance (NMR) spectroscopic analysis was performed on a Varian Unity Plus 400 MHz spectrometer using deuterated chloroform ( $\text{CDCl}_3$ ) as the solvent. Attenuated total reflection-Fourier transform infrared spectroscopy (ATR-FTIR) spectroscopy was carried out using a Bruker Tensor 27 FTIR, with GladiATR ATR attachment obtained from Pike Technologies. The FTIR was equipped with OPUS 6.5 spectroscopy software from Bruker Optik GmbH. X-ray diffraction (XRD) spectroscopy was carried out on a Bruker D8 Advance Diffractometer, using standard Ni-filtered Cu  $\text{K}\alpha$  radiation. Fluorescent images of ThT stained gel networks were acquired on a Leica TCS SP2 confocal laser scanning microscope (CLSM), using excitation wavelength of 490 nm. Scanning electron microscope (SEM) images were acquired using a FEI Quanta 200 ESEM FEG. Samples were pre-coated with gold using a Dynavac Mini Sputter Coater prior to imaging. Thermogravimetric analysis (TGA) was performed on a TGA/SDTA851e, Mettler Toledo in air with heating rate of  $10\text{ }^\circ\text{C}\cdot\text{min}^{-1}$ .

**Determination of conversion within networks.** A calibration curve was generated from  $^1\text{H NMR}$  analysis of Val NCA solutions (100  $\mu\text{L}$ ) at 5 different concentrations (15, 30, 60, 120, 180 mg/mL) diluted with  $\text{CDCl}_3$  (900  $\mu\text{L}$ ). Integration of the Val NCA doublet peak at 0.92 ppm relative to the methyl DMF signals at 2.88 ppm and 2.96 ppm determined for the 5 Val NCA concentrations, afforded a calibration curve as shown in Supplementary Fig. 6.

Thus, Val NCA conversions were determined by taking 100  $\mu\text{L}$  aliquots of reaction solutions after  $\beta$ -sheet incorporation into the networks and diluting with  $\text{CDCl}_3$  (900  $\mu\text{L}$ ). These solutions were analysed by  $^1\text{H NMR}$  by normalising against the same peaks of DMF, to determine Val NCA concentrations of each solution. This was then used to calculate the monomer conversion (as shown in Supplementary Fig. 7).

Gly NCA conversions were determined by  $^1\text{H NMR}$  integration of the cyclic amine peak at 8.84 ppm relative to the Val NCA doublet at 0.92 ppm. Thus, the amount of NCA in solution due to Gly NCA and not Val NCA could be determined (see Supplementary Fig. 8).

**Swell ratio measurement.** To measure the equilibrium swell ratio ( $Q$ ), the network was dried under heat in vacuo (60 °C, 20 mbar) for 24 h and then swollen in water until it reached equilibrium swelling. The weight of dry and fully swollen samples was determined by analytical balance and denoted as  $W_d$  and  $W_s$ , respectively. The equilibrium swell ratio ( $Q$ ) is defined by Eq. (1).

$$Q = \frac{W_s}{W_d} \quad (1)$$

**Degradation studies.** Dried networks were weighed and placed into different solutions. The vials were capped and placed into a temperature controlled orbital shaker (37 °C, 100 rpm). The samples were removed from each vial at certain time point and washed in deionised water. Then the samples were dehydrated by soaking in ethanol for 1 h followed by drying in vacuo (60 °C, 20 mbar) for 24 h. Finally, the samples were weighed, and the mass values obtained were plotted against time to obtain the degradation profiles.

**Mechanical tests.** The compressive strain-stress curves were obtained using an Instron Microtester 5848 equipped with a 2 kN static load cell and Bluehill material testing software. cylindrical hydrated network samples (diameter: ~9 mm; height: ~8.5 mm) were compressed to their maximum strain between two parallel plates at a crosshead speed of 0.1 mm/second. Engineering stresses and strains were recorded.

#### Data availability

All data that support the findings of this study are available in the Figshare repository at <https://doi.org/10.26188/5e1ff5e18580a>. Additional data for this article are available as a Supplementary Information file.

Received: 27 June 2019; Accepted: 24 February 2020;

Published online: 02 April 2020

## References

- Matsura, K., Murasato, K. & Kimizuka, N. Artificial peptide-nanospheres self-assembled from three-way junctions of  $\beta$ -sheet-forming peptides. *J. Am. Chem. Soc.* **127**, 10148–10149 (2005).
- Hartgerink, J. D., Beniash, E. & Stupp, S. I. Self-assembly and mineralization of peptide-amphiphile nanofibers. *Science* **294**, 1684–1688 (2001).
- Banwell, E. F. et al. Rational design and application of responsive  $\alpha$ -helical peptide hydrogels. *Nat. Mater.* **8**, 596–600 (2009).
- Wibowo, S. H., Sulistio, A., Wong, E. & Blenkowe, A. Functional and well-defined  $\beta$ -sheet-assembled porous spherical shells by surface-guided peptide formation. *Adv. Funct. Mater.* **25**, 3147–3156 (2015).
- Oh, K. J., Cash, K. J. & Plaxco, K. W. Beyond molecular beacons: optical sensors based on the binding-induced folding of proteins and polypeptides. *Chem. Eur. J.* **15**, 2244–2251 (2009).
- Vázquez, M. E. et al. 6-N,N-Dimethylamino-2,3-naphthalimide: a new environment-sensitive fluorescent probe in  $\delta$ - and  $\mu$ -selective opioid peptides. *J. Med. Chem.* **49**, 3653–3658 (2006).
- Noël, S. et al. Use of a new water-soluble Zn sensor to determine Zn affinity for the amyloid- $\beta$  peptide and relevant mutants. *Metalomics* **6**, 1220–1222 (2014).
- Chow, E., Ebrahimi, D., Gooding, J. J. & Hibbert, D. B. Application of N-PLS calibration to the simultaneous determination of Cu<sup>2+</sup>, Cd<sup>2+</sup> and Pb<sup>2+</sup> using peptide modified electrochemical sensors. *Analyst* **131**, 1051–1057 (2006).
- Markland, P., Zhang, Y., Amidon, G. L. & Yang, V. C. A pH- and ionic strength-responsive polypeptide hydrogel: synthesis, characterization, and preliminary protein release studies. *J. Biomed. Mater. Res.* **47**, 595–602 (1999).
- Rising, A. & Johansson, J. Toward spinning artificial spider silk. *Nat. Chem. Biol.* **11**, 309–315 (2015).
- Arnott, S., Dover, S. D. & Elliott, A. Structure of  $\beta$ -poly-L-alanine: refined atomic co-ordinates for an anti-parallel beta-pleated sheet. *J. Mol. Biol.* **30**, 201–208 (1967).
- Smith, C. K., Withka, J. M. & Regan, L. A thermodynamic scale for the  $\beta$ -sheet forming tendencies of the amino acids. *Biochemistry* **33**, 5510–5517 (1994).
- Keten, S., Xu, Z., Ihle, B. & Buehler, M. J. Nanoconfinement controls stiffness, strength and mechanical toughness of  $\beta$ -sheet crystals in silk. *Nat. Mater.* **9**, 359–367 (2010).
- Wibowo, S. H., Sulistio, A., Wong, E. H. H., Blenkowe, A. & Qiao, G. G. Tailoring substrate hydrophilicity using grafted polypeptide nanocoatings. *Aust. J. Chem.* **67**, 598–602 (2014).
- Rathore, O. & Sogah, D. Y. Self-assembly of  $\beta$ -sheets into nanostructures by poly(alanine) segments incorporated in multiblock copolymers inspired by spider silk. *J. Am. Chem. Soc.* **123**, 5231–5239 (2001).
- Ortony, J. H. et al. Internal dynamics of a supramolecular nanofiber. *Nat. Mater.* **13**, 812–816 (2014).
- Ling, S. et al. Polymorphic regenerated silk fibers assembled through bioinspired spinning. *Nat. Commun.* **8**, 1387 (2017).
- Peng, Q., Shao, H., Hu, X. & Zhang, Y. Role of humidity on the structures and properties of regenerated silk fibers. *Prog. Nat. Sci.: Mater. Int.* **25**, 430–436 (2015).
- Marsano, E. et al. Wet spinning of Bombyx mori silk fibroin dissolved in N-methyl morpholine N-oxide and properties of regenerated fibres. *Int. J. Biol. Macromol.* **37**, 179–188 (2005).
- Schafer-Nolte, F. et al. Biomechanics and biocompatibility of woven spider silk meshes during remodeling in a rodent fascia replacement model. *Ann. Surg.* **259**, 781–792 (2014).
- Kim, S., Kim, J. H., Lee, J. S. & Park, C. B. Beta-sheet-forming, self-assembled peptide nanomaterials towards optical, energy, and healthcare applications. *Small* **11**, 3623–3640 (2015).
- De Leon Rodriguez, L. M., Hemar, Y., Cornish, J. & Brimble, M. A. Structure-mechanical property correlations of hydrogel forming  $\beta$ -sheet peptides. *Chem. Soc. Rev.* **45**, 4797–4824 (2016).
- Xia, X.-X., Xu, Q., Hu, X., Qin, G. & Kaplan, D. L. Tunable self-assembly of genetically engineered silk-elastin-like protein polymers. *Biomacromolecules* **12**, 3844–3850 (2011).
- Greish, K. et al. Silk-elastinlike protein polymer hydrogels for localized adenoviral gene therapy of head and neck tumors. *Biomacromolecules* **10**, 2183–2188 (2009).
- Dinerman, A. A., Cappello, J., Ghandehari, H. & Hoag, S. W. Swelling behavior of a genetically engineered silk-elastinlike protein polymer hydrogel. *Biomaterials* **23**, 4203–4210 (2002).
- Wu, H., Zhou, T., Tian, L., Xia, Z. & Xu, P. Self-assembling RADA16-I peptide hydrogel scaffold loaded with tamoxifen for breast reconstruction. *BioMed. Res. Int.* **2017**, 3656193 (2017).
- Wu, X. et al. Functional self-assembling peptide nanofiber hydrogel for peripheral nerve regeneration. *Regenerative Biomater.* **4**, 21–30 (2017).
- Salick, D. A., Kretsinger, J. K., Pochan, D. J. & Schneider, J. P. Inherent antibacterial activity of a peptide-based  $\beta$ -hairpin hydrogel. *J. Am. Chem. Soc.* **129**, 14793–14799 (2007).
- Kretsinger, J. K., Haines, L. A., Ozbas, B., Pochan, D. J. & Schneider, J. P. Cytocompatibility of self-assembled  $\beta$ -hairpin peptide hydrogel surfaces. *Biomaterials* **26**, 5177–5186 (2005).
- Huang, J. et al. Supramolecular hydrogels with reverse thermal gelation properties from (Oligo)tyrosine containing block copolymers. *Biomacromolecules* **14**, 200–206 (2013).
- Nowak, A. P. et al. Rapidly recovering hydrogel scaffolds from self-assembling diblock copolypeptide amphiphiles. *Nature* **417**, 424–428 (2002).
- Nowak, A. P., Breedveld, V., Pine, D. J. & Deming, T. J. Unusual salt stability in highly charged diblock co-polypeptide hydrogels. *J. Am. Chem. Soc.* **125**, 15666–15670 (2003).
- Zhang, S., Alvarez, D. J., Sofroniew, M. V. & Deming, T. J. Design and synthesis of nonionic copolypeptide hydrogels with reversible thermoresponsive and tunable physical properties. *Biomacromolecules* **16**, 1331–1340 (2015).
- Zou, J. et al. Responsive organogels formed by supramolecular self assembly of PEG-block-allyl-functionalized racemic polypeptides into  $\beta$ -sheet-driven polymeric ribbons. *Soft Matter* **9**, 5951–5958 (2013).
- Thornton, P. D., Billah, S. M. R. & Cameron, N. R. Enzyme-degradable self-assembled hydrogels from polyalanine-modified poly(ethylene glycol) star polymers. *Macromol. Rapid Commun.* **34**, 257–262 (2013).
- Lam, S. J. et al. Combating multidrug-resistant Gram-negative bacteria with structurally nanoengineered antimicrobial peptide polymers. *Nat. Microbiol.* **1**, 16162 (2016).
- Goh, S. L., Platt, A. P., Rutledge, K. E. & Lee, I. Synthesis and aggregation of poly(valine)-poly(ethylene glycol) block copolymers. *J. Polym. Sci. Part A Polym. Chem.* **46**, 5381–5389 (2008).
- Drumheller, P. D. & Hubbell, J. A. Polymer networks with grafted cell adhesion peptides for highly biospecific cell adhesive substrates. *Anal. Biochem.* **222**, 380–388 (1994).
- Drumheller, P. D., Elbert, D. L. & Hubbell, J. A. Multifunctional poly(ethylene glycol) semi-interpenetrating polymer networks as highly selective adhesive substrates for bioadhesive peptide grafting. *Biotechnol. Bioeng.* **43**, 772–780 (1994).
- Clarke, D. E., Pashuck, E. T., Bertazzo, S., Weaver, J. V. M. & Stevens, M. M. Self-Healing, self-assembled  $\beta$ -sheet peptide-poly( $\gamma$ -glutamic acid) hybrid hydrogels. *J. Am. Chem. Soc.* **139**, 7250–7255 (2017).
- Vanhalbe, M., Cornillie, S., Smet, M., Van Puyvelde, P. & Goderis, B. Poly(alanine): structure and stability of the d and l-enantiomers. *Biomacromolecules* **17**, 183–191 (2016).
- Fujie, A., Komoto, T., Oya, M. & Kawai, T. Crystallization of polypeptides in the course of polymerization, III. Further studies on the growth mechanisms of poly(L-alanine). *Cryst. Die Makromol. Chem.* **169**, 301–321 (1973).
- Yang, A.-S. & Honig, B. Free energy determinants of secondary structure formation: I.  $\alpha$ -helices. *J. Mol. Biol.* **252**, 351–365 (1995).
- Shirbin, S. J., Karimi, F., Chan, N. J.-A., Heath, D. E. & Qiao, G. G. Macroporous hydrogels composed entirely of synthetic polypeptides: biocompatible and enzyme biodegradable 3D cellular scaffolds. *Biomacromolecules* **17**, 2981–2991 (2016).
- Lifson, S. & Sander, C. Antiparallel and parallel  $\beta$ -strands differ in amino acid residue preferences. *Nature* **282**, 109–111 (1979).
- Noël, S., Cadet, S., Gras, E. & Hureau, C. The benzazole scaffold: a SWAT to combat Alzheimer's disease. *Chem. Soc. Rev.* **42**, 7747–7762 (2013).
- Biancalana, M., Makabe, K., Koide, A. & Koide, S. Molecular mechanism of thioflavin-T binding to the surface of  $\beta$ -rich peptide self-assemblies. *J. Mol. Biol.* **385**, 1052–1063 (2009).
- Zhang, Y. P., Lewis, R. N. A. H., Hodges, R. S. & McElhaney, R. N. FTIR spectroscopic studies of the conformation and amide hydrogen exchange of a peptide model of the hydrophobic transmembrane  $\alpha$ -helices of membrane proteins. *Biochemistry* **31**, 11572–11578 (1992).
- Miyazawa, T. & Blout, E. R. The infrared spectra of polypeptides in various conformations: amide I and II bands. *J. Am. Chem. Soc.* **83**, 712–719 (1961).
- Miyazawa, T., Masuda, Y. & Fukushima, K. Chain conformation and amide V band of polypeptides. *J. Polym. Sci.* **62**, S62–S64 (1962).
- El Khoury, Y., Hielscher, R., Voicescu, M., Gross, J. & Hellwig, P. On the specificity of the amide VI band for the secondary structure of proteins. *Vibrational Spectrosc.* **55**, 258–266 (2011).
- Rösler, A., Klok, H.-A., Hamley, I. W., Castelletto, V. & Mykhaylyk, O. O. Nanoscale structure of poly(ethylene glycol) hybrid block copolymers containing amphiphilic  $\beta$ -strand peptide sequences. *Biomacromolecules* **4**, 859–863 (2003).
- Gu, D., Tan, S., Xu, C., O'Connor, A. J. & Qiao, G. G. Engineering tough, highly compressible, biodegradable hydrogels by tuning the network architecture. *Chem. Commun.* **53**, 6756–6759 (2017).

54. Zhang, C., Aung, A., Liao, L. & Varghese, S. A novel single precursor-based biodegradable hydrogel with enhanced mechanical properties. *Soft Matter* **5**, 3831–3834 (2009).
55. Cui, J., Lackey, M. A., Tew, G. N. & Crosby, A. J. Mechanical properties of end-linked PEG/PDMS hydrogels. *Macromolecules* **45**, 6104–6110 (2012).
56. Hartgerink, J. D., Granja, J. R., Milligan, R. A. & Ghadiri, M. R. Self-assembling peptide nanotubes. *J. Am. Chem. Soc.* **118**, 43–50 (1996).
57. Rusu, A. G., Popa, M. I., Lisa, G. & Vereștiuc, L. Thermal behavior of hydrophobically modified hydrogels using TGA/FTIR/MS analysis technique. *Thermochim. Acta* **613**, 28–40 (2015).
58. Cho, S. Y. et al. Carbonization of a stable  $\beta$ -sheet-rich silk protein into a pseudographitic pyroprotein. *Nat. Commun.* **6**, 7145 (2015).
59. Kavitha, A. A. & Singha, N. K. “Click Chemistry” in tailor-made polymethacrylates bearing reactive furfuryl functionality: a new class of self-healing polymeric material. *ACS Appl. Mater. Interfaces* **1**, 1427–1436 (2009).
60. Li, C. et al. Rapid formation of a supramolecular polypeptide–DNA hydrogel for in situ three-dimensional multilayer bioprinting. *Angew. Chem. Int. Ed.* **54**, 3957–3961 (2015).
61. Murphy, R. et al. Degradable 3D-printed hydrogels based on star-shaped copolypeptides. *Biomacromolecules* **19**, 2691–2699 (2018).
62. Murphy, R. D., Kimmins, S., Hibbitts, A. J. & Heise, A. 3D-extrusion printing of stable constructs composed of photoresponsive polypeptide hydrogels. *Polym. Chem.* **10**, 4675–4682 (2019).
63. Skoulas, D., Stavroulaki, D., Santorinaios, K. & Iatrou, H. Synthesis of hybrid-polypeptides m-PEO-b-poly (His-co-Gly) and m-PEO-b-poly (His-co-Ala) and study of their structure and aggregation. influence of hydrophobic copolypeptides on the properties of poly (L-histidine). *Polymers* **9**, 564 (2017).

### Acknowledgements

This work was performed in part at the Materials Characterization and Fabrication Platform (MCFP) at the University of Melbourne. N.J.C. thanks The University of Melbourne for providing Australian Government Research Training Program Scholarship (AGRTP). D.G. thanks The University of Melbourne for providing Melbourne International Research Scholarships (MIRS). The authors would also like to thank Dr. Ke Xie and Mr. Min Liu for assistance with SEM measurements. We are also grateful to the Particulate Fluids Processing Centre (PFPC) for infrastructure support.

### Author contributions

N.J.C., D.G., S.T. and Q.F. established the reaction conditions of hydrogels and cryogels. N.J.C. performed the work introducing a new monomer into the system. S.T.

and D.G. proposed the characterisation framework. N.J.C. and D.G. prepared samples and characterised the networks. N.J.C. and T.G.P. established the reaction conditions for the 3D-printed networks and subsequent characterisation. G.G.Q. and A.J.O. both supervised the project. N.J.C., D.G., S.T., Q.F. and G.G.Q. wrote the manuscript.

### Competing interests

The authors declare no competing interests.

### Additional information

Supplementary information is available for this paper at <https://doi.org/10.1038/s41467-020-15312-x>.

Correspondence and requests for materials should be addressed to G.G.Q.

Peer review information *Nature Communications* thanks Paul Thornton and the other anonymous reviewer(s) for their contribution to the peer review of this work. Peer reviewer reports are available.

Reprints and permission information is available at <http://www.nature.com/reprints>

Publisher's note Springer Nature remains neutral with regard to jurisdictional claims in published maps and institutional affiliations.



**Open Access** This article is licensed under a Creative Commons Attribution 4.0 International License, which permits use, sharing, adaptation, distribution and reproduction in any medium or format, as long as you give appropriate credit to the original author(s) and the source, provide a link to the Creative Commons license, and indicate if changes were made. The images or other third party material in this article are included in the article's Creative Commons license, unless indicated otherwise in a credit line to the material. If material is not included in the article's Creative Commons license and your intended use is not permitted by statutory regulation or exceeds the permitted use, you will need to obtain permission directly from the copyright holder. To view a copy of this license, visit <http://creativecommons.org/licenses/by/4.0/>.

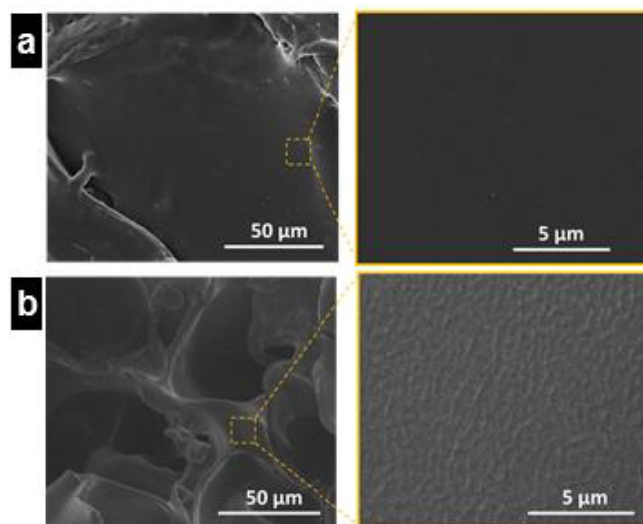
© The Author(s) 2020

## 2.3. Supporting Information

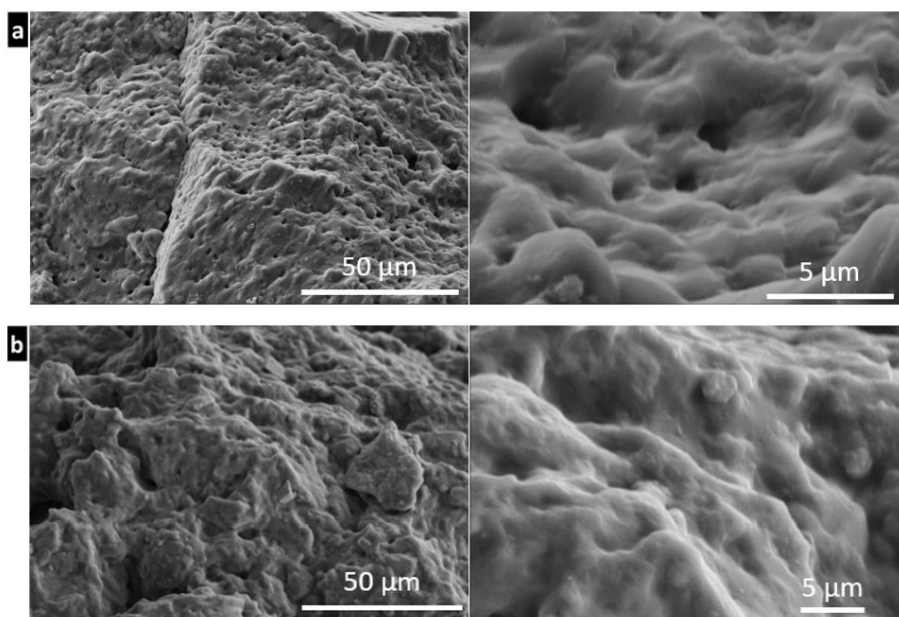
### **Supplementary Information**

**Spider-silk inspired polymeric networks by harnessing the mechanical potential of  $\beta$ -sheets through network guided assembly**

Nicholas Jun-An Chan, et al.

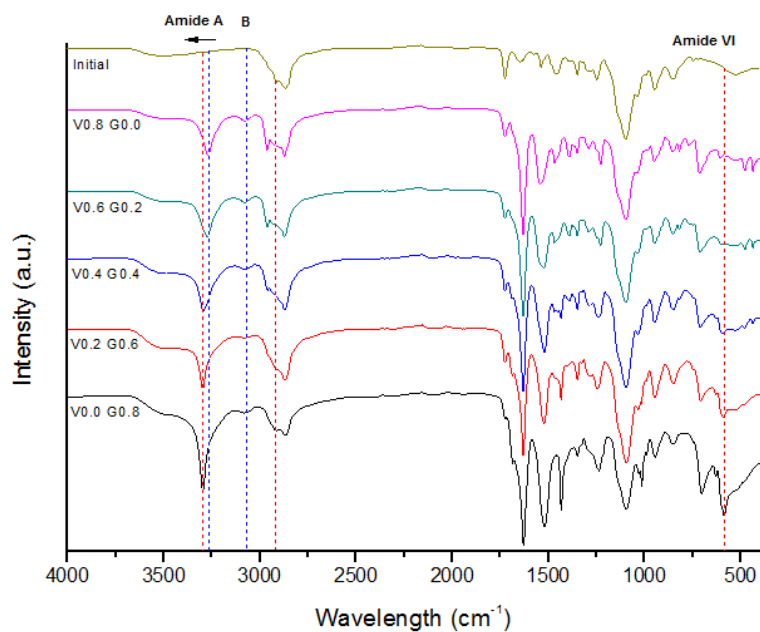


**Supplementary Figure 1.** SEM cross-sectional images of initial networks at various magnifications (from left to right, scale bars are 50 μm, 5 μm with increasing magnification) with different morphologies showing **(a)** hydrogel and **(b)** cryogels.

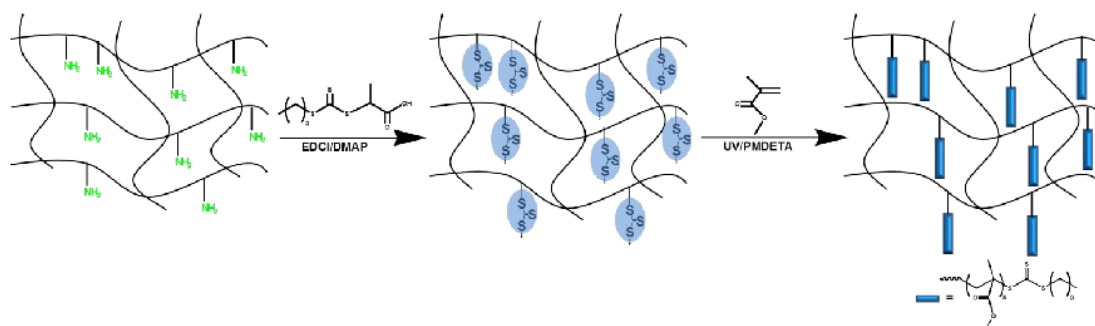


**Supplementary Figure 2.** SEM cross-sectional images of  $\beta$ -sheets incorporated hydrogel networks at various magnifications (from left to right, scale bars are 50  $\mu\text{m}$ , 5  $\mu\text{m}$  with increasing magnification): **(a)** 50:50 valine to glycine monomer at 0.8M ( $\sim$ 120 mg/mL of val NCA); **(b)** glycine 100% 0.8M.



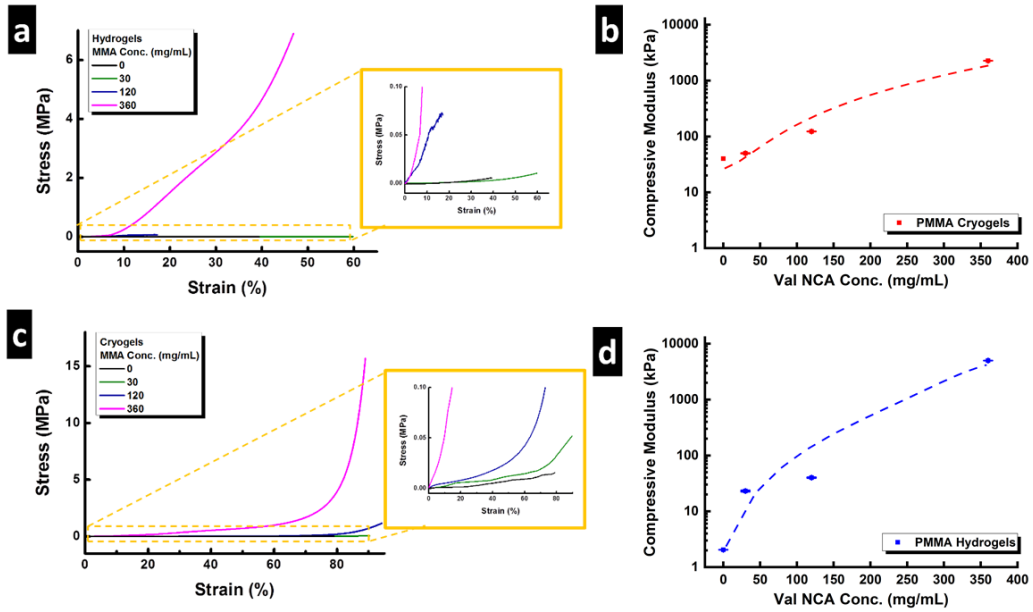


**Supplementary Figure 3.** ATR-FTIR Spectra showing characterizations of initial network and  $\beta$ -sheet ( $400 - 4000 \text{ cm}^{-1}$ ) incorporated final networks obtained using different glycine concentrations at a constant monomer molar concentration (0.8M)

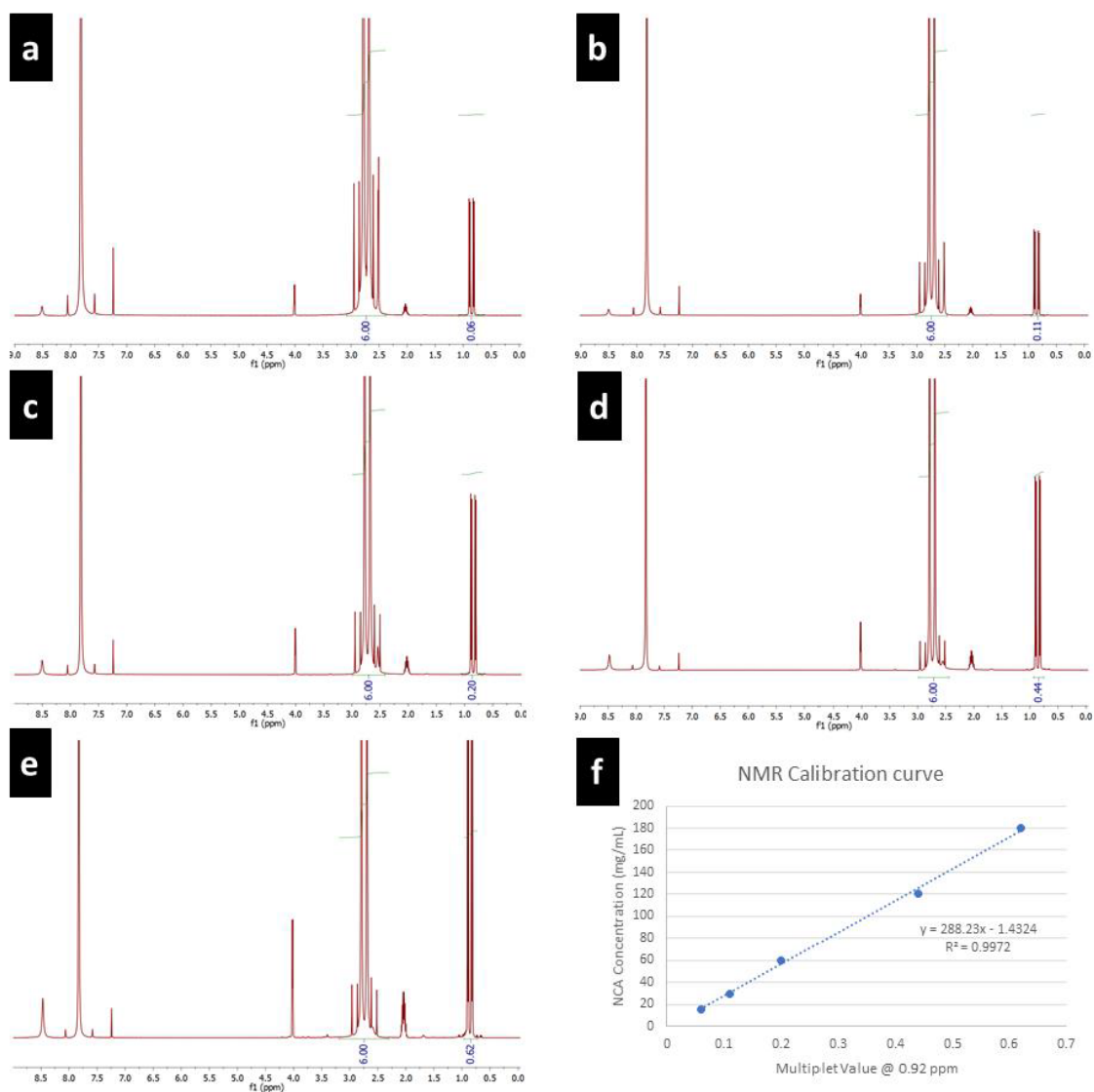


**Supplementary Figure 4.** Preparation of PMMA-grafted networks (hydrogels & cryogels) through functionalization of initial network with trithiocarbonate initiators (TTC); ii) insertion of PMMA chains via UV-initiated RAFT polymerization based on the attached TTC initiators, in the presence of MMA monomers at three different concentrations (30, 120, and 360 mg/mL).

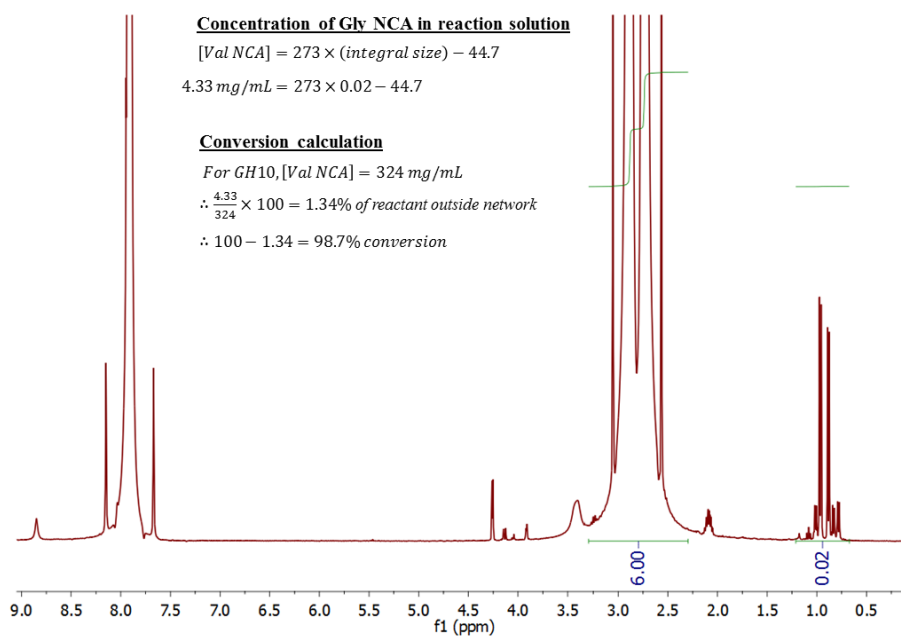




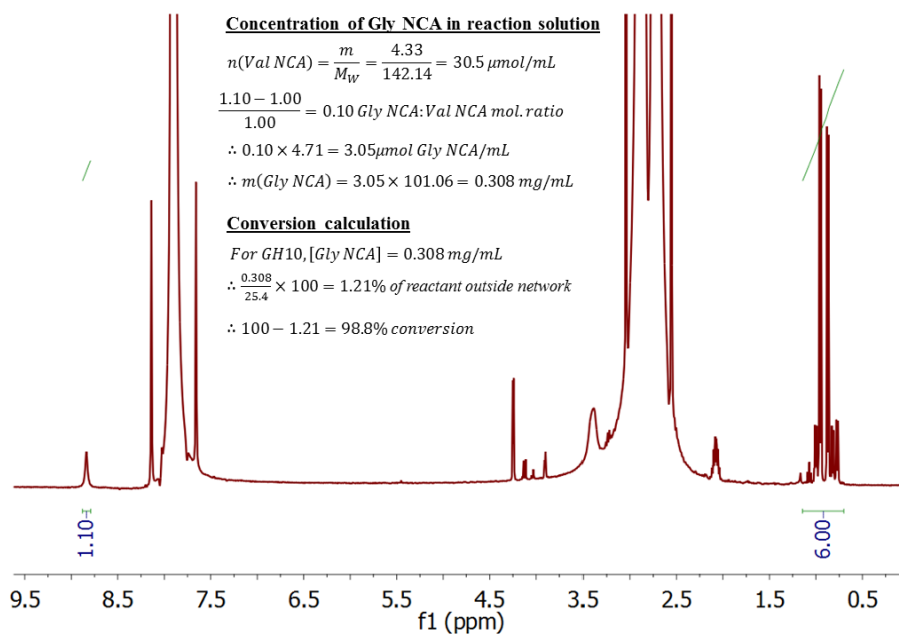
**Supplementary Figure 5 (a) & (c)** Compression strain-stress curves of PMMA grafted networks, hydrogels and cryogels respectively, prepared with different MMA concentrations (30, 120, and 360 mg/mL); **(b) & (d)** compression moduli (stiffness) of PMMA grafted networks vs. those of  $\beta$ -sheets incorporated counterparts, hydrogels and cryogels respectively, as a function of corresponding monomer concentrations. Error bars determined by experimental error.



**Supplementary Figure 6:**  $\text{H}^1$  NMR spectra for (a) 15, (b) 30, (c) 60, (d) 120 and (e) 180 mg/mL of Val NCA in DMF with integral of the Val NCA doublet at 0.92 ppm analysed using the two singlets at 2.88 ppm and 2.96 ppm of the two methyl groups from DMF being used to normalize these integrals. (f) Val NCA concentration plotted against value of the integral at 0.92 ppm.



**Supplementary Figure 7:**  $^1H$  NMR spectrum of GH10 reaction solution and calculation of conversion of Val NCA in GH10



**Supplementary Figure 8:**  $^1\text{H}$  NMR spectrum of GH10 reaction solution and calculation of conversion of Gly NCA in GH10

## ***Chapter 3:***

# **Crosslinked Polypeptide Films via RAFT-Mediated Continuous Assembly of Polymers**

---

### 3.1. Chapter Perspectives

The structure of polypeptide-based films and surfaces dictates their properties, functionality and subsequent applications and, thus, control of this morphology is imperative. Traditionally polymer-based films are based on the deposition of the polymer on the surface and subsequent evaporation of solvent. NCA ROP further allows the use of polymerization methods, resulting in the covalent bonding of polypeptides to functionalized surfaces and a unique brush morphology where the polymer chain is perpendicular to the surface. Additionally, other morphologies are available using this technique such as chemically crosslinked films formed through the continuous assembly of polymers (CAP). Such molecular morphologies are expected to impact both the secondary structures and nanostructures within the material, though the impact of CAP on polypeptide films has yet to be investigated.

This chapter reports the development of polypeptide films using reversible addition–fragmentation chain-transfer (RAFT) mediated CAP. Poly(L-lysine) modified with methacrylated side chains (PLLMA) films was utilized to form films. Multiple different parameters were tested and optimized, resulting in films with a thickness of  $94.9 \pm 8.2$  nm after multiple applications of the technique. Secondary structure analysis found increased random coil content compared to others poly(L-lysine) films. The versatility of the technique was found using poly(L-glutamate) (PLGMA)-based films, which also produced an increased random coil content.

This chapter has produced a research article in *Angewandte Chemie International Edition*, published on 3.12.2021 (<https://doi.org/10.1002/anie.202112842>). In this paper, I was responsible for developing and optimizing film synthesis.

**Polypeptide Films**
How to cite: *Angew. Chem. Int. Ed.* **2022**, *61*, e202112842

International Edition: doi.org/10.1002/anie.202112842

German Edition: doi.org/10.1002/ange.202112842

## Crosslinked Polypeptide Films via RAFT-Mediated Continuous Assembly of Polymers

Nicholas J. Chan, Sarah Lentz, Paul A. Gurr, Shereen Tan, Thomas Scheibel,\* and Greg G. Qiao\*

**Abstract:** Polypeptide coatings are a cornerstone in the field of surface modification due to their widespread biological potential. As their properties are dictated by their structural features, subsequent control thereof using unique fabrication strategies is important. Herein, we report a facile method of precisely creating densely crosslinked polypeptide films with unusually high random coil content through continuous assembly polymerization via reversible addition–fragmentation chain transfer (CAP-RAFT). CAP-RAFT was fundamentally investigated using methacrylated poly-L-lysine (PLLMA) and methacrylated poly-L-glutamic acid (PLGMA). Careful technique refinement resulted in films up to  $36.1 \pm 1.1$  nm thick which could be increased to  $94.9 \pm 8.2$  nm after using this strategy multiple times. PLLMA and PLGMA films were found to have 30–50% random coil conformations. Degradation by enzymes present during wound healing reveals potential for applications in drug delivery and tissue engineering.

### Introduction

For decades, scientists have been deeply fascinated in surface modification via the introduction of synthetic polypeptides for a wide range of applications including biosensing,<sup>[1]</sup> active molecule release<sup>[2]</sup> and antibiofouling/antimicrobial applications.<sup>[3]</sup> Polypeptides can be designed to bear application specific chemical and physical properties which largely is afforded by their ability to fold into different well-defined conformations known as secondary structures based on their specific amino acid sequence.<sup>[4]</sup> Thus, the design and manipulation of secondary structures (e.g.

$\alpha$ -helices,  $\beta$ -sheets, random coils) forms a core directive for material scientists.<sup>[5]</sup> While conventional techniques for coatings and film formation are well established, synthetic polypeptides formed through *N*-carboxyanhydride ring-opening polymerization (NCA ROP) offers the opportunity to lean into grafting polymerization techniques for the fabrication of polypeptide films.<sup>[6]</sup> Grafting-to and grafting-from strategies both result in linear polymers with a terminal group anchored to the surface.<sup>[7]</sup> However, films formed through grafting-to techniques tend to be limited by steric hindrance associated with tethering a large molecule to a surface, while films fabricated through a grafting-from approach are difficult to characterize after more than one monomer is introduced to the system.<sup>[7]</sup> Grafting-through strategies aim to mitigate these issues, by using macromonomers with polymerizable end groups, instead of monofunctional monomers resulting in thicker films with well-defined polymer bottlebrushes.<sup>[8a,8]</sup> With all the advantages that result from using grafting-through methods, our group has developed a unique methodology, which yields unique, robust, crosslinked films, called continuous assembly polymerization (CAP).<sup>[9]</sup>

As with grafting-through techniques, CAP utilizes polymers with a polymerizable group, but unlike traditional grafting-through techniques, these polymerizable groups are not restricted to a singular endgroup resulting in a macrocrosslinker.<sup>[10]</sup> The result is a dense crosslinked polymeric network forming a robust film on the substrate surface with often a unique morphology, compared to even traditional grafting through methods. The technique itself is robust enough that multiple other macrocrosslinkers have already been utilized using this technique such as polyethylene glycol (PEG)-based,<sup>[11]</sup> 2-hydroxyethylacrylate (HEA)-based,<sup>[9a,c]</sup> and polythiophene<sup>[12]</sup> polymers. Uniquely, this can be combined with macrocrosslinkers which already bear unique morphologies. For example, polyrotaxane-based macrocrosslinkers have been utilized to afford a film with the densely crosslinked nature of CAP films, along with the stimuli sensitivity associated with the “host–guest” chemistry of a cyclodextrin-based polyrotaxane network.<sup>[13]</sup> The unique morphology afforded through CAP and the wide variety of macrocrosslinkers amenable to this process has enabled the synthesis of a range of films targeting a variety of different applications.<sup>[10a,11a]</sup> Antifogging qualities of a PEG-based film have been shown using this technique after exposure of the film at  $-20$  °C to ambient conditions, and films retained high light transmittance with a relatively low crosslinking density.<sup>[11b]</sup> However, despite the aforemen-

[\*] N. J. Chan, S. Lentz, P. A. Gurr, S. Tan, G. G. Qiao  
Polymer Science Group, Department of Chemical Engineering  
University of Melbourne  
Parkville, Melbourne, Victoria 3010 (Australia)  
E-mail: gregghq@unimelb.edu.au

N. J. Chan, S. Lentz, T. Scheibel  
Lehrstuhl Biomaterialien  
Universität Bayreuth  
Prof.-Rüdiger-Bormann-Str. 1, 95447 Bayreuth (Germany)  
E-mail: thomas.scheibel@uni-bayreuth.de

© 2021 The Authors. Angewandte Chemie International Edition published by Wiley-VCH GmbH. This is an open access article under the terms of the Creative Commons Attribution Non-Commercial License, which permits use, distribution and reproduction in any medium, provided the original work is properly cited and is not used for commercial purposes.

tioned versatility of polypeptides, they have yet to be utilized with this technique. In parallel to the established library of crosslinkers is the variety of techniques for CAP, which have since been established including various fabrication conditions.<sup>[9a]</sup> Recently a unique patterning method has been developed employing CAP through microcontact printing which involves delivering material via a polymeric stamp.<sup>[14]</sup> Alongside these advances, the development of CAP includes different polymerization methods such as ring-opening metathesis polymerization (ROMP)<sup>[12,13]</sup> and atom transfer radical polymerization (ATRP).<sup>[11]</sup> Fundamentally, the method of polymerization utilized impacts film properties due to the mechanistic differences and as such developing CAP using different polymerization techniques is of profound interest. A blue-light mediated system employed a thiocarbamate as a photoiniferter, but the film thickness's being limited to approximately 5 nm.<sup>[9a]</sup> It is this variability in properties that highlights the need for investigating, the as yet unreported, reversible addition–fragmentation chain transfer (RAFT) polymerization as a CAP technique.

RAFT is identified as one of the most robust and versatile reversible-deactivation radical polymerization techniques.<sup>[15]</sup> In a RAFT polymerization system, polymerization is controlled by the degenerative chain transfer of the chain transfer agent (CTA) in the form of a thiocarbonylthio compound (known as a RAFT agent) to the polymer chains, leading to the sequential insertion of monomer units to the initial RAFT agent.<sup>[15d,16]</sup> As initiation is still free-radical based, there are numerous approaches to RAFT polymerization including initiation through enzymes, thermal initiators or acoustic cavitation of bubbles in the system via ultrasound. However, for a surface-initiated polymerization, light-based RAFT techniques provide a facile method of yielding grafted polymers.<sup>[7c,17]</sup> Using our already developed techniques in both RAFT polymerization<sup>[18]</sup> and NCA ROP,<sup>[19]</sup> we aim to further develop the potential of CAP-RAFT while fabricating polypeptide-based films with secondary structure morphologies based on a fabrication technique rather than solely on polypeptide structure.

Herein, we expand on this film formation strategy, to perform blue light-mediated CAP-RAFT using synthetic polypeptide based macrocrosslinkers. This is the first instance of fabricating a chemically crosslinked NCA ROP/based polypeptide film with precision control of thickness in one-step, controlled multilayer structures with designed composition and specifically formed peptide secondary structure resulting from the fabrication technique itself rather than solely on the polypeptide structure. Photoinitiator lithium phenyl-2,4,6-trimethylbenzoylphosphinate (LAP) was used in conjunction with two different model RAFT agents. A dithiobenzoate and a trithiocarbonate with differing kinetics were chosen to investigate their influence on the ability to form thick uniform films. Furthermore, we investigated the importance of RAFT agent in solution, which historically has been required to develop films of uniform thickness and its effects on both kinetics and uniformity. In furthering this work, we also explored the ability to produce stratified, multi-layered cross-linked films

by coupling RAFT agent to the initiating surface to re-initiate the CAP-RAFT process at the growing polymer surface. As a demonstration of versatility, a second polypeptide based macrocrosslinker was introduced into the system. In both cases, an unusually high random coil conformation was produced which, combined with the evident enzymatic degradation demonstrated, presents unique opportunities in drug delivery and tissue engineering.

## Results and Discussion

Polypeptide macroinitiators were synthesized through NCA ROP, subsequent deprotection and methacrylation (Supporting Information Figure S1, S2). NCA ROP is known to be a facile method for creating long chain, non-sequence specific polypeptides.<sup>[4b,20]</sup> With a selection of 21 canonical amino acids with varying degrees of hydrophobicity, physical properties and chemical functionality, it makes them a highly versatile polymer class for a wide range of applications.<sup>[20b,21]</sup> To synthesize a model polypeptide macroinitiator, the homopolypeptide  $\epsilon$ -carboxybenzyl-protected poly(L-lysine(Z)) (PZLL) was synthesized using hexylamine as the initiator. The use of PLL as the base polypeptide is rooted in its pendant amines which are ideal for material functionalization. The polypeptide was then treated with hydrobromic acid (HBr), removing the carboxybenzyl protecting group and revealing pendant primary amines of poly(L-lysine) (PLL) which would be amenable to methacrylation. This methacrylation was performed by first deprotonating the polypeptide in a 10 wt% aqueous solution by raising the pH to 10–11 and then addition of methacrylic anhydride, resulting in a methacrylation of 15% (Supporting Information Table S1). It should be noted that increasing macrocrosslinker functionalization will generally yield increased film thickness when utilizing CAP as demonstrated in a previous study.<sup>[10c]</sup> However, 10% of repeat units with double bonds is generally sufficient for CAP process. While this results in poly(L-lysine-*g*-methacrylate) (PLLMA) as intended, a fortuitous side-effect is that the polypeptide remains deprotonated allowing for CAP to be performed in organic solvents (Figure 1).

To prepare the surfaces for CAP, RAFT agent was immobilized onto aminated silica surfaces. Silica surfaces were aminated with 3-aminopropargyl triethoxysilane (APTES) using previously established methods.<sup>[22]</sup> The subsequent amine groups were susceptible to carbodiimide coupling with carboxylic acid-terminated RAFT agents (Supporting Scheme S3). To establish the validity of this method, 4-cyano-4-(phenylcarbonothioylthio)pentanoic acid (CPADB) was anchored as a model dithiobenzoate RAFT agent, allowing CAP-RAFT to be performed using PLLMA macrocrosslinker. CPADB has been used previously as a model dithiobenzoate RAFT agent for the study of methacrylamine monomers in solution,<sup>[23]</sup> and thus was deemed an appropriate model RAFT agent in this instance.

CAP-RAFT was performed by soaking the treated surfaces in a DMSO solution of PLLMA macrocrosslinker and LAP photoinitiator and irradiated under blue light



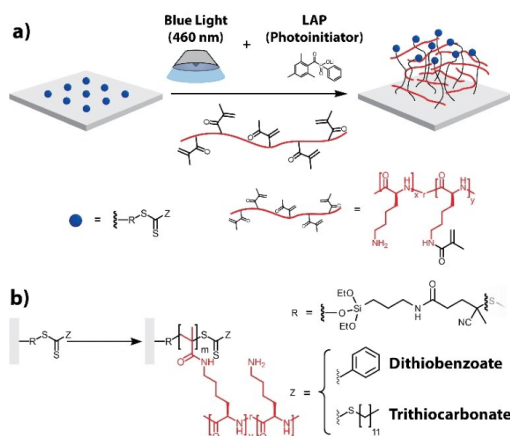


**Figure 1.** Schematic for CAP-RAFT using a polypeptide macroinitiator onto a surface functionalized with RAFT agent. a) Graphical schematic of CAP-RAFT of PLLMA macrocrosslinker through the use of blue light ( $4\text{ mW cm}^{-2}$ ,  $\lambda_{\text{max}} = 460\text{ nm}$ ). b) Chemical schematic representing the use of model dithiobenzoate and trithiocarbonate RAFT agents.

( $4\text{ mW cm}^{-2}$ ,  $\lambda_{\text{max}} \approx 460\text{ nm}$ ). To confirm that film formation is due to CAP rather than solely adhesion of the macroinitiator to the surface, control experiments were performed with specific elements absent from the system (Supporting Information Table S2). All samples showed very small amount ( $1.31\text{--}5.60\text{ nm}$ ) of film formation due to adhesion of deposited polypeptide. As would be expected, surfaces without surface initiator resulted in films of similar thicknesses, indicating a lack of surface confined polymerization (Figure 1). Furthermore, samples kept in the dark (i.e. no blue light exposure) also showed a lack of surface confined polymerization confirming the requirement for blue light for RAFT polymerization. Our group has previously shown that RAFT polymerization can be initiated with blue light without the use of a photoinitiator with a significantly lowered rate of polymerization, compared to other known RAFT mechanisms.<sup>[24]</sup> However, only samples with photoinitiator showed any evidence of polymerization, with film thickness of at least  $30\text{ nm}$  observed, providing strong evidence of surface confined RAFT polymerization.

Previous papers have shown that surface initiated RAFT polymerization in general requires the use of a RAFT agent in solution to ensure consistent film thickness.<sup>[7c]</sup> Recently, Seo et al. demonstrated the use of SI-PET-RAFT without RAFT agent in the solution to yield patternable polymer brushes.<sup>[25]</sup> This is in agreement with our results indicating polymerization is confined to the film surface. Thus, to observe the degree of polymerization occurring both with and without RAFT agent in solution, analysis of the aggregate size was performed. DLS revealed an increase in particle size after irradiation under blue light as long as photoinitiator was present in solution (from  $0.901 \pm 0.0590\text{ nm}$  to  $2.47 \pm 0.210\text{ nm}$  with LAP and without func-

tionized surfaces) (Supporting Figure S6 and S7). A decrease in particle size correlating to a decrease in polymerization in the supernatant was observed with the introduction of functionalized surfaces, signifying an increase in control upon their introduction; for reactions without RAFT agent in solution, particles with a diameter of  $2.47 \pm 0.210\text{ nm}$  were observed after reaction without surfaces compared to  $2.04 \pm 0.360\text{ nm}$  with surfaces. With RAFT agent in solution, particles with a diameter of  $4.01 \pm 0.513\text{ nm}$  without surfaces were observed compared to  $3.19 \pm 0.41\text{ nm}$  with surfaces. However, the degree of polymerization in solution was found to be decreased without any free RAFT agent in solution signifying greater surface confinement of the reaction.

To further investigate the necessity of sacrificial RAFT agent when using polymeric macroinitiators, experiments with and without RAFT agent in solution were performed (Figure 2). In the presence of sacrificial RAFT agent, films were found to reach a maximum of  $36.1 \pm 1.1\text{ nm}$  after 16 h (Figure 2ai) with an RMS roughness of  $6.1\text{ nm}$  (Figure 2aii). Without RAFT agent in solution, surfaces grew slower (24 h maximum), rougher and thinner ( $31.5 \pm 2.4\text{ nm}$  with an RMS roughness of  $9.4\text{ nm}$ ), however remained relatively uniform in thickness, despite more regions of varied thickness (Figure 2b). In both cases, surfaces were found to have relatively high RMS roughness with respect to the film thickness. Furthermore, the overall homogeneity of the surface was found to be decreased without RAFT agent in solution. Though both films were relatively homogeneous, large regions with denser films were also observed. This has been observed in previous instances of the use of CAP which is due to the decreased availability of initiator at the film surface as it is covered by macrocrosslinker during film growth, with differences in homogeneity emerging based on the polymerization technique utilized and the macromonomers.<sup>[10]</sup> Furthermore, RAFT agents are susceptible to aminolysis by primary amines, potentially causing the degradation.<sup>[26]</sup> To determine if this was occurring, analysis of the supernatant after reaction both with and without RAFT agent in solution was performed. Dialysis was performed to remove excess CPADB (RAFT agent) and LAP, with the resulting  $^1\text{H NMR}$  revealing splitting patterns consistent with aromatic rings which would only be present due to aminolysis of CPADB (Supporting Figure S8). Although solution experiments have confirmed that aminolysis can occur with PLLMA, direct confirmation on the surface is challenging due to the low concentration of the RAFT end groups. On the other hand, uneven growth of CAP layer can also be due to other reasons such as monomer type, polymerization methods as well as efficiency of re-initiation as observed before in other systems. Furthermore, while there is a relatively significant impact upon the introduction of RAFT agent in solution, it is not a crucial requirement in this system.

To observe if this trend remained consistent with other initiators, 4-cyano-4-[(dodecylsulfanylthiocarbonyl)sulfanyl]pentanoic acid (CDTPA)—a trithiocarbonate-based RAFT agent—was introduced in the same manner as the dithiobenzoate initiator. Trithiocarbonates typically have a high



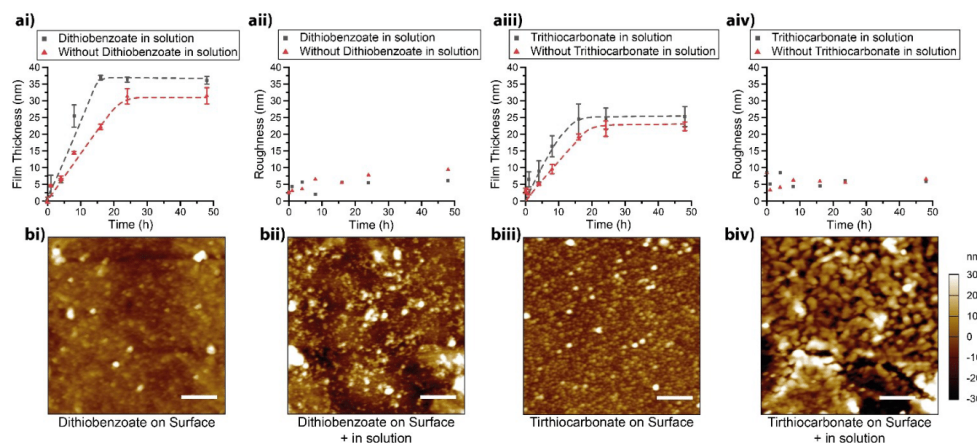


**Figure 2.** AFM imaging and analysis of CAP-RAFT films using a PLLMA macrocrosslinker utilizing different model RAFT agents. ai, aii) Analysis of film growth utilizing a dithiobenzoate RAFT agent observing kinetics of film growth (ai) and film roughness (aii) both with and without RAFT agent in solution. aiii, aiv) Analysis of film growth utilizing a trithiocarbonate RAFT agent observing kinetics of film growth (aiii) and film roughness (aiv) both with and without RAFT agent in solution. b) Surface morphology after 48 h of CAP-RAFT utilizing systems imaged using AFM with b) a dithiobenzoate RAFT agent anchored to the surface as well as in RAFT agent in solution; bii) a dithiobenzoate RAFT agent anchored to the surface but not in the reaction solution; biii) a trithiocarbonate RAFT agent anchored to the surface as well as in RAFT agent in solution; and biv) a trithiocarbonate anchored to the surface but not in the reaction solution (scale bars = 1  $\mu\text{m}$ ).

affinity towards methacrylamides<sup>[27]</sup> and would provide some insight toward specific variability associated with using CAP (Figure 2). The time to reach maximum film thickness was the same as with the dithiobenzoate initiator, with and without sacrificial RAFT agent (16 h and 24 h respectively), but thicknesses were significantly reduced both with and without RAFT agent ( $25.3 \pm 3.0$  and  $22.3 \pm 1.3$  nm respectively) (Figure 2aiii–iv). Furthermore, the morphologies of the films were found to have more significant aggregation (Figure 2biii–iv). This appears to concur with the general principal that trithiocarbonates are known to be less active than their dithiobenzoate counterparts.<sup>[15d]</sup> However, they are less susceptible to aminolysis,<sup>[26c]</sup> supporting the hypothesis that the lower overall homogeneity of the dithiobenzoate samples is due to RAFT agent degradation by aminolysis. Nonetheless, as we aim to develop this method by keeping polymerization surface confined, we continued testing without RAFT agent in solution.

One advantage of CAP is the ability to increase the film thickness without concern for maintaining chain-end fidelity through re-initiation. As lysine residues have primary amine side chains, these films are uniquely susceptible to modification using the same carbodiimide chemistry employed for immobilization of the carboxylic acid-functional RAFT agent. From this RAFT agent-functionalized layer, a second layer of CAP could be performed (Figure 3a). This process could theoretically be continuously repeated to yield thicker films based on desired functionality. Using this strategy, we were able to grow films with  $94.9 \pm 8.24$  nm in thickness after 4 layers (Figure 3b). It should be noted that a prominent increase in regions aggregation was also observed as more

and more layers were introduced to the system (Figure 3d). Furthermore, these pendant primary amines are no longer available for carbodiimide coupling after attacking another immobilized RAFT agent. While this did not seem to have a significant effect on the first or second layers, this irregular morphology was much more pronounced in the third and fourth layers. Nonetheless, this demonstrates the potential to develop multilayered systems which can be increased further based on previous works demonstrating similar capabilities.<sup>[10]</sup>

With the use of polypeptides in the formation of these films comes the presence of secondary structures typical for proteins and polypeptides with poly-L-lysine being no exception.<sup>[28]</sup> ATR-FTIR spectra around the Amide I band ( $1600\text{--}1720\text{ cm}^{-1}$ ) are often used to analyze the secondary structure content of proteins.<sup>[28]</sup> By observing this region of the spectra, the bottom three layers were found to share similar structures based on the major peaks (Figure 3c). However, the introduction of the fourth layer appeared to have a drastic effect with the peak at  $1649\text{ cm}^{-1}$  splitting into two peaks ( $1658$  and  $1642\text{ cm}^{-1}$ ) and a drop of the peak at  $1696\text{ cm}^{-1}$  both indicating a drop in  $\beta$ -sheet formation.

To further determine the secondary structures present, lineshape analysis was performed according to Chirgadze et al.<sup>[29]</sup> for IR analysis of polypeptides. High molecular weight poly-L-lysine is well known to form random coils in solution while charged,<sup>[30]</sup> which is changed to a primarily  $\alpha$ -helical structure under alkali aqueous conditions (i.e. uncharged primary amines).<sup>[28d]</sup> Poly-L-lysine films formed utilizing different methodologies including dip coating quartz in an alkali aqueous media or grafting the polypep-

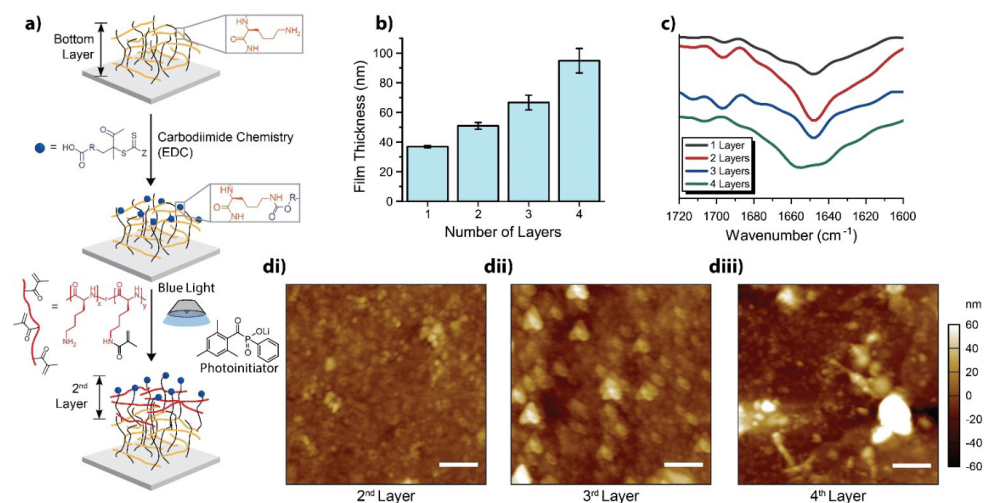


**Figure 3.** Multiple layers synthesized using CAP-RAFT. a) Schematic for reinitiation and execution of multiple layers of CAP-RAFT. b) Film thickness for multiple layers with PLLMA macrocrosslinker determined using AFM. c) FTIR spectra of the Amide I band of each layer. d) Surface morphology as revealed by AFM imaging of the di) 2nd, dii) 3rd and diii) 4th layers. (scale bars = 1 μm). EDC is 1-ethyl-3-(3-dimethylaminopropyl) carbodiimide.

tion directly to the surface showed this  $\alpha$ -helical structure while in their uncharged state.<sup>[31]</sup> Subsequently, it might be reasonable to assume that since polylysine favors  $\alpha$ -helices,<sup>[32]</sup> the films may form the same secondary structure. However, this was not the case when using CAP-RAFT as they instead preferentially formed random coils and  $\beta$ -sheets in the majority of the films (Table 1). While random coil content tended to vary significantly between 30 to 50%, the  $\beta$ -sheet content remained between 32 to 39%. This deviation from the expected  $\alpha$ -helical structures is likely due to the unique covalently crosslinked morphology of films formed through CAP, resulting in reduced mobility of the PLLMA chains and thus preventing their usual favored conformation. Interestingly, the four-layer films seem to trend back towards the expected norm with  $\beta$ -sheet and random coil content dropping to 21 and 19% respectively, while  $\alpha$ -helical structure rose from around 13–19% to 26%. Furthermore,  $\beta$ -turns were observed in a far more significant quantity at 27%. The issues stated before, pertaining to localized film growth, would also lead to lower crosslinking density. Subsequently, chain mobility would be increased, allowing the PLLMA chains to begin to take on their more favorable conformations. This unusually high random coil conformation grants these films a more amorphous structure which can assist with accessibility to functional groups or motifs desired for further surface modification or the specific binding of molecules making them a prime candidate for drug delivery or tissue engineering where such signaling molecules and molecular payloads are desired.

To further establish the versatility of this technique, poly(L-glutamic acid-r-L-lysine-g-methacrylate) (PLGMA)

was investigated in a similar fashion as PLLMA (Supporting Information Figure S3, Table S3) with similarly modifiable functional group side chains (i.e. carboxylic acids). By performing CAP with PLGMA in aqueous media, a slightly thicker film of  $41.2 \pm 1.4$  nm was observed, possibly attributed to PLGMA's inability to undergo aminolysis (Figure 4a). However, the comparative increase in film thickness was more pronounced when CAP was performed on a reinitiated PLLMA layer with a jump to  $76.0 \pm 9.4$  nm. Since the reaction was performed at pH 7 (deionized water), PLLMA and PLGMA layers exist in both the cationic and anionic forms. This would potentially result in ionic attraction of the layers accounting for the observed increased film thickness.

Despite one sample including a PLLMA layer below the PLGMA layer, both samples with PLGMA share similar FTIR spectra around the Amide I band (Figure 4b). Using the same logic as before, as poly-L-glutamic acid is expected to take predominantly random coil conformations at neutral pH,<sup>[33]</sup> the high random coil content of the PLGMA films ( $37 \pm 2\%$ ) is unsurprising, though there are still significant quantities of other secondary structures which might be due to localised confinement afforded by the unique morphology of CAP films. However, analogous to layer-by-layer (LbL) films fabricated from poly-L-glutamic acid and poly-L-lysine<sup>[34]</sup> our PLLMA/PLGMA films would be expected to form primarily  $\beta$ -sheet formations, due to polyionic complexation. In contrast, this was not observed and, instead, a similar secondary structure breakdown to the solely PLGMA films (with the exception of  $\beta$ -turns at  $23 \pm 14\%$ ) was elucidated. It can be surmised that after the initial layer

**Table 1:** Secondary structure elements of multi-layered PLLMA and PLGMA films (determined using ATR-FTIR).

Layer Number	2	3	4 (top)	$\beta$ -Sheets [%]	$\alpha$ -Helices [%]	Random Coils [%]	$\beta$ -Turns [%]	Others <sup>[a]</sup> [%]
PLLMA	–	–	–	37 ± 6	19 ± 11	35 ± 11	9 ± 5	N/A
PLLMA	PLLMA	–	–	32 ± 7	13 ± 3	50 ± 5	5 ± 2	N/A
PLLMA	PLLMA	PLLMA	–	39 ± 2	15 ± 3	40 ± 2	6 ± 2	N/A
PLLMA	PLLMA	PLLMA	PLLMA	21 ± 4	26 ± 1	19 ± 2	27 ± 4	6 ± 4
PLGMA	–	–	–	19 ± 1	29 ± 2	37 ± 2	13 ± 2	2 ± 1
PLLMA	PLGMA	–	–	14 ± 4	25 ± 8	37 ± 12	23 ± 14	2 ± 1

[a] In some cases, the amount of “other” secondary structure was negligible and thus denoted as “N/A”.

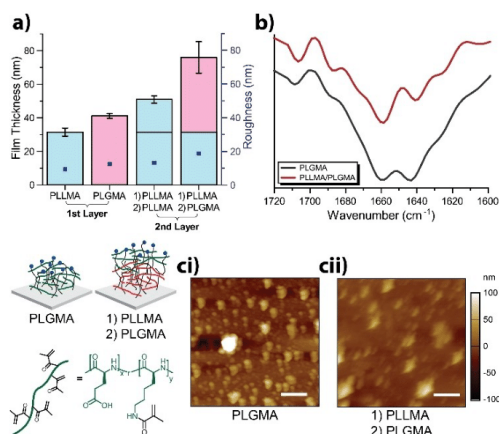


**Figure 4.** a) Comparative film thickness and roughness upon introduction of PLGlu as the initial layer and the second layer; b) FTIR spectra of top PLGlu layer; c) surface morphology of PLGlu layer as the ci) initial layer and cii) the second layer (scale bars = 1  $\mu$ m).

of PLGMA, the subsequently deposited PLGMA layer no longer interacts strongly with the preceding PLLMA layer to form the polyionic complex as before.

Alongside their ability to form secondary structures, polypeptides are favourable in bio applications such as drug delivery and tissue engineering due to their ability to undergo enzymatic degradation.<sup>[55]</sup> To evaluate this susceptibility, the PLLMA- and PLGMA-based films were incubated with both  $\alpha$ -chymotrypsin and protease type XIV as model proteases.  $\alpha$ -chymotrypsin is a digestive enzyme present in the mammalian gut,<sup>[56]</sup> while protease type XIV is a protease mixture known to break down  $\beta$ -sheet structures and is often used in wound healing studies since it mimics the cocktail of metalloproteases (MMP's) found in wounds.<sup>[37]</sup> In general, proteases are expected to hydrolyse the amide bonds of the polypeptide backbone in multiple locations while leaving the hydrocarbon backbone formed through RAFT polymerization intact (Figure 5a). Thus, while it is expected that residual polymer remains, the majority of the film is degraded. AFM analysis of films at the same site of the PLLMA-based films before and after incubation (Figure 5b and d) revealed significant change

using both enzymes. After the use of  $\alpha$ -chymotrypsin, a noticeable increase in roughness was observed with both higher and lower regions of the films expanding relative to each other as a result of degradation in these lower regions in particular (Figure 5b). While this could also be observed in presence of protease type XIV (Figure 5d), a large piece was found missing after incubation indicating successful degradation. Interestingly, treatment of PLGMA films with these enzymes also yielded degradation, but it had little changes in the presence of  $\alpha$ -chymotrypsin (Figure 5c), and none in the presence of protease type XIV showing resistance to this protease (Figure 5d). This suggests that degradation against certain enzymes can be controlled through selection of different amino acids though as is typical for proteases, since this control is enzyme specific. Thus, evidence of controllable enzymatic degradation has been demonstrated using both model enzymes, further suggesting potential in biological systems as scaffolds and drug delivery systems.

## Conclusion

In summary, the first instance of CAP-RAFT has been established to form crosslinked polypeptide films with unique secondary structure features. Through the use of PLLMA as an initial model macrocrosslinker, investigations were performed with model dithiobenzoate and trithiocarbonate initiators and with and without sacrificial RAFT agent in solution. While the thickest films were obtained using surface confined dithiobenzoate RAFT agent (thickness of  $36.1 \pm 1.1$  nm), films of comparable thickness ( $31.5 \pm 2.4$  nm) and uniformity were obtained with sacrificial RAFT agent in solution. As a result, further experiments which ensured greater surface confinement were performed in the absence of RAFT agent in solution. In this way, multi-layered films reaching a thickness of  $94.9 \pm 8.24$  nm were achieved. Secondary structure analysis showed an unusually high proportion of random coil structures (35–50%), despite expected high  $\alpha$ -helical formation for PLLMA. This is likely due to the reduced mobility of the surface confined PLLMA, and hence its ability to form the usually favored secondary structure. Similar trends were observed when the PLGMA macrocrosslinker was utilized. As a result, we have established CAP-RAFT as a viable strategy to create surface confined polypeptide crosslinked films with precision thick-





ness control and unique properties such as specific secondary structure formations and degradation. This secondary structure control combined with enzymatic degradation shows high potential for numerous biological applications including drug delivery and tissue engineering which will be subject to further investigation in future studies.

### Acknowledgements

This work was performed in part at the Materials Characterization and Fabrication Platform (MCFP) at the University of Melbourne. We further thank Prof. Laforch for access to the Harrick VariGATR. S.L. thanks Markus Hund for technical assistance with AFM measurements. N.J.C. thanks The University of Melbourne for providing Australian Government Research Training Program Scholarship (AGRTP) for providing funds for travel. This work is supported by grants DFG SCHE603/ 23-1. N.J.C., S.L., G.G.Q. and T.S. acknowledge funding from the German Academic Exchange Service (DAAD) through its thematic network Bayreuth-Melbourne Colloid/Polymer Network sponsored from funds of the Federal Ministry of Education and Research (BMBF). Open Access funding enabled and organized by Projekt DEAL.

### Conflict of Interest

The authors declare no conflict of interest.

**Keywords:** CAP-RAFT · Crosslinked · Polypeptide · Surface-initiated polymerization · Secondary structure

- [1] a) G. Bozokalfa, H. Akbulut, B. Demir, E. Guler, Z. P. Gumus, D. Odaci Demirkol, E. Aldemir, S. Yamada, T. Endo, H. Coskunol, S. Timur, Y. Yagci, *Anal. Chem.* **2016**, *88*, 4161–4167; b) B. Demir, T. Yilmaz, E. Guler, Z. P. Gumus, H. Akbulut, E. Aldemir, H. Coskunol, D. G. Colak, I. Cianga, S. Yamada, S. Timur, T. Endo, Y. Yagci, *Talanta* **2016**, *161*, 789–796; c) T. Yilmaz Sengel, E. Guler, Z. P. Gumus, E. Aldemir, H. Coskunol, H. Akbulut, D. Goen Colak, I. Cianga, S. Yamada, S. Timur, T. Endo, Y. Yagci, *Sens. Actuators B* **2017**, *246*, 310–318.
- [2] a) K. Park, H. Jeong, J. Tanum, J.-C. Yoo, J. Hong, *J. Ind. Eng. Chem.* **2019**, *69*, 263–268; b) B. Jiang, B. Li, *Int. J. Nanomed.* **2009**, *4*, 37–53; c) B. Jiang, E. DeFusco, B. Li, *Biomacromolecules* **2010**, *11*, 3630–3637.
- [3] a) Q. Gao, M. Yu, Y. Su, M. Xie, X. Zhao, P. Li, P. X. Ma, *Acta Biomater.* **2017**, *51*, 112–124; b) G. P. Sakala, M. Reches, *Adv. Mater. Interfaces* **2018**, *5*, 1800073; c) J. S. Rudra, K. Dave, D. T. Haynie, *J. Biomater. Sci. Polym. Ed.* **2006**, *17*, 1301–1315; d) Q. Yang, L. Wang, W. Lin, G. Ma, J. Yuan, S. Chen, *J. Mater. Chem. B* **2014**, *2*, 577–584.
- [4] a) T. J. Deming, *J. Polym. Sci. Part A* **2000**, *38*, 3011–3018; b) T. J. Deming, *Nature* **1997**, *390*, 386–389; c) C. Nacar, *Protein J.* **2020**, *39*, 21–32; d) K. Fujiwara, H. Toda, M. Ikeguchi, *BMC Struct. Biol.* **2012**, *12*, 18.
- [5] a) N. J.-A. Chan, D. Gu, S. Tan, Q. Fu, T. G. Pattison, A. J. O'Connor, G. G. Qiao, *Nat. Commun.* **2020**, *11*, 1630; b) D. T. Haynie, L. Zhang, J. S. Rudra, W. Zhao, Y. Zhong, N. Palath, *Biomacromolecules* **2005**, *6*, 2895–2913; c) S. H. Wibowo, A. Sulistio, E. H. H. Wong, A. Blencowe, G. G. Qiao, *Chem. Commun.* **2014**, *50*, 4971–4988; d) T. Borase, A. Heise, *Adv. Mater.* **2016**, *28*, 5725–5731.
- [6] a) C. Zhang, J. Yuan, J. Lu, Y. Hou, W. Xiong, H. Lu, *Biomaterials* **2018**, *178*, 728–737; b) A. Heise, H. Menzel, H. Yim, M. D. Foster, R. H. Wieringa, A. J. Schouten, V. Erb, M. Stamm, *Langmuir* **1997**, *13*, 723–728; c) Y.-C. Chang, C. W. Frank, *Langmuir* **1996**, *12*, 5824–5829; d) F. Audouin, M. Fox, R. Larragy, P. Clarke, J. Huang, B. O'Connor, A. Heise, *Macromolecules* **2012**, *45*, 6127–6135.
- [7] a) K. Kato, E. Uchida, E.-T. Kang, Y. Uyama, Y. Ikada, *Prog. Polym. Sci.* **2003**, *28*, 209–259; b) Y. Uyama, K. Kato, Y. Ikada, *Grafting/Characterization Techniques/Kinetic Modeling* **1998**, 1–39; c) M. Li, M. Fromel, D. Ranaweera, S. Rocha, C. Boyer, C. W. Pester, *ACS Macro Lett.* **2019**, *8*, 374–380.
- [8] a) E. Roeven, A. R. Kuzmyn, L. Scheres, J. Baggerman, M. M. J. Smulders, H. Zuilhof, *Langmuir* **2020**, *36*, 10187–10199; b) Y. Zhang, K. Kang, N. Zhu, G. Li, X. Zhou, A. Zhang, Q. Yi, Y. Wu, *J. Mater. Chem. B* **2020**, *8*, 7428–7437.
- [9] a) E. H. H. Wong, S. N. Guntari, A. Blencowe, M. P. van Koe-verden, F. Caruso, G. G. Qiao, *ACS Macro Lett.* **2012**, *1*, 1020–1023; b) T. K. Goh, S. N. Guntari, C. J. Ochs, A. Blencowe, D. Mertz, L. A. Connal, G. K. Such, G. G. Qiao, F. Caruso, *Small* **2011**, *7*, 2863–2867; c) D. Mertz, C. J. Ochs, Z. Zhu, L. Lee, S. N. Guntari, G. K. Such, T. K. Goh, L. A. Connal, A. Blencowe, G. G. Qiao, F. Caruso, *Chem. Commun.* **2011**, *47*, 12601–12603; d) E. Nam, J. Kim, S. N. Guntari, H. Seyler, Q. Fu, E. H. H. Wong, A. Blencowe, D. J. Jones, F. Caruso, G. G. Qiao, *Chem. Sci.* **2014**, *5*, 3374–3380.
- [10] a) S. N. Guntari, A. C. H. Khin, E. H. H. Wong, T. K. Goh, A. Blencowe, F. Caruso, G. G. Qiao, *Adv. Funct. Mater.* **2013**, *23*, 5159–5166; b) E. H. H. Wong, M. P. van Koe-verden, E. Nam, S. N. Guntari, S. H. Wibowo, A. Blencowe, F. Caruso, G. G. Qiao, *Macromolecules* **2013**, *46*, 7789–7796; c) S. N. Guntari, T. K. Goh, A. Blencowe, E. H. H. Wong, F. Caruso, G. G. Qiao, *Polym. Chem.* **2013**, *4*, 68–75.
- [11] a) Q. Fu, J. Kim, P. A. Gurr, J. M. P. Scofield, S. E. Kentish, G. G. Qiao, *Energy Environ. Sci.* **2016**, *9*, 434–440; b) E. Nam, E. H. H. Wong, S. Tan, Q. Fu, A. Blencowe, G. G. Qiao, *Macromol. Mater. Eng.* **2017**, *302*, 1600199.
- [12] E. Nam, E. H. H. Wong, S. Tan, S. N. Guntari, Q. Fu, J. Kim, B. Delalat, A. Blencowe, G. G. Qiao, *Polym. Chem.* **2016**, *7*, 3251–3258.
- [13] S. Tan, E. Nam, J. Cui, C. Xu, Q. Fu, J. M. Ren, E. H. H. Wong, K. Ladewig, F. Caruso, A. Blencowe, G. G. Qiao, *Chem. Commun.* **2015**, *51*, 2025–2028.
- [14] T. G. Pattison, A. Spanu, A. M. Friz, Q. Fu, R. D. Miller, G. G. Qiao, *ACS Appl. Mater. Interfaces* **2020**, *12*, 4041–4051.
- [15] a) G. Moad, E. Rizzardo, S. H. Thang, *Chem. Asian J.* **2013**, *8*, 1634–1644; b) G. Moad, *Polym. Chem.* **2017**, *8*, 177–219; c) M. D. Nothling, Q. Fu, A. Reyhani, S. Allison-Logan, K. Jung, J. Zhu, M. Kamigaito, C. Boyer, G. G. Qiao, *Adv. Sci.* **2020**, *7*, 2001656; d) G. Moad, E. Rizzardo, S. H. Thang, *Polymer* **2008**, *49*, 1079–1131; e) R. Whitfield, K. Parkatzidis, N. P. Truong, T. Junkers, A. Anastasaki, *Chem* **2020**, *6*, 1340–1352; f) K. Parkatzidis, H. S. Wang, N. P. Truong, A. Anastasaki, *Chem* **2020**, *6*, 1575–1588.
- [16] a) S. Allison-Logan, F. Karimi, Y. Sun, T. G. McKenzie, M. D. Nothling, G. Bryant, G. G. Qiao, *ACS Macro Lett.* **2019**, *8*, 1291–1295; b) A. Reyhani, S. Allison-Logan, H. Ranji-Burachaloo, T. G. McKenzie, G. Bryant, G. G. Qiao, *J. Polym. Sci. Part A* **2019**, *57*, 1922–1930.
- [17] a) A. R. Kuzmyn, A. T. Nguyen, L. W. Teunissen, H. Zuilhof, J. Baggerman, *Langmuir* **2020**, *36*, 4439–4446; b) Q. Wang, L. Hu, Z. Cui, P. Fu, M. Liu, X. Qiao, X. Pang, *ACS Appl. Mater. Interfaces* **2020**, *12*, 42161–42168.

- [18] a) S. Allison-Logan, Q. Fu, Y. Sun, M. Liu, J. Xie, J. Tang, G. G. Qiao, *Angew. Chem. Int. Ed.* **2020**, *59*, 21392–21396; *Angew. Chem.* **2020**, *132*, 21576–21580; b) T. G. McKenzie, E. H. H. Wong, Q. Fu, A. Sulistio, D. E. Dunstan, G. G. Qiao, *ACS Macro Lett.* **2015**, *4*, 1012–1016.
- [19] a) S. J. Lam, N. M. O'Brien-Simpson, N. Pantarat, A. Sulistio, E. H. H. Wong, Y.-Y. Chen, J. C. Lenzo, J. A. Holden, A. Blencowe, E. C. Reynolds, G. G. Qiao, *Nat. Microbiol.* **2016**, *1*, 16162; b) S. J. Shirbin, S. J. Lam, N. J.-A. Chan, M. M. Ozmen, Q. Fu, N. O'Brien-Simpson, E. C. Reynolds, G. G. Qiao, *ACS Macro Lett.* **2016**, *5*, 552–557.
- [20] a) G. J. M. Habraken, K. H. R. M. Wilsens, C. E. Koning, A. Heise, *Polym. Chem.* **2011**, *2*, 1322–1330; b) Z. Song, Z. Tan, J. Cheng, *Macromolecules* **2019**, *52*, 8521–8539; c) G. J. M. Habraken, M. Peeters, C. H. J. T. Dietz, C. E. Koning, A. Heise, *Polym. Chem.* **2010**, *1*, 514–524.
- [21] a) H. Lu, J. Wang, Z. Song, L. Yin, Y. Zhang, H. Tang, C. Tu, Y. Lin, J. Cheng, *Chem. Commun.* **2014**, *50*, 139–155; b) N. Hadjichristidis, H. Iatrou, M. Pitsikalis, G. Sakellariou, *Chem. Rev.* **2009**, *109*, 5528–5578.
- [22] M. D. Nothling, T. G. McKenzie, I. A. Eastland, H.-C. Chien, J. Collins, A. S. Meyer, G. G. Qiao, *Chem. Commun.* **2019**, *55*, 8544–8547.
- [23] a) Y. A. Vasilieva, C. W. Scales, D. B. Thomas, R. G. Ezell, A. B. Lowe, N. Ayres, C. L. McCormick, *J. Polym. Sci. Part A* **2005**, *43*, 3141–3152; b) P. Singhsa, H. Manuspiya, R. Narain, *Polym. Chem.* **2017**, *8*, 4140–4151.
- [24] T. G. McKenzie, Q. Fu, E. H. H. Wong, D. E. Dunstan, G. G. Qiao, *Macromolecules* **2015**, *48*, 3864–3872.
- [25] S. E. Seo, E. H. Discekici, Y. Zhang, C. M. Bates, C. J. Hawker, *J. Polym. Sci.* **2020**, *58*, 70–76.
- [26] a) J. Xu, J. He, D. Fan, X. Wang, Y. Yang, *Macromolecules* **2006**, *39*, 8616–8624; b) C. Boyer, A. Granville, T. P. Davis, V. Bulmus, *J. Polym. Sci. Part A* **2009**, *47*, 3773–3794; c) G. B. Desmet, D. R. D'hooge, M. K. Sabbe, M.-F. Reyniers, G. B. Marin, *J. Org. Chem.* **2016**, *81*, 11626–11634.
- [27] a) Y. Shi, E. T. A. van den Dungen, B. Klumperman, C. F. van Nostrum, W. E. Hennink, *ACS Macro Lett.* **2013**, *2*, 403–408; b) K. Luo, J. Yang, P. Kopečková, J. Kopeček, *Macromolecules* **2011**, *44*, 2481–2488.
- [28] a) X. Zhou, Z. Li, *Adv. Healthcare Mater.* **2018**, *7*, 1800020; b) J. Huang, A. Heise, *Chem. Soc. Rev.* **2013**, *42*, 7373–7390; c) N. H. Lee, L. M. Christensen, C. W. Frank, *Langmuir* **2003**, *19*, 3525–3530; d) K. Ciešlik-Boczula, *Biochimie* **2017**, *137*, 106–114.
- [29] a) A. Barth, *Biochim. Biophys. Acta Bioenerg.* **2007**, *1767*, 1073–1101; b) Y. N. Chirgadze, B. V. Shestopalov, S. Y. Vennyaminov, *Biopolymers* **1973**, *12*, 1337–1351.
- [30] D. Huesmann, A. Birke, K. Klinker, S. Türk, H. J. Räder, M. Barz, *Macromolecules* **2014**, *47*, 928–936.
- [31] a) A. Di Mauro, F. Mirabella, A. D'Urso, R. Randazzo, R. Purrello, M. E. Fragalà, *J. Colloid Interface Sci.* **2015**, *437*, 270–276; b) Y. Wang, Y. C. Chang, *Macromolecules* **2003**, *36*, 6511–6518.
- [32] A. Mirti, J. Grdadolnik, *Biophys. Chem.* **2013**, *175–176*, 47–53.
- [33] K. Inoue, N. Baden, M. Terazima, *J. Phys. Chem. B* **2005**, *109*, 22623–22628.
- [34] A.-M. Pilbat, V. Ball, P. Schaaf, J.-C. Voegel, B. Szalontai, *Langmuir* **2006**, *22*, 5753–5759.
- [35] a) S. J. Shirbin, F. Karimi, N. J.-A. Chan, D. E. Heath, G. G. Qiao, *Biomacromolecules* **2016**, *17*, 2981–2991; b) M. Byrne, P. D. Thornton, S.-A. Cryan, A. Heise, *Polym. Chem.* **2012**, *3*, 2825–2831; c) M. K. Joo, D. Y. Ko, S. J. Jeong, M. H. Park, U. P. Shinde, B. Jeong, *Soft Matter* **2013**, *9*, 8014–8022.
- [36] a) D. M. Blow, *Acc. Chem. Res.* **1976**, *9*, 145–152; b) W. Appel, *Clin. Biochem.* **1986**, *19*, 317–322.
- [37] a) J. Brown, C.-L. Lu, J. Coburn, D. L. Kaplan, *Acta Biomater.* **2015**, *11*, 212–221; b) S. Müller-Herrmann, T. Scheibel, *ACS Biomater. Sci. Eng.* **2015**, *1*, 247–259.

Manuscript received: September 21, 2021

Accepted manuscript online: December 3, 2021

Version of record online: January 12, 2022

### 3.3. Supporting Information



Supporting Information

#### **Crosslinked Polypeptide Films via RAFT-Mediated Continuous Assembly of Polymers**

*N. J. Chan, S. Lentz, P. A. Gurr, S. Tan, T. Scheibel\*, G. G. Qiao\**

## Materials and Methods

### Materials

Acetone (>99.5%, AR Grade, Merck), 3-aminopropargyl triethoxysilane (APTES, 99%, Merck), diethyl ether (Et<sub>2</sub>O, AR grade, Chem-Supply), *N*-(3-(dimethylamino)propyl)-*N*-ethylcarbodiimide hydrochloride (EDCI, ≥98%, Merck), 4-cyano-4-[(dodecylsulfanylthiocarbonyl)sulfanyl]pentanoic acid (CDTPA, 98%, Aldrich) 4-cyano-4-(phenylcarbonothioylthio)pentanoic acid (CPADB; 98%, Aldrich), dimethyl sulfoxide (DMSO; AR grade, Ajax Finechem), glacial acetic acid (AcOH; AR Grade, Chem-Supply), hydrobromic acid (HBr; 33% in acetic acid, Merck), hexylamine (≥98%, Merck), *N*-hydroxysuccinimide (NHS; ≥98%, Fluka), isopropanol (iPrOH, AR grade, Chem-Supply), lithium phenyl-2,4,6-trimethylbenzoylphosphinate (LAP, >98% HPLC grade, Tokyo Chemical Industry), H-L-Lys(Z)-OH (>99%, Mimotopes), H-L-Glu(OBzl)-OH (>99%, Mimotopes), magnesium sulfate (anh. MgSO<sub>4</sub>, ≥97%, Merck), methanol (AR grade, Chem-Supply), α-pinene (98%, Merck), sodium hydrogen carbonate (NaHCO<sub>3</sub>, AR grade, Chem-Supply), triphosgene (≥98%, Merck), sodium hydroxide (NaOH; ≥97%, Merck), trifluoroacetic acid (TFA; Merck) were used as received without further purification. Saturated brine solution was prepared from sodium chloride (NaCl, AR grade, Chem-Supply) in DI water. Tetrahydrofuran (anh. THF, inhibitor free, >99.9%, Merck), ethyl acetate (anh. EtOAc, >99.9 Honeywell) and dimethylformamide (anyhd. DMF, 99.8%, Acros) were purified by passage through a solvent purification system (SBPT-1, LC Technologies, USA) containing 4Å sieves under Argon gas. Hexane (AR, Chem-Supply) was distilled over calcium hydride under nitrogen prior to use.

### Instrumentation



$^1\text{H}$  NMR analysis was performed using a Varian Unity Plus 400 MHz NMR spectrometer using referenced deuterated solvent ( $\text{D}_2\text{O}$ ,  $d_6$ -DMSO or  $\text{CDCl}_3$ ).

GPC analysis was performed on a Shimadzu liquid chromatography system fitted with a PostNova Analytics MALS detector ( $\lambda = 658$  nm), a Shimadzu RID-10 refractometer ( $\lambda = 633$  nm), and a Shimadzu SPD-20A UV-vis detector, using three phenogel columns (Phenomenex,  $5 \mu\text{m}$ ) in series and HPLC grade DMF with 0.05 M LiBr as the mobile phase (1 mL/min). The oven temperature was set to  $50^\circ\text{C}$  to maintain an acceptable pressure across the system, and the detectors were temperature controlled to  $25^\circ\text{C}$ . Nova MALS software (PostNova) was used to determine the molecular weights and PDI using poly(ethylene glycol) standards.

DLS was performed using ZetaSizer NanoZS (Malvern Instruments, Worcestershire, U.K.) to analyze aggregation of macromonomer post-modification at concentrations of 0.01 mg/mL in reaction solution and diluted with DMSO.

The characterization of the thin films was performed using ATR-FTIR spectroscopy with a Bruker Hyperion 1000 microscope with a dedicated ATR-objective (Bruker Optics GmbH, Ettlingen, Germany). The ATR-crystal was brought into contact with the sample. The microscope was continuously purged with dry air, and the MCT detector was cooled with liquid nitrogen. The FTIR spectra were recorded with a resolution of  $2 \text{ cm}^{-1}$ . One hundred scans per measurement were performed. Three samples per layer with three spots per sample were measured.

Atomic force microscopy (AFM) for surface morphology and film thickness was performed in air-tapping mode on an Asylum Research Cypher (Asylum Research, Santa Barbara) with a silicon tip. CAP film thicknesses were estimated by film scratching (mechanical removal) and by tracing a profile along the film and the scratched zone. The thickness measurements reported represent mean values over 3 different analysis sites per substrates.

AFM was used to identify surface morphology before and after enzyme degradation and was acquired with a Dimension Icon (Bruker Nano Inc.) in tapping mode in air with a resolution of 512 to 512 datapoints at 0.5 to 1 Hz. Silicon cantilevers (OTESPA-R3, Bruker, Karlsruhe, Germany) were used with a force constant of 26 Nm<sup>-1</sup>. The x- and y positions were exactly stored and used before and after enzymatic degradation. The same cantilever was used for the measurements.

## Macromonomer Synthesis

### *Z-protected lysine N-Carboxyanhydride (Lys(Z) NCA) and Benzyl-protected Glutamic Acid (Glu(OBzl) NCA)*

Both NCAs were synthesized using modified versions of previous reported methods. In a typical experiment Lys(Z) (5.00 g, 17.8 mmol) was added to a 500 mL three-necked RBF and suspended in 200 mL of anh. THF with  $\alpha$ -pinene (6.00 mL, 37.5 mmol, 1.15 excess moles) under nitrogen. After heating to 60 °C, triphosgene (2.11 g, 7.14 mmol, 1.2 excess moles) was added and the mixture was stirred at temperature for 2 h. Solvent was then removed from the now clear solution under reduced pressure and replaced with 100 mL of anh. EtOAc. The solution was cooled to -18 °C before washing with sat. brine and 5 w/v% sodium hydrogen carbonate and the organic phase was dried over MgSO<sub>4</sub>. The filtered solution was reduced under reduced pressure and recrystallized using anh. hexane at -18 °C over 16 h. The solids were then filtered and redissolved into anh. EtOAc before being precipitated into anh. hexane. The precipitate was then dried under vacuum over 24 h and stored under argon at -80 °C (yields ~80%).

Lys(z) NCA: <sup>1</sup>H NMR (400 MHz, CDCl<sub>3</sub>):  $\delta$  1.30–1.60 (m, 4H, -NH-CH<sub>2</sub>-CH<sub>2</sub>-CH<sub>2</sub>-), 1.81–2.07 (m, 2H, -NH-CH<sub>2</sub>-CH<sub>2</sub>-CH<sub>2</sub>-), 3.20 (m, 2H, -NH-CH<sub>2</sub>-CH<sub>2</sub>-CH<sub>2</sub>-), 4.27 (t, 1H,  $J = 5.6$  Hz, CHN), 4.92 (s, 1H, side chain NH), 5.10 (s, 2H, CH<sub>2</sub>-ArH), 6.83 (s, 1H, ring NH), 7.22–7.37 (m, 5H, ArH).

Glu(OBzl) NCA:  $^1\text{H}$  NMR (400 MHz,  $\text{CDCl}_3$ ):  $\delta$  2.06–2.32 (m, 2H,  $\text{CH}_2\text{-CH}_2\text{-CO}$ ), 2.58 (t, 2H,  $J = 6.8$  Hz,  $\text{CH}_2\text{-CH}_2\text{-CO}$ ), 4.36 (t, 1H,  $J = 6.0$  Hz, CHN), 5.12 (s, 2H,  $\text{CH}_2\text{-ArH}$ ), 6.59 (s, 1H, ring NH), 7.29–7.41 (m, 5H, ArH).

***Poly(L-glutamic acid(OBzl)-r-L-lysine(Z)) synthesis***

Both Glu(OBzl) NCA (3.00 g, 11.4 mmol, 80 mol% of overall NCA monomer) and Lys(Z) NCA (0.873 g, 2.85 mmol, 20 mol% of overall NCA monomer) were dissolved in anh. DMF under nitrogen in a 50 mL RBF. To the stirring solution was added hexylamine (23.5  $\mu\text{L}$ , 54.3  $\mu\text{mol}$ ,  $M/I = 90$ ), and the clear solution was stirred under an argon bleed at room temperature for 24 h. The reaction mixture was then precipitated into and subsequently rinsed with  $\text{Et}_2\text{O}$  which was then dried and stored under vacuum to afford a clear tacky solid as the final product (2.84 g, yield: 78.5%).

$M_n$  (GPC) = 7.2 kDa; PDI 1.30.  $^1\text{H}$  NMR ( $d_6\text{-DMSO}$ ):  $\delta$  1.20–1.90 (m, Lys  $\text{-NH-CH}_2\text{-CH}_2\text{-CH}_2\text{-CH}_2\text{-}$ ), 2.0–2.40 (m, Glu  $\text{-CH}_2\text{-CH}_2\text{-CO-}$ ), 2.94 (s, Lys  $\text{-NH-CH}_2\text{-CH}_2\text{-CH}_2\text{-CH}_2\text{-}$ ), 3.92 (s, CH-NH backbone), 4.99 (m,  $\text{CH}_2\text{-ArH}$ ), 5.76 (m,  $\text{CH}_2\text{-CH-}$ ), 7.26 (s, ArH), 8.38 (brs, CO-NH)

***Deprotection of poly(L-glutamic acid(OBzl)-r-L-lysine(Z))***

To a 25 mL RBF was added the protected poly(L-glutamic acid(OBzl)-r-L-lysine(Z)) (2.84 g, 0.12 mmol) followed by 20 mL of TFA. The solution was stirred until the polymer was completely dissolved, followed by the dropwise addition of HBr (33 vol% in AcOH diluted to 16.7 vol% with AcOH, 20 mL). The resulting solution was stirred with thick precipitate observed soon after. The reaction mixture was stirred for a total of 16 h with the suspension then dropwise precipitated into diethyl ether, washed in ether ( $\times 2$ ), then dried in vacuo overnight. The solid was then dissolved in DI water and added to 3.5 kDa dialysis tubing for dialysis against 2 L DI water ( $\times 3$ ) for 24 h before being freeze-dried to obtain a white, fluffy solid ( $\sim 1.4$  g).

#### ***Deprotection of poly(L-glutamic acid(OBzl)-r-L-lysine(Z))***

To a 25 mL RBF was added the protected poly(L-glutamic acid(OBzl)-r-L-lysine(Z)) (2.84 g, (0.12 mmol) followed by 20 mL of TFA. The solution was stirred until the polymer was completely dissolved, followed by the dropwise addition of HBr (33 vol% in AcOH diluted to 16.7 vol% with AcOH, 20 mL). The resulting solution was stirred with thick precipitate observed soon after. The reaction mixture was stirred for a total of 16 h with the suspension then dropwise precipitated into diethyl ether, washed in ether (×2), then dried in vacuo overnight. The solid was then dissolved in DI water and added to 3.5 kDa dialysis tubing for dialysis against 2 L DI water (×3) for 24 h before being freeze-dried to obtain a white, fluffy solid (~ 1.4 g). <sup>1</sup>H NMR (D<sub>2</sub>O, 400 MHz): 1.06–1.43 (m, 4H, -NH-CH<sub>2</sub>-CH<sub>2</sub>-CH<sub>2</sub>-), 1.89–1.99 (m, Glu -CH<sub>2</sub>-CH<sub>2</sub>-CO-), 2.23 (m, Glu -CH<sub>2</sub>-CH<sub>2</sub>-CO-), 2.56 (m, 2H, Lys -NH-CH<sub>2</sub>-CH<sub>2</sub>-CH<sub>2</sub>-), 4.27 (m, CH-NH backbone).

#### ***Methacrylation of poly(L-lysine) to form PLLMA***

In a 28 mL glass vial, poly(L-lysine) (1.00 g, 4.78 mmol lysine units) was dissolved in DI water. pH was adjusted to 10 using 2.5 M NaOH before being chilled in an ice bath while stirring. Methacrylic anhydride (143 μL, 0.957 mmol, 20% mole equivalent to lysine units), was then added dropwise and the mixture was allowed to stir for 24 h. The resulting mixture was added to 3.5 kDa dialysis tubing for dialysis against 2 L DI water (×3) for 24 h before being freeze-dried to obtain a white fluffy solid (~300 mg). The polymer was purged with argon and stored at -18 °C. <sup>1</sup>H NMR (D<sub>2</sub>O, 400 MHz): δ 1.04–1.40 (m, 4H, Lys methacrylated -NH-CH<sub>2</sub>-CH<sub>2</sub>-CH<sub>2</sub>-), 1.41–1.73 (m, 4H, Lys NH<sub>2</sub>-CH<sub>2</sub>-CH<sub>2</sub>-CH<sub>2</sub>-), 1.84 (m, 3H, methacrylate -CO-C(CH<sub>3</sub>)=CH<sub>2</sub>), 2.78 (m, Lys NH<sub>2</sub>-CH<sub>2</sub>-CH<sub>2</sub>-CH<sub>2</sub>-), 3.13 (m, Lys methacrylated -NH-CH<sub>2</sub>-CH<sub>2</sub>-CH<sub>2</sub>-), 4.12 (m, CH-NH backbone), 5.27 (s, 1H, methacrylate -NH-CO-C(CH<sub>3</sub>)=CH<sub>2</sub>), 5.56 (s, 1H, methacrylate -NH-CO-C(CH<sub>3</sub>)=CH<sub>2</sub>)

### ***Methacrylation of poly(L-lysine-r-L-glutamic acid) to form PLGMA***

In a 28 mL glass vial, poly(L-glutamic acid-r-L-lysine) (1.00 g, 0.868 mmol of lysine units) was dissolved in DI water. pH was adjusted to 10 using 2.5 M NaOH before being chilled in an ice bath while stirring. Excess methacrylic anhydride (388  $\mu$ L, 2.60 mmol, 3 times excess mole equivalent to lysine units) was then added dropwise, and the mixture was stirred for 24 h. The resulting mixture was added to 3.5 kDa dialysis tubing for dialysis against 2 L DI water ( $\times 3$ ) for 24 h before being freeze-dried to obtain a white, fluffy solid ( $\sim 300$  mg). The polymer was purged with argon and stored at  $-18$   $^{\circ}$ C.  $^1$ H NMR ( $D_2O$ , 400 MHz):  $\delta$  1.06–1.53 (m, 4H, Lys methacrylated -NH-CH<sub>2</sub>-CH<sub>2</sub>-CH<sub>2</sub>-CH<sub>2</sub>-), 1.77 (m, 3H, methacrylate -CO-C(CH<sub>3</sub>)=CH<sub>2</sub>), (m, 4H, Lys NH<sub>2</sub>-CH<sub>2</sub>-CH<sub>2</sub>-CH<sub>2</sub>-CH<sub>2</sub>-), 1.84 (m, 3H, methacrylate -CO-C(CH<sub>3</sub>)=CH<sub>2</sub>), 1.87-2.12 (m, Glu -CH<sub>2</sub>-CH<sub>2</sub>-CO-), 2.24-2.55 (m, 2H, Lys -NH-CH<sub>2</sub>-CH<sub>2</sub>-CH<sub>2</sub>-CH<sub>2</sub>-), 3.21 (m, Lys methacrylated -NH-CH<sub>2</sub>-CH<sub>2</sub>-CH<sub>2</sub>-CH<sub>2</sub>-), 3.85-4.27 (m, CH-NH backbone), 5.24 (s, 1H, methacrylate -NH-CO-C(CH<sub>3</sub>)=CH<sub>2</sub>), 5.58 (s, 1H, methacrylate -NH-CO-C(CH<sub>3</sub>)=CH<sub>2</sub>)

### **Wafer Modification**

Silica wafers were sonicated in acetone (30 m) and isopropanol (30 m) before being rinsed in isopropanol and dried *in vacuo*. Surfaces were silanized using previously established procedures. Silica wafers were soaked in a solution of APTES in acetone (4 v/v%) at 45  $^{\circ}$ C for 24 h. Wafers were then rinsed in acetone thoroughly before being dried *in vacuo*. Using CDTPA as an example, CDTPA (50.0 mg, 0.179 mmol, 1 mol eq.), EDCI (137 mg, 0.716 mmol, 4 mol eq.) and NHS (20.6 mg, 0.179 mmol, 1 mol eq.) were added to a 100 mL RBF and dissolved in anh. DCM (50 mL). The solution was stirred for 2 h under nitrogen before adding to a beaker containing the washed silicon wafers. The beaker was placed in a desiccator purged with N<sub>2</sub> (g) which was shaken on a plate agitator at 80 RPM for 48 h. The wafers were

removed and washed thoroughly with DCM and isopropanol and left to dry in vacuo. Wafers were stored in methanol at 4 °C for later use.

***PLLMA CAP-RAFT on pretreated silica substrates***

PLLMA (30.0 mg, 31.9  $\mu\text{mol}$  of methacrylated units) dissolved in DMSO (973.8  $\mu\text{L}$ , totalling to 30 mg/mL concentration after addition of stock solutions) was treated with DMSO solutions of CTA (25.8  $\mu\text{L}$ , 1.00 mg/mL, 63.8 nmol, 1/500 mole equivalent of methacrylate units) and LAP (0.470  $\mu\text{L}$ , 1.00 mg/mL, 1.56 nmol, 1/40 mole equivalent of CTA). Functionalized wafers were submersed face up in solution, and high purity argon was bubbled through the solution for 20 min. The degassed mixture was left sealed and irradiated in blue light (4 mW/cm<sup>2</sup>,  $\lambda_{\text{max}}$  = 460 nm) for various intervals up to 24 h. Upon completion, the wafers were sonicated for 10 s in fresh DMSO, and the supernatant was extracted. The wafers themselves were thoroughly washed with DMSO (x3), DCM and iPrOH, before being dried under a nitrogen stream for 1 min. Treated wafers were then stored *in vacuo* prior to analysis.

The supernatant was also added to 3.5 kDa dialysis tubing for dialysis against 1 L DMSO (x3) for 24 h to remove leftover CTA and LAP and then analyzed by <sup>1</sup>H NMR.

***PLGMA CAP-RAFT on pretreated silica substrates***

PLGMA (30.0 mg, 27.5  $\mu\text{mol}$  of methacrylated units) dissolved in DI water (984.2  $\mu\text{L}$ , totalling to 30 mg/mL concentration after addition of stock solutions) was treated with DI water of CTA (15.4  $\mu\text{L}$ , 1.00 mg/mL, 55.1 nmol, 1/500 mole equivalent of methacrylate units) and LAP (0.405  $\mu\text{L}$ , 1.00 mg/mL, 1.38 nmol, 1/40 mole equivalent of CTA). Functionalized wafers were submersed face up in solution and high purity argon was bubbled through the solution for 20 min. The degassed mixture was left sealed and irradiated in blue light for various intervals up to 24 h. Upon completion, the wafers were sonicated for 10 s in fresh DI water, and then

thoroughly washed with DI water (x3), then DMSO and isopropanol, before being dried under a nitrogen stream for 1 min. Treated wafers were then stored *in vacuo* prior to analysis.

## Characterization

### Line shape analysis (LSA) for the quantification of secondary structure elements from FTIR

Line shape analysis was performed according to Chirgadze for IR analysis of polypeptides. The sum of the measured absorbance  $A(\nu)$  of the components (i) was calculated using Equation (1).

$$A(\nu) = \sum A_i(\nu) \quad (1)$$

The maximum  $\nu_i^{max}$  and the half-width at half-weight ( $w_i$ ) and the integral of the component ( $B_i$ ) were calculated. The starting values for the curve fit (Local-least-squares and Levenberg-Marquardt) were a mixture of 50% Lorentzian and 50% Gaussian lineshape.<sup>[1]</sup> For curve fitting, the OPUS software 8.1 (Bruker Optics GmbH, Ettlingen, Germany) was used. The recorded spectra were cut before curve fitting to the amide I region ( $1590 \text{ cm}^{-1}$  -  $1720 \text{ cm}^{-1}$ ), smoothed by 9 points, and baseline corrected with one iterative step. The number of components was determined by calculating the second derivative of the spectra. The negative peaks of the second derivative were used as wavenumber positions for the LSA. The half-widths for each component except the unordered random coil component around  $1655\text{-}1660 \text{ cm}^{-1}$  were set to  $w_i = 20 \text{ cm}^{-1}$  and for the random coil structure  $w_{\text{random coil}}$  was set to  $50 \text{ cm}^{-1}$  according to Chirgadze.<sup>[1]</sup> All spectra were fitted according to this procedure. The secondary structure proportions were calculated by summing up all the component integrals assigned to the respective secondary structures.<sup>[1]</sup> The quotient of the integral of one secondary structure component and the sum of all integrals multiplied by 100 is the secondary proportion in percent as shown in Equations (2) – (6).<sup>[2]</sup>

$$Q_{\text{random coil}} = \frac{\sum B_{1638-1655 \text{ cm}^{-1}}}{(B_{(\text{random coil})} + B_{(\beta\text{-sheet})} + B_{(\beta\text{-turn})} + B_{(\alpha\text{-helices})} + B_{(\text{Other})})} \quad (2)$$

$$Q_{\beta\text{-sheets}} = \frac{\sum B_{1614-1638 \text{ cm}^{-1}} + B_{1696-1708 \text{ cm}^{-1}}}{(B_{(\text{random coil})} + B_{(\beta\text{-sheet})} + B_{(\beta\text{-turn})} + B_{(\alpha\text{-helices})} + B_{(\text{Other})})} \quad (3)$$

$$Q_{\alpha\text{-helices}} = \frac{B_{1655-1664 \text{ cm}^{-1}}}{(B_{(\text{random coil})} + B_{(\beta\text{-sheet})} + B_{(\beta\text{-turn})} + B_{(\alpha\text{-helices})} + B_{(\text{Other})})} \quad (4)$$

$$Q_{\beta\text{-turns}} = \frac{\sum B_{1664-1696\text{ cm}^{-1}}}{(B_{(\text{random coil})} + B_{(\beta\text{-sheet})} + B_{(\beta\text{-turn})} + B_{(\alpha\text{-helices})} + B_{(\text{Other})})} \quad (5)$$

$$Q_{\text{Other (side chains, aggregated chain strands)}} = \frac{B_{1604-1613\text{ cm}^{-1}}}{(B_{(\text{random coil})} + B_{(\beta\text{-sheet})} + B_{(\beta\text{-turn})} + B_{(\alpha\text{-helices})} + B_{(\text{Other})})} \quad (6)$$

### ***Film Degradation***

Degradation experiments were performed according to Müller-Herrmann and Scheibel.<sup>[3]</sup> Experiments were performed in TCNB buffer (50 mM Tris/HCl, 10 mM CaCl<sub>2</sub>, 150 mM NaCl, 0.05% Brij 35, pH 7.5) at room temperature. The samples were incubated with 250 µL of PXIV or CHC solution (175 µg/mL in TCNB buffer) for 24 h. Control experiments without enzymes were conducted in 250 µL TCNB buffer. AFM analysis was performed with a Dimension Icon (Bruker Nano Inc.) in tapping mode as previously stated elaborated.



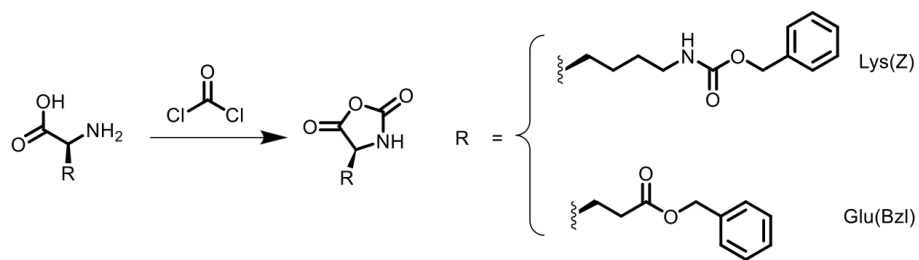


**Figure S1:** Scheme for synthesis of *N*-carboxyanhydrides

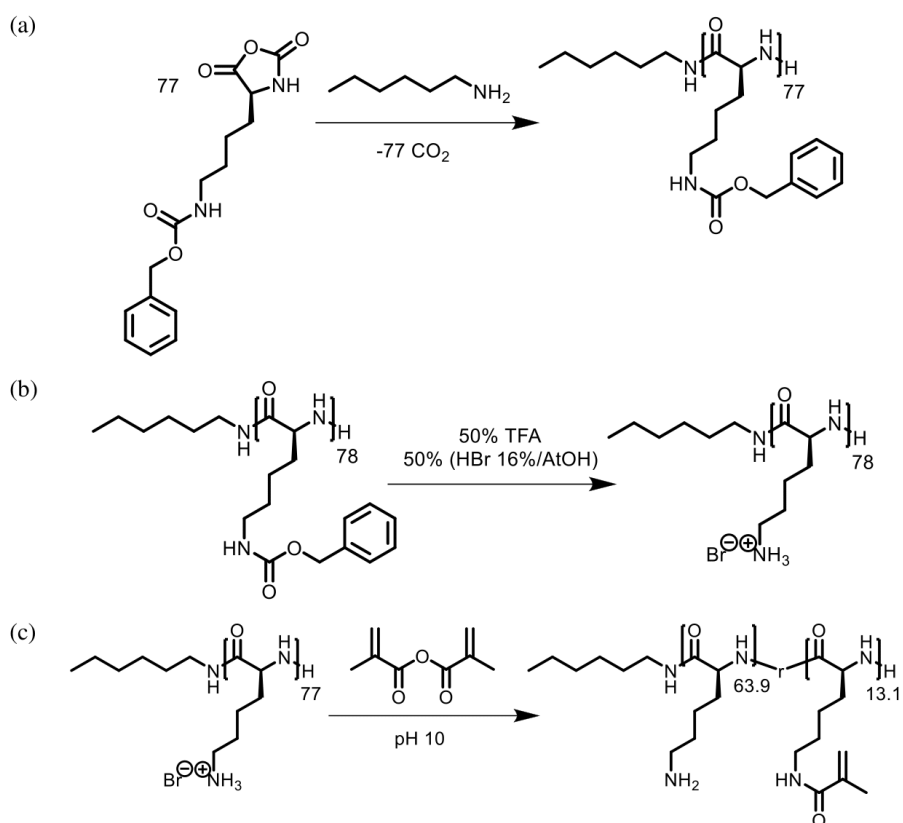


**Figure S2:** Synthesis of poly(L-lysine-*r*-L-lysine-*g*-methacrylamide) (PLLMA) (a) NCA ROP of Lys(Z) NCA using hexylamine as an initiator; (b) Deprotection of Z-protecting group using HBr. (c) Methacrylation of exposed amine groups with methacrylic anhydride.

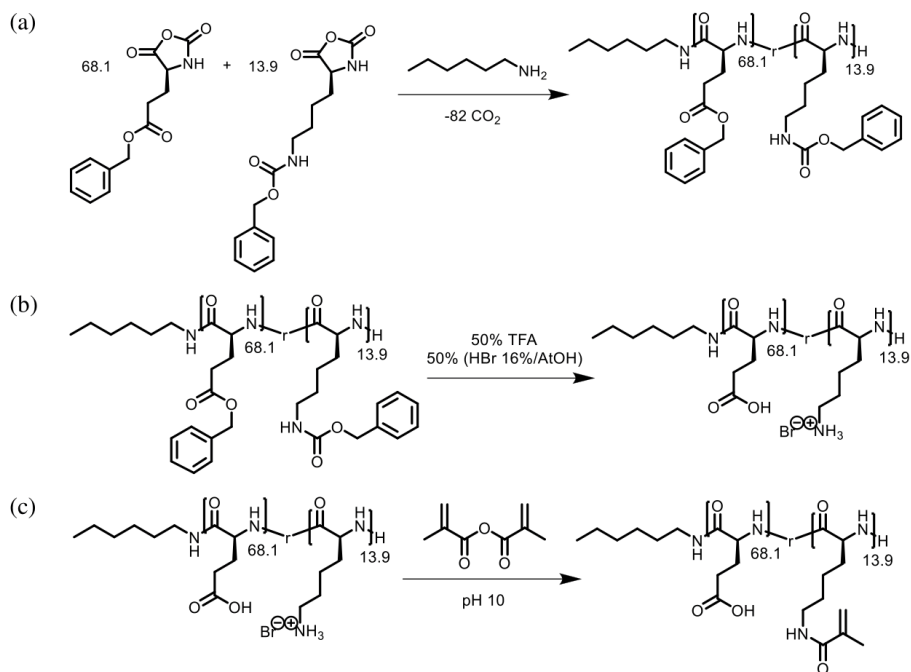


**Figure S3:** Synthesis of poly(L-glutamic acid-*r*- L-lysine-*g*-methacrylamide) (PLGMA) (a) NCA ROP of Lys(Z) and Glu(Bzl) NCA using hexylamine as an initiator; (b) Deprotection of Z-protecting group using HBr, (c) Methacrylation of exposed amine groups with methacrylic anhydride.

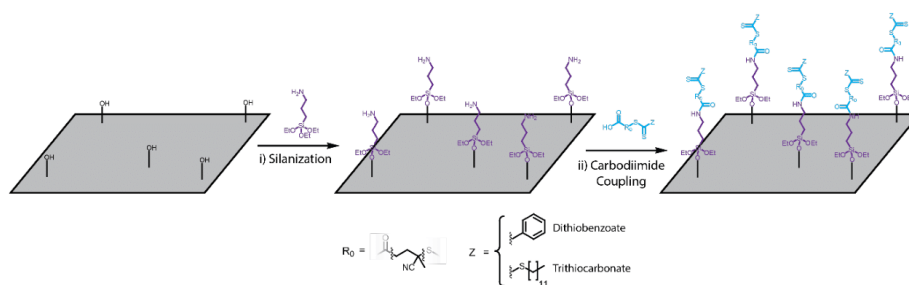


**Figure S4:** Anchoring of initiator to silicon wafers

**Table S1:** Summary of PLLMA macromonomer

$M_w^{[a]}$	DP <sup>[a]</sup>	PDI <sup>[a]</sup>	Methacrylation <sup>[b]</sup>
8318	77.9	1.22	15%

<sup>[a]</sup>Molecular weight (and subsequently degree of polymerization) and PDI determined using GPC with PEG standards; <sup>[b]</sup>Methacrylation determined by <sup>1</sup>H NMR.

**Table S2:** Thickness of films in the absence of specific elements used in the CAP-RAFT procedure

Surface Initiator <sup>[a]</sup>	Free CTA in solution <sup>[a]</sup>	Photoinitiator <sup>[a]</sup>	Light <sup>[a]</sup>	Thickness (nm) <sup>[b]</sup>	RMS (nm) <sup>[b]</sup>
N	N	Y	Y	3.45 ± 0.15	3.12
N	Y	Y	Y	5.60 ± 0.29	2.74
Y	N	N	Y	4.05 ± 0.26	3.67
Y	Y	N	Y	1.31 ± 0.51	1.15
Y	N	Y	N	4.98 ± 0.75	3.55
Y	Y	Y	N	4.37 ± 1.10	3.31
Y	N	Y	Y	31.46 ± 2.41	9.39
Y	Y	Y	Y	36.09 ± 1.13	6.11

<sup>[a]</sup> “N” indicates element absent in experiment, “Y” indicates element present in experiment;

<sup>[b]</sup> Thickness and RMS roughness determined using AFM

**Table S3:** Summary of PLGMA macromonomer

$M_n^{[a]}$	DP <sup>[a]</sup>	PDI <sup>[a]</sup>	Methacrylation <sup>[b]</sup>
8723	82.1	1.39	17%

<sup>[a]</sup> Number average molecular weight ( $M_n$ ) (and subsequently degree of polymerization) and PDI determined using GPC with PEG standards; <sup>[b]</sup> Methacrylation determined using <sup>1</sup>H NMR.

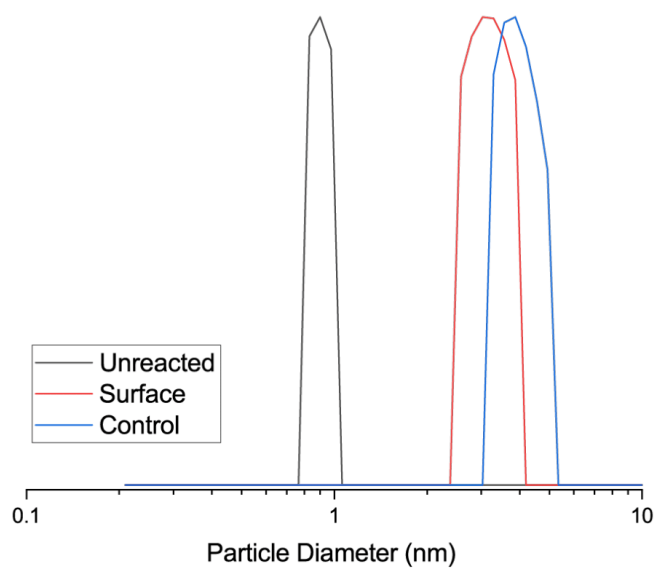


**Figure S6:** DLS of supernatant with CTA present in 0.5 mg/mL solutions of DMSO.

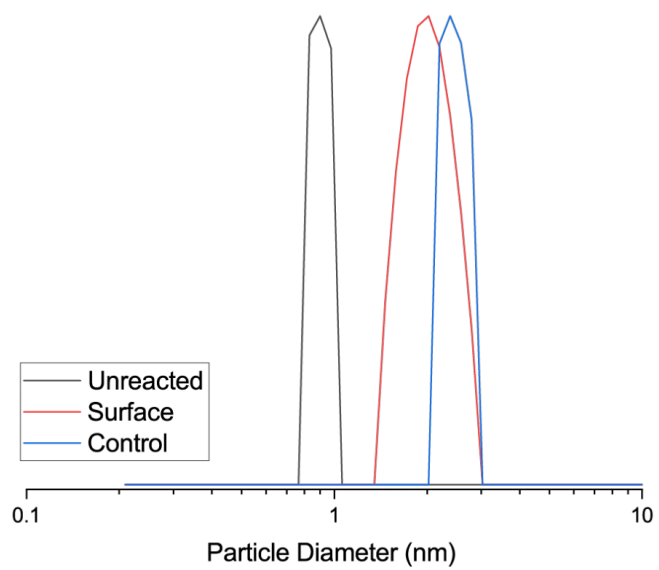


**Figure S7:** DLS of supernatant without CTA present in 0.5 mg/mL solutions of DMSO.

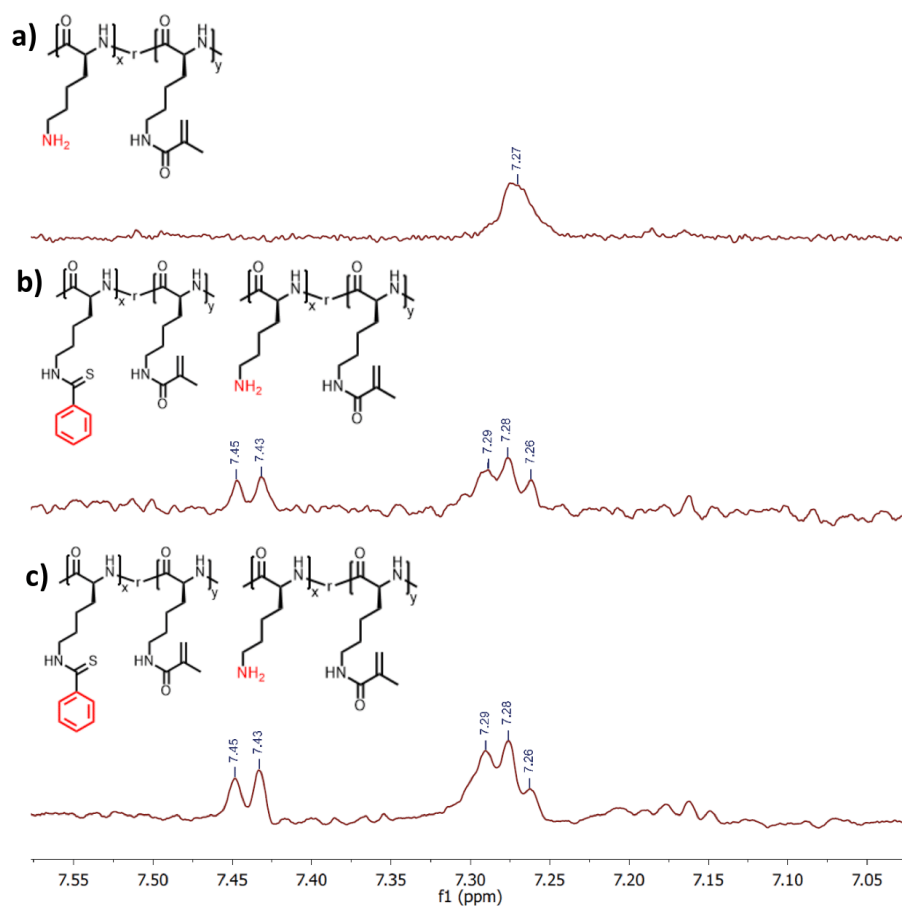


**Figure S8:**  $^1\text{H}$  NMR (in DMSO) between 7.0 and 7.6 ppm of PLLMA a) before reaction and b) after reaction without CTA in solution and c) after reaction with CTA in solution. Reaction supernatant was dialysed against DMSO, revealing splitting patterns consistent with aromatic rings which would only be present after degradation of RAFT agent by free amines on the PLLMA.

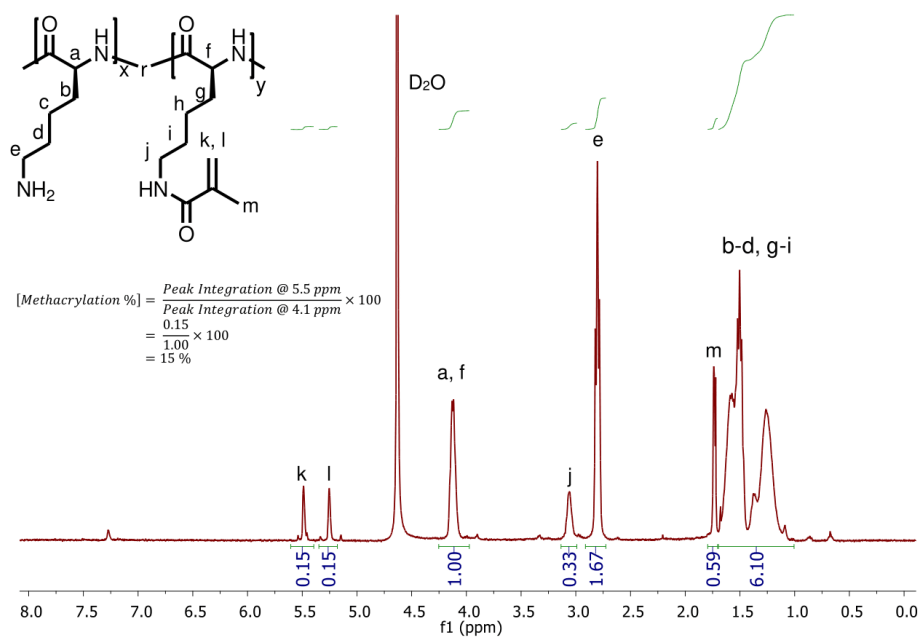


**Figure S9:**  $^1\text{H}$  NMR of PLLMA including calculation for methacrylation percentage

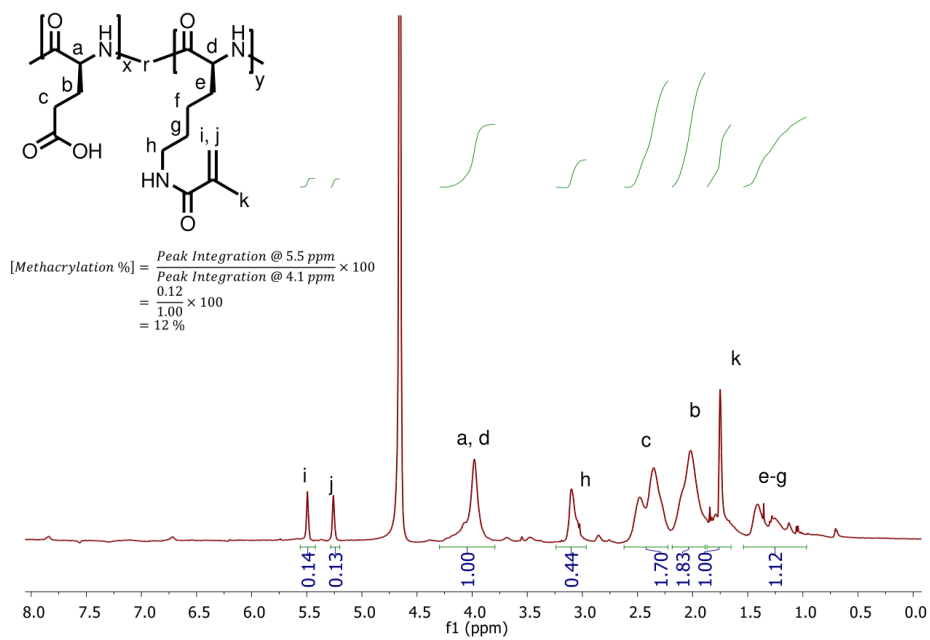


**Figure S10:**  $^1\text{H}$  NMR of PLGMA including calculation for methacrylation percentage

## References

- [1] Y. N. Chirgadze, B. V. Shestopalov, S. Y. Venyaminov, *Biopolymers* **1973**, *12*, 1337-1351.
- [2] A. Barth, *Biochimica et Biophysica Acta (BBA) - Bioenergetics* **2007**, *1767*, 1073-1101.
- [3] S. Müller-Herrmann, T. Scheibel, *ACS Biomaterials Science & Engineering* **2015**, *1*, 247-259.

## ***Chapter 4:***

# **Robust $\beta$ -sheet reinforced fibers fabricated from unmodified polymers**

---

### 4.1. Chapter Perspectives

The aforementioned issues with  $\beta$ -sheet aggregation further complicate their inclusion into one-dimensional fibers, where aggregation of polymer first occurs during fiber formation without suitable morphological control. Polypeptides-based fibers primarily utilize synthetic recombinant or purified natural structural proteins as the sole component of the fiber due to its precise sequencing. This forms a natural issue for NCA ROP based fibers, and, thus, hybrids with synthetic polymers have been developed to form  $\beta$ -sheet laden fibers. Such hybrids have multi-step procedures towards polymer synthesis with the use of chemical linkers and coupling chemistry, making them non-facile and thus difficult to scale up.

In this chapter, we report a facile strategy for introducing  $\beta$ -sheet forming polypeptides into wet spun microfibers from unmodified polymers and yield robust fibers. By introducing Val NCA into the spinning solution as a monomer and polymerizing the  $\beta$ -sheet forming polypeptide (PLV) after fiber formation instead of as part of the fiber polymer, uncontrolled aggregation is no longer an issue, as now intermolecular forces between the  $\beta$ -sheet structure and the polymer fibers largely dictate the conformation of both structures. Polymers with low hydrogen bonding potential (polycaprolactone (PCL) and cellulose acetate) were found to undergo polymer crystallization, leading to an increase in mechanical strength. Other fibers without significant polymer crystal disruption (nylon 6 and poly(benzyl-L-glutamate)) were found to have an increased strain at break. Furthermore, disruption to natural occurring polymer structures did result in either minor or reduced mechanical properties in the case of cellulose and the recombinant spider silk respectively.

This chapter is to be submitted to *Advanced Functional Materials*. In this paper, I was responsible for fabricating polymeric fibers, obtaining FTIR and tensile mechanical data and analyzing all data.



## 4.2. Main Text

WILEY-VCH

### **Robust $\beta$ -sheet reinforced fibers fabricated from unmodified polymers**

*N. J. Chan, S. Lentz, P. A. Gurr, S. Tan, M. Schultebeyring, S. Rosenfeldt, A. Schenk, T. Scheibel\*, G. G. Qiao\**

N. J. Chan, S. Lentz, P. A. Gurr, S. Tan, G. G. Qiao  
Polymer Science Group, Department of Chemical Engineering  
University of Melbourne  
Parkville, Melbourne, Victoria 3010, Australia  
Email: [gregghq@unimelb.edu.au](mailto:gregghq@unimelb.edu.au)

N. J. Chan, S. Lentz, M. Schultebeyring, T. Scheibel  
Lehrstuhl Biomaterialien  
Universität Bayreuth  
Prof.-Rüdiger-Bormann-Str. 1, D-95447 Bayreuth  
Email: [thomas.scheibel@bm.uni-bayreuth.de](mailto:thomas.scheibel@bm.uni-bayreuth.de)

S. Rosenfeldt, A. Schenk  
Bavarian Polymer Institute (BPI)  
Universität Bayreuth  
D-95447 Bayreuth, Germany

S. Rosenfeldt  
Physical Chemistry 1  
Universität Bayreuth  
D-95447 Bayreuth, Germany

A. Schenk  
Physical Chemistry - Colloidal Systems  
Universität Bayreuth  
D-95447 Bayreuth, Germany

Keywords: wet-spinning, NCA ROP, secondary structure, crystallization, biofabrication, fiber

In natural silks,  $\beta$ -sheet crystals are embedded within an amorphous matrix in natural silks, resulting in natural polypeptide-based nanocomposites and contributing to their subsequent high strength and toughness. Consequently, imitation and mimicry of such concepts utilizing polypeptides provides a pathway towards achieving similar properties. Herein, we investigate the introduction of poly(L-valine) (PVal)  $\beta$ -sheet nanocrystals into nylon 6, polycaprolactone (PCL), cellulose acetate, cellulose, poly(benzyl-L-glutamate) (PBLG) and synthetic recombinant spider silk protein eADF4(C16) fibers. Subsequent morphological changes are probed through observation of lattice structure, nanoscale and mesoscale features and microscale morphology. While evidence of  $\beta$ -sheet formation is observed in all fibers, further crystallization of polymer fibers (PCL and cellulose acetate fibers) is also triggered. This crystallization manifests in physical properties with tensile strength increasing from  $614 \pm 63$  to  $1342 \pm 194$  kPa (2.2 times increase) and  $36.1 \pm 5.2$  to  $154.4 \pm 13.4$  MPa (4.3 times increase) respectively for PCL and cellulose acetate fibers upon  $\beta$ -sheet introduction. Thus, it is shown that when used in combination with specific polymer,  $\beta$ -sheet introduction is able to induce crystallization and thus providing an intriguing method of tuning physical properties of such fibers.

### **1. Introduction**

Nature provides a near infinite number of blueprints for the bioinspiration of robust synthetic materials.<sup>[1]</sup> At the forefront of these are materials derived from polypeptides as the monomeric amino acid units, experience various intermolecular interactions such as hydrogen bonding and van der Waals forces to conform into higher order structures – namely secondary structures – including  $\alpha$ -helices and  $\beta$ -sheets.<sup>[2]</sup> Both of such structures are rigid and contribute to material strength due to their lattice packing structures and subsequent intermolecular interactions with each other, with crystal formation resulting from the coiled coil and layered lamellae structures in the case of  $\alpha$ -helices and  $\beta$ -sheets respectively.<sup>[3]</sup> However, such structure alone are very brittle and thus natural nanocomposites provide an avenue to yield tough materials where such rigid structures exist within a more amorphous continuous phase. One prime example is the protein-based dragline spider-silk with a high tensile strength comparable to high tensile steel and orders of magnitude higher toughness.<sup>[4]</sup> The silk protein consists of two categories of repetitive motifs; i) short poly(L-alanine) segment (approximately 5-8 residues in length) which form rigid  $\beta$ -sheet nanocrystals and ii) glycine-rich segments which result in less ordered

structures including random coils. As a tensile load is applied to silk, energy is dissipated between the  $\beta$ -sheet nanocrystals within the less ordered semi-amorphous matrix, before aligning and eventually unravelling prior to rupture.<sup>[5]</sup> The net result is a fiber with a tensile strength between 0.88–1.5 GPa and an extension at break of 21–27%.<sup>[6]</sup> As such, the fabrication of composite fibers with peptidic component capable of forming rigid structures responsible for superior mechanical properties such as  $\beta$ -sheets and synthetic polymeric components similar to spider-silk pose great potential.<sup>[7]</sup>

Multiple strategies have focused on the design and optimization of  $\beta$ -sheet forming peptide-polymer composites.<sup>[8]</sup> The general design strategy for nanocomposite materials involves introducing nanoparticles (such as graphene-based nanoparticles, nanocellulose or clays) into the material precursor solution as a dispersion within a polymeric matrix.<sup>[9]</sup> In the case of polypeptide composites, the polypeptide often forms a 3-D matrix instead of individual nanoparticle components.<sup>[10]</sup> Alternatively, polypeptide hydrogels have been designed to induce the deposition of molecules after hydrogelation to form nanoparticles after hydrogelation – a strategy primarily used for bio-silicification. Through the use of cationic poly-L-lysine blocks, acidic silica-bearing molecules can be deposited within the polypeptide matrix. The morphology of the biosilica deposits was subsequently controlled through the overall structure and morphology as influenced by the matrix secondary structure.<sup>[11]</sup> Polypeptide nanoparticle introduction into a polymeric matrix has also been well researched, but primarily as a micelle for payload delivery, rather than explicitly for mechanical reinforcement.<sup>[12]</sup> The development of discrete  $\beta$ -sheet nanostructures for reinforcement are largely complicated by the uncontrolled aggregation of secondary structures, although strategies to control this such as templating are beginning to develop.<sup>[13]</sup> Predominantly, the design of materials utilizing polypeptides as the reinforcing components primarily utilize a building block approach where polypeptide sequences are attached to a synthetic polymer either through coupling or the use of a synthetic polymer as a macroinitiator, to influence  $\beta$ -sheet formation.<sup>[14]</sup> The resulting microphase separation during material fabrication yields the desired composite on a mesoscale. ABA triblock polymer conformations are particularly popular for such work with a central soft synthetic polymer flanked by peptidic components.<sup>[15]</sup>

While the interactions between different components in any composite are an important factor, this is further complicated by inherent changes in self-assembly of both the polymer composite

and the peptidic component itself.<sup>[16]</sup> Interactions between the peptide and the non-peptidic component, inherently affects the folding of both polymers.<sup>[17]</sup> The studies of the Korley group into films developed from ABA triblocks exemplifies this combined morphological impact.<sup>[18]</sup> This influence extends into impacting the morphology of the other non-peptidic component affecting synthetic polymer crystallinity and spherulite formation specifically in poly(ethylene glycol) (PEG) and poly(Cbz-L-lysine).<sup>[19]</sup> As the peptidic component (poly(Cbz-L-lysine)) was introduced, hydrogen bonding between PEG and peptide bonds resulted in the disruption of the usual intermolecular bonds of PEG, leading to reduced crystallinity. Secondary structure was found to have some degree of impact as well, as samples containing  $\beta$ -sheets were found to have lower crystallinity than their  $\alpha$ -helical counterparts at the same mass concentration. Furthermore, stimuli sensitivity can be altered as has been observed with PEG-polyalanine conjugates. Due to the dehydration of PEG molecules upon heating, resulting in tighter packing of the conjugates and thus induced  $\beta$ -sheet formation.<sup>[20]</sup> Such design traits, while universally useful, do not perfectly translate between different material morphologies, with microfibers being a particularly interesting morphology.

Polypeptides-based fibers primarily utilize synthetic recombinant or purified natural structural proteins as the sole component of the fiber. While keratin, collagen and caesin have all been utilized for such artificial material,<sup>[21]</sup> it is the aforementioned spider silk which forms the basis of the majority of works, whereby either synthetic mimicry or subtle derivatives are investigated. Regenerated silk fibroin derived from silkworms (*i.e. Bombyx mori* spider silk) offers a close natural facsimile sharing similar polypeptide sequence motifs with spider silk despite not bearing the same mechanical superiority.<sup>[22]</sup> Recombinant spider silk provides a synthetic pathway to achieving similar mechanical properties.<sup>[23]</sup> However, recombinant methods require specialization not required by other methods, whilst having limitations of throughput.<sup>[24]</sup> Although *N*-carboxyanhydride ring opening polymerization (NCA ROP) is amenable to high throughput production of polypeptides, its application in polypeptide based microfibers is under investigated.<sup>[25]</sup> To date, only two others studies have explored the use of NCA ROP derived polypeptides within a microfiber.<sup>[26]</sup> However, both strategies required molecular changes to the polymer yielding multiple step processes to even synthesize and purify the desired polymer. Thus, a more facile approach to polypeptide integration is desirable. Building on our previous published work which utilized  $\beta$ -sheet forming polypeptides, derived from NCA ROP poly-L-

valine (PVal), with increased strength, we seek to extend this concept in the formation of microfibers.<sup>[27]</sup>

Herein, we present a novel and broadly applicable technique for introducing  $\beta$ -sheet forming polypeptides into wet spun microfibers from unmodified polymers for mechanical or physical reinforcement by the introduction of L-valine NCA (Val NCA) monomer into the spinning dope and thus controlling the subsequent  $\beta$ -sheet formation. Through this method, we have presented a novel methodology of inducing polymer crystallization through  $\beta$ -sheet formation. This comprehensive investigation includes a diverse range of synthetic and natural polymers – specifically nylon 6, polycaprolactone (PCL), cellulose acetate, cellulose, poly(benzyl-L-glutamate) (PBLG) and a synthetic recombinant spider silk protein eADF4(C16) – to elucidate the nature of this crystallization on a structural level and correlating this to their mechanical properties. Based on polymer crystallization and structures, fibers with higher  $\beta$ -sheet morphology were found to have significant increases in strength (in the case of cellulose acetate and polycaprolactone) or strain at break (in the cases of nylon 6 and poly(benzyl-L-glutamate)). Through this study we have developed a greater understanding of the structural and physical effects of introducing  $\beta$ -sheets to microfibers.

## 2. Results and Discussion

Wet spinning was utilized to fabricate fibers by dissolving NCA and polymer within the spinning dope and extruding the solution into a coagulation bath designed to initiate NCA ROP and produce a  $\beta$ -sheet forming polypeptide within the fiber (Figure 1a, b). The solvent/nonsolvent system was designed such that polymerization would only occur upon extrusion into the coagulation bath. As such, anhydrous solvents or a mixture of anhydrous and acidic solvents were utilized in the spinning dope and 1% triethylamine (TEA) was introduced into the coagulation bath to initiate polymerization. Nonsolvent coagulation baths containing diethyl ether were initially tested but were found to cause the polymers to precipitate too quickly to form continuous fibers. Thus, the nonsolvent coagulation baths of a high fraction of water (or even 100% water) which normally would cause the indiscriminate ring opening of NCA. However, with the inclusion of a small amount of TEA, as in our case, was shown by Heise *et al.* to successfully initiate, NCA ROP within a O/W colloid system.<sup>[28]</sup> PVal was utilized as the  $\beta$ -sheet forming polypeptide due to its high  $\beta$ -sheet forming propensity (especially compared to high molecular weight poly(L-alanine)).<sup>[2b]</sup> Six different polymers were spun using wet



chemical schematic within each fiber during each stage. c) Chemical structure of all spun polymers.

Table 1: Summary of processing conditions for wet-spinning of polymers both with and without Val NCA

Polymer	Spinning Dope Concentration [%]	Spinning Dope Solvent	Coagulation Bath (with 2% TEA)	Configuration	Extrusion Rate [ $\mu\text{L}/\text{min}$ ]
Nylon 6	30	80% MeCOOH 20% DMF	Water	Vertical	30
PCL	15	DMF	Water	Horizontal	45
Cellulose Acetate	15	DMF	Water	Horizontal	35
Cellulose <sup>a)</sup>	-	-	-	-	-
PBLG	10	DMF	Water	Horizontal	30
eADF4(C16)	30	90% MeCOOH 10% DCM	30% Water 30% Diethyl Ether 40% Isopropanol	Vertical	30

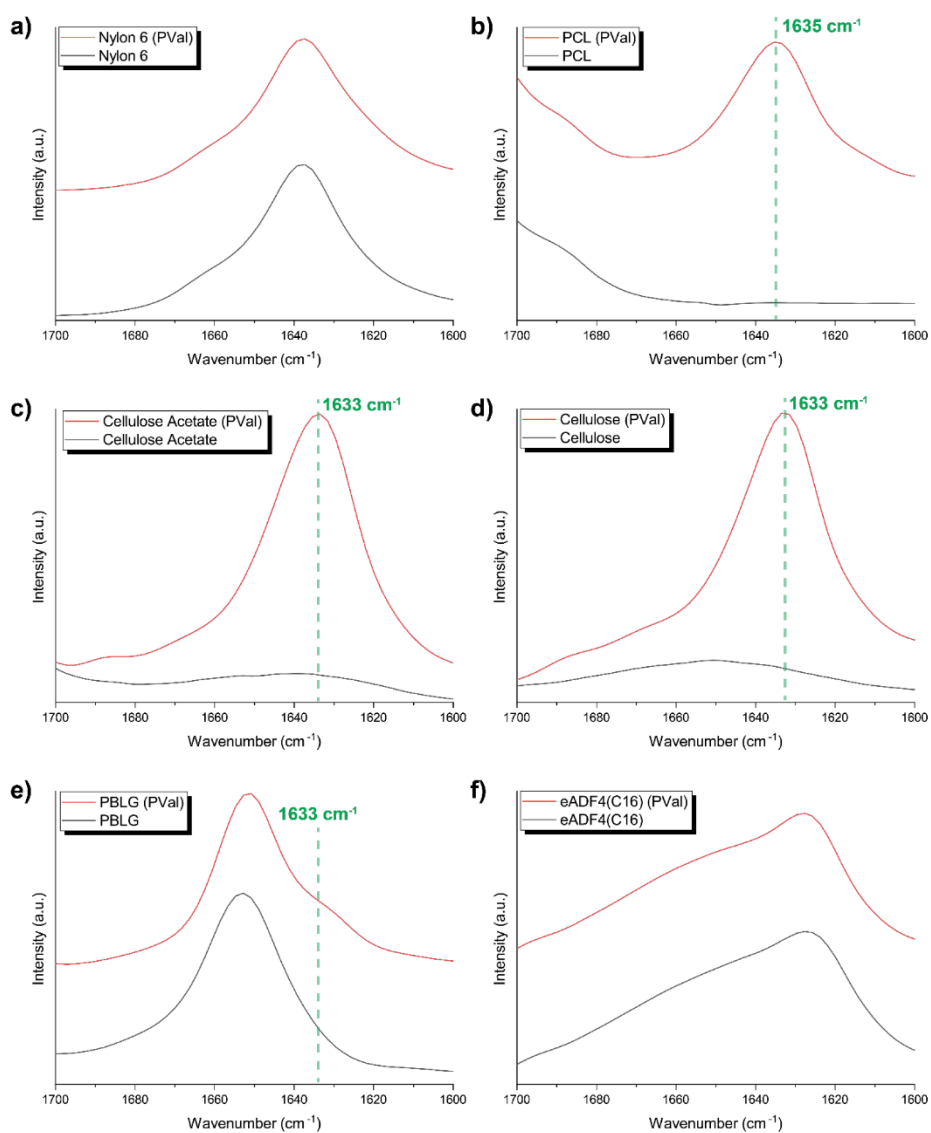
<sup>a)</sup> Cellulose fibers are derived from cellulose acetate fibers after deacetylation.

Fundamentally, elucidating details of the internal structure of the fibers is important in determining why specific mechanical trends may occur. Fourier transform infrared (FTIR) spectroscopy was used to confirm both the introduction of polypeptides and their  $\beta$ -sheet conformation (Figure S1, Supporting Information). Analysis of the Amide I band ( $1600 - 1700 \text{ cm}^{-1}$ ) is common practice for not only indicating the presence of the amide bond in general, but the secondary structure of polypeptides (Figure 2). For fibers derived from non-polyamides, a clear peak is observed at  $1633 \text{ cm}^{-1}$  which specifically correlates to antiparallel  $\beta$ -sheet formation (Figure 2b-d). The PBLG fibers have a peak correlating to  $\alpha$ -helical conformation ( $1652 \text{ cm}^{-1}$ ), while the introduction of PVal yields a shoulder indicating antiparallel  $\beta$ -sheet structures, as with the non-polyamide polymers (Figure 2e). For Nylon 6, however, the peak indicating  $\beta$ -sheet formation does not appear as a distinct shoulder from the close neighbouring peak already present without PVal at  $1638 \text{ cm}^{-1}$  (Figure 2a). Similarly, eADF4(C16) fibers do not show an easily distinguishable shoulder with a prominent peak at  $1625 \text{ cm}^{-1}$  due to  $\beta$ -sheet structure (Figure 2f). Fourier self-deconvolution (FSD) over the whole Amide I band on both peaks failed to determine a separate peak at  $1633 \text{ cm}^{-1}$  and so an alternative analysis was performed.

In each case, the relative intensity of the prominent  $\beta$ -sheet peak compared to other peaks was determined (Table S2, Supporting Information). Here for each polymer, either the appearance or increase in relative signal of the  $\beta$ -sheet peak was determined upon the introduction of PVal. In the case of Nylon 6, the relative Amide I signal was compared to the CH and CH<sub>2</sub> aliphatic

stretch at  $2850 - 2950 \text{ cm}^{-1}$  showing a distinct increase, attributed to an increase in the amide structure of  $\beta$ -sheets. For the two polypeptide-based fibers, Fourier self-deconvolution (FSD) could be restricted to the Amide I band as this would conveniently give a secondary structure content breakdown (Table S3, Supporting Information). For PBLG, the  $\beta$ -sheet content rose from 2 % to 11 % while in the case of eADF4(C16),  $\beta$ -sheet content was found to increase from 46 % to 54 % which is correlated to PVal. For Nylon 6 and eADF4(C16), this shift of the  $\beta$ -sheet band to preexisting amide I peaks, may be due to numerous factors with one likely reason being the incorporation of the  $\beta$ -sheet into the polymer's natural substructures.





**1623 - 1637  $\text{cm}^{-1}$  =  $\beta$  sheet**

Figure 2: Fourier transform infrared (FTIR) spectroscopy of Amide I band (1600-1700  $\text{cm}^{-1}$ ) for fiber samples with and without PVal for a) nylon 6, b) poly(caprolactone) (PCL), c) cellulose acetate, d) cellulose, e) poly(benzyl-L-glutamate) and f) eADF4(C16).

Changes in both cross sectional and surface morphology due to PVal introduction were visualized using scanning electron microscopy (SEM). Broadly, the overall roughness of the surface of all fibers was increased upon introduction of PVal (Figure 3). This can be attributed to three different factors; i) the precipitation of the Val NCA disrupting the precipitation of the primary polymer matrix, ii) the conformational changes after aggregation and folding of the Val NCA and iii) the production of carbon dioxide during NCA ROP. The first of these points is well shown in the overall fiber structure where samples without any PVal were found to remain straight (Figure 3i) while those containing PVal were found to twist to some degree (Figure 3iii). Nylon 6 samples were all found to have an undulated surface consistent with previous studies, but upon introduction of PVal (Figure 3aiii-iv), regions with greatly increased roughness are present on the surface of the fiber, consistent with  $\beta$ -sheet aggregates close to the surface. In contrast, PCL fibers were found to have comparatively little change in morphology despite being somewhat chemically similar to nylon 6 (both are linear synthetic polymers with no pendant groups), with fibers being extremely porous both with and without  $\beta$ -sheet introduction (Figure 3b). A drastic decrease in homogeneity can be observed on the surface of cellulose acetate fibers with  $\beta$ -sheet introduction and jagged ridges and edges appearing along the surface at a greater frequency, which is likely a product of the combination of aforementioned three factors (Figure 3c). This morphological difference between  $\beta$ -sheet loaded samples and their control counterpart is absent in cellulose fibers which were already porous without the introduction of PVal. The lack of change can be attributed to molecular rearrangement upon deacetylation, which then alters rearrangement after  $\beta$ -sheet has been formed as opposed to during molecular rearrangement as with other fibers (Figure 3d). Interestingly, the two polypeptide-based fibers both resulted in clear morphological changes though with different impact. In both cases, aggregation was not found to show any distinct visual difference from the rest of the polymer matrix. Striations on the PBLG fibers were still present, although non-directional bumps were also found across the surface (Figure 3e). Control eADF4(C16) fibers were found to have globule-like aggregates on the surface, but upon introduction of PVal the surface is a lot smoother (Figure 3f).

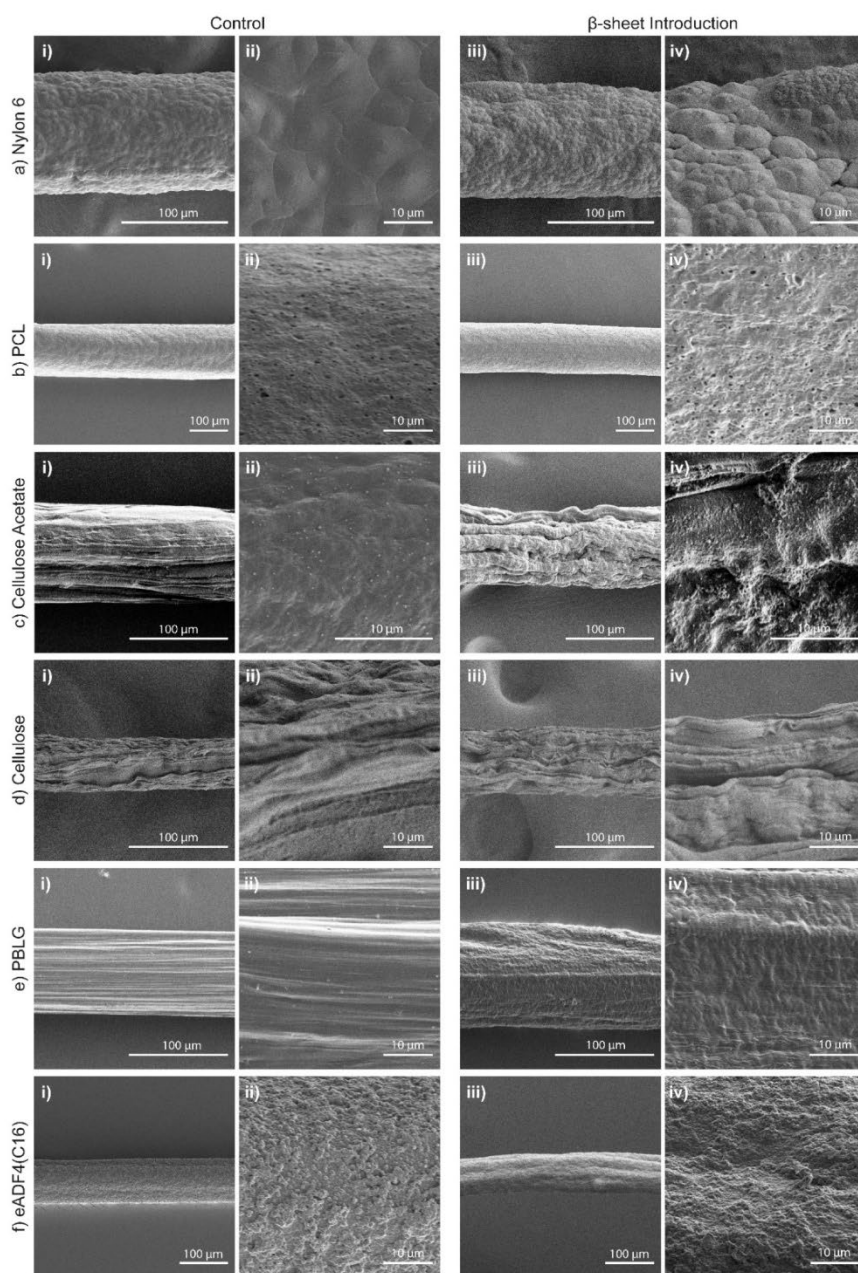


Figure 3: Scanning electron microscopy (SEM) of fiber surface at i, iii) low magnification and ii, iv) high magnification for fiber samples i, ii) with and iii, iv) without PVal for a) nylon 6, b) poly(caprolactone) (PCL), c) cellulose acetate, d) cellulose, e) poly(benzyl-L-glutamate) and f) eADF4(C16).

Cross sectional visualization of fibers further demonstrates the impact of introducing  $\beta$ -sheet forming polypeptides within the materials (Figure 4). Interestingly, distinct regions of aggregation were only clearly visible in commercially available synthetic polymers (*i.e.* those with long chain aliphatic backbones). In the case of Nylon 6, these distinct regions required close inspection as regions were less than 2  $\mu\text{m}$  in scale (Figure S2, Supporting Information) while these regions in PCL samples were found to be more continuous at a larger scale. Furthermore, PCL fibers both have hollow interiors as a byproduct of the fast coagulation. Due to their long aliphatic backbones, repetitive regions between hydrogen bonding groups are molecularly distant, hence resulting in the discrete regions where PVal chains will favor hydrogen bonding with solely PVal in these two fibers. In contrast, all other fibers displayed a more homogeneous and continuous integration of  $\beta$ -sheets. Cellulose acetate fibers displayed much larger pores compared to Nylon 6 due to processing. The introduction of PVal does appear to be homogeneously distributed clearly showing aggregates on a micrometer scale. The internal porous structure changes during the deacetylation process and the formation of cellulose fibers, though it is hard to discern any obvious changes in aggregation at a micrometer scale. The two polypeptide fibers do not possess the same macroporous nature of the other fibers. PBLG fibers did not show discernable internal differences upon introduction of PVal. However, eADF(C16) fibers without PVal were found to possess a corona surrounding the core, which was no longer present once PVal was included, implying reduced microphase separation during spinning. While it is confirmed that the introduction of PVal has introduced  $\beta$ -sheets within all fibers and presented microscale morphological changes, a further analysis of mesoscale structures is required to determine the molecular influence of  $\beta$ -sheet introduction.

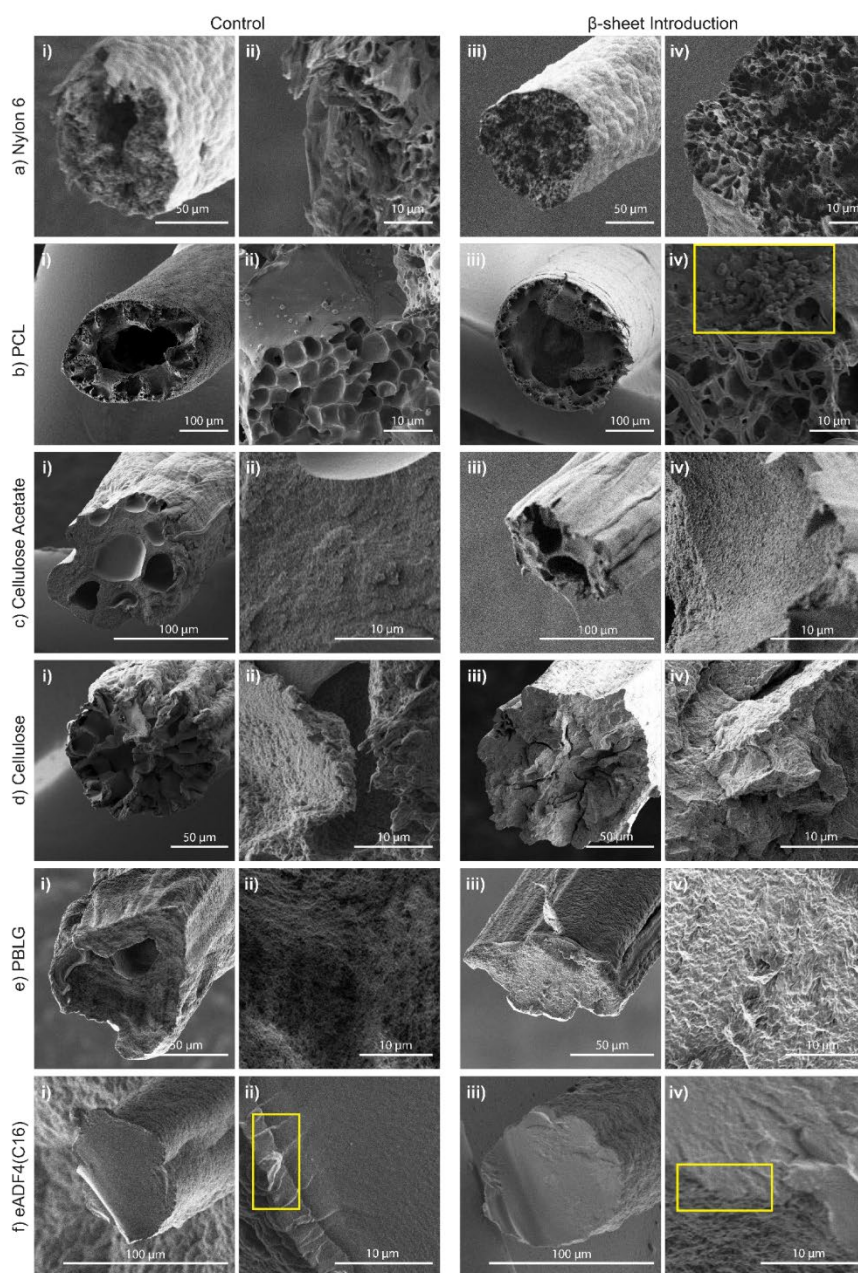


Figure 4: Scanning electron microscopy (SEM) of fiber cross-section at i, iii) low magnification and ii, iv) high magnification for fiber samples i, ii) with and iii, iv) without PVal for a) nylon 6, b) poly( $\epsilon$ -caprolactone) (PCL), c) cellulose acetate, d) cellulose, e) poly( $\epsilon$ -benzyl-L-glutamate) and f) eADF4(C16). Features mentioned in text highlighted in yellow.



Further analysis of molecular confirmation within fibers provides insight into both the arrangement of PVal  $\beta$ -sheet structures and the polymer itself. Previous studies have correlated  $d$  spacings of 4.6–4.7 Å to the interstrand spacing between  $\beta$ -strands; and 10 Å to the intersheet spacing within  $\beta$ -sheet nanocrystals, cumulating in a cross- $\beta$  structure indicative of antiparallel  $\beta$ -sheet nanocrystals.<sup>[29]</sup> X-ray diffraction (XRD) reveals a peak indicative of a  $d$ -spacing of 10 Å, within all samples upon introduction of PVal with the exception of eADF4(C16) (Figure 5). Notably, this peak is not visible within Nylon 6,<sup>[30]</sup> PCL,<sup>[31]</sup> cellulose<sup>[32]</sup> and PBLG<sup>[33]</sup> without PVal as is in accordance with literature, indicating this  $d$ -spacing can solely be attributed to the intersheet spacing of antiparallel  $\beta$ -sheets. Cellulose acetate contains a broad peak within this region indicating minor crystallinity with a broad range of crystal sizes,<sup>[34]</sup> but ultimately this peak is much more defined and slightly shifted upon introduction of PVal and the slight shift in the position of the peak maximum indicates the presence of the intersheet spacing. Interestingly, a  $d$ -spacing of 4.6 Å was observed as a slight shoulder in most instances, but most prominently in cellulose acetate and PCL in particular remaining consistent with previous reports of  $\beta$ -sheet structures.<sup>[35]</sup> eADF4(C16) is an exception in this case as well where a peak is observed at  $2\theta = 20.1^\circ$ ,  $d = 4.4$  Å in both samples implying alanine-based  $\beta$ -sheet packing due to the reduced side chain size.<sup>[26b, 35b]</sup> However, there is no notable comparative difference between samples with and without PVal, though this affirms FTIR results where the  $\beta$ -sheet peak from PVal is not distinct from the  $\beta$ -sheet peak in eADF4(C16) fibers without PVal. Overall and in conjunction with FTIR,  $\beta$ -sheet nanocrystal formation with regular inter-strand and interplanar spacings is confirmed. However, two distinct peaks are also observed in cellulose acetate and PCL at 4.1 and 3.7 Å which are unique to both polymers and require further investigation.

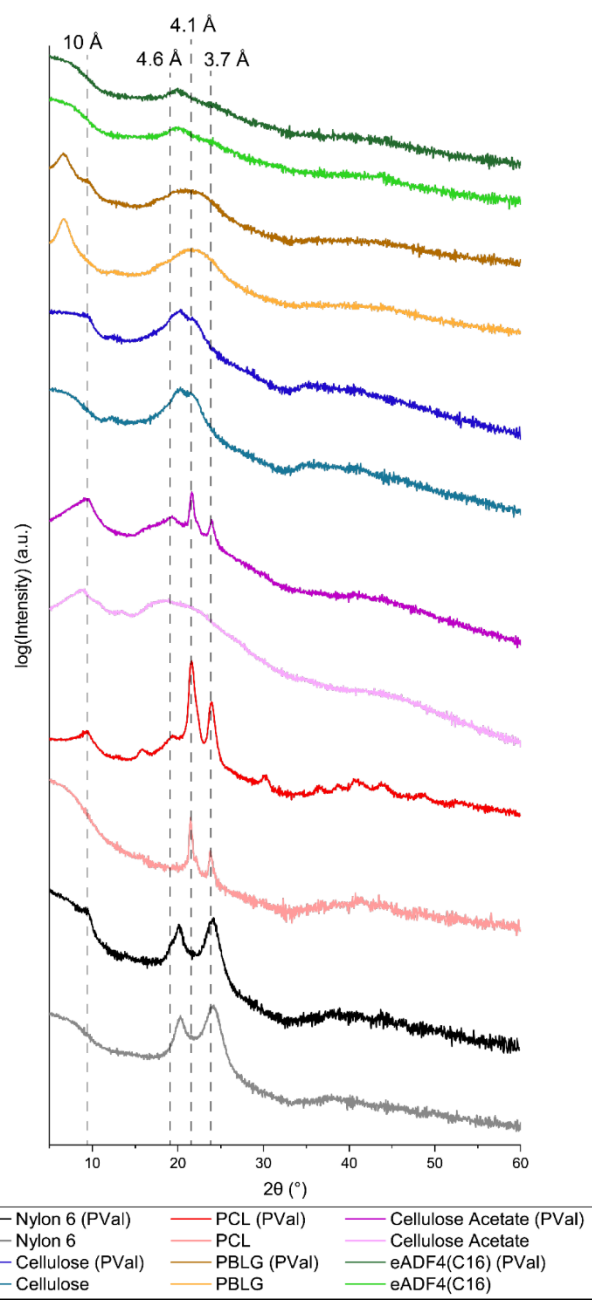


Figure 5: X-ray diffraction (XRD) spectra for fiber samples with and without PVal for nylon 6, poly( $\epsilon$ -caprolactone) (PCL), cellulose acetate, cellulose, poly( $\epsilon$ -benzyl-L-glutamate) (PBLG) and eADF4(C16).

The two unknown peaks indicate the induced crystallization of the polymer itself through this method of introducing  $\beta$ -sheets. In the case of cellulose acetate fibers, a  $d$ -spacing of 3.7 Å has previously been assigned to lattices structures of cellulose and its derivatives,<sup>[36]</sup> though they have also been assigned to natural  $\beta$ -sheets and thus cannot be specifically assigned to either component. However, the peak at  $2\theta = 21.6^\circ$ ,  $d = 4.1$  Å has previously been assigned to crystalline cellulose.<sup>[37]</sup> In the case of PCL, these peaks emerge at the characteristic crystalline peaks of the polymer itself and thus differential scanning calorimetry (DSC) was used to determine if this correlates to a change in bulk crystallinity of the PCL itself (Figure S3, Supporting Information). Upon introduction of  $\beta$ -sheets fiber crystallinity was increased from 40% to 47% (7% increase in crystallinity). Interestingly, the most distinguishing feature of cellulose acetate and PCL from a molecular standpoint is a comparative lack of hydrogen bond donors compared to other polymers (pendant hydroxyl groups on cellulose and the amide backbone of the other polymers). This is supported by Matolyak *et al.* who have previously shown a reduction in PEG crystallinity with increased  $\beta$ -sheet content in peptide-polyurea hybrid films, due to enhanced interaction between the synthetic and peptide components and subsequent disruption of the crystalline structures within the polymer matrix.<sup>[19]</sup> It should be noted that matrix polymer crystallinity was reduced in their work in all samples compared to the control without peptide due to the hydrogen bonding of peptidic units, but this difference is due to the utilization of materials of different classes and the subsequent different fabrication techniques rather than a discrepancy. Furthermore, this also supports why other polymers with greater hydrogen bonding capabilities were found to not have this increase in crystallinity which is likely due to disruption and subsequent intercalation of pre-existing crystalline regions.

Small angle x-ray scattering (SAXS) was further utilized for the assessment of subsequent nanostructures (Figure S4, Supporting Information). Despite molecular alterations, fibers lacked the introduction of unique nanoscale features upon introduction of  $\beta$ -sheets. Interestingly, a small peak in cellulose fibers can be observed at  $\sim 0.053$  Å<sup>-1</sup> ( $\sim 1.8$  nm) which has been observed in cellulose fiber previously as cellulose nanocrystals,<sup>[38]</sup> but this is lost upon introduction of the PVal, implying the intercalation of  $\beta$ -sheet structures within the material. This is contrast to the PCL fibers which retain their feature at  $\sim 0.046$  Å<sup>-1</sup> ( $\sim 2.1$  nm) both with and without  $\beta$ -sheets.

To determine the geometric organization of fibers, power law analysis (Equation 1) was used on SAXS spectra to calculate the mass fractal dimension  $n$  (i.e. dictates the degree of order where lower values indicate more ordered structures) giving insight into the nanoscale



arrangement of polymers (Table 2).<sup>[39]</sup> For all fibers (except for eADF4(C16)),  $n \sim 4.0$ , indicating overall low structural order. In the cases of nylon 6, PCL and cellulose acetate,  $\beta$ -sheet introduction did not significantly affect this dimensionality, indicating insignificant nanoscale geometric alterations. Cellulose and PBLG both exhibit a shift to  $n \sim 3.5$  and  $\sim 3.3$  respectively, indicating a partial increase in order within the bulk polymer matrix as caused by PVal introduction and intercalation of  $\beta$ -sheets. Conversely, however, eADF4(C16) the opposite effect was observed below approximately  $\sim 0.01 \text{ \AA}^{-1}$  ( $\sim 10 \text{ nm}$ ), represented by a shift from  $n \sim 3.5$  to  $\sim 3.9$ . A shift at higher scanning vectors to  $n \sim 2$  indicates more ordered disc-like structures throughout the fiber. As eADF4(C16) is precisely designed to assemble into  $\beta$ -sheet favoring geometries, the inclusion of a disruptive second polypeptide in the form of PVal is expected to reduce this order as observed.

$$I(q) \propto q^{-n} \quad (1)$$

Where  $I$  is the scattering intensity

$q$  is the scanning vector size ( $\text{\AA}^{-1}$ )

$n$  is the mass fractal dimension

Table 2: Summary of the mass fractal dimensions of all polymers with and without PVal.

Polymer	Power law exponent ( $n$ )	
	Without PVal	With PVal
Nylon 6	4.0	4.0
PCL	4.1	4.0
Cellulose Acetate	3.9	3.9
Cellulose <sup>a)</sup>	4.0	3.5
PBLG	3.9	3.3
eADF4(C16)	3.5 ( $q < 0.01 \text{ \AA}^{-1}$ ) 2.2 ( $q > 0.01 \text{ \AA}^{-1}$ )	3.9 ( $q < 0.01 \text{ \AA}^{-1}$ ) 2.0 ( $q > 0.01 \text{ \AA}^{-1}$ )

As would be expected with the wide array of morphological changes exhibited over the range of tested polymers, the impact on mechanical properties is varied (Figure 6). Almost all fibers experience an increased Young's modulus which can be correlated to the presence of more rigid structures. Notably, only the two polymers which experienced internal polymer crystallization experienced a significantly increased strength upon PVal introduction (outlined in red), with an increase from  $614 \pm 63$  to  $1342 \pm 194 \text{ kPa}$  (2.2 times increase) and  $36.1 \pm 5.2$  to  $154.4 \pm 13.4 \text{ MPa}$  (4.3 times increase) for PCL and cellulose acetate respectively (Figure 6b, c). Thus, it can be concluded that the introduction of  $\beta$ -sheet alone is insufficient for increasing mechanical strength but is also a result of induced polymer crystallization. Only nylon 6 and PBLG exhibited increases in elongation at break from  $31.8 \pm 2.2 \%$  to  $90.9 \pm 5.9 \%$  (2.9 times increase)

and  $87.8 \pm 8.3 \%$  to  $159.2 \pm 29 \%$  (1.8 times increase) respectively (Figure 6a, d, outlined in blue). While the polymer matrix may not be greatly affected in both cases, the strong hydrogen bonding between their polyamide backbones still allows for energy dispersion throughout the fiber during tensile load. This potential for high degrees of hydrogen bonding further extends to both cellulose and eADF4(C16) fibers (outlined in green), however both have undergone fundamental structural changes that counteract this potential. The loss of nanocrystalline structure due to structural disruption in cellulose fibers would contribute to reduced mechanical properties, but the increase in nanoscale order counteracts this to yield fibers with no statistically significant difference in mechanical properties. eADF4(C16) is the only polymer fiber to result in reduced mechanical capabilities in all assessments including Young's modulus which can be correlated to the lack of cross- $\beta$  structures and a reduction in fractal dimensionality upon  $\beta$ -sheet introduction (Figure 6f). Due to the design of eADF4(C16) leading to precise self-assembly characteristics, the disruption of the polymer matrix with PVal was expected to have a much more pronounced effect compared to other polymers resulting in the structural and consequential mechanical changes as described.

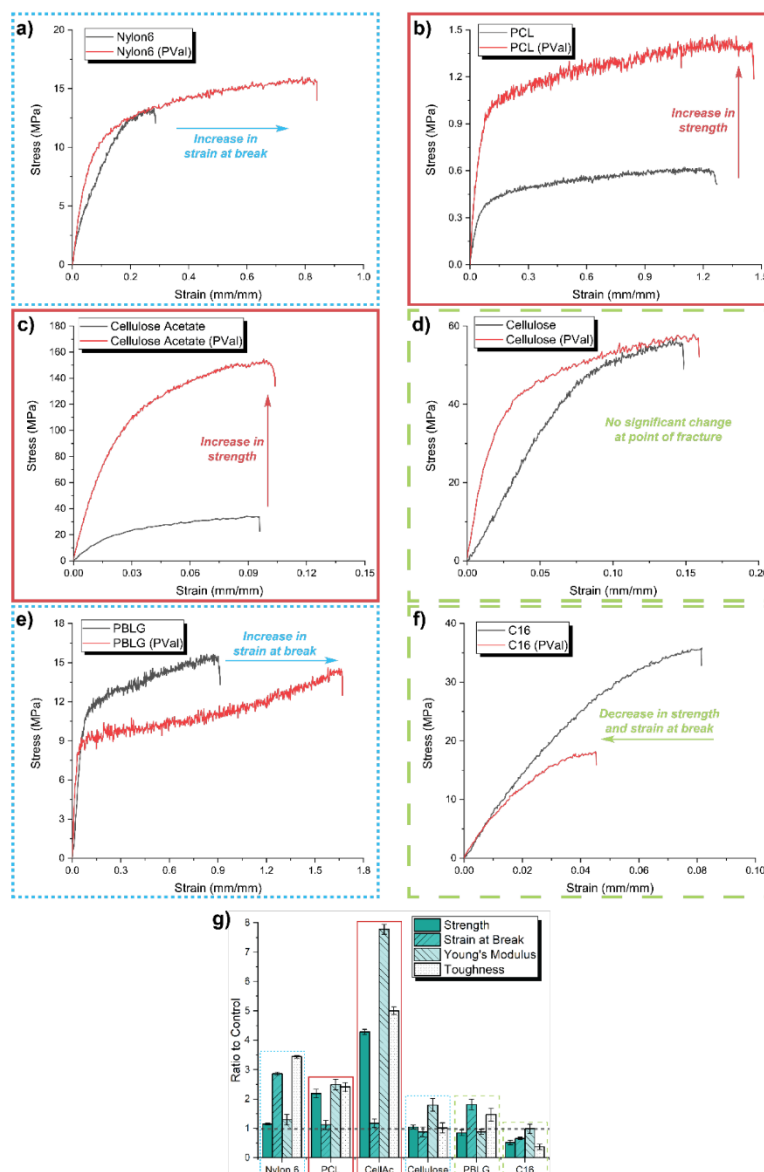


Figure 6: Example tensile mechanical testing curves for fibers without polypeptide and with Pval and PGly for a) nylon 6, b) poly( $\epsilon$ -caprolactone) (PCL), c) cellulose acetate, d) cellulose, e) poly( $\epsilon$ -benzyl-L-glutamate) and f)  $\epsilon$ ADF4(C16). g) Summary of relative impact of PVal on strength, extension at break, Young's modulus and toughness for all polymers. Samples which experience a strength increase outlined in red, samples which experience an increase in strain at break outlined in dashed blue and samples which experience no significant difference or reduced mechanical properties outlined in green.

### 3. Conclusion

In summary, we have developed a novel and facile methodology for introducing  $\beta$ -sheets into a range of different polymer fibers and investigated the subsequent changes in morphology due to this technique. By introducing Val NCA monomer into the spinning dope, polymerization could be initiated during the fabrication of different synthetic, polysaccharide, and polypeptide fibers. Upon investigation into substructures, cross- $\beta$  structures typical of  $\beta$ -sheet inclusion were found to be present in the majority of fibers. However, further intermolecular interactions between the subsequent PVal-based  $\beta$ -sheets and the polymer, increased the bulk crystallization in PCL and cellulose acetate fibers, which both have a low density of hydrogen bond acceptors compared to the other polymers. Such fibers were found to have increases in tensile strength upon  $\beta$ -sheet introduction of up to 4.3 times. Other polymers which did not exhibit a loss in structure – namely nylon 6 and PBLG – exhibited an increase in extensibility at break of up to 2.9 times instead due to the increased density of hydrogen bonding. However, this increased hydrogen bonding was found to disrupt the internal structure of other polymers more significantly. No significant mechanical change in the case of cellulose where a loss of nanoscale structure was found to be counterbalanced by an overall increase in nanoscale structural order. In the case of the recombinant spider silk mimic (eADF4(C16)), the reduced nanoscale structural order resulted in all mechanical properties being significantly inferior to the counterpart without PVal. Thus, we have established a novel and facile fiber fabrication system to introduce  $\beta$ -sheet structures without complex or multi-step reactions, garnering significant changes in fiber properties and thus guide the future development of tough materials and fibers.

### 4. Materials and Methodology

*Materials:* Acetone (tech. grade, VWR chemicals), alginate sodium salt (300-350 kDa, Carl Roth), *N,N*-dimethyl formamide (DMF, 99.8%, anhydrous, Sigma-Aldrich), diethyl ether (Et<sub>2</sub>O, AR grade, Chem-Supply), cellulose acetate (MW 100,000, Arcos Chemicals), ethanol (tech. grade, VWR chemicals), formic acid (puriss. p. a.  $\geq 98\%$ , Sigma Aldrich), L-valine-OH ( $>99\%$ , Mimotopes), L-Glu(OBzl)-OH ( $>99\%$ , Mimotopes), magnesium sulfate (anh. MgSO<sub>4</sub>,  $\geq 97\%$ , Merck),  $\alpha$ -pinene (98%, Merck), sodium hydrogen carbonate (NaHCO<sub>3</sub>, AR grade, Chem-Supply), sodium hydroxide (NaOH;  $\geq 97\%$ , Merck), triethylamine (TEA,  $\geq 99.5\%$ , Sigma-Aldrich), triphosgene ( $\geq 98\%$ , Merck), and Nylon 6 (Sigma Aldrich) were all used as received without further purification. Saturated brine solution was prepared from sodium chloride (NaCl,

AR grade, Chem-Supply) in DI water. Tetrahydrofuran (anh. THF, inhibitor free, >99.9%, Merck), ethyl acetate (anh. EtOAc, >99.9% Honeywell) and were purified by passage through a solvent purification system (SBPT-1, LC Technologies, USA) containing 4Å sieves under Argon gas. Hexane (AR, Chem-Supply) was distilled over calcium hydride under nitrogen prior to use.

*Synthesis of Valine NCA (Val NCA) and Benzyl-protected Glutamic Acid (Glu(OBzl) NCA):*

Both NCAs were synthesized using modified versions of previous reported methods.<sup>[27]</sup> In a typical experiment Val (10.0 g, 42.2 mmol) was added to a 500 mL three-necked RBF and suspended in 200 mL of anh. THF with  $\alpha$ -pinene (31.1 mL, 96.9 mmol, 1.15 excess moles) under nitrogen. After heating to 60 °C, triphosgene (10.1 g, 16.9 mmol, 1.2 excess moles) was added and the mixture was stirred at temperature for 2 h. Solvent was then removed from the clear solution under reduced pressure and replaced with 100 mL of anh. EtOAc. The solution was cooled to -18 °C before washing with sat. brine (1 × 100 mL) and then 5 w/v% aq. NaHCO<sub>3</sub> (1 × 100 mL) and the organic phase dried over MgSO<sub>4</sub>. The filtered solution was reduced to dryness *in vacuo* and recrystallized using anh. hexane at -18 °C over 16 h. The solids were then filtered and redissolved into anh. EtOAc before being precipitated into anh. hexane. The precipitate was then dried *in vacuo* over 24 h to afford a colorless solid and stored under argon at -80 °C.

Val NCA (10.2 g, 83% yield): <sup>1</sup>H NMR (400 MHz, CDCl<sub>3</sub>,  $\delta$ ): 1.00-1.09 (m, J = 7.0 Hz, 3H; -CH-(CH<sub>3</sub>)<sub>2</sub>), 2.27 (1, 1H; -CH-(CH<sub>3</sub>)<sub>2</sub>), 4.24 (d, J = 4.4 Hz, 1H; -CH-NH-), 6.79 (s, 1H; ringNH)

Glu(OBzl) NCA (9.7 g, 87 % yield): <sup>1</sup>H NMR (400 MHz, CDCl<sub>3</sub>,  $\delta$ ): 2.08–2.31 (m, 2H; -CH<sub>2</sub>-CH<sub>2</sub>-CO-), 2.55 (t, J = 6.8 Hz, 2H; -CH<sub>2</sub>-CH<sub>2</sub>-CO-), 4.42 (t, J = 6.0 Hz, 1H; -CH-NH-), 5.11 (s, 2H; -CH<sub>2</sub>-ArH), 6.47 (s, 1H; ringNH), 7.35–7.40 (m, 5H; ArH).

*Synthesis of Poly(benzyl-L-glutamic acid) (PBLG):*

Glu(OBzl) NCA (1.50 g) was dissolved in 50 mL of anh. DCM under nitrogen in a 100 mL RBF. To the stirring solution was added TEA, and the clear solution was stirred under an argon bleed at room temperature for 24 h. The reaction mixture was then precipitated into and subsequently rinsed with Et<sub>2</sub>O which was then dried and stored under vacuum to afford a clear tacky solid as the final product (2.84 g, 78.5% yield). <sup>1</sup>H NMR (400 MHz, DMSO-*d*<sub>6</sub>,  $\delta$ ): 2.04–2.48 (m, 2H; -CH<sub>2</sub>-CH<sub>2</sub>-CO-), 3.90 (t, 1H; -CH-N-CO-), 5.00 (s, 2H, -CH<sub>2</sub>-ArH), 5.59 (s, 1H; ringNH), 7.19–7.30 (m, 5H; ArH).

*Wet Spinning of Polymeric Fibers:* Polymer solutions with assigned spinning dope concentrations were dissolved over 4 h (until complete dissolution in anhydrous spinning dope solvent under nitrogen according to Table 1. For samples loaded with NCA, NCA was then introduced into the solution at a 4:1 ratio of polymer to NCA. The subsequent solution was extruded into the coagulation bath with 2% TEA as an initiator at a continuous rate. Upon precipitation, the fiber was drawn out of the coagulation bath and dried under an infrared lamp before being collected. After 24 h, the collected fibers were washed in the coagulation bath solution without TEA, 3 times and subsequently dried under an air stream for 48 h.

*Deacetylation of Cellulose Acetate Fibers:* Cellulose acetate fibers were soaked in a solution of 0.5 N aq. 50% EtOH / 50% H<sub>2</sub>O for 24 h. Subsequent cellulose fibers were washed progressively in 50% EtOH / 50% H<sub>2</sub>O, 25% EtOH / 75% H<sub>2</sub>O solution and H<sub>2</sub>O before subsequent drying under an air stream for 48 h.

*Mechanical Testing:* Tensile mechanical testing was performed using an ElectroForce 3200 (TA Instruments, DE, USA) with 2.5 N load cells. Small sections of fibers were randomly selected and fixed onto plastic frames with a gap of 3 mm using two-component glue in case of dry samples. The glue was left to dry under a fume hood for at least 24 h. The frames were then fixed between the clamps of the testing device and pulled apart until failure at a rate of 0.01 mm s<sup>-1</sup> at a relative humidity of 65%, and room temperature. The Young's modulus was obtained by calculating the slope of the stress–strain curve in the linear elastic region. The fiber toughness was calculated by integrating the stress–strain curve. The measurements were repeated for a minimum of five individual samples.

*Equipment:* ATR-FTIR spectroscopy was performed with a Bruker Hyperion 1000 microscope with a dedicated ATR-objective (Bruker Optics GmbH, Ettlingen, Germany). The ATR-crystal was brought into contact with the sample. The microscope was continuously purged with dry air, and the MCT detector was cooled with liquid nitrogen. The FTIR spectra were recorded with a resolution of 4 cm<sup>-1</sup>. One hundred scans per measurement were performed. Three samples per layer with three spots per sample were measured. Scanning electron microscopy (SEM) was attained using a Leo 1530 Gemini (Zeiss, Oberkochen, Germany) at an accelerating voltage of 3 kV. Samples were sputtered with 1.3 nm platinum. SAXS was performed using

the small-angle X-ray system “Double Ganesha AIR” (SAXSLAB, Denmark). The X-ray source is a rotating anode (copper, MicoMax 007HF, Rigaku Corporation, Japan) providing a microfocused beam. XRD patterns were obtained on a Bragg–Brentano-type diffractometer (Empyrean, Malvern Panalytical BV, The Netherlands) equipped with a PIXcel-1D detector using Cu K $\alpha$  radiation ( $\lambda = 1.54187 \text{ \AA}$ ). All patterns were analyzed using Malvern Panalyticals’s HighScore Plus software. Differential scanning calorimetry (DSC) measurements on PCL were carried out on a PerkinElmer DSC 8500 with a heating rate of  $40 \text{ }^\circ\text{C min}^{-1}$ . Subsequent crystallization was determined by determining the heat of melting of crystalline structures and determining it as a percentage of the heat of melting of 100 % crystalline PCL.<sup>[40]</sup>

### Supporting Information

Supporting Information is available from the Wiley Online Library.

### Acknowledgements

This work was performed in part at the Materials Characterization and Fabrication Platform (MCFP) at the University of Melbourne. N.J.C thanks The University of Melbourne for providing Australian Government Research Training Program Scholarship (AGRTP) for providing funds for travel. This work is supported by grants DFG SCHE603/23-1. N.J.C., S.L., G.G.Q. and T.S. acknowledge funding from the German Academic Exchange Service (DAAD) through its thematic network Bayreuth-Melbourne Colloid/Polymer Network sponsored from funds of the Federal Ministry of Education and Research (BMBF).

Received: ((will be filled in by the editorial staff))

Revised: ((will be filled in by the editorial staff))

Published online: ((will be filled in by the editorial staff))

### References

- [1] a) C. Zhang, D. A. Mcadams II, J. C. Grunlan, *Advanced Materials* **2016**, 28, 6292; b) M. S. Ganewatta, Z. Wang, C. Tang, *Nature Reviews Chemistry* **2021**, 5, 753.
- [2] a) C. Bonduelle, *Polymer Chemistry* **2018**, 9, 1517; b) K. Fujiwara, H. Toda, M. Ikeguchi, *BMC Structural Biology* **2012**, 12, 18.
- [3] S. Mondal, G. Jacoby, M. R. Sawaya, Z. A. Arnon, L. Adler-Abramovich, P. Rehak, L. Vuković, L. J. W. Shimon, P. Král, R. Beck, E. Gazit, *Journal of the American Chemical Society* **2019**, 141, 363.

- [4] a) A. E. Brooks, H. B. Steinkraus, S. R. Nelson, R. V. Lewis, *Biomacromolecules* **2005**, 6, 3095; b) M. Saric, L. Eisoldt, V. Döring, T. Scheibel, **2021**, 33, 2006499; c) S. M. Correa-Garhwal, T. H. Clarke, M. Janssen, L. Crevecoeur, B. N. McQuillan, A. H. Simpson, C. J. Vink, C. Y. Hayashi, *Scientific Reports* **2019**, 9, 13656; d) M. Xu, R. V. J. P. o. t. N. A. o. S. Lewis, **1990**, 87, 7120.
- [5] a) G. R. Plaza, J. Pérez-Rigueiro, C. Riekkel, G. B. Perea, F. Agulló-Rueda, M. Burghammer, G. V. Guinea, M. Elices, *Soft Matter* **2012**, 8, 6015; b) D. T. Grubb, L. W. Jelinski, *Macromolecules* **1997**, 30, 2860; c) C. Riekkel, C. Bränden, C. Craig, C. Ferrero, F. Heidelbach, M. Müller, *International Journal of Biological Macromolecules* **1999**, 24, 179.
- [6] O. Hakimi, D. P. Knight, F. Vollrath, P. Vadgama, *Composites Part B: Engineering* **2007**, 38, 324.
- [7] J. C. Johnson, L. T. J. Korley, *Soft Matter* **2012**, 8, 11431.
- [8] S. Mondal, S. Das, A. K. Nandi, *Soft Matter* **2020**, 16, 1404.
- [9] a) S. Murugesan, T. Scheibel, *Advanced Functional Materials* **2020**, 30, 1908101; b) S. Mondal, *Polymer-Plastics Technology and Engineering* **2018**, 57, 1377; c) A. Kumar, K. Sharma, A. R. Dixit, *Journal of Materials Science* **2019**, 54, 5992.
- [10] Y. Qian, S. Di, L. Wang, Z. Li, *Journal of Materials Chemistry B* **2021**, 9, 6521.
- [11] a) J.-S. Jan, T.-H. Chuang, P.-J. Chen, H. Teng, *Langmuir* **2011**, 27, 2834; b) K.-J. Chen, H.-L. Chen, C.-C. Tang, H.-H. Wu, J.-S. Jan, *Journal of Colloid and Interface Science* **2019**, 542, 243; c) L. Xia, Y. Liu, Z. Li, *Macromolecular Bioscience* **2010**, 10, 1566.
- [12] a) L. Wei, C. Cai, J. Lin, T. Chen, *Biomaterials* **2009**, 30, 2606; b) M. Patel, T. Nakaji-Hirabayashi, K. Matsumura, *Journal of Biomedical Materials Research Part A* **2019**, 107, 1094.
- [13] a) S. Goh, A. Platt, K. Rutledge, I. Lee, *Journal of polymer science. Part A, Polymer chemistry* **2008**, 46, 5381; b) S. H. Wibowo, A. Sulistio, E. H. H. Wong, A. Blencowe, G. G. Qiao, *Aust J Chem* **2014**, 67, 598.
- [14] a) M. A. Gauthier, H.-A. Klok, *Chemical Communications* **2008**, DOI: 10.1039/B719689J2591; b) L. A. Canalle, D. W. P. M. Löwik, J. C. M. van Hest, *Chemical Society Reviews* **2010**, 39, 329; c) J. Y. Shu, B. Panganiban, T. Xu, *Annual Review of Physical Chemistry* **2013**, 64, 631.
- [15] a) E. Ibarboure, E. Papon, J. Rodríguez-Hernández, *Polymer* **2007**, 48, 3717; b) H. J. Moon, B. G. Choi, M. H. Park, M. K. Joo, B. Jeong, *Biomacromolecules* **2011**, 12, 1234.
- [16] a) A. Maslovskis, J. B. Guilbaud, I. Grillo, N. Hodson, A. F. Miller, A. Saiani, *Langmuir* **2014**, 30, 10471; b) R. Murphy, T. Borase, C. Payne, J. O'Dwyer, S. A. Cryan, A. Heise, *RSC Advances* **2016**, 6, 23370; c) P. G. Gudeangadi, K. Uchida, A. Tateishi, K. Terada, H. Masunaga, K. Tsuchiya, H. Miyakawa, K. Numata, *Polymer Chemistry* **2020**, 11, 4920.
- [17] a) H. Lai, X. Chen, Q. Lu, Z. Bian, Y. Tao, X. Wang, *Chemical Communications* **2014**, 50, 14183; b) H. Huang, J. Hu, Y. Zhu, *Macromolecular Bioscience* **2013**, 13, 161.
- [18] a) L. E. Matolyak, J. K. Keum, K. M. Van de Voorde, L. T. J. Korley, *Organic & Biomolecular Chemistry* **2017**, 15, 7607; b) J. C. Johnson, N. D. Wanasekara, L. T. J. Korley, *Biomacromolecules* **2012**, 13, 1279; c) D. Jang, C. B. Thompson, S. Chatterjee, L. T. J. Korley, *Molecular Systems Design & Engineering* **2021**, 6, 1003; d) J. C. Johnson, N. D. Wanasekara, L. T. J. Korley, *Journal of Materials Chemistry B* **2014**, 2, 2554.
- [19] L. E. Matolyak, C. B. Thompson, B. Li, J. K. Keum, J. E. Cowen, R. S. Tomazin, L. T. J. Korley, *Biomacromolecules* **2018**, 19, 3445.



- [20] a) B. G. Choi, M. H. Park, S. H. Cho, M. K. Joo, H. J. Oh, E. H. Kim, K. Park, D. K. Han, B. Jeong, *Biomaterials* **2010**, 31, 9266; b) E. J. Yun, B. Yon, M. K. Joo, B. Jeong, *Biomacromolecules* **2012**, 13, 1106.
- [21] a) J. Zhang, Y. Liu, J. Sun, R. Gu, C. Ma, K. Liu, *Materials Today Advances* **2020**, 8, 100095; b) C. Haynl, E. Hofmann, K. Pawar, S. Förster, T. Scheibel, *Nano Letters* **2016**, 16, 5917; c) B. Mu, F. Hassan, Y. Yang, *Green Chemistry* **2020**, 22, 1726; d) M. C. Bier, S. Kohn, A. Stierand, N. Grimmelsmann, S. V. Homburg, A. Rattenholl, A. Ehrmann, *IOP Conference Series: Materials Science and Engineering* **2017**, 254, 192004.
- [22] a) J. Yan, G. Zhou, D. P. Knight, Z. Shao, X. Chen, *Biomacromolecules* **2010**, 11, 1; b) F. Zhang, Q. Lu, X. Yue, B. Zuo, M. Qin, F. Li, D. L. Kaplan, X. Zhang, *Acta Biomaterialia* **2015**, 12, 139; c) S. Ling, Z. Qin, C. Li, W. Huang, D. L. Kaplan, M. J. Buehler, *Nature Communications* **2017**, 8, 1387.
- [23] a) A. Heidebrecht, L. Eisoldt, J. Diehl, A. Schmidt, M. Geffers, G. Lang, T. Scheibel, *Advanced Materials* **2015**, 27, 2189; b) X.-X. Xia, Z.-G. Qian, C. S. Ki, Y. H. Park, D. L. Kaplan, S. Y. Lee, *Proceedings of the National Academy of Sciences* **2010**, 107, 14059.
- [24] M. Saric, T. Scheibel, *Current Opinion in Biotechnology* **2019**, 60, 213.
- [25] A. Rasines Mazo, S. Allison-Logan, F. Karimi, N. J.-A. Chan, W. Qiu, W. Duan, N. M. O'Brien-Simpson, G. G. Qiao, *Chemical Society Reviews* **2020**, 49, 4737.
- [26] a) L. Gu, Y. Jiang, J. Hu, *Advanced Materials* **2019**, 31, 1904311; b) O. Rathore, D. Y. Sogah, *Journal of the American Chemical Society* **2001**, 123, 5231.
- [27] N. J.-A. Chan, D. Gu, S. Tan, Q. Fu, T. G. Pattison, A. J. O'Connor, G. G. Qiao, *Nature Communications* **2020**, 11, 1630.
- [28] J. Jacobs, D. Pavlović, H. Prydderch, M.-A. Moradi, E. Ibarboure, J. P. A. Heuts, S. Lecommandoux, A. Heise, *Journal of the American Chemical Society* **2019**, 141, 12522.
- [29] a) D. A. Kirschner, C. Abraham, D. J. Selkoe, *Proceedings of the National Academy of Sciences* **1986**, 83, 503; b) J. Zou, F. Zhang, Y. Chen, J. E. Raymond, S. Zhang, J. Fan, J. Zhu, A. Li, K. Seetho, X. He, D. J. Pochan, K. L. Wooley, *Soft Matter* **2013**, 9, 5951.
- [30] G. Rusu, K. Ueda, E. Rusu, M. Rusu, *Polymer* **2001**, 42, 5669.
- [31] W. Li, Y. Hu, L. Shi, X. Zhang, L. Xiong, W. Zhang, I. Ullah, *Journal of Biomaterials Science, Polymer Edition* **2018**, 29, 1155.
- [32] J. Gong, J. Li, J. Xu, Z. Xiang, L. Mo, *RSC Advances* **2017**, 7, 33486.
- [33] A. Nakajima, T. Hayashi, K. Kugo, K. Shinoda, *Macromolecules* **1979**, 12, 840.
- [34] X. Sun, C. Lu, W. Zhang, D. Tian, X. Zhang, *Carbohydrate Polymers* **2013**, 98, 405.
- [35] a) K. Devarayan, S. Nakagami, S. Suzuki, I. Yuki, K. Ohkawa, *Polymers* **2020**, 12, 327; b) J. Greenwald, M. P. Friedmann, R. Riek, *Angewandte Chemie International Edition* **2016**, 55, 11609.
- [36] a) K. Arai, Y. Horikawa, T. Shikata, H. Iwase, *RSC Advances* **2020**, 10, 19059; b) Y. E. Kim, S. J. Yeom, J.-E. Lee, S. Kang, H. Kang, G.-H. Lee, M. J. Kim, S. G. Lee, H.-W. Lee, H. G. Chae, *Journal of Power Sources* **2020**, 468, 228371.
- [37] a) T. Cui, J. Li, Z. Yan, M. Yu, S. Li, *Biotechnology for Biofuels* **2014**, 7, 134; b) A. Nabili, A. Fattoum, M.-C. Brochier-Salon, J. Bras, E. Elaloui, *Iranian Polymer Journal* **2017**, 26, 137.
- [38] a) F. Pignon, M. Challamel, A. De Geyer, M. Elchamaa, E. F. Semeraro, N. Hengl, B. Jean, J.-L. Putaux, E. Gicquel, J. Bras, S. Prevost, M. Sztucki, T. Narayanan, H. Djeridi, *Carbohydrate Polymers* **2021**, 260, 117751; b) A. Sharma, P. Wankhede, R. Samant, S. Nagarkar, S. Thakre, G. Kumaraswamy, *ACS Applied Polymer Materials* **2021**, 3, 2598.
- [39] D. Johansen, J. Trehwella, D. P. Goldenberg, *Protein Sci* **2011**, 20, 1955.

- [40] V. Crescenzi, G. Manzini, G. Calzolari, C. Borri, *European Polymer Journal* **1972**, *8*, 449.

## 4.3. Supporting Information

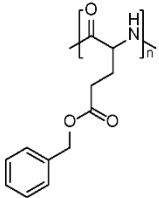
WILEY-VCH

Supporting Information

**$\beta$ -sheet reinforced robust fibers fabricated from unmodified polymers**

*N. J. Chan, S. Lentz, P. A. Gurr, M. Schulteberyng, S. Rosenfeldt, A. Schenk, T. Scheibel\*, G. Qiao\**

Table S3: Chemical Information on Poly(benzyl-L-glutamate)

Polymer	Structure	Molecular Weight (MDa)	Polydispersity Index
PBLG		333	1.21

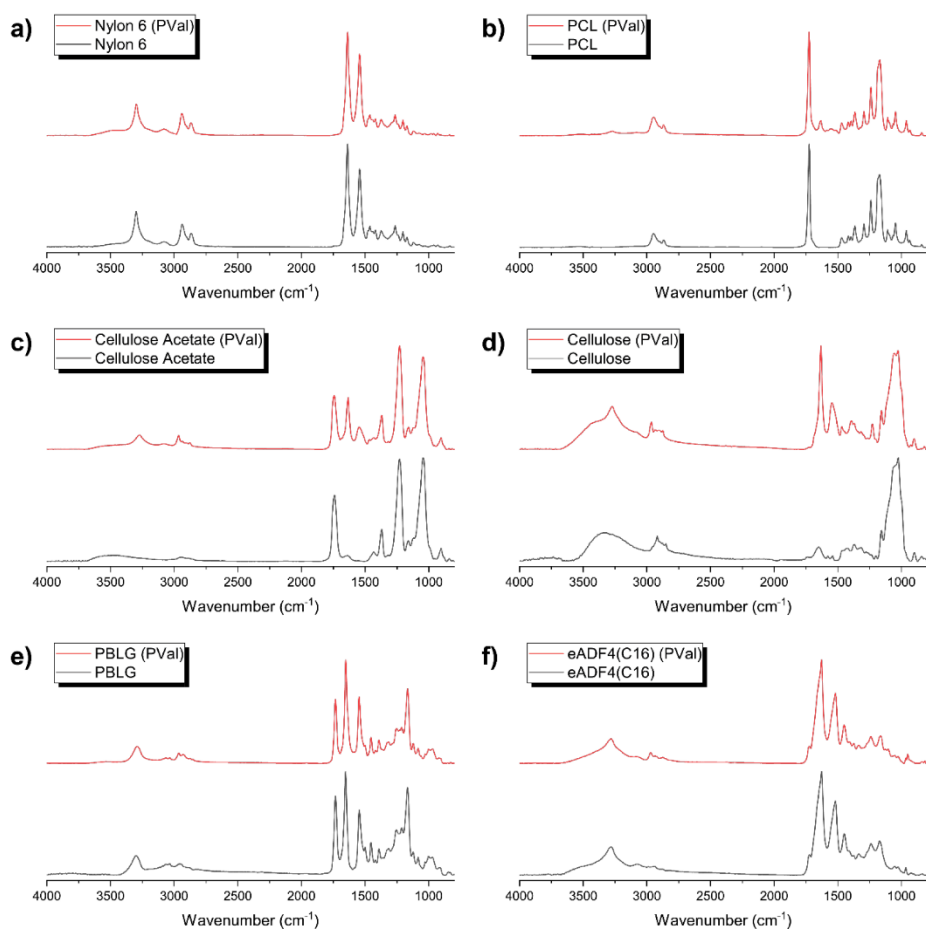


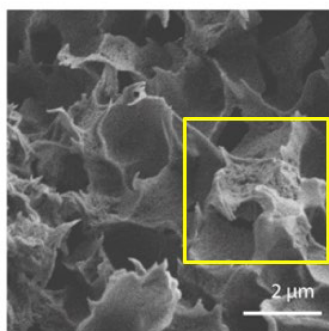
Figure S1: Full Fourier transform infrared (FTIR) spectra for fiber samples without polypeptide and with Pval and PGly for a) nylon 6, b) poly(caprolactone) (PCL), c) cellulose acetate, d) cellulose, e) poly(benzyl-L-glutamate) and f) eADF4(C16).

Table S2: Summary of relative intensity of  $\beta$ -sheet peak relative to key non  $\beta$ -sheet peak within polymer.

Polymer	FTIR band reference peak ( $\text{cm}^{-1}$ )	Deconvoluted relative intensity (to 1625-1634 $\text{cm}^{-1}$ )	
		Unmodified	With $\beta$ -sheet
<b>Nylon 6</b>	2850 – 2950 (CH and $\text{CH}_2$ aliphatic stretch)	1.55 $\pm$ 0.03	2.09 $\pm$ 0.08
<b>PCL</b>	1726 (C=O stretch)	Not present	0.12 $\pm$ 0.02
<b>Cellulose Acetate</b>	1737-1755 (C=O + O-H stretch)	0.09 $\pm$ 0.04	0.44 $\pm$ 0.06
<b>Cellulose</b>	1740 (O-H stretch)	Not present	0.67 $\pm$ 0.14
<b>PBLG</b>	1652 ( $\alpha$ -helix N-H)	0.02 $\pm$ 0.04	0.12 $\pm$ 0.02
<b>eADF(C16)</b>	1647 (random coil N-H)	1.62 $\pm$ 0.07	8.66 $\pm$ 2.74

Table S3: Secondary structure content of polypeptide-based fibers with and without PVal inclusion

Fiber	$\beta$ -sheets (%)	$\alpha$ -helices (%)	Random coils (%)	$\beta$ -turns (%)
<b>PBLG</b>	2 $\pm$ 2	98 $\pm$ 2	-	-
<b>PBLG (PVal)</b>	11 $\pm$ 2	89 $\pm$ 2	-	-
<b>eADF4(C16)</b>	47 $\pm$ 3	-	35 $\pm$ 4	18 $\pm$ 14
<b>eADF4(C16) (PVal)</b>	56 $\pm$ 1	15 $\pm$ 1	10 $\pm$ 3	19 $\pm$ 5

Figure S2: Scanning electron microscopy (SEM) fiber cross-section at high magnification for fiber samples of nylon 6 with PVal with highlighted  $\beta$ -sheet region.

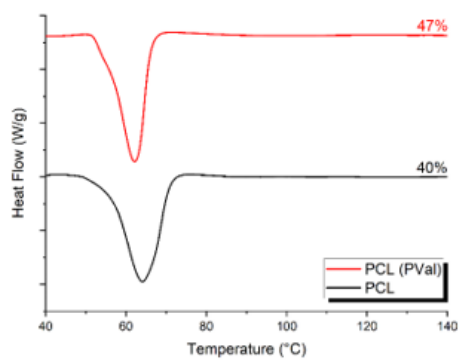


Figure S3: Differential scanning calorimetry (DSC) thermogram of PCL fibers with and without  $\beta$ -sheets with crystallinity quoted

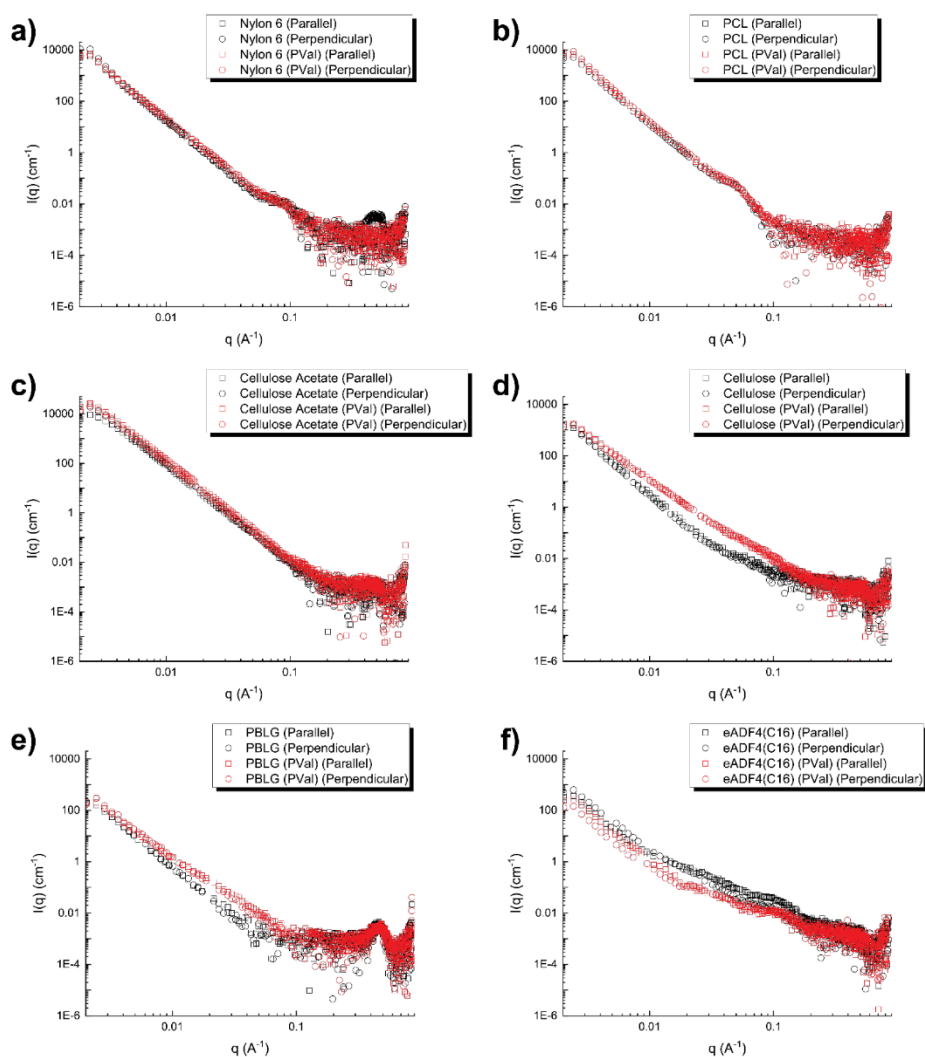


Figure S4: Small angle X-ray scattering (SAXS) spectra for fiber samples with and without PVal for a) nylon 6, b) poly(caprolactone) (PCL), c) cellulose acetate, d) cellulose, e) poly(benzyl-L-glutamate) and f) eADF4(C16).



## Chapter 5:

# Conclusions and Future Perspectives

---

### 5.1 Conclusion

The incorporation of synthetic polypeptides into materials offers a broad range of potential physical and chemical qualities based on their structure. However, this control of structure is traditionally based on the specific sequence of amino acids in the polypeptide, and, thus, the control non-sequence specific polypeptides for the fabrication of materials becomes far more intriguing. This thesis reports the advancement of multiple different novel material fabrication methods towards the control of synthetic polypeptides, the resulting substructures as controlled during fabrication including secondary structure, and their subsequent physical properties.

In **Chapter 2**, the fabrication of  $\beta$ -sheet laden hydrogels by grafting-from  $\beta$ -sheet forming poly(L-valine-*r*-glycine) polypeptides was reported, yielding tough materials. High molecular weight polypeptide chains could be formed without the uncontrolled aggregation usually observed when developing  $\beta$ -sheets within hydrogels, which usually leads to soft materials. Instead, a continuous brittle  $\beta$ -sheet network could be formed, which could be made more amorphous by increasing the glycine to L-valine ratio. As a result, compressive mechanical properties could be greatly enhanced, with compressive strength increasing from 2 kPa without polypeptide to 9.4 MPa upon poly(L-valine) introduction. By introducing PLVG at different ratios of Val NCA to Gly NCA, mechanical toughness was maintained ( $\sim 2 \text{ MJ/m}^3$ ), while strain at break increased from 40.4 % to 63.2 %. Versatility was further shown through the integration of this method with 3D printed networks.

In **Chapter 3**, the development of chemically crosslinked polypeptide modified surfaces was thoroughly investigated, yielding materials with unusual secondary structure formation. By utilizing methacrylated polypeptides (methacrylated poly(L-lysine) and methacrylated poly(L-glutamic acid)), surfaces were modified by polymerizing through these side chains using reversible addition-fragmentation (RAFT). After optimization of the technique, multilayer films with a thickness of  $94.9 \pm 8.2 \text{ nm}$  were developed using a dithiobenzoate RAFT agent without external RAFT agent in the reaction solution. Secondary structure analysis revealed increased random coil content compared to other films developed using the same polypeptides. Furthermore, the films were found to be susceptible to protease degradation (specifically  $\alpha$ -

chymotrypsin and Protease XIV) and found to be tunable depending on the amino acid residues used.

In **Chapter 4**, a strategy towards introducing  $\beta$ -sheet aggregates in a controlled manner into fibers of unmodified polymer was developed. Instead of developing the  $\beta$ -sheet forming polypeptide before spinning, soluble Val NCA monomer was introduced into the spinning dope with the subsequent growth of PVal occluding during and after spinning, resulting in the desired  $\beta$ -sheet formation. Polymer crystallization was found with low hydrogen bonding potential (polycaprolactone (PCL) and cellulose acetate), leading to an increase in tensile strength of up to 4.3 times the unmodified control. Other fibers without significant polymer crystal disruption (nylon 6 and poly(benzyl-L-glutamate)) were found to have an increased strain at break of up to 2.9 times the unmodified control. Conversely, a loss of natural occurring polymer structures resulted in either minor or reduced mechanical properties in the case of cellulose and the recombinant spider silk respectively.

## 5.2 Future Perspectives

This thesis primarily focuses on the structural control of polypeptides through the development of novel fabrication platforms. Future expansion on this work centers around two overarching paradigms – process optimization and developing application specific properties.

The  $\beta$ -sheet laden hydrogels reported in **Chapter 2**, were largely based on the use of PLVG-based  $\beta$ -sheets. Valine was chosen as the primary  $\beta$ -sheet forming residue on the premise of its high  $\beta$ -sheet forming propensity from computational studies<sup>1</sup> and previous experimental work.<sup>2</sup> However, the resulting materials were brittle with a reduced extensibility. While secondary structure is important, previous studies have shown that the conformation of such secondary structures on a nanoscale still differs from residue to residue even if they possess the similar secondary structure content.<sup>3</sup> Specifically, fibrillar structures as present in nature have the nanostructural order to endow the desired superior mechanical properties.<sup>4</sup> Thus to attain such structures in the pursuit of even stronger materials, residues which have already previously demonstrated  $\beta$ -sheet fibrillar formation without excessive control required to prevent uncontrolled aggregation such as using threonine should also be explored.<sup>5</sup> Furthermore, investigating multiblock block conformations upon introduction of glycine similar to that present in natural spider silk instead of the random polymerization as reported may offer greater control towards this fibrillar morphology.<sup>6</sup> While the work as reported provides a strong platform for developing tough materials, there is room for further sequential optimization.

Further to this, we also presented the potential of this work in 3D printed systems, opening up multiple different potential applications. As these materials are primarily polypeptide-based they have further potential as a degradable material to be used in high-strength applications. Optimization of degradation properties – particularly in regards to naturally occurring proteases available in natural ecosystems – provides a potential alternative to traditional plastics with potential to mitigate microplastic accumulation.<sup>7</sup> With further optimization to mechanical properties, this system can meet the requirements of cancellous bone tissue engineering, where a compressive strength and Young's modulus within the range of ~10 MPa and ~100 MPa respectively has already been met by the reported study.<sup>8</sup> Thus further studies with osteoblast and osteocyte culture provide a pathway towards this specific application.

**Chapter 3** reports the fabrication of polypeptide-based films with tunable degradation. In terms of optimization, further modifications to the macromonomer should be focused on controlling both thickness and degradation. Aminolysis of the RAFT agent was a potential issue using the poly(L-lysine)-based macromonomer, thus utilizing strategies to mitigate this such as the use of protecting groups should be investigated to garner greater control of film growth.<sup>9</sup> Previous studies have shown that film thickness is a function of macrocrosslinker functionalization.<sup>10</sup> However, this is likely to further impact degradation and thus opens one avenue for potential investigation. Furthermore, the reported degradation of copolypeptides relies on the non-sequence specific targeting of enzymes— however this degradation can be more precisely controlled by introducing sequences which can be identified (and thus hydrolyzed) by specific enzymes such as matrix metalloproteinases.<sup>11</sup>

Functionalization for drug delivery and tissue engineering applications are a natural pathway for such polypeptide films. For drug delivery in particular, the aforementioned control of degradation properties can be used to control the delivery of either entrapped or covalently bonded drugs (**Error! Reference source not found.**). The macromonomer itself can be functional either through the use of homopolypeptide blocks, which are known to assist with cell growth, proliferation and differentiation such as variants of poly(alanine),<sup>12</sup> or the use of antimicrobial polypeptide-based macrocrosslinkers such as poly(L-lysine-*r*-DL-valine).<sup>13</sup> A further feature of RAFT CAP which has yet to be explored is the potential of functionalization of the RAFT agent itself post-fabrication. Aminolysis yields a thiol group, which allows for many click chemistry to be performed.<sup>14</sup> This inherently decouples the chemical functionalization of the film from the structural potential of the polypeptide film itself.

Enzymatic degradation over time

+

Drug release over time

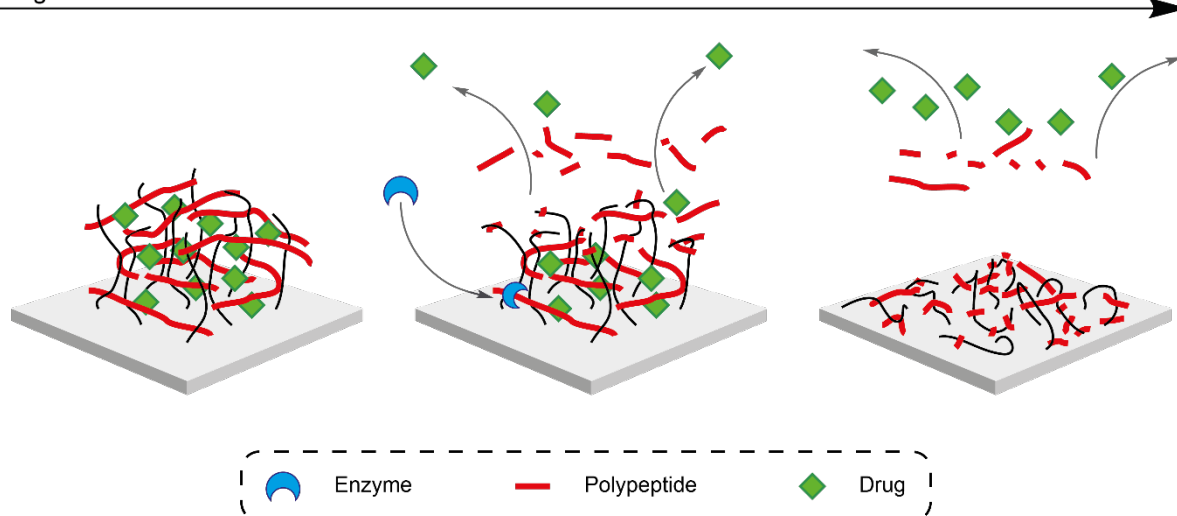


Figure 18: Schematic of drug release over time in relation to enzyme degradation

The fiber fabrication system reported in **Chapter 4** focused on a range of polymers. Of these polymers, cellulose acetate was found to have the greatest increase in mechanical toughness, thus optimization of this system as a focus provides the greatest potential. Determining the limit of  $\beta$ -sheet loading before adverse impacts on polymer crystallization and subsequent mechanical properties will equate to a practical upper limit for subsequent work. Attaining crystallite alignment is also imperative to further developing the system for tough materials.<sup>15</sup> This has previously been executed through the addition of a post-stretching stage to the system.<sup>16</sup>

While wet spinning was presented as the focus of the reported study, electrospinning provides another route for developing nanofibers. Typically, electrospinning emits the polymer jet into the atmosphere, which would be devoid of reactive initiators making traditional setups unfeasible. However, a dual syringe system, where initiator and monomer are kept in separate solutions and only combined at the electrospinning nozzle, provides one method of ensuring initiator integration into the fiber, while still preventing unwanted aggregation within the spinning dope (**Error! Reference source not found.**)<sup>17</sup> By further expanding work into electrospun mats, further applications where mechanically favorable electrospun mats such as bone tissue engineering become available.<sup>18</sup>

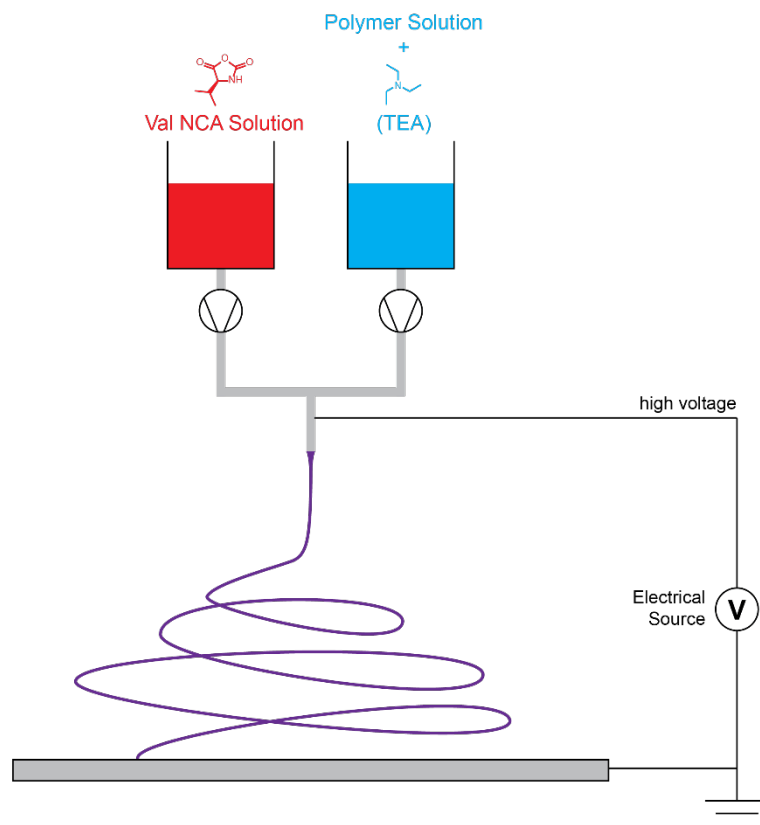


Figure 19: Schematic of dual syringe electrospinning, with NCA in one syringe and polymer with initiator in another solution

### 5.3 References

- (1) Fujiwara, K.; Toda, H.; Ikeguchi, M. Dependence of  $\alpha$ -helical and  $\beta$ -sheet amino acid propensities on the overall protein fold type. *BMC Structural Biology* **2012**, *12* (1), 18.
- (2) Wibowo, S. H.; Sulistio, A.; Wong, E. H. H.; Blencowe, A.; Qiao, G. G. Functional and Well-Defined  $\beta$ -Sheet-Assembled Porous Spherical Shells by Surface-Guided Peptide Formation. *Advanced Functional Materials* **2015**, *25* (21), 3147.
- (3) Matolyak, L. E.; Thompson, C. B.; Li, B.; Keum, J. K.; Cowen, J. E.; Tomazin, R. S.; Korley, L. T. J. Secondary-Structure-Mediated Hierarchy and Mechanics in Polyurea–Peptide Hybrids. *Biomacromolecules* **2018**, *19* (8), 3445.
- (4) Bortolini, C.; Jones, N. C.; Hoffmann, S. V.; Wang, C.; Besenbacher, F.; Dong, M. Mechanical properties of amyloid-like fibrils defined by secondary structures. *Nanoscale* **2015**, *7* (17), 7745.
- (5) Hou, S.-S.; Fan, N.-S.; Tseng, Y.-C.; Jan, J.-S. Self-Assembly and Hydrogelation of Coil–Sheet Poly(l-lysine)-block-poly(l-threonine) Block Copolypeptides. *Macromolecules* **2018**, *51* (20), 8054.
- (6) Rising, A.; Johansson, J. Toward spinning artificial spider silk. *Nat Chem Biol* **2015**, *11* (5), 309.
- (7) Oliveira, J.; Belchior, A.; da Silva, V. D.; Rotter, A.; Petrovski, Ž.; Almeida, P. L.; Lourenço, N. D.; Gaudêncio, S. P. Marine Environmental Plastic Pollution: Mitigation by Microorganism Degradation and Recycling Valorization. *Frontiers in Marine Science* **2020**, *7*.
- (8) Amini, A. R.; Laurencin, C. T.; Nukavarapu, S. P. Bone tissue engineering: recent advances and challenges. *Crit Rev Biomed Eng* **2012**, *40* (5), 363.
- (9) De Alwis Watuthanthrige, N.; Kurek, P. N.; Konkolewicz, D. Photolabile protecting groups: a strategy for making primary amine polymers by RAFT. *Polymer Chemistry* **2018**, *9* (13), 1557.
- (10) Guntari, S. N.; Goh, T. K.; Blencowe, A.; Wong, E. H. H.; Caruso, F.; Qiao, G. G. Factors influencing the growth and topography of nanoscale films fabricated by ROMP-mediated continuous assembly of polymers. *Polymer Chemistry* **2013**, *4* (1), 68.
- (11) Verma, R. P.; Hansch, C. Matrix metalloproteinases (MMPs): Chemical–biological functions and (Q)SARs. *Bioorganic & Medicinal Chemistry* **2007**, *15* (6), 2223.
- (12) Yun, E. J.; Yon, B.; Joo, M. K.; Jeong, B. Cell Therapy for Skin Wound Using Fibroblast Encapsulated Poly(ethylene glycol)-poly(l-alanine) Thermogel. *Biomacromolecules* **2012**, *13* (4), 1106.
- (13) Lam, S. J.; O'Brien-Simpson, N. M.; Pantarat, N.; Sulistio, A.; Wong, E. H. H.; Chen, Y.-Y.; Lenzo, J. C.; Holden, J. A.; Blencowe, A.; Reynolds, E. C. et al. Combating multidrug-resistant Gram-negative bacteria with structurally nanoengineered antimicrobial peptide polymers. *Nature Microbiology* **2016**, *1* (11), 16162.
- (14) Hess, A.; Schmidt, B. V. K. J.; Schlaad, H. Aminolysis induced functionalization of (RAFT) polymer-dithioester with thiols and disulfides. *Polymer Chemistry* **2020**, *11* (48), 7677.
- (15) Xu, G.; Gong, L.; Yang, Z.; Liu, X. What makes spider silk fibers so strong? From molecular-crystallite network to hierarchical network structures. *Soft Matter* **2014**, *10* (13), 2116.
- (16) Weatherbee-Martin, N.; Xu, L.; Hupe, A.; Kreplak, L.; Fudge, D. S.; Liu, X.-Q.; Rainey, J. K. Identification of Wet-Spinning and Post-Spin Stretching Methods Amenable to Recombinant Spider Aciniform Silk. *Biomacromolecules* **2016**, *17* (8), 2737.

- (17) Ji, Y.; Ghosh, K.; Li, B.; Sokolov, J. C.; Clark, R. A. F.; Rafailovich, M. H. Dual-Syringe Reactive Electrospinning of Cross-Linked Hyaluronic Acid Hydrogel Nanofibers for Tissue Engineering Applications. *Macromolecular Bioscience* **2006**, *6* (10), 811.
- (18) Jang, J.-H.; Castano, O.; Kim, H.-W. Electrospun materials as potential platforms for bone tissue engineering. *Advanced drug delivery reviews* **2009**, *61* (12), 1065.

## ***Chapter 6:***

### ***Experimental***

---

This chapter describes the experimental procedures and subsequent experimental methods utilized in all works within this thesis. Methods have been isolated based on specific Chapters as specific materials and protocols were altered based on location during the construction of this thesis.

#### **6.1. Methods for Chapter 2**

##### **6.1.1. Materials**

L-valine ( $\geq 98\%$ ) and glycine ( $\geq 98\%$ ) were purchased from Merck and used as received. Triphosgene (98%), (+)- $\alpha$ -pinene (99%), anhydrous n-pentane ( $>99\%$ ), anhydrous N,N-Dimethylformamide (DMF) ( $>99.8\%$ ), 2-aminoethyl methacrylate hydrochloride (97%), triethylamine ( $\geq 99.5\%$ , TEA), oligo(ethylene glycol) methylether methacrylate ( $M_n = 1100$ , OEGMEMA), oligo(ethylene glycol) dimethacrylate ( $M_n = 750$ , OEGDMA), ammonium persulfate (APS,  $>98\%$ ), N, N, N', N'-Tetramethyl ethylenediamine (TEMED,  $\geq 99.5\%$ ), Diphenyl(2,4,6-trimethylbenzoyl)phosphine oxide (TPO, 97%) Thioflavin T (ThT), Guanidine hydrochloride (GdnCl,  $\geq 99\%$ ), phosphate buffered saline (PBS) tablets, protease from streptomyces griseus (Type XIV), N-(3-Dimethylaminopropyl)-N'-ethyl carbodiimide (EDCI), 4-(Dimethylamino)pyridine (DMAP,  $\geq 99\%$ ) and N, N, N', N'', N''-pentamethyl diethylenetriamine (PMDETA, 99%) were all purchased from Sigma Aldrich and used as received. Anhydrous and deoxygenated Tetrahydrofuran (THF) (Honeywell, 99.9%, HPLC grade) was obtained by distillation from benzophenone and sodium metal under argon. AR grade hydrochloric acid (HCl), sodium hydroxide (NaOH) and other solvents were purchased from Chem-Supply Pty. Ltd. and used without further purification. L-valine ( $\geq 98\%$ ) was purchased from Merck and used as received. Anhydrous and deoxygenated Tetrahydrofuran (THF) (Honeywell, 99.9%, HPLC grade) was obtained by distillation from benzophenone and sodium metal under argon. Deuterated chloroform ( $CDCl_3$ ) was purchased from Cambridge Isotope Laboratories and used as received. 2-(((butylthio)carbonothioyl)thio)propanoic acid (TTC-1) was received from Dulux Group Australia and used as received. Methyl methacrylate (MMA, 99%, Sigma Aldrich) was de-inhibited by basic alumina prior to use.



### 6.1.2. Synthesis of *L*-valine *N*-carboxyanhydride (Val NCA)

Val NCA was synthesized using modified versions of previous reported methods.<sup>1,2</sup> Briefly, *L*-valine (43 mmol, 5 g) was suspended within 80 mL of anhydrous THF in a two-necked round bottom flask under argon. Triphosgene (1.2× excess: 17 mmol, 5.1 g) was added and the mixture was continuously stirred 60 °C for 2 h or until all valine had dissolved. The reaction mixture was sparged with argon into a saturated NaOH solution for 1 h after which solvent was removed in vacuo (20 mbar, 40 °C) until equilibrium. The reduced mixture was redissolved in anhydrous 50 mL ethyl acetate which was chilled in 5 °C and then washed with saturated brine at 5 °C and 0.5 w/v % sodium bicarbonate aqueous solution at 5 °C with the organic phase being washed after separation each time. The resulting organic phase was dried using magnesium sulphate with the filtrate being reduced in vacuo (20 mbar, 50 °C) until equilibrium. The residue was recrystallised using *n*-pentane overnight. The resulting crystals were filtered and reprecipitated to afford a white powder (~60% Yield). <sup>1</sup>H NMR (400 MHz, CDCl<sub>3</sub>): δ 0.92 (dd, 6 H, CH<sub>3</sub>), 2.00–2.18 (m, 1 H, CH), 4.08 (dd, 1 H, cyclic CH), 8.84 (s, 1 H, cyclic NH).

### 6.1.3. Synthesis of glycine *N*-carboxyanhydride (Gly NCA)

Glycine NCA was synthesised using a modified procedure from previously reported literature <https://www.nature.com/articles/s41467-020-15312-x> - ref-CR63.<sup>3</sup> Glycine (67 mmol, 5 g) was suspended within a mixture of 250 mL of anhydrous THF and 21.2 mL (+)- $\alpha$ -pinene (133 mmol) in a two-necked round bottom flask under argon. Triphosgene (1.2× excess: 27 mmol, 7.9 g) was dissolved and added dropwise over 1.5 h while mixture was continuously stirred 70 °C and stirred for a further 1 h. The reaction mixture was sparged with argon into a saturated NaOH solution for 1 h after which the suspension was filtered and the filtrate was reduced in vacuo (20 mbar, 60 °C) until equilibrium. The resulting suspension was redissolved in THF and recrystallized using *n*-pentane overnight. The supernatant was removed and recrystallization was repeated two more times. The resulting white solid was filtered and washed with *n*-pentane (Yield 1.83 g, 27.2%). <sup>1</sup>H NMR (400 MHz, DMSO): δ 4.33 (s, 2 H, cyclic CH<sub>2</sub>), 8.84 (s, 1 H, cyclic NH).

### 6.1.4. Synthesis of initial OEGMA hydrogel network

2-aminoethyl methacrylate hydrochloride (1.56 mmol, 258 mg) was first deprotonated with TEA (1.88 mmol, ~300  $\mu$ L) in 20 mL of DI water overnight. The mixture was mixed with comonomer OEGMEMA (1.04 mmol, 1.14 g) and crosslinker OEGDMA (0.87 mmol, 650 mg) and degassed with N<sub>2</sub> for a few minutes. After addition of APS (20 mg) and TEMED (25  $\mu$ L)

(solids content ~10 w/w %, APS and TEMED 1–1.2 w/w% of solids), the solution was sonicated and separated into 1 mL batches in 3 mL syringes and allowed to stand at room temperature for 3 days. The resulting gels were swelled in DI water and washed six times to remove unreacted reactant. They were dehydrated in vacuo (20 mbar, 30 °C) for 2 days and stored in vacuo at room temperature for further use.

#### 6.1.5. Synthesis of initial OEGMA cryogel networks

The gel precursor solution was prepared and transferred to the syringes in the same procedures as described above. Then the solution in the mould was frozen at  $-18\text{ }^{\circ}\text{C}$  and kept at this temperature for 3 days. After thawing and being washed with water, the cryogel sample was dried and stored in vacuo for further use.

#### 6.1.6. Synthesis of $\beta$ -sheets-incorporated networks

The following synthesis of HB360 is used as an example of the formation of  $\beta$ -sheet incorporated networks. Dehydrated initial hydrogel network was immersed in the anhydrous DMF (3 mL) for 2 days to achieve swelling equilibrium. The swollen network was transferred to a monomer solution (in 3 mL anhydrous DMF) containing 360 mg/mL of Val NCA. The reaction vials were sealed at room temperature under vacuum for 3 days. The network was washed with DMF ( $3 \times 3\text{ mL}$ ) and sonicated in DMF (3 mL) for 30 min. To further remove potential non-grafted monomers/polymers, the network was then washed with THF ( $6 \times 3\text{ mL}$ ).

#### 6.1.7. Synthesis of PMMA-grated networks

The initial network hydrogel or cryogel was swollen in 3 mL of TTC-1 (RAFT agent) (~40 mg/mL, 0.503 mmol, 6.5 equiv. of amine groups in networks) dissolved in anhydrous DMF. EDCI (90 mg, 0.468 mmol, 6 equiv.) and DMAP (1 mg, 0.0078 mmol, 0.1 equiv.) was then added in the mixture with the reaction sealed at room temperature with occasional agitation under vacuum for 2 days to the RAFT agent. Afterwards, the network was washed with anhydrous DMF for several times to remove the free RAFT agent and remaining catalyst until the network colour did not fade. The network attached with RAFT agent was then transferred to the MMA monomer solutions (in 3 mL anhydrous DMF) at different concentrations (60, 120, 360 mg/mL) in presence of PMDETA (~5  $\mu\text{L}$ , 0.024 mmol, 0.33 equiv.). The reaction mixture was sealed and degassed using nitrogen for approximately 1 h. The UV light source ('Beauflly-nail lamp', 220 V,  $\lambda_{\text{max}} \sim 365\text{ nm}$ ,  $4 \times 9\text{ W}$ ) was then switched on, and the reaction mixture was left at room temperature with occasional agitation under positive  $\text{N}_2$  pressure for 3 days. A small aliquot (~100  $\mu\text{L}$ ) of the supernatant was taken for 1 H

NMR analysis to check monomer conversion rate, according to an established calibration curve as described below. After the reaction, the supernatant was removed, and the network was washed with DMF ( $3 \times 3$  mL) and sonicated in DMF (3 mL) for 30 min. To further remove potential non-grafted monomers/polymers, the network was then washed with THF ( $6 \times 3$  mL). Finally, the network was dried and stored under vacuum.

### 6.1.8. Synthesis of 3D-printed initial networks

2-Aminoethyl methacrylate hydrochloride (6.00 mmol, 994 mg), co-monomer OEGMEMA (4.00 mmol, 4.40 g) and crosslinker OEGDMA (10.0 mmol, 7500 mg) were dissolved in 25.8 mL of DMF: deionised water (7:3), with TPO photoinitiator (129 mg, 1 w/w% of solids) dissolved into the solution just prior to printing. The 3D printing was performed on an ANYCUBIC Photon 3D Printer with a  $\lambda_{\max} \sim 405$  nm and a layer height of 0.5 mm, bottom layer exposure time of 120 s, bottom layer count of 8 and layer exposure time of 80 s. 3D Models were designed using Autodesk® Tinkercad and sliced using ChiTuBox 3D Slicer software. The subsequent networks were then soaked in a solution of DMF (10 mL) and TEA (600  $\mu$ L) overnight and then washed with anhydrous DMF ( $6 \times 10$  mL).

### 6.1.9. Synthesis of $\beta$ -sheets-incorporated 3D-printed networks

The swollen networks were transferred to vials containing 50 mL of valine NCA in anh. DMF (120 mg/mL). The vials were then sealed and agitated at room temperature under vacuum for 3 days. The resulting networks were then washed with six aliquots of DI water, followed by subsequent washing with DMF ( $3 \times 3$  mL) before being sonicated in DMF (3 mL) for 30 min.

## 6.2. Methods for Chapter 3

### 6.2.1. Materials

Acetone (>99.5%, AR Grade, Merck), 3-aminopropargyl triethoxysilane (APTES, 99%, Merck), diethyl ether (Et<sub>2</sub>O, AR grade, Chem-Supply), N-(3-(dimethylamino)propyl)-N'-ethylcarbodiimide hydrochloride (EDCI,  $\geq 98\%$ , Merck), 4-cyano-4-[(dodecylsulfanylthiocarbonyl)sulfanyl]pentanoic acid (CDTPA, 98%, Aldrich) 4-cyano-4-(phenylcarbonothioylthio)pentanoic acid (CPADB; 98%, Aldrich), dimethyl sulfoxide (DMSO; AR grade, Ajax Finechem), glacial acetic acid (AcOH; AR Grade, Chem-Supply), hydrobromic acid (HBr; 33% in acetic acid, Merck), hexylamine ( $\geq 98\%$ , Merck), N-hydroxysuccinimide (NHS;  $\geq 98\%$ , Fluka), isopropanol (iPrOH, AR grade, Chem-Supply), lithium phenyl-2,4,6-trimethylbenzoylphosphinate (LAP, >98% HPLC grade, Tokyo Chemical

Industry), H-L-Lys(Z)-OH (>99%, Mimotopes), H-L-Glu(OBzl)-OH (>99%, Mimotopes), magnesium sulfate (anh. MgSO<sub>4</sub>, ≥97%, Merck), methanol (AR grade, Chem-Supply),  $\alpha$ -pinene (98%, Merck), sodium hydrogen carbonate (NaHCO<sub>3</sub>, AR grade, Chem-Supply), triphosgene (≥98%, Merck), sodium hydroxide (NaOH; ≥97%, Merck), trifluoroacetic acid (TFA; Merck) were used as received without further purification. Saturated brine solution was prepared from sodium chloride (NaCl, AR grade, Chem-Supply) in DI water. Tetrahydrofuran (anh. THF, inhibitor free, >99.9%, Merck), ethyl acetate (anh. EtOAc, >99.9 Honeywell) and dimethylformamide (anyhd. DMF, 99.8%, Acros) were purified by passage through a solvent purification system (SBPT-1, LC Technologies, USA) containing 4Å sieves under Argon gas. Hexane (AR, Chem-Supply) was distilled over calcium hydride under nitrogen prior to use.

### 6.2.2. Synthesis of Z-protected lysine *N*-carboxyanhydride (Lys(Z) NCA) and Benzyl-protected Glutamic Acid *N*-carboxyanhydride (Glu(OBzl) NCA)

Z-protected lysine (Lys(Z) NCA) and Benzyl-protected Glutamic Acid (Glu(OBzl) NCA) NCAs were synthesized using modified versions of previous reported methods.<sup>1,2</sup> In a typical experiment Lys(Z) (5.00 g, 17.8 mmol) was added to a 500 mL three-necked RBF and suspended in 200 mL of anh. THF with  $\alpha$ -pinene (6.00 mL, 37.5 mmol, 1.15 excess moles) under nitrogen. After heating to 60 °C, triphosgene (2.11 g, 7.14 mmol, 1.2 excess moles) was added and the mixture was stirred at temperature for 2 h. Solvent was removed from the now clear solution under reduced pressure and replaced with 100 mL of anh. EtOAc. The solution was cooled to -18 °C before washing with sat. brine and 5 w/v% sodium hydrogen carbonate and the organic phase was dried over MgSO<sub>4</sub>. The filtered solution was reduced under reduced pressure and recrystallized using anh. hexane at -18 °C over 16 h. The solids were then filtered and redissolved into anh. EtOAc before being precipitated into anh. hexane. The precipitate was then dried under vacuum over 24 h and stored under argon at -80 °C (yields ~80%).

Lys(Z) NCA: <sup>1</sup>H NMR (400 MHz, CDCl<sub>3</sub>):  $\delta$  1.30–1.60 (m, 4H, -NH-CH<sub>2</sub>-CH<sub>2</sub>-CH<sub>2</sub>-CH<sub>2</sub>-), 1.81–2.07 (m, 2H, -NH-CH<sub>2</sub>-CH<sub>2</sub>-CH<sub>2</sub>-CH<sub>2</sub>-), 3.20 (m, -NH-CH<sub>2</sub>-CH<sub>2</sub>-CH<sub>2</sub>-CH<sub>2</sub>-), 4.27 (t, 1H, J = 5.6 Hz, CHN), 4.92 (s, 1H, side chain NH), 5.10 (s, 2H, CH<sub>2</sub>-ArH), 6.83 (s, 1H, ring NH), 7.22–7.37 (m, 5H, ArH).

Glu(OBzl) NCA: <sup>1</sup>H NMR (400 MHz, CDCl<sub>3</sub>):  $\delta$  2.06–2.32 (m, 2H, CH<sub>2</sub>-CH<sub>2</sub>-CO), 2.58 (t, 2H, J = 6.8 Hz, CH<sub>2</sub>-CH<sub>2</sub>-CO), 4.36 (t, 1H, J = 6.0 Hz, CHN), 5.12 (s, 2H, CH<sub>2</sub>-ArH), 6.59 (s, 1H, ring NH), 7.29–7.41 (m, 5H, ArH).

### 6.2.3. Synthesis of Poly(L-gluatamic acid(OBzl)-*r*-L-lysine(Z))

Both Glu(OBzl) NCA (3.00 g, 11.4 mmol, 80 mol% of overall NCA monomer) and Lys(Z) NCA (0.873 g, 2.85 mmol, 20 mol% of overall NCA monomer) were dissolved in anh. DMF under nitrogen in a 50 mL RBF. To the stirring solution was added hexylamine (23.5  $\mu$ L, 54.3  $\mu$ mol, M/I = 90), and the clear solution was stirred under an argon bleed at room temperature for 24 h. The reaction mixture was then precipitated into and subsequently rinsed with Et<sub>2</sub>O which was then dried and stored under vacuum to afford a clear tacky solid as the final product (2.84 g, yield: 78.5%).  $M_n$  (GPC) = 7.2 kDa;  $D$  1.30. <sup>1</sup>H NMR (d<sub>6</sub>-DMSO):  $\delta$  1.20–1.90 (m, Lys -NH-CH<sub>2</sub>-CH<sub>2</sub>-CH<sub>2</sub>-CH<sub>2</sub>-), 2.0–2.40 (m, Glu -CH<sub>2</sub>-CH<sub>2</sub>-CO-), 2.94 (s, Lys -NH-CH<sub>2</sub>-CH<sub>2</sub>-CH<sub>2</sub>-CH<sub>2</sub>-), 3.92 (s, CH-NH backbone), 4.99 (m, CH<sub>2</sub>-ArH), 5.76 (m, CH<sub>2</sub>-CH-), 7.26 (s, ArH), 8.38 (brs, CO-NH)

### 6.2.4. Deprotection of Poly(L-gluatamic acid(OBzl)-*r*-L-lysine(Z))

To a 25 mL RBF was added the protected poly(L-lysine(Z)) (3.22 g, 0.12 mmol) followed by 20 mL of TFA. The solution was stirred until the polymer was completely dissolved, followed by the dropwise addition of HBr (33 vol% in AcOH diluted to 16.7 vol% with AcOH, 20 mL). The resulting solution was stirred with thick precipitate observed soon after. The reaction mixture was stirred for a total of 16 h with the suspension then dropwise precipitated into diethyl ether, washed in ether ( $\times$ 2), then dried in vacuo overnight. The solid was then dissolved in DI water and added to 3.5 kDa dialysis tubing for dialysis against 2 L DI water ( $\times$ 3) for 24 h before being freeze-dried to obtain a white, fluffy solid ( $\sim$  1.4 g). <sup>1</sup>H NMR (D<sub>2</sub>O, 400 MHz): 1.06–1.43 (m, 4H, -NH-CH<sub>2</sub>-CH<sub>2</sub>-CH<sub>2</sub>-CH<sub>2</sub>-), 2.56 (m, 2H, -NH-CH<sub>2</sub>-CH<sub>2</sub>-CH<sub>2</sub>-CH<sub>2</sub>-), 4.27 (m, CH-NH backbone).

### 6.2.5. Deprotection of Poly(L-gluatamic acid(OBzl)-*r*-L-lysine(Z))

To a 25 mL RBF was added the protected poly(L-glutamic acid(OBzl)-*r*-L-lysine(Z)) (2.84 g, (0.12 mmol) followed by 20 mL of TFA. The solution was stirred until the polymer was completely dissolved, followed by the dropwise addition of HBr (33 vol% in AcOH diluted to 16.7 vol% with AcOH, 20 mL). The resulting solution was stirred with thick precipitate observed soon after. The reaction mixture was stirred for a total of 16 h with the suspension then dropwise precipitated into diethyl ether, washed in ether ( $\times$ 2), then dried in vacuo overnight. The solid was then dissolved in DI water and added to 3.5 kDa dialysis tubing for dialysis against 2 L DI water ( $\times$ 3) for 24 h before being freeze-dried to obtain a white, fluffy solid ( $\sim$  1.4 g). <sup>1</sup>H NMR (D<sub>2</sub>O, 400 MHz): 1.06–1.43 (m, 4H, -NH-CH<sub>2</sub>-CH<sub>2</sub>-CH<sub>2</sub>-CH<sub>2</sub>-),

1.89–1.99 (m, Glu -CH<sub>2</sub>-CH<sub>2</sub>-CO-), 2.23 (m, Glu -CH<sub>2</sub>-CH<sub>2</sub>-CO-), 2.56 (m, 2H, Lys -NH-CH<sub>2</sub>-CH<sub>2</sub>-CH<sub>2</sub>-CH<sub>2</sub>-), 4.27 (m, CH-NH backbone).

#### 6.2.6. Methacrylation of poly(L-lysine) to form PLLMA

In a 28 mL glass vial, poly(L-lysine) (1.00 g, 4.78 mmol lysine units) was dissolved in DI water. pH was adjusted to 10 using 2.5 M NaOH before being chilled in an ice bath while stirring. Methacrylic anhydride (143  $\mu$ L, 0.957 mmol, 20% mole equivalent to lysine units), was then added dropwise and the mixture was allowed to stir for 24 h. The resulting mixture was added to 3.5 kDa dialysis tubing for dialysis against 2 L DI water ( $\times$ 3) for 24 h before being freeze-dried to obtain a white fluffy solid ( $\sim$ 300 mg). The polymer was purged with argon and stored at -18  $^{\circ}$ C. <sup>1</sup>H NMR (D<sub>2</sub>O, 400 MHz):  $\delta$  1.04–1.40 (m, 4H, Lys methacrylated -NH-CH<sub>2</sub>-CH<sub>2</sub>-CH<sub>2</sub>-CH<sub>2</sub>-), 1.41–1.73 (m, 4H, Lys NH<sub>2</sub>-CH<sub>2</sub>-CH<sub>2</sub>-CH<sub>2</sub>-CH<sub>2</sub>-), 1.84 (m, 3H, methacrylate -CO-C(CH<sub>3</sub>)=CH<sub>2</sub>), 2.78 (m, Lys NH<sub>2</sub>-CH<sub>2</sub>-CH<sub>2</sub>-CH<sub>2</sub>-CH<sub>2</sub>-), 3.13 (m, Lys methacrylated -NH-CH<sub>2</sub>-CH<sub>2</sub>-CH<sub>2</sub>-CH<sub>2</sub>-), 4.12 (m, CH-NH backbone), 5.27 (s, 1H, methacrylate -NH-CO-C(CH<sub>3</sub>)=CH<sub>2</sub>), 5.56 (s, 1H, methacrylate -NH-CO-C(CH<sub>3</sub>)=CH<sub>2</sub>)

#### 6.2.7. Methacrylation of poly(L-lysine-r-L-glutamic acid) to form PLGMA

In a 28 mL glass vial, poly(L-glutamic acid-r-L-lysine) (1.00 g, 0.868 mmol of lysine units) was dissolved in DI water. pH was adjusted to 10 using 2.5 M NaOH before being chilled in an ice bath while stirring. Excess methacrylic anhydride (388  $\mu$ L, 2.60 mmol, 3 times excess mole equivalent to lysine units) was then added dropwise, and the mixture was stirred for 24 h. The resulting mixture was added to 3.5 kDa dialysis tubing for dialysis against 2 L DI water ( $\times$ 3) for 24 h before being freeze-dried to obtain a white, fluffy solid ( $\sim$ 300 mg). The polymer was purged with argon at stored at -18  $^{\circ}$ C. <sup>1</sup>H NMR (D<sub>2</sub>O, 400 MHz):  $\delta$  1.06–1.53 (m, 4H, Lys methacrylated -NH-CH<sub>2</sub>-CH<sub>2</sub>-CH<sub>2</sub>-CH<sub>2</sub>-), 1.77 (m, 3H, methacrylate -CO-C(CH<sub>3</sub>)=CH<sub>2</sub>), (m, 4H, Lys NH<sub>2</sub>-CH<sub>2</sub>-CH<sub>2</sub>-CH<sub>2</sub>-CH<sub>2</sub>-), 1.84 (m, 3H, methacrylate -CO-C(CH<sub>3</sub>)=CH<sub>2</sub>), 1.87–2.12 (m, Glu -CH<sub>2</sub>-CH<sub>2</sub>-CO-), 2.24–2.55 (m, 2H, Lys -NH-CH<sub>2</sub>-CH<sub>2</sub>-CH<sub>2</sub>-CH<sub>2</sub>-), 3.21 (m, Lys methacrylated -NH-CH<sub>2</sub>-CH<sub>2</sub>-CH<sub>2</sub>-CH<sub>2</sub>-), 3.85–4.27 (m, CH-NH backbone), 5.24 (s, 1H, methacrylate -NH-CO-C(CH<sub>3</sub>)=CH<sub>2</sub>), 5.58 (s, 1H, methacrylate -NH-CO-C(CH<sub>3</sub>)=CH<sub>2</sub>).

#### 6.2.8. Silanization of silica wafers

Silica wafers were sonicated in acetone (30 m) and isopropanol (30 m) before being rinsed in isopropanol and dried in vacuo. Surfaces were silanized using previously established procedures. Silica wafers were soaked in a solution of APTES in acetone (4 v/v%) at 45  $^{\circ}$ C for 24 h. Wafers were then rinsed in acetone thoroughly before being dried in vacuo. Using

CDTPA as an example, CDTPA (50.0 mg, 0.179 mmol, 1 mol eq.), EDCI (137 mg, 0.716 mmol, 4 mol eq.) and NHS (20.6 mg, 0.179 mmol, 1 mol eq.) were added to a 100 mL RBF and dissolved in anh. DCM (50 mL). The solution was stirred for 2 h under nitrogen before adding to a beaker containing the washed silicon wafers. The beaker was placed in a desiccator purged with N<sub>2</sub> (g) which was shaken on a plate agitator at 80 RPM for 48 h. The wafers were removed and washed thoroughly with DCM and isopropanol and left to dry in vacuo. Wafers were stored in methanol at 4 °C for later use.

6.2.9. PLLMA reversible addition fragmentation chain transfer-mediated continuous assembly of polymers (CAP-RAFT) on pretreated silica substrates  
PLLMA (30.0 mg, 31.9 μmol of methacrylated units) dissolved in DMSO (973.8 μL, totalling to 30 mg/mL concentration after addition of stock solutions) was treated with DMSO solutions of CTA (25.8 μL, 1.00 mg/mL, 63.8 nmol, 1/500 mole equivalent of methacrylate units) and LAP (0.470 μL, 1.00 mg/mL, 1.56 nmol, 1/40 mole equivalent of CTA). Functionalized wafers were submersed face up in solution, and high purity argon was bubbled through the solution for 20 min. The degassed mixture was left sealed and irradiated in blue light (4 mW/cm<sup>2</sup>, λ<sub>max</sub> = 460 nm) for various intervals up to 24 h. Upon completion, the wafers were sonicated for 10 s in fresh DMSO, and the supernatant was extracted. The wafers themselves were thoroughly washed with DMSO (x3), DCM and iPrOH, before being dried under a nitrogen stream for 1 min. Treated wafers were then stored in vacuo prior to analysis.

The supernatant was also added to 3.5 kDa dialysis tubing for dialysis against 1 L DMSO (×3) for 24 h to remove leftover CTA and LAP and then analysed by <sup>1</sup>H NMR.

#### 6.2.10. PLGMA CAP-RAFT on pretreated silica substrates

PLGMA (30.0 mg, 27.5 μmol of methacrylated units) dissolved in DI water (984.2 μL, totalling to 30 mg/mL concentration after addition of stock solutions) was treated with DI water of CTA (15.4 μL, 1.00 mg/mL, 55.1 nmol, 1/500 mole equivalent of methacrylate units) and LAP (0.405 μL, 1.00 mg/mL, 1.38 nmol, 1/40 mole equivalent of CTA). Functionalized wafers were submersed face up in solution and high purity argon was bubbled through the solution for 20 min. The degassed mixture was left sealed and irradiated in blue light for various intervals up to 24 h. Upon completion, the wafers were sonicated for 10 s in fresh DI water, and then thoroughly washed with DI water (x3), then DMSO and isopropanol, before being dried under a nitrogen stream for 1 min. Treated wafers were then stored *in vacuo* prior to analysis.

## 6.3. Methods for Chapter 4

### 6.3.1. Materials

Acetone (tech. grade, VWR chemicals), alginic acid sodium salt (300-350 kDa, Carl Roth), *N,N*-dimethyl formamide (DMF, 99.8%, anhydrous, Sigma-Aldrich), diethyl ether (Et<sub>2</sub>O, AR grade, Chem-Supply), cellulose acetate (MW 100,000, Arcos Chemicals), ethanol (tech. grade, VWR chemicals), formic acid (puriss. p.a. ≥98%, Sigma Aldrich), H-L-valine-OH (>99%, Mimotopes), H-L-Glu(OBzl)-OH (>99%, Mimotopes), magnesium sulfate (anh. MgSO<sub>4</sub>, ≥97%, Merck), α-pinene (98%, Merck), sodium hydrogen carbonate (NaHCO<sub>3</sub>, AR grade, Chem-Supply), sodium hydroxide (NaOH; ≥97%, Merck), triethylamine (TEA, ≥99.5%, Sigma-Aldrich), triphosgene (≥98%, Merck), and Nylon 6 (Sigma Aldrich) were all used as received without further purification. Saturated brine solution was prepared from sodium chloride (NaCl, AR grade, Chem-Supply) in DI water. Tetrahydrofuran (anh. THF, inhibitor free, >99.9%, Merck), ethyl acetate (anh. EtOAc, >99.9% Honeywell) and were purified by passage through a solvent purification system (SBPT-1, LC Technologies, USA) containing 4Å sieves under Argon gas. Hexane (AR, Chem-Supply) was distilled over calcium hydride under nitrogen prior to use.

### 6.3.2. Synthesis of Valine NCA (Val NCA) and Benzyl-protected Glutamic Acid (Glu(OBzl) NCA)

Both NCAs were synthesized using modified versions of previous reported methods.<sup>1,2</sup> In a typical experiment Val (10.0 g, 42.2 mmol) was added to a 500 mL three-necked RBF and suspended in 200 mL of anh. THF with α-pinene (31.1 mL, 96.9 mmol, 1.15 excess moles) under nitrogen. After heating to 60 °C, triphosgene (10.1 g, 16.9 mmol, 1.2 excess moles) was added and the mixture was stirred at temperature for 2 h. Solvent was then removed from the clear solution under reduced pressure and replaced with 100 mL of anh. EtOAc. The solution was cooled to -18 °C before washing with sat. brine (1 × 100 mL) and then 5 w/v% aq. NaHCO<sub>3</sub> (1 × 100 mL) and the organic phase dried over MgSO<sub>4</sub>. The filtered solution was reduced to dryness *in vacuo* and recrystallized using anh. hexane at -18 °C over 16 h. The solids were then filtered and redissolved into anh. EtOAc before being precipitated into anh. hexane. The precipitate was then dried *in vacuo* over 24 h to afford a colorless solid and stored under argon at -80 °C.



Val NCA (10.2 g, 83% yield):  $^1\text{H}$  NMR (400 MHz,  $\text{CDCl}_3$ ,  $\delta$ ): 1.00–1.09 (m,  $J = 7.0$  Hz, 3H;  $-\text{CH}-(\text{CH}_3)_2$ ), 2.27 (s, 1H;  $-\text{CH}-(\text{CH}_3)_2$ ), 4.24 (d,  $J = 4.4$  Hz, 1H;  $-\text{CH}-\text{NH}-$ ), 6.79 (s, 1H; ringNH)

Glu(OBzl) NCA (9.7 g, 87 % yield):  $^1\text{H}$  NMR (400 MHz,  $\text{CDCl}_3$ ,  $\delta$ ): 2.08–2.31 (m, 2H;  $-\text{CH}_2-\text{CH}_2-\text{CO}-$ ), 2.55 (t,  $J = 6.8$  Hz, 2H;  $-\text{CH}_2-\text{CH}_2-\text{CO}-$ ), 4.42 (t,  $J = 6.0$  Hz, 1H;  $-\text{CH}-\text{NH}-$ ), 5.11 (s, 2H;  $-\text{CH}_2-\text{ArH}$ ), 6.47 (s, 1H; ringNH), 7.35–7.40 (m, 5H; ArH).

### 6.3.3. Synthesis of Poly(benzyl-L-gluatamic acid) (PBLG)

Glu(OBzl) NCA (1.50 g) was dissolved in 50 mL of anh. DCM under nitrogen in a 100 mL RBF. To the stirring solution was added TEA, and the clear solution was stirred under an argon bleed at room temperature for 24 h. The reaction mixture was then precipitated into and subsequently rinsed with  $\text{Et}_2\text{O}$  which was then dried and stored under vacuum to afford a clear tacky solid as the final product (2.84 g, 78.5% yield).  $^1\text{H}$  NMR (400 MHz,  $\text{DMSO}-d_6$ ,  $\delta$ ): 2.04–2.48 (m, 2H;  $-\text{CH}_2-\text{CH}_2-\text{CO}-$ ), 3.90 (t, 1H;  $-\text{CH}-\text{N}-\text{CO}-$ ), 5.00 (s, 2H,  $-\text{CH}_2-\text{ArH}$ ), 5.59 (s, 1H; ringNH), 7.19–7.30 (m, 5H; ArH).

### 6.3.4. Wet Spinning of Polymeric Fibers

Polymer solutions with assigned spinning dope concentrations were dissolved over 4 h (until complete dissolution in anhydrous spinning dope solvent under nitrogen. For samples loaded with NCA, NCA was then introduced into the solution at a 4:1 ratio of polymer to NCA. The subsequent solution was extruded into the coagulation bath with 2% TEA as an initiator at a continuous rate. Upon precipitation, the fiber was drawn out of the coagulation bath and dried under an infrared lamp before being collected. After 24 h, the collected fibers were washed in the coagulation bath solution without TEA, 3 times and subsequently dried under an air stream for 48 h.

### 6.3.5. Deacetylation of Cellulose Acetate Fibers

Cellulose acetate fibers were soaked in a solution of 0.5 N aq. 50% EtOH / 50%  $\text{H}_2\text{O}$  for 24 h. Subsequent cellulose fibers were washed progressively in 50% EtOH / 50%  $\text{H}_2\text{O}$ , 25% EtOH / 75%  $\text{H}_2\text{O}$  solution and  $\text{H}_2\text{O}$  before subsequent drying under an air stream for 48 h.

## 6.4. Instrumentation and Characterization

### 6.4.1. Nuclear magnetic resonance (NMR)

Proton ( $^1\text{H}$ ) Nuclear Magnetic Resonance (NMR) spectroscopic analysis was performed on a Varian Unity Plus 400 MHz spectrometer.

#### 6.4.1.1. Conversion within $\beta$ -sheet laden networks

A calibration curve was generated from  $^1\text{H}$  NMR analysis of Val NCA solutions (100  $\mu\text{L}$ ) at 5 different concentrations (15, 30, 60, 120, 180 mg/mL) diluted with  $\text{CDCl}_3$  (900  $\mu\text{L}$ ). Integration of the Val NCA doublet peak at 0.92 ppm relative to the methyl DMF signals at 2.88 ppm and 2.96 ppm determined for the 5 Val NCA concentrations, afforded a calibration curve.

Thus, Val NCA conversions were determined by taking 100  $\mu\text{L}$  aliquots of reaction solutions after  $\beta$ -sheet incorporation into the networks and diluting with  $\text{CDCl}_3$  (900  $\mu\text{L}$ ). These solutions were analysed by  $^1\text{H}$  NMR by normalising against the same peaks of DMF, to determine Val NCA concentrations of each solution. This was then used to calculate the monomer conversion.

Gly NCA conversions were determined by  $^1\text{H}$  NMR integration of the cyclic amine peak at 8.84 ppm relative to the Val NCA doublet at 0.92 ppm. Thus, the amount of NCA in solution due to Gly NCA and not Val NCA could be determined.

### 6.4.2. Attenuated total reflection – Fourier transform infrared spectroscopy (ATR-FTIR)

In **Chapter 2**, attenuated total reflection- Fourier transform infrared spectroscopy (ATR-FTIR) spectroscopy was carried out using a Bruker Tensor 27 FTIR, with GladiATR ATR attachment obtained from Pike Technologies. The FTIR was equipped with OPUS 6.5 spectroscopy software from Bruker Optik GmbH and recorded with a resolution of 4  $\text{cm}^{-1}$ .

In **Chapter 4**, ATR-FTIR spectroscopy was performed with a Bruker Hyperion 1000 microscope with a dedicated ATR-objective (Bruker Optics GmbH, Ettlingen, Germany). The ATR-crystal was brought into contact with the sample. The microscope was continuously purged with dry air, and the MCT detector was cooled with liquid nitrogen. The FTIR spectra were recorded with a resolution of 4  $\text{cm}^{-1}$ . One hundred scans per measurement were performed. Three samples per layer with three spots per sample were measured.

### 6.4.3. Fluorescent imaging of Thioflavin T (ThT) stained networks

Fluorescent images of ThT stained gel networks were acquired on a Leica TCS SP2 confocal laser scanning microscope (CLSM), using excitation wavelength of 490 nm.

### 6.4.4. Scanning electron microscopy (SEM)

In **Chapter 2**, scanning electron microscope (SEM) images were acquired using a FEI Quanta 200 ESEM FEG. Samples were pre-coated with gold using a Dynavac Mini Sputter Coater prior to imaging.

### 6.4.5. Differential scanning calorimetry (DSC)

Differential scanning calorimetry (DSC) measurements on PCL were carried out on a PerkinElmer DSC 8500 with a heating rate of 40 °C min<sup>-1</sup>. Subsequent crystallization was determined by determining the heat of melting of crystalline structures and determining it as a percentage of the heat of melting of 100 % crystalline PCL.<sup>4</sup>

### 6.4.6. Swelling ratio measurement

To measure the equilibrium swell ratio ( $Q$ ), the network was dried under heat in vacuo (60 °C, 20 mbar) for 24 h and then swollen in water until it reached equilibrium swelling. The weight of dry and fully swollen samples was determined by analytical balance and denoted as  $W_d$  and  $W_s$ , respectively. The equilibrium swell ratio ( $Q$ ) is defined by Eq. (1).

$$Q = \frac{W_s}{W_d} \quad (1)$$

### 6.4.7. Compressive mechanical testing

The compressive strain-stress curves were obtained using an Instron Microtester 5848 equipped with a 2 kN static load cell and Bluehill material testing software. cylindrical hydrated network samples (diameter: ~9 mm; height: ~8.5 mm) were compressed to their maximum strain between two parallel plates at a crosshead speed of 0.1 mm/second. Engineering stresses and strains were recorded.

### 6.4.8. Tensile mechanical testing

Tensile mechanical testing was performed using an ElectroForce 3200 (TA Instruments, DE, USA) with 2.5 N load cells. Small sections of fibers were randomly selected and fixed onto plastic frames with a gap of 3 mm using two-component glue in case of dry samples. The glue was left to dry under a fume hood for at least 24 h. The frames were then fixed between the

clamps of the testing device and pulled apart until failure at a rate of  $0.01 \text{ mm s}^{-1}$  at a relative humidity of 65%, and room temperature. The Young's modulus was obtained by calculating the slope of the stress–strain curve in the linear elastic region. The fiber toughness was calculated by integrating the stress–strain curve. The measurements were repeated for a minimum of five individual samples.

## 6.5. References

- (1) Shirbin, S. J.; Insua, I.; Holden, J. A.; Lenzo, J. C.; Reynolds, E. C.; O'Brien-Simpson, N. M.; Qiao, G. G. Architectural Effects of Star-Shaped “Structurally Nanoengineered Antimicrobial Peptide Polymers” (SNAPPs) on Their Biological Activity. *Advanced Healthcare Materials* **2018**, *7* (21), 1800627.
- (2) Shirbin, S. J.; Karimi, F.; Chan, N. J.-A.; Heath, D. E.; Qiao, G. G. Macroporous Hydrogels Composed Entirely of Synthetic Polypeptides: Biocompatible and Enzyme Biodegradable 3D Cellular Scaffolds. *Biomacromolecules* **2016**, *17* (9), 2981.
- (3) Skoulas, D.; Stavroulaki, D.; Santorinaios, K.; Iatrou, H. Synthesis of Hybrid-Polypeptides m-PEO-b-poly(His-co-Gly) and m-PEO-b-poly(His-co-Ala) and Study of Their Structure and Aggregation. Influence of Hydrophobic Copolypeptides on the Properties of Poly(L-histidine). *Polymers* **2017**, *9* (11), 564.
- (4) Crescenzi, V.; Manzini, G.; Calzolari, G.; Borri, C. Thermodynamics of fusion of poly- $\beta$ -propiolactone and poly- $\epsilon$ -caprolactone. comparative analysis of the melting of aliphatic polylactone and polyester chains. *European Polymer Journal* **1972**, *8* (3), 449.

# Appendix A: Mimicry of silk utilizing synthetic polypeptides

## Mimicry of silk utilizing synthetic polypeptides

*Nicholas J. Chan<sup>†§#</sup>, Sarah Lentz<sup>†§#</sup>, Paul A. Gurr<sup>†</sup>, Thomas Scheibel<sup>§\*</sup>, Greg G. Qiao<sup>†\*</sup>*

<sup>†</sup>Polymer Science Group, Department of Chemical Engineering, and University of Melbourne, Parkville, Melbourne, Victoria 3010, Australia

<sup>§</sup>Chair of Biomaterials, University of Bayreuth, Prof.-Rüdiger-Bormann-Str. 1, D-95447

Bayreuth

<sup>#</sup> contributed equally

\* Corresponding author emails: Thomas Scheibel: [thomas.scheibel@bm.uni-bayreuth.de](mailto:thomas.scheibel@bm.uni-bayreuth.de); Greg

G. Qiao: [gregghq@unimelb.edu.au](mailto:gregghq@unimelb.edu.au)

ABSTRACT. For thousands of years, silks have been utilized by mankind for various reasons, and silk-based materials are increasingly used in modern biomedical and technical applications nowadays. However, natural silks show some limitations (especially for the latter set of applications). In this respect, chemical polymerization methods have been developed, providing a potential avenue to synthesize materials with silk-like features. This article reviews the physicochemical properties of silks and how this relationship has been used to integrate  $\beta$ -sheet forming polypeptide regions. Strategies that utilize N-carboxyanhydride ring-opening polymerization (NCA ROP) for polypeptide synthesis are the primary focus of this review as a versatile and unique polypeptide synthesis methodology. The anticipated advancements in this

field of mechanical applications aim to utilize  $\beta$ -sheet structures more effectively within an amorphous matrix to yield tough materials.

KEYWORDS: Silk inspired materials, biomimicry,  $\beta$ -sheet, synthetic polymerization, NCA ROP, chemoenzymatic

## Contents

Abbreviations.....	5
Nomenclature.....	6
1. Introduction.....	8
2. The Structure of Silk and the Impact on Properties.....	10
2.1 Silkworm Silk.....	14
2.2 Dragline Spider Silk.....	14
3. Polypeptide Synthesis Through <i>N</i> -carboxyanhydride Ring Opening Polymerization.....	15
4. Strategies towards silk-like polymer synthesis.....	20
4.1. Polypeptides with modified silk-like motifs.....	24
4.1.1. Spacer residues within PLAla blocks.....	25
4.1.2. The impact of hydrophobic blocks outside of PAla chains.....	26
4.1.3. The impact of ionic components outside of PAla chains.....	28
4.1.4 Non-linear precursors.....	29
4.2. Alternative polypeptides for $\beta$ -sheet fibrils.....	31
4.2.1. $\beta$ -Sheet Fibrils Formed through Canonical Amino Acids.....	33
4.2.2. $\beta$ -Sheet Fibrils Formed Through Side Chain Modified Amino Acids.....	39
5. Material Morphology and Fabrication Strategies towards silk-like polymer synthesis.....	43
5.1. Fiber Processing.....	44
5.2. Film Casting and Surface Modification.....	45
5.3. Polypeptide Based Gels.....	48
6. Applications.....	50
6.1. Drug/Payload Delivery.....	50
6.2. Cell toxicity and antimicrobial behavior.....	51
6.3. Tissue Engineering.....	52
6.4. Further Applications.....	56
7. Conclusions and Future Perspectives.....	58
8. Acknowledgements.....	59
9. References.....	60
Appendix A: Overview of different $\beta$ -sheet forming polypeptides, synthetic methods, and architectures for silk mimicry with the respective natural construct used as a blueprint and characterization methods.....	89
Appendix B: Overview of different poly(alanine)-based polymers, secondary structure, and other applicable properties.....	92

Appendix C: Overview of different  $\beta$ -sheet fibril forming copolymers, synthesis methods and morphologies with mechanical and other applicable properties..... 109  
Appendix D: Chemical Structure of Polymers Presented..... 118



## Abbreviations

<sup>13</sup> C-NMR	Carbon-13 nuclear magnetic resonance
Abz	Aminobenzoic
ACN	Acetonitrile
ADSCs	Adipose-derived stem cells
AFM	Atomic force microscopy
ATR-FTIR	Attenuated total reflection Fourier transform infrared spectroscopy
ATRP	Atom transfer radical polymerization
<i>b</i>	Block
Bzl	Benzyl
CD	Circular dichroism
CGC	Critical gelation concentration
DCM	Dichloromethane
DLS	Dynamic light scattering
DMF	Dimethylformamide
DMSO	Dimethyl sulfoxide
DOX	Doxorubicin
DP	Degree of polymerization
E. Coli	Escherichia Coli
ECM	Extracellular matrix
EDTA	Ethylenediamine tetraacetic acid
FTIR	Fourier transform infrared spectroscopy
<i>g</i>	Grafted
GPa	Gigapascal
HDI	Hexamethylene diisocyanate
HEMA	2- Hydroxyethylmethacrylat
HFIP	Hexafluoroisopropanol
M®	Matrigel TM
MALDI-TOF	Matrix-assisted Laser Desorption Ionisation Time of Flight
MeOH	Methanol
MJ	Megajoule
MMA	Methyl methacrylate
NCA ROP	N-carboxyanhydride ring-opening polymerization
PDI	Polydispersity index
pH	Potential of hydrogen
<i>r</i>	Random
SAXS	Small-angle X-ray scattering
SEM	Scanning electron microscope
sGAG	Sulfonated glycosaminoglycan
SWCNT	Single-wall carbon nanotubes
TEM	Transmission electron microscopy

THF	Tetrahydrofuran
UV	Ultraviolet
XRD	X-Ray diffraction

## Nomenclature

A	Ala	Alanine
C	Cys	Cysteine
D	Asp	Aspartic acid
E	Glu	Glutamic acid
F	Phe	Phenylalanine
G	Gly	Glycine
H	His	Histidine
I	Ile	Isoleucine
K	Lys	Lysine
L	Leu	Leucine
M	Met	Methionine
N	Asn	Asparagine
P	Pro	Proline
P	Pro	Proline
PADLG		Poly(DL-allylglycine)
PBLA		Poly( $\beta$ -benzyl-L-aspartate)
PBLG		Poly( $\gamma$ -benzyl- $\alpha$ , L-glutamate)
PCL		Poly( $\epsilon$ -caprolactone)
PDAla		Poly(D-alanine)
PDGlu		Poly(D-glutamic acid)
PDLAla		Poly(DL-alanine)
PDLGlu		Poly(DL-glutamic acid)
PDMS		Polydimethylsiloxane
PEG		Polyethylene glycol
PEI		Polyethylenimine
PGI		Polyglobalide
PGly		Poly(glycine)
PHLG		Poly [N5-(2-hydroxyethyl)-L-glutamine]
PLAla		Poly(L-alanine)
PLArg		Poly(L-arginine)
PLAsp		Poly(L-aspartic acid)
PLGlu		Poly(L-glutamic acid)
PLHis		Poly(L-histidine)
PLIle		Poly(L-isoleucine)
PLLys		Poly(L-lysine)

PLLeu		Poly(L-leucine)
PLPhe		Poly(L-phenylalanine)
PLThr		Poly(L-threonine)
PLTyr		Poly(L-tyrosine)
PLX		Poloxamer
PMLL		Poly(L-lysine-g-methylacrylate)
PMMA		Polymethylmethacrylate
PNIPAM		Poly(N-isopropylacrylamide)
POLM		Poly(sulfoxide methanoimine)
POSS		Polyhedral oligomeric silsesquioxane
PPDL		Polypentdecylactone
PPLG		Amino propanol-modified PLGlu
PPO		Poly(p-phenylene oxide)
PZLL		Poly(carboxybenzyl-L-lysine)
Q	Gln	Glutamine
R	Arg	Arginine
T	Thr	Threonine
V	Val	Valine
Y	Tyr	Tyrosine

## 1. Introduction

Through evolution, nature often constructs materials with outstanding properties, providing inspiration for material scientists, and forming the basis of biomimicry. The range of properties is wildly diverse – mussel feet show strong adhesion to wet surfaces,[1, 2] *Morpho* butterfly wings have stunning structural color,[3, 4] and shark skin-inspired surfaces achieve minimal drag and subsequently increased aerodynamic efficiency.[5, 6] One of the most highly investigated natural materials with excellent mechanical properties is animal silks.[7-11]

The superior strength of spider silk is well-reported exemplary with the dragline silk of the European garden spider, possessing a tensile strength, extension at break, and toughness around 1.1 GPa, 30 % and 160 MJ/m<sup>3</sup>, respectively, which can reach up to 500 MJ/m<sup>3</sup> in case of other species.[12-15] For comparison, high tensile steel has a similar strength of 1.5 GPa, but a far inferior extension at break of 0.8%, resulting in a much lower toughness (6 MJ/m<sup>3</sup>). *Bombyx mori* (*B. mori*, i.e., silkworm) silk has a lower tensile strength, extension at break, and toughness than its spider silk counterpart (0.6 GPa, 18%, and 70 MJ/m<sup>3</sup>, respectively). However, its overall toughness is still far superior to tensile steel.[10] In addition to their remarkable mechanical properties, certain silks have been found to be biocompatible with human cells and provide sufficient support for cellular adhesion.[16-18] Furthermore, as with other proteins, silks are susceptible to enzymatic degradation, making them a strong candidate for utilization in many bioapplications.[17, 19, 20] Although *B. mori* silkworm silk and the regeneration of silk fibers can overcome the issue of scaling up,[9] its overall mechanical properties still leave a lot to be desired for technical applications. In contrast, spider silk is naturally available only at an incredibly low quantity due to the cannibalistic behavior of spiders upon spider farming making it impractical for large-scale use.[9]

As silks are protein-based, research into mimicry often starts at a molecular level. The synthesis of polypeptides can be performed using many different techniques. Recombinant methods involve the manipulation of bacterial plasmids to force microorganisms to produce proteins with specific sequences.[21, 22] Silk-like proteins synthesized in this fashion are amongst the most popular and extensively studied methods for achieving silk mimicry and have already been extensively reviewed.[23-25] The other common method for synthesizing specific sequences is using solid-state peptide synthesis, but the size of these peptides is restricted and lacks a high mass throughput.[26, 27] The polymerization methods for synthesizing polypeptides – *N*-carboxyanhydride ring-opening polymerization (NCA ROP) [28-31] and chemoenzymatic polymerization[32, 33] – provide alternative techniques which can lead to the desired constructs. Comparatively, chemoenzymatic polypeptide synthesis is a less developed technique than NCA ROP, and while interesting work exists in the field, these works have previously been well reviewed. As NCA ROP has been well developed, multiple strategies uniquely available to polymerization-based techniques have emerged with interesting methods for synthesizing polypeptides with homopoly(amino acids) or copoly(amino acids) (random or alternating depending on the polymerization method) blocks.

As interest in the field of biomimicry expands, and with the studies into synthetic methods ever-increasing, silk-inspired chemically synthesized polymers have intriguing prospects, with this review mainly focusing on the potential for NCA ROP to develop silk-mimetic polymers based on amino acid motifs that are typically not found in silk proteins. Previous bioinspired methods for silk-inspired chemical synthesis have been reviewed as well as other parallel strategies which share specific structural similarities with silk, and which can lead to bio-inspired pathways in the future. As with any attempts at biomimicry, a firm grasp of the structure-property relationship of silks is

imperative. From there, the appropriate strategy for polypeptide synthesis can be determined. The Tang group has most recently reviewed the synthesis of bioinspired polymers,[34] while the Zha [35] and Numata [36] groups have recently reviewed the chemical synthesis of silk-like polymers specifically but were limited only to the synthesis of such materials. In contrast, this review expands into the properties of materials yielded from these polymers and their subsequent applications. Beyond these works, the chemical synthesis and applications of other structures are reviewed, which are responsible for silk properties at a nanostructural and molecular level.

## **2. The Structure of Silk and the Impact on Properties**

Before discussing the specifics of silk structure and the sequence-structure-function relationship, a fundamental understanding of the hierarchical structural nature of proteins is required.

Natural proteins are large folded biomacromolecules comprising up to 21 natural amino acids. Almost all amino acids consist of three unique groups extending from a chiral carbon (the  $\alpha$ -carbon) – a carboxylic acid functional group, an amino-functional group, and a unique side chain different for each amino acid. As such, amino acids generally have two stereoisomers, with the L-isomer being the natural form of amino acids, though the D-isomer does occur in rare cases due to modifications after biological synthesis (referred to as posttranslational modifications). Conjugation of the carboxyl and amino functional groups stemming from the  $\alpha$ -carbon results in peptide bonds, and the amino acid sequence in the polypeptides is called the protein primary structure. Supramolecular interactions between the amino acid residue side chains, such as hydrophobic interactions,  $\pi$ - $\pi$  stacking, Van der Waals forces, and ionic bonding, cause this polypeptide chain to adopt thermodynamically stable secondary structures such as  $\alpha$ -helices,  $\beta$ -sheets, and random coils. The spatial configuration of these secondary structure elements yields a

3D structure called the tertiary structure. In some cases, individual proteins will associate with each other to form a multimeric protein complex called a quaternary structure. Of these structural levels, the secondary structure is thermodynamically controlled and relies on the design of the primary structure.

Silks are best defined as a family of fibrous structural proteins consisting of highly repetitive sequences, which are processed from a concentrated protein solution (the protein itself is silk fibroin) before assembling into fibers outside the body.[37] Fibrous proteins consist of amino acid motifs that persist intrinsically unstructured in solution but can fold into rigid or flexible structures upon distinct processing, imparting high strength and toughness required for the fiber's performance.[38] This is distinct from globular proteins which have often a compact and spherical structure implying their function in solution to begin with.[14] In natural silks, the host organism stores the concentrated silk protein solution (otherwise referred to as a silk dope) within its silk glands.[12] From these glands, shear forces induce a highly controlled phase transition from an unfolded, soluble protein solution into a structured solid fiber alongside ion and pH gradients.[39] This spinning process induces structure formation resulting in a semicrystalline structure semicrystalline structure based on both protein primary structure and spinning conditions. It is these crystallites which regulate mechanical properties, with crystallite fraction, size and orientation differentiating between species and subsequent mechanical properties.[40, 41] It should be noted that while shear forces are applied within the body in most organisms, exceptions occur where spinning occurs post-excretion with rheological stress triggering assembly.[42, 43] While a variety of arthropods produce silks, this section focuses on the two most prominent producers of silk – silkworms (*Bombyx mori* larvae) and spiders.[8, 44]

Silk crystallites can comprise one of five major secondary structures: extended  $\beta$ -sheets, cross  $\beta$ -sheets,  $\alpha$ -helical coiled coils, collagen triple helices and polyglycine II.[45] The thermodynamically favorable packing of  $\beta$ -sheets dictates that amino acid side chains orientated towards the same face possess similar hydrophobicity and size. The orientation of such structures relative to the fiber axis is dictated through primary structure and spinning and defines the subcategory of structure. Extended  $\beta$ -sheet structures result from the packing of  $\beta$ -strands parallel to the fiber axis.[46, 47] Cross- $\beta$  structures instead result from the protein folding back on itself in a  $\beta$ -turn – usually due to periodic glycine within the crystallite.[45, 48, 49] Apart from  $\beta$ -sheet based structures, helix based structures are also present, though derived from different helical conformations.  $\alpha$ -helical coiled-coils are particularly prevalent in acniform silk (primarily used by spiders for wrapping prey), consisting of  $\alpha$ -helices (right-handed twisting) winding around each other into a superhelix.[50, 51] This is characterized by a repetitive heptad sequence with bulky nonpolar residues in the first and fourth position.[52] Collagen triple helices structures are far more rare, though are present in some silks (e.g. sawfly silk).[38] They are characterized by the repetitive triad sequence GXY where X & Y are proline or hydroxyproline), resulting in left-handed helices which intertwine into a superhelix.[53] Polyglycine II structures are also rare, though are found in specific silks such as *Argiope trifasciata* flagelliform silk.[54] They consist of right-handed helices ( $3_1$  helices), though more tightly wound than  $\alpha$ -helices but instead of forming superhelices, they pack into a hexagonal lattice structure. The composition of such structures within crystallites subsequently contributes to mechanical properties, with coiled-coils contributing to high extension-at-break while  $\beta$ -sheet structures are far more rigid, contributing to mechanical strength.[55]



In this review, the focus lies on the mimicry of silk-derived  $\beta$ -sheet structures and the resulting properties. Therefore, from now on the focus lies on the internal structure of the silks and not on the hierarchical structure of the silks. Another important aspect reviewing silks is that they can be regarded from a polymer chemistry view as block copolymer-like materials, since they comprise a defined amino acid sequence.[56]

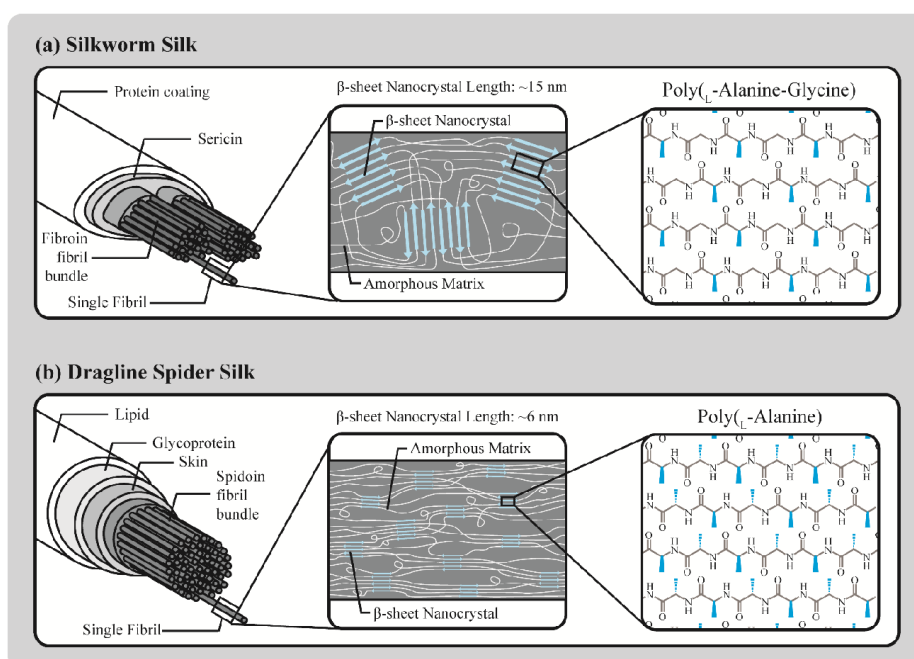


Figure 1: Overall structure of a) silkworm silk and b) dragline spider silk. Both silks employ a “core-shell” structure with the core consisting of bundles of  $\beta$ -sheet nanofibrils. In spider silk, the  $\beta$ -sheet nanocrystals are based on poly(L-alanine) structure with methyl group side chains alternating on a different side of the  $\beta$ -sheet plane (blue coming out of the page while red going

into the page). Silkworm silk rather contains poly (glycine-L-alanine) motifs where side-chain alanine methyl groups would all remain on the same side of the plane (all coming out of the page).

## **2.1 Silkworm Silk**

*Bombyx mori* silk consists of a heavy chain fibroin (~350-400 kDa), a small light chain fibroin (~25 kDa) linked to the heavy chain *via* disulfide bonds, and the P25 protein (a ~30 kDa glycoprotein) bonded to the other two components *via* hydrophobic interactions. [57-59] The heavy chain is a hydrophobic polypeptide consisting primarily of glycine alternating with another amino acid (*i.e.*, multiple repetitive GX motifs where G is glycine and X is another amino acid). Serine, tyrosine, valine, and threonine are all found in significant quantities as the second amino acid, while prominent motifs are GAGAGS, GAGAGY and GAAS (A is alanine, S is serine and Y is tyrosine) appearing in ~70 residue blocks and thus resulting in alanine-rich  $\beta$ -sheet nanocrystal forming blocks (Figure 1a). The light chain, in contrast, making up the amorphous section of this protein is far less ordered with no repetition, consisting primarily of anionic glutamic acid and bulky hydrophobic and aromatic residues. [60-62]

## **2.2 Dragline Spider Silk**

The properties of dragline spider silk can significantly differ based on species but generally the fibers consist primarily of two different major ampullate spidroins (MaSps) (~200-350 kDa) (Figure 1b) notated as MaSp1 and MaSp2, though recent studies have begun to research additional proteins such as MaSp3 and MaSp4. [63-66] Numerous motifs are common within these, including poly(L-alanine) (PLAla), GGX and GPGXX motifs (almost exclusively in MaSp2), where P is proline and X is often tyrosine, glutamine, or leucine. The frequency of these motifs primarily affects the overall amino acid composition. It helps to differentiate the two MaSps – for example, the proline content in MaSp1 is less than 1% while it is greater than 10% for MaSp2. These MaSps consist of highly repetitive units of around 30-60 residues, including these motifs. The  $\beta$ -sheet

nanocrystalline regions partially responsible for the superior mechanical properties are due to the PLAla blocks. These are made up of 5-14 residues depending on their species of origin and respective MaSp. Subsequently, hydrophobic association stacks these  $\beta$ -sheets to form aligned nanocrystals much smaller than that of silkworm silk, with spider silk  $\beta$ -sheet nanocrystals with dimensions in the range of 1 – 10 nm, although this varies between species. Importantly, silkworm silk  $\beta$ -sheet nanocrystals are at least twice as big as the dragline spider silk nanocrystals. The combination of nanocrystals alignment parallel to the fiber axis and size results in spider silk's significantly superior mechanical properties – precisely, strength and toughness are approximately double that of silkworm silk.[67-69] Apart from these regions are the glycine-rich regions which include the GGX as mentioned above and GPGXX motifs and, subsequently, are less well-defined, consisting of a mix of secondary structures.[70-74] This more amorphous region then provides the desired matrix for the  $\beta$ -sheet crystals to attain the desired mobility and thus achieve the superior flexibility and elasticity observed in such fibers. Besides from this repetitive core are flanking non-repetitive regions existing at the ends of the polypeptide sequence called the primarily helical terminal domains. These terminal domains function as molecular switches preventing aberrant aggregation pre-spinning while promoting self-assembly during spinning.[66, 75]

### **3. Polypeptide Synthesis Through *N*-carboxyanhydride Ring Opening Polymerization**

Many strategies have implemented the previously detailed natural blueprints of the silkworm *B. mori* or different spider species like *N. clavipes*, with biocompatibility, biodegradability, and outstanding mechanical properties of natural silks driving this motivation. The aim is to produce a material that combines these properties, specifically synthetic polymers with silk-inspired polypeptide components using NCA ROP.

NCA ROP can be performed using numerous initiation methods (Scheme 1).[29] The most common initiation method is through nucleophilic attack (Scheme 1a) (most commonly a primary amine), resulting in chain-growth ring-opening polymerization *via* the normal amine mechanism. As the initiator remains attached to the polypeptide, facile synthesis of polypeptides with functional end groups can be performed. Furthermore, multiple initiating sites can be employed to design molecules with alternative architectures such as graft polypeptides and core-first stars. Alternatively, initiation *via* metal complexes (Scheme 1b) has been employed by the Deming group, which utilized nickel and cobalt initiators.[76-78] Through oxidative addition and amide proton migration upon reaction with other NCAs, five-membered amido-alkyl metallacycles, susceptible to further reaction by NCA monomers through the same sequences, are formed to achieve polymerization. Though residual metals must be removed, metal complex initiation offers reduced polydispersity and faster kinetics than nucleophilic attack. A third initiation strategy is to take advantage of the activated monomer mechanism (Scheme 1c) *via* deprotonation of the cyclic amine on the NCA monomers through a base. The deprotonated anionic amine acts as an initiator, ring-opening another NCA monomer resulting in a single NCA ring with a ring-opened amino acid installed onto the cyclic amine. Thus, it can act both as an initiator *via* the primary amine of the ring-opened amino acid group or as a cyclic monomer *via* this NCA ring. Though uncontrolled, this method yields high molecular weight polypeptides.

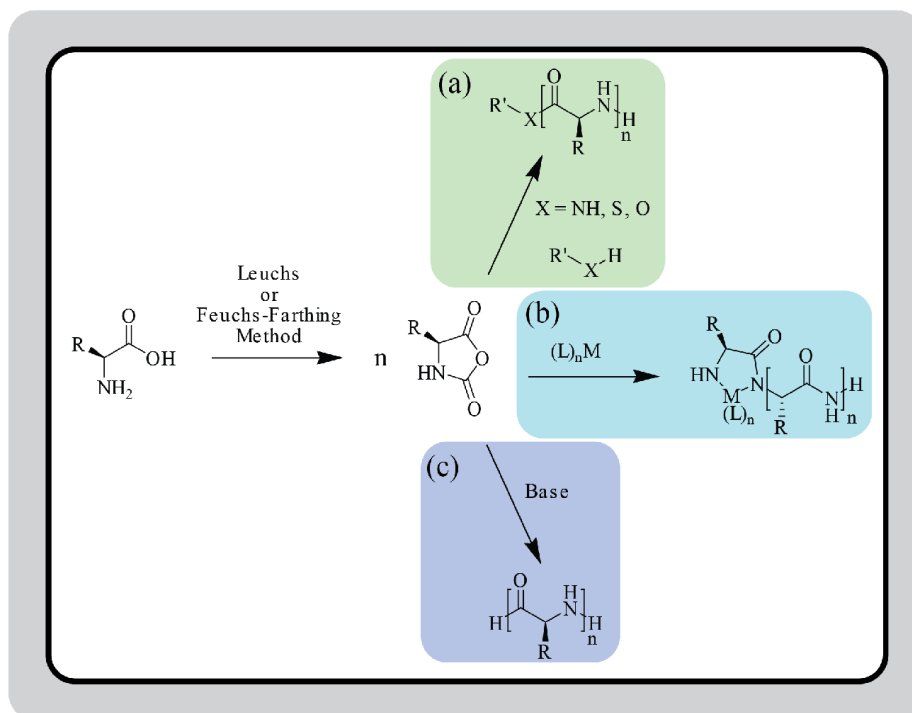
As with any synthetic technique, NCA ROP possesses specific qualities which inherently make them both more and less favorable to developing silk mimics. As a polymer synthesis technique, NCA ROP can yield polymers of high molecular weight (molecular weights on the order of 10 MDa have previously been reported) at a multigram scale within a comparable or shorter timescale compared to other techniques (24 h reaction times are often reported for the polymerization

reaction). However, as they are synthetic polymers, they share characteristics which hinder their versatility. Of these characteristics, its non-sequence specific nature is the most notable as this complicates secondary structure-centered design considerably. This is even more pertinent in the pursuit of silk mimicry where the conformation of secondary structures is important. Furthermore, resultant polypeptides have a distribution of molecular weights centered around a targeted degree of polymerization (DP), otherwise known as a polydispersity index (PDI), instead of a specific molecular weight. In general, this means that polymers with a lower molecular weight distribution (i.e., lower PDI) will form more consistent substructures, but in the case of some polypeptide monoblocks residues such as poly(L-alanine) where the size of such blocks specifically dictates their secondary structure conformation, PDI in combination with molecular weight can ultimately determine secondary structure distribution and substructures.

The range of available residues for NCA ROP is also greatly increased beyond the traditional 21 canonical amino acids compared to other strategies. An NCA specific issue comes in the form of its susceptibility to nucleophilic attack and as such side-chain protection must commonly be employed for functional residues (e.g., glutamic acid, lysine). This introduces an extra deprotection step, though such modified amino acids have been utilized in their protected forms as the modified intermolecular interactions of such groups results in drastically altered secondary structure conformations. Furthermore, such modified amino acids cannot be easily utilized by techniques which require the identification of canonical amino acid (i.e., recombinant methods or chemoenzymatic polymerization). Another detail is the facile introduction of the unnatural D-isomer. In recombinant techniques, the introduction of the D-isomer is only possible through post-translational processes and clever design whereas NCA ROP allows introduction of the isomer during polymerization, allowing for physical and biological tuning of properties. While these

perspectives must be taken into consideration during synthesis, its potential as a polymerization method allows for unique strategies unavailable to other polypeptide synthesis strategies.

While coupling techniques are often required to append non-peptidic molecules, polymerization from an initiating group of preexisting molecules allows for a more facile approach with further capabilities. Compared to coupling, such strategies assure high functionalization efficiency due to the reduced steric hinderance of a monomer instead of a polymer. Functional initiators allow for end-group functionalization with a functional group or polymer. Grafting-from strategies (or in the case of star polymers, core-first strategies) also become available for the purposes of developing graft polymers and polymer-based surfaces. In both cases, grafting from approaches yield high PDI, but can still yield high grafting efficiency or, in the case of surfaces, thicker surfaces. NCA ROP is established as a versatile and facile methodology for yielding silk-mimicking materials, but with its lack of sequence-control in particular, much can be garnered from studying the control of substructures using this technique.



*Scheme 1: Synthesis of polypeptides via NCA ROP using the most common initiation methods: a) nucleophile initiated ROP, often initiated by a primary amine; b) transition metal initiated ROP; c) base initiated ROP resulting in chain propagation via the activated monomer mechanism.*

#### **4. Strategies towards silk-like polymer synthesis**

Many strategies have implemented the previously detailed natural blueprints of the silkworm *B. Mori* or different spider species like *Nephila clavipes*, with biocompatibility and biodegradability, utilizing NCA ROP to yield such structures.[34, 79] Besides from precise strategies which mimic genetic blueprints to form the peptide sequence, the exploration of peripheral approaches, including poly(alanine) utilization and  $\beta$ -sheet fibrilization, gives further insight into the potential of silk-inspired polymers (Figure 2). The general strategy implements rigid polypeptide secondary structures within an amorphous matrix as with natural silks to yield materials that can harness the following desired properties. Based on the primary structure of silks, typically, amino acids glycine and alanine are modified to act as monomers. Then in further steps, the amino acids are coupled to polypeptides. Appendix A summarizes the strategies with specific sequences designed to mimic silk and their resulting secondary structure.



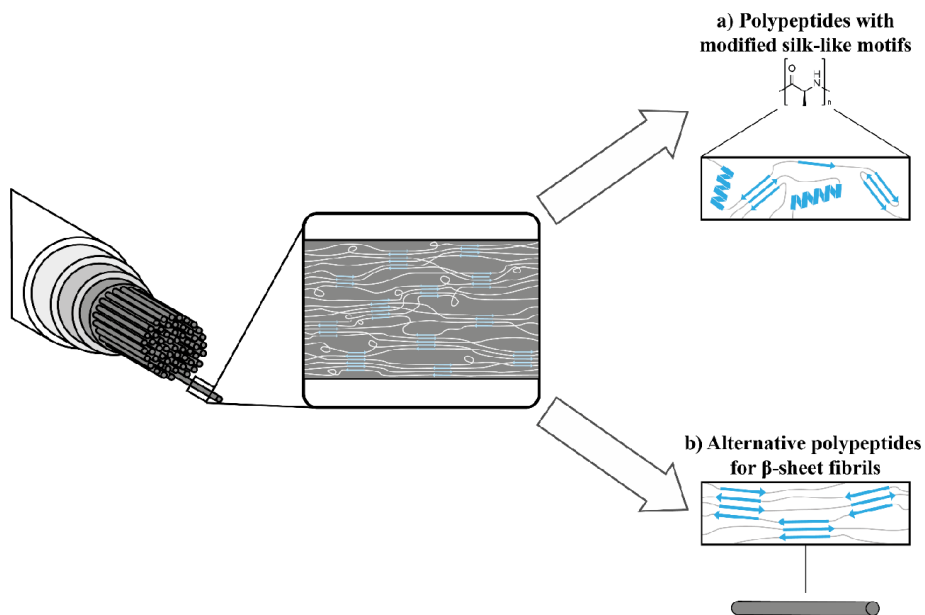


Figure 2: Techniques toward silk-inspired synthetic polymeric materials using a) polypeptides with chemical similarity to  $\beta$ -sheet forming silk motifs, and b) polypeptides with  $\beta$ -sheet fibrillar conformations after processing

The Sogah group established the desired synthetic hybrid silk-mimic structures by catenating preformed building blocks with defined structure and functionality. [80, 81] This strategy – which they have dubbed the Lego method – employs a combination of NCA ROP and anionic polymerization to link macromonomers consisting of soft synthetic polymeric segments such as poly(ethylene glycol) (PEG) already covalently coupled with the crystalline peptide sequence of alanine-glycine-alanine-glycine (Ala-Gly-Ala-Gly).[80, 81] Thus, it was possible to generate a library of protein-inspired polymers in which some segments are replaced with synthetic segments. NCA ROP strategies were particularly useful in such cases as the use of bifunctional polyethylene

glycol (PEG) initiators prevented the need to multiple protection and deprotection steps. This enabled new opportunities to investigate the structure-property correlation, which is necessary to design new targeted bioinspired materials.[80, 81] Their earlier templated approach used the rigid aromatic hairpin turn phenoxathiine as a template for  $\beta$ -sheet formation, even for weak hydrogen acceptors (Figure 3).[82, 83] The second was a non-templated linear approach. The linking with PEG was performed in the same way as the templated approach.[80-83] Due to their linear architecture, the polymer can freely assemble into parallel or anti-parallel  $\beta$ -sheets via inter-or intramolecular interactions.[81]

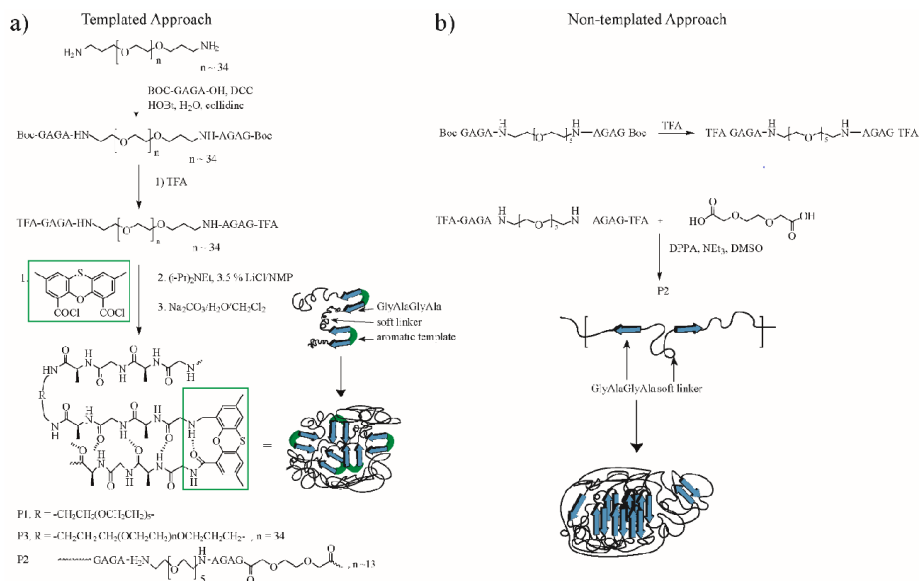


Figure 3: The use of the molecular Lego method by the Sogah group. There are two different approaches presented: a) the templated approach and b) the non-templated approach. [81], Copyright 2001. Adapted with permission from the American Chemical Society.

Such strategies also include studies where NCA ROP has not been utilized to develop the peptidic component, but its utilization provides simpler alternative pathways. One such aspect is the development of simpler methods of utilizing specific peptides with polymerizable end groups, resulting in a polymer with pendant peptides.[84] Ayres *et al.* utilized the  $\beta$ -sheet forming sequence from silkworm silk modified with methacrylate end groups to employ atom-transfer radical polymerization (ATRP). However, the  $\beta$ -sheet forming sequence required a multi-step protocol involving multiple protection and deprotection steps whereas NCA ROP would allow for the single-step synthesis of the desired peptide with a methacrylate-ended initiator. In other cases,

the utilization of the end group amine still present after ROP can provide a versatile group for coupling. Smeenk *et al.*, inspired by the triblock approach of the Sogah group, recombinantly produced polypeptide ((AG)<sub>3</sub>EG)<sub>10</sub> which was coupled *via* maleimide coupling to PEG chains through the use of terminal tag peptides with cysteine.[85] In contrast, the use of a diamine initiator could have yielded the desired polypeptide with highly reactive amine groups which could be either modified themselves or directly coupled to the desired PEG chains. Thus, the potential of producing similar work utilizing NCA ROP as a synthetic strategy provides more versatility which in turn expands the field and provides potential scalability.

#### **4.1. Polypeptides with modified silk-like motifs**

Poly(alanine) is the major  $\beta$ -sheet forming unit in spider silk.[58, 71, 74] Poly(alanine) motifs natively found in silks remain below nine alanine units in length, thus achieving good thermodynamic stability in  $\beta$ -sheet conformations. However, beyond this upper threshold, these blocks favor  $\alpha$ -helical structures.[86] Thus, careful design and manipulation are required to achieve  $\beta$ -sheets in pursuing primary and secondary structure mimicry. In this section, we focus on studies that utilize poly(alanine) in some way, including those which have poly(alanine) blocks interspersed with other residues (somewhat similar to silkworm silk and its GAGAGS motifs), with studies summarized in Appendix B. As mechanical properties are primarily dependent on the system, further clarification of general trends within studies have been stated.

#### 4.1.1. Spacer residues within PLAla blocks

Early studies of alanine and glycine copolymerization investigated the relationship between the amino acid sequence and secondary structure using the simplest possible model.[87] In the late 1960s, Iwakura and coworkers reported the NCA-copolymerization of L-alanine, D-alanine, and glycine in different ratios and combinations in acetonitrile (ACN) or dimethylsulfoxide (DMSO).[88-90] Poly(L-alanine) (PLAla) folded into  $\alpha$ -helical structures, whereas a 1:1 mixture of glycine and L-alanine resulted in  $\beta$ -sheet conformations.[89] The resulting secondary structure was also dependent on the solvent used for polymerization. DMSO led to mainly  $\beta$ -sheet form like polypeptides similar to silk fibroin. The use of ACN resulted in  $\alpha$ -helical form like PLAla.[88, 89]

Studies from Iio *et al.* showed that the incorporation of higher ratios of glycine behaved destructively towards the  $\alpha$ -helix formation of PAla in various organic solvents and water.[87] Conversely, it was found that the stability of an  $\alpha$ -helix was higher in a polymer, in which glycine was at a ratio of 1:2 with alanine than a polymer where the ratio was 1:3 (glycine to alanine). The solubility of these copolymers depends on their molecular weight. Additionally, adding a D, L-glutamic acid (Glu) at the end of each polypeptide block increased the solubility without significant change to the resulting secondary structure. The introduction of charged amino acids like Glu can lead to a steric hindrance and favors the formation of inter- or intramolecular  $\beta$ -sheets.

It is important to note that upon the secondary structure change associated with introducing such residues, the stability and mechanical properties of these materials also change. For example, the Chen group has shown in their PLAla-*r*-poly(L-phenylalanine) (PLPhe)-*b*-PEG-*b*-PLAla-*r*-PLPhe based hydrogels the impact of introducing phenylalanine residues.[91] As LPhe is known to have a high  $\beta$ -sheet propensity, its insertion into PLAla blocks of around 30-40 units resulted in stiffer

self-assembling hydrogels, with a storage moduli increase of 138 Pa up to 579 Pa with an increased LPhe to LAla ratio. Furthermore, the stereoisomerism of residues in the PAla block impacted overall stability. In a PEG-*b*-PAla-*r*-PLPhe hydrogel system (PAla DP ~10, PLPhe ~5), the introduction of D-alanine into blocks with primarily L-alanine led to a reduction in  $\beta$ -sheet structures (with an increase in other ordered structures) and a subsequent drop in mechanical stability with a storage modulus of ~500 Pa dropping to ~0.15 Pa with a racemic mixture. Interestingly, the use of solely D-isomers (i.e., poly(D-alanine) (PDAla)) led to a slight increase in storage modulus (~100 Pa increase).

#### 4.1.2. The impact of hydrophobic blocks outside of PAla chains

Hydrophobic components outside of the main PAla chain inherently affect intermolecular packing of chains either by improving the packing *via* hydrophobic association or disrupting the packing *via* the presence of bulky components.

Intriguingly, the Jeong group introduced a light-sensitive azobenzene unit within their linear polymers, resulting in molecular kinks, which impacted morphology alongside the effects of  $\pi$ - $\pi$  stacking (Figure 4).[92] The N-termini of PEG<sub>22.7</sub>-*b*-PLAla<sub>7.7,9</sub> molecules were coupled together with an azobenzene-based diacyl chloride (azobenzene-4,4'-dicarbonyl dichloride), resulting in PEG<sub>22.7</sub>-*b*-PLAla<sub>7.7,9</sub>-Abz(azobenzene)-*b*-PLAla<sub>7.7,9</sub>-*b*-PEG<sub>22.7</sub>. A drastic decrease in  $\beta$ -sheet formation was observed compared to uncoupled copolymers (58% to below 45%), possibly due to the rigidity of the azobenzene group limiting interactions between L-alanine residues of the same polymer chain. The trans-to-cis configurational change of the central azobenzene group upon exposure to ultraviolet (UV) light (365 nm) was found to influence the  $\pi$ - $\pi$  stacking of the molecules and thus the overall morphology of the hydrogels. In its cis configuration (under UV light), tighter, circular packing of the PLAla blocks resulted, with transmission electron

microscopy (TEM) and dynamic light scattering (DLS) revealing the presence of spherical micellar structures of 60-82 nm in diameter. In its trans configuration (under visible light), the overall linear PLAla segments were found to stack upon each other with a slightly increased  $\beta$ -sheet content (44.1% compared to 40.8% in the cis configuration) with larger micellar structures of 95-147 nm being formed. Interestingly, these micelles remained spherical instead of worm-like nature, which may be expected from the parallel intermolecular stacking.

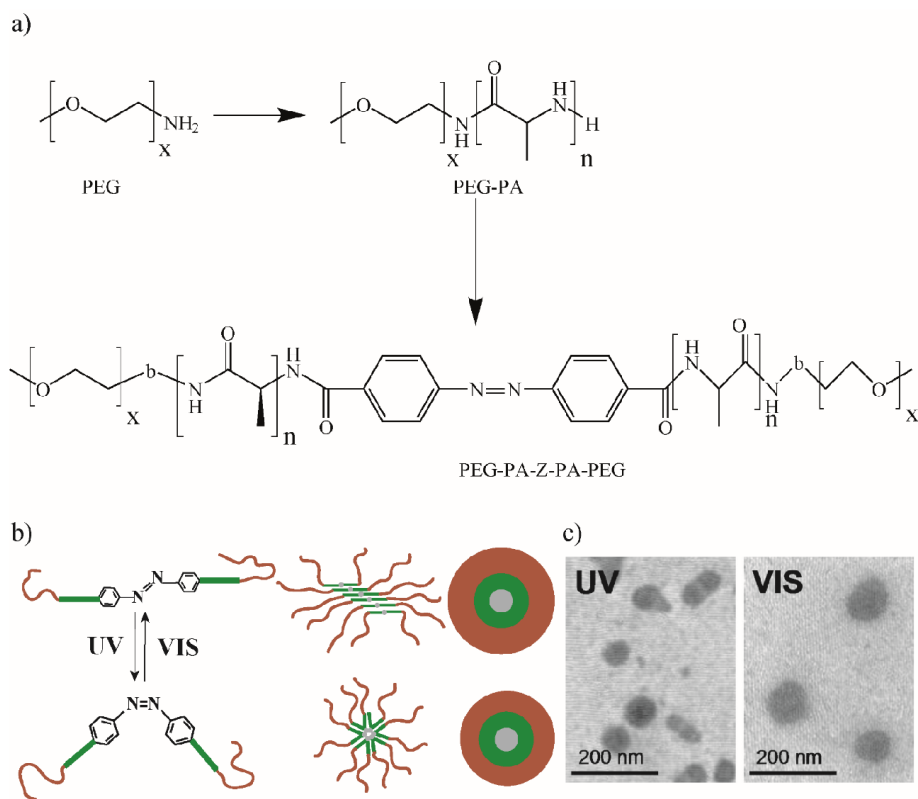


Figure 4: a) Synthetic route of azobenzene-centered copolymer with PLAla blocks. b) Schematic of transformation to cis (under UV) and trans (under visible light) forms. c) TEM of micellar structures in the two conformations. [92], Copyright 2012. Adapted with permission from John Wiley and Sons and Copyright Clearance Center, license number: 5067640310938.

#### 4.1.3. The impact of ionic components outside of PAla chains

Ionic bonding and repulsion profoundly affect the secondary structures and dominate the resulting secondary structures. This impact can be most easily observed in the poly(L-lysine) (PLLys)<sub>0.8-b-</sub>



PLA<sub>4.5</sub>-*b*-polaxmer (PLX)-*b*-PLA<sub>4.5</sub>-*b*-PLL<sub>ys0.8</sub> hydrogels synthesized by the Chu group.[93] The introduction of cationic L-lysine units prevented  $\beta$ -sheet formation *via* the short PLA blocks despite being introduced at a minimal concentration (*i.e.*, less than one-fifth of the amount of L-alanine). Upon heating from 20 to 60 °C,  $\alpha$ -helical and  $\beta$ -sheet content decreased and increased respectively ( $\alpha$ -helices: 60-58%;  $\beta$ -sheets: 2-4%), which was enough of a change to thermally induce gelation from an initial micellar formation, though these hydrogels remained relatively soft with a storage modulus of  $\sim$ 200 Pa. Conversely, ionic bonding can be amplified using polyionic complexation – using mixtures of polyanionic and polycationic polymers to induce  $\beta$ -sheet formation – as demonstrated by the Deming group, through the use of multiblock copolypeptides.[94] In their work,  $\beta$ -sheet formation was dominated by the number of polyionic blocks (*i.e.*, PLL<sub>ys</sub> and poly(L-glutamic acid) (PLGlu)) instead of the poly(sulfoxide methanoinine) (POLM)-*co*-PLA blocks, reconfirming the dominance of ionic effects on such polypeptides. This led to a subsequent increase in storage moduli upon an increase from a diblock ( $\sim$ 40 Pa at 10 wt%) to a pentablock polypeptide ( $\sim$ 3000 Pa at 10 wt%). As such, it can be concluded that ionic components tend to dominate the secondary structure formation of these polypeptides, with the role of PLA in such polypeptides not significantly extending into morphology.

#### 4.1.4 Non-linear precursors

Asides from linear architectures, other molecular architectures have been employed with PA blocks branching from a core or backbone, resulting in increased proximity between PA blocks. Murphy *et al.* studied a series of hydrogels based on 8-arm stars with polypeptide arms terminated with hydrophobic, 5-unit homopolypeptide blocks, one of which was a PLA<sub>5</sub> block.[95] Interestingly, despite the natural proclivity for PLA<sub>5</sub> blocks to form  $\beta$ -sheets, 8-poly(carboxybenzyl-L-lysine) (PZLL)<sub>40</sub>-PLA<sub>5</sub> formed random coils identified by Fourier

transform infrared spectroscopy (FTIR) and circular dichroism (CD) spectra, unable to gelate. Thornton *et al.* investigated their star-based system with a far more significant presence of  $\alpha$ -helices and  $\beta$ -sheets.[96] Using a 4-arm PEG<sub>56.8</sub> initiator, PLAla arms were polymerized with lengths ranging from DP 4-100. In contrast, Murphy *et al.* reported that their 4-PEG<sub>56.8</sub>-*b*-PLAla<sub>5</sub> and 4-PEG<sub>56.8</sub>-*b*-PLAla<sub>10</sub> stars were both found to gelate and exhibit significant  $\alpha$ -helical structures, with the latter also possessing significant  $\beta$ -sheet content. This also contrasts against the expected primarily  $\beta$ -sheet conformations expected at low molecular weight PLAla. The explanation for the drastically observed difference in secondary structure is unclear but may be related to the relative bulkiness of side chains. While the PEG units of the 4-PEG<sub>56.8</sub>-*b*-PLAla stars have no side chains, the bulk aromatic side chains of the PZLL blocks of the 8-PZLL<sub>40</sub>-PLAla<sub>5</sub> likely hindered the interactions between neighboring arms. Furthermore, it should be noted that critical gelation and, presumably, mechanical stability increased upon increasing the PLAla length beyond five units.

Like stars, graft polymers potentially offer increased packing of neighboring PLAla blocks resulting in increased  $\alpha$ -helical formation. Jeong and coworkers developed graft polymers by first synthesizing polypeptide-based arms and grafting them to a chitosan backbone.[97] On their own, the PLAla<sub>9.9</sub>-*b*-PEG<sub>45</sub> copolymers would be expected to form  $\beta$ -sheets primarily. However, upon carbodiimide coupling *via* the N-terminus of the PLAla block to the dicarboxylic acid linker to couple to the amine of chitosan units, the subsequent graft polymer was found to possess a significant mix of both  $\alpha$ -helical and  $\beta$ -sheet structures as shown by FTIR. Interestingly, the pH-sensitive behavior of the chitosan-containing hydrogel was not only altered upon the introduction of PLAla-*b*-PEG branches but outright reversed. As chitosan contains side chain amines (not coupled to by PLAla-*b*-PEG), their expected ionization under acidic conditions would usually

result in electrostatic repulsion and thus softer hydrogels – a feature observed in other amine-based hydrogels.[98] However, storage moduli were instead found to increase with a decreasing pH (at 6 wt%, 43 Pa at pH 9.0 to 396 Pa at pH 3.0). This could partially be attributed to the slightly greater  $\alpha$ -helical content at acidic pH. A shift in the ethylene oxide group of the carbon-13 nuclear magnetic resonance ( $^{13}\text{C}$ -NMR) spectra from 72.4 ppm at pH 6.5 to 72.1 ppm at pH 3.0, as well as the broadening of the peak, suggest increased hydrogen bonding between the PEG and chitosan and restricted molecular motion which would further increase gelation.

#### **4.2. Alternative polypeptides for $\beta$ -sheet fibrils**

As motif-based design does not exclusively render  $\beta$ -sheet conformations, the mimicry of silk-like structures without silk-like motifs provides an interesting alternative. Silk nanofibrils are similar but not identical to  $\beta$ -sheet-dominated amyloid fibrils at molecular and nanostructural levels.[99-102] Further to this, all amino acid sequences show some level of propensity towards  $\beta$ -sheet formation, though may be sterically hindered by side chains, and thus can be forced into this conformation.[103, 104] As a result, much research has gone into investigating  $\beta$ -sheet-rich fibril structures for their individually strong nature, manipulation, and the subsequent impact on materials on a larger scale.[48, 105, 106] While these structures are not entirely congruent to those observed in silks, the pursuit of  $\beta$ -sheet fibrillar nanostructures is more easily attainable and thus presents more opportunities for investigation. Naturally, these structures tend to be larger than their silk-based counterparts, but with less stringent design criterion in relation to molecular weight, there is potentially more flexibility in tuning such materials to achieve specific properties. Specifically, this manifests in different  $\beta$ -strand spacings with the associated cross- $\beta$  structures possessing interstrand spacings of 4.6 – 4.7 Å compared to the spacing of around 4.4 Å in spider silks due to glycine-rich components and the small side chains of this residue. Beyond this different

spacing, however, the way in which such fibrillar structures manifest is largely based on the residue used and the strategies which have been employed to control their packing structure. This section seeks to observe how  $\beta$ -sheet fibrils have been produced, their conformations in relation to the residues used and subsequent implementation into different materials, with works summarized in Appendix C.

While this section is not focused on gel formation, the vast majority of the papers published on  $\beta$ -sheet fibrils focus on gelation. The self-assembly of  $\beta$ -sheet fibrils is primarily based on the system (e.g., spontaneous self-assembly, temperature-driven) instead of a singular universal environmental trigger. As the concentration of  $\beta$ -sheet-forming peptides are increased, the fibrils continue to increase in length before physical entanglement ensues.

#### 4.2.1. $\beta$ -Sheet Fibrils Formed through Canonical Amino Acids

Branched side chains on the  $\beta$ -carbon and aromatics have an affinity toward  $\beta$ -sheet formation, though this often manifests in uncontrolled aggregation,[107] often complicating the formation of specific nanostructures, with even micellar  $\beta$ -sheets potentially forming instead of an expected fibrillar state.[108] Amino acids which satisfy this prerequisite include isoleucine,[109] tyrosine,[110] phenylalanine, and threonine.

The hydrophobicity afforded by the formation of  $\beta$ -sheet structures and the large aromatic groups of poly(L-phenylalanine) (PLPhe) side chains makes them challenging to handle. The net result is far larger intersheet spacings than would usually be expected, as Puiggali and coworkers reported when using poly(L-lactic acid) (PLLA)-PLPhe.[111, 112] Here, PPhe and PLLA blocks varied significantly concerning length and ratio, with FTIR providing evidence of high  $\beta$ -sheet content. [111, 112] Throughout both works, PPhe and PLLA blocks varied significantly concerning length and ratio, with FTIR providing evidence of high  $\beta$ -sheet content. X-ray diffraction (XRD) spectra revealed the typical  $\beta$ -strand spacing of 4.7 Å typically associated with  $\beta$ -sheet crystals. Intriguingly, a reflection at 1.186 nm was also observed for all PLPhe lengths which is greater than

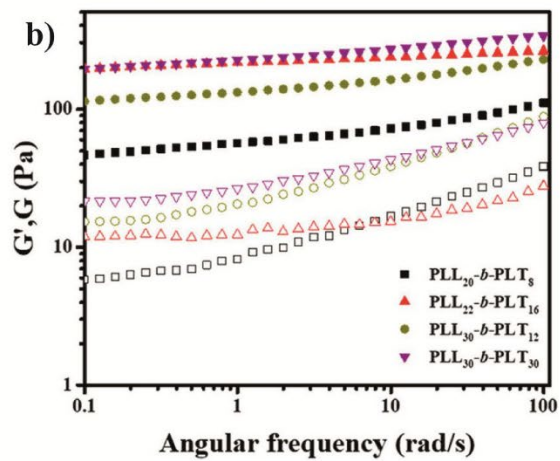
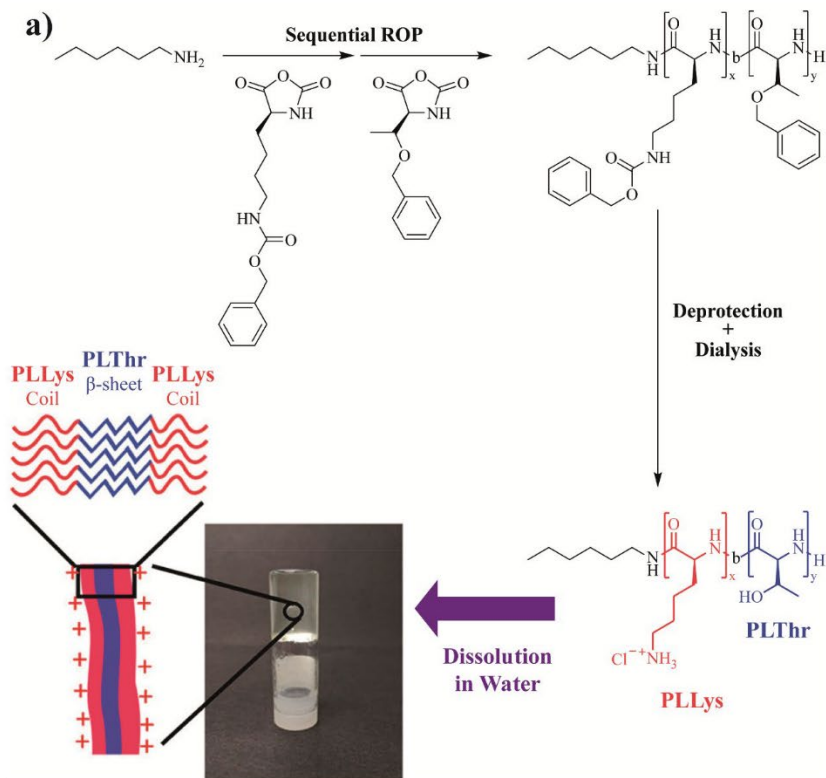
typical cross- $\beta$  structures assignment of interplanar spacing but can be attributed to the bulky aromatic rings causing this significant lamellar packing distance.

In direct contrast to the high hydrophobicity of PLPhe blocks, L-threonine blocks (PLThr) are the only polar block with high  $\beta$ -sheet forming potential under benign conditions. Extensive publications by the Jan group reported using the coil-sheet forming poly(L-lysine) (PLLys)-PLThr to form a range of different  $\beta$ -sheet fibril-based assemblies (nanosheet/ribbons, hydrogel particles known as nanogels, hydrogels[113]). In all cases, copolyptide formation was achieved using sequential NCA ROP. The impact of the  $\beta$ -sheet formation on these assemblies can be partially reflected in the hydrogels, where a series of copolymers with a PLLys length of  $\sim$ 20 DP and increasing PLThr sizes (DPs of 8, 16, and 41) correlated to an increase in  $\beta$ -sheet content determined by CD (45.3%, 46.6%, 54.8%).[113] The presence of the cationic PLLys block was still required, as PLThr<sub>20</sub> was unable to form a gel at concentrations below 10 wt% despite attaining the highest  $\beta$ -sheet content (80.2%), though whether this was due to uncontrolled aggregation was unconfirmed. It was surmised that the charge-repulsion afforded by the PLLys blocks assisted with packing the PLThr blocks to achieve fibrillar formations. Investigation of small-angle X-ray scattering (SAXS) spectra revealed largely one-dimensional fibril assemblies with the XRD spectra revealing the typical  $d$  spacing of 4.6 Å associated with antiparallel  $\beta$ -sheets.[114]

The inherently polar nature of threonine results in an increased chain length requirement to observe comparable mechanical properties to peptidic blocks with non-polar side chains. Despite having similar  $\beta$ -sheet propensities to other  $\beta$ -branched and aromatic amino acids,[107] they are also less hydrophobic.[115-118] Due to the results of microphase separation of hydrophobic domains increasing crosslinking and thereby mechanical properties,[119, 120] this reduced hydrophobicity

means that longer PLThr blocks are required resulting in an increased  $\beta$ -sheet content, increased hydrophobic microdomain density and subsequently increased mechanical properties. This impact can be seen from a mechanical standpoint in the Jan group's PLLys-PLThr system, where increasing PLThr resulted in increased  $\beta$ -sheet content and thus storage moduli in two separate cases (Figure 5).[113] At 5 wt% concentration, storage moduli increased from  $\sim 45$  Pa for PLLys<sub>20</sub>-*b*-PLThr<sub>8</sub> to  $\sim 200$  Pa for PLLys<sub>22</sub>-*b*-PLThr<sub>16</sub>; and from  $\sim 100$  Pa for PLLys<sub>30</sub>-*b*-PLThr<sub>12</sub> to  $\sim 200$  Pa for PLLys<sub>30</sub>-*b*-PLThr<sub>30</sub> (Figure 5b). In contrast, the PEG<sub>45.4</sub>-poly(L-tyrosine) (PLTyr) of the Heise group only required a peptide length of 6 units to achieve similar mechanical properties, though higher temperatures were required ( $\sim 200$  Pa at 2 wt%, 60 °C).[110]

While other hydrophobic residues also share a propensity towards  $\beta$ -sheet conformations, they simultaneously show a high propensity towards  $\alpha$ -helix formation.[107] Thus, ingenious design strategies have been employed to force the tight packing required for preferential  $\beta$ -sheet formation.



36



Figure 5: a) Schematic of PLThr-PLLys block polypeptide synthesis and hydrogelation. After deprotection and subsequent dispersion in water, the repulsion forces of the PLLys help to force the PLThr blocks into the desired  $\beta$ -sheet nanoribbon conformation. b) Storage modulus of hydrogels with differing block lengths at 5.0 wt%. [113], Copyright 2018. Adapted with permission from the American Chemical Society.

Poly(L-leucine) (PLLeu) blocks follow a length-dependent secondary structure formation similar to PLAla,[121] though  $\beta$ -sheet fibrils have been much less extensively explored. Generally, PLLeu blocks with DPs less than 10 primarily favor  $\beta$ -sheet conformation with increasing block length, leading to a slow evolution from  $\beta$ -sheet to  $\alpha$ -helix.[121, 122] The Deming group has performed extensive research on the use of PLLeu in diblock copolypeptides, but primarily as  $\alpha$ -helical fibril formers.[122-125] As such, similar to PLAla, the use of non-peptidic components which may influence packing are used to modify secondary structure conformation. Higuschi *et al.* reported the design of poly(allylamine) with PLLeu grafted from the backbone. [126] Notably, the graft polymers were designed to have only 55% of allylamine group functionalized with PLLeu of DP 15, resulting in a backbone with pendant amine groups and thus in pH dependent morphology. With increased acidity and thus increased cationic charge of pendant amine groups, repulsive forces force a shift towards  $\beta$ -sheet formation in a similar fashion to the aforementioned effect of charge on PLAla chains. Furthermore, the alignment of such structures caused a transition from globular to fibrillar conformations which over a large time scale (18 days) would organize into sheet and eventually plate structures.

The influence of charge extends to charged amino acids which are susceptible to salt- and pH-dependent changes, which, in turn, affect their secondary structure. Typically, their charged state results in random coils due to the electrostatic repulsion preventing hydrogen bonding between

peptide backbones. However, these repulsive forces can be rendered moot and thus strengthen their packing by either increasing the ionic strength of the solution [127] or reverting the residues to their uncharged states and thus increasing their hydrophobicity.

While not specifically an NCA ROP-based paper, the insights afforded by Dzwolak and coworkers into the conditions under which PLGlu and poly(D-glutamic acid) (PDGlu) form  $\beta$ -sheet fibrils provides a useful insight into design (Figure 6).[128] Acidification to pH  $\sim$ 4.1 and heating to temperatures above 65 °C resulted in the slow evolution of  $\beta$ -sheets from  $\alpha$ -helical conformations after at least a 44 h incubation period. Stereoisomerism is an essential factor in structure formation as with other polypeptide blocks, with pure solutions of PLGA and PDGA of various molecular weights (15 – 50 kDa  $\sim$  116 – 388 DP, center at DP 200) resulting in large, twisted bunches approximately 200 nm thick, with individual fibrils of 5 – 10 nm in width after incubation. Interestingly, scanning electron microscopy (SEM) uncovered the chirality-dependent twisting nature of these bundles, with PLGA and PDGA exhibiting left-handed and right-handed spirals, respectively. Equimolar mixtures of these polypeptides exhibited a slower transition to  $\beta$ -sheet fibrils (evolution still occurring up to 99 h), with a lack of consistent twisting nature. A DP of 4 was found to be the critical length required for fibrillar aggregation of PLGlu, though the fibrillar bunches did not readily form until DP 10.[129]

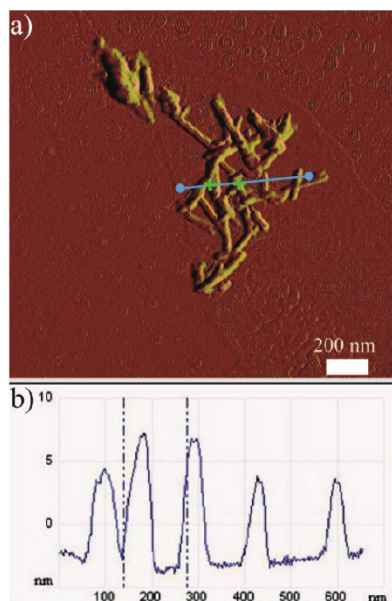


Figure 6: Atomic force microscopy (AFM) images of PLGlu at acidic conditions at pH 4.5. a) Topography image of PLGlu nanofibers. b) Cross-section height profiles of PLGlu nanofibers following the blue line in the topographical map. Green crosses on the blue line correlate to the position of the dotted lines on the height profile.[128], Copyright 2010. Adapted with permission from the American Chemical Society.

#### 4.2.2. $\beta$ -Sheet Fibrils Formed Through Side Chain Modified Amino Acids

As stated before, protecting groups are often required with functional residues while using NCA ROP, though the altered intermolecular interactions results in  $\beta$ -sheet fibrils. Aromatic protecting groups are amongst the most investigated sidechain protecting groups. While they share the same

ability to form  $\pi$ - $\pi$  stacking bonds as their canonical counterparts, this does not translate to similar  $\beta$ -sheet forming propensities, with longer chains resulting in  $\alpha$ -helical conformations.[130]

Poly(benzyl-L-glutamate) (PBLG) stands out as a popular amino acid for fundamental studies. Though often used for its  $\alpha$ -helical propensity, PBLG also experiences length dependent secondary structure though this cutoff is less than canonical amino acids with similar length dependence, with blocks with a DP less than 18 yielding  $\beta$ -sheets.[130] As with these residues though, non-peptidic components can influence this packing. Rodríguez-Hernández and coworkers interestingly worked on PBLG-polydimethylsiloxane (PDMS)-PBLG triblock polymers to observe the nanostructures that would form (Figure 7).[131, 132] With increasing peptide length came the expected evolution of  $\alpha$ -helical structures, with PBLG<sub>5</sub> maintaining primarily  $\beta$ -sheet structures (Figure 10b) and with PBLG<sub>10</sub> attaining a more even mix of the two structures. Atomic force microscopy (AFM) revealed fibrillar morphologies up to 23 units in length, with a fibril thickness of 9 nm for DP 10 (Figure 10c). It was surmised that PDMS formed coils while the flanking peptides would form the  $\beta$ -sheet structures in the low DP range. It can be extrapolated that non-peptidic components with stronger intermolecular influences such as the aforementioned charged backbones of PLLeu graft polymers could see a similar influence with PBLG.

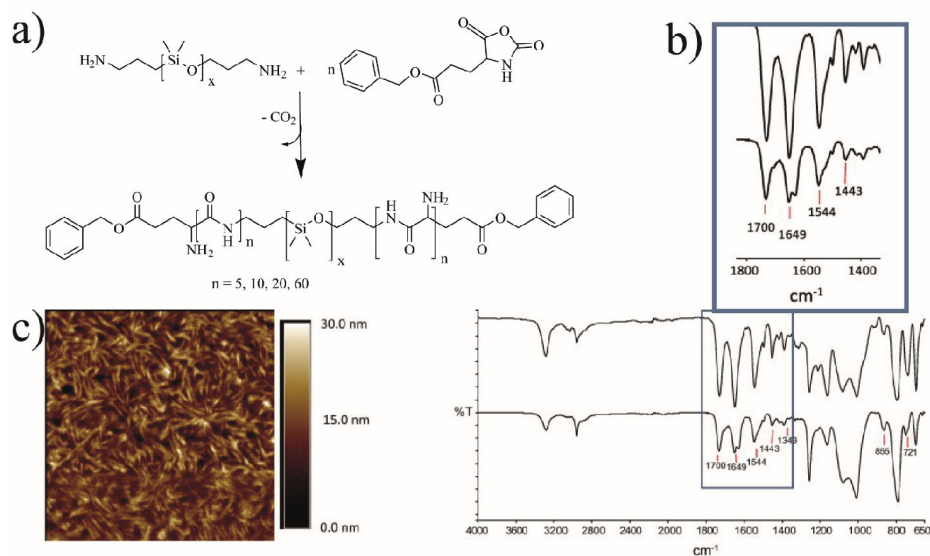


Figure 7: a) Synthetic route of PBLG-b-PDMS-b-PBLG copolyptide via bifunctional PDMS. b) FTIR of PBLG<sub>60</sub>-b-PDMS-b-PBLG<sub>60</sub> (top) and PBLG<sub>5</sub>-b-PDMS-b-PBLG<sub>5</sub> (bottom). c) AFM images of PBLG<sub>10</sub>-b-PDMS-b-PBLG<sub>10</sub>. [131, 132], Copyright 2007 & 2010. Adapted with permission from Elsevier and Copyright Clearance Center.

Oligo(ethylene glycol)-functionalized L-glutamate blocks (PEGLG) are particularly interesting concerning their thermoresponsive secondary structure conformation. Much like poly(alanine), PEGLG tends to favor  $\alpha$ -helical conformations. However, the Li group revealed through NMR spectroscopy that reversible dehydration of the ethylene glycol side chains of the PEG<sub>45</sub>-PEGLG<sub>43</sub> copolymers through temperature increase resulted in increased hydrophobicity and subsequent  $\beta$ -sheet conformations as confirmed by FTIR.[133] TEM imaging revealed ribbon-like structures with a width of 60-80 nm in solutions at 80 °C – far larger than the fibrils reported using other residues. It was proposed that copolymers would first form wormlike micelles with  $\alpha$ -helices

associating to form cylindrical cores upon elevated temperatures. Further heating would result in the aforementioned  $\beta$ -sheet formation *via* intermolecular hydrogen bonding, resulting in nanoribbon packing.

The Li group further reported PEGLG in numerous fibrillar  $\beta$ -sheet organo- and hydrogel studies. A series of PEG-PEGLG diblock copolymers with shorter PEGLG blocks would spontaneously gelate when dispersed into water.[134] Larger PEGLG blocks were found to form gels at lower concentrations, with PEG<sub>44</sub>-PEGLG<sub>28</sub> and PEG<sub>44</sub>-PEGLG<sub>15</sub> due to an increase in  $\beta$ -sheet content. TEM and AFM imaging both presented significantly thinner fibrils with widths and heights of  $\sim$ 7-9 nm and  $\sim$ 1.0-1.5 nm, respectively, which may contribute to a continuous fibrillar network formation. Star polypeptides in a later work were found to produce gels with a far greater degree of mechanical tunability with storage moduli ranging between 24-3350 Pa solely via adjustment of arm length (DP 15-50) and number (8 and 32).[135] However, the fibrillar hydrogels were only observed with the 8-arm copolypeptides.

$\beta$ -sheet fibril organogels formed from poly(D,L-allylglycine) (PADLG) assembly have been reported by the Wooley group.[136] Copolymers were synthesized using mono- and bi-functional PEG-based initiators to polymerize 12-residue long PADLG blocks. Using racemic blocks instead of a single consistent stereoisomer contradicts the usual strategy of triggering secondary structure formation. Nonetheless, gelation occurred after dissolution in polar solvents such as dimethylformamide (DMF), DMSO, and methanol (MeOH), with the sol-gel transition, found to reverse upon sonication. Attenuated total reflection Fourier transform infrared spectroscopy (ATR-FTIR) spectroscopy of dried diblock gels confirmed the role of secondary structure in gelation with primarily parallel  $\beta$ -sheet formation as well as significant antiparallel  $\beta$ -sheets.[136]

Of note is the increased CGC (and hence, lower hydrogel stability) with increasing solvent polarity (where DMF has the lowest polarity and methanol has the highest) due to increased ease of dissolution. TEM and AFM imaging both revealed the fibrillar conformation of these structures, and AFM imaging of spin-coated mica samples showed exposed ribbon-like morphologies with heights and widths of  $\sim 2.5$  and  $\sim 18$  nm, respectively. Physically, these ribbon structures stacked similarly to monolayers, with hydrophilic tails flanking the hydrophobic core of the ribbons leading to  $\beta$ -sheet fibrillar structures, resulting in a stiff organogel in DMF (storage modulus of 15.2 kPa, compressive Young's modulus of 25.1 kPa).

## **5. Material Morphology and Fabrication Strategies towards silk-like polymer synthesis**

A natural progression from mimicking silk polypeptides at a chemical level is to process them into materials for practical applications. A common theme with all fabrication methods is the reliance on a high amount intermolecular bonds between molecules thus requiring high molecular weight polymers. Furthermore, the use of protected and modified residues is available using NCA ROP as stated before, resulting in potential strategies which have cannot be emulated with other synthetic polypeptide techniques. Most of the reports utilizing NCA ROP result in the formation of gels as the final product. This is likely due to the minimal design constraints associated with homopolypeptides, block copolypeptides or random copolypeptides spontaneously forming the desired secondary structures and form the physical crosslinks necessary for gel formation in solution after the reaction. In some studies, further processing was performed to develop either films or fibers. Although this subset of studies is relatively small, many material morphologies for a vast suite of applications have been highlighted.

### 5.1. Fiber Processing

Fiber processing is most successful through the utilization of long chain polymer precursors with a high density of intermolecular bonds, thus altering the approach available by NCA ROP polypeptides. Utilization multiblock polymer-polypeptide hybrids as previously described is limited, thus step-growth polymerization *via* the end-to-end coupling of the hybrids as a prepolymer, allowing for the synthesis of high molecular weight polymers for spinning. Alternatively, the polypeptide itself can be designed to be high molecular weight using a base as an initiator, though this results in a less controlled reaction. Either of these strategies has been shown to yield NCA ROP polypeptides suitable for fiber formation

The control of the molecular weight of peptidic components becomes an issue specifically related to NCA ROP. Based on the relationship between the size of some homopeptidic blocks and protein folding, the use of materials with minor molecular weight changes may yield significant changes in physical or chemical properties. Sogah and coworkers fabricated fibers from their PLAla<sub>4-6</sub>-b-PEG<sub>5</sub>-b-PLAla<sub>4-6</sub> triblocks *via* wet spinning using the previously mentioned Lego method, developing fibers with PLAla blocks of DP 4 and 6 separately.[80] Integration across the radial axes found *d* spacings of 4.45 and 5.36 Å in both cases which are consistent with the spacing between β-sheets formed from PLAla. Alignment of such structures was found to be more pronounced with PLAla blocks of DP 6. The net result was a comparatively more brittle but stronger fiber with the increase in Young's modulus and strength corresponding to an increase in β-sheet content ( $410 \pm 35$  to  $750 \pm 156$  and  $13.0 \pm 1.4$  to  $14.2 \pm 2.7$ , respectively), as well as the corresponding drop in elongation at break ( $22.9 \pm 13.6\%$  to  $5.4 \pm 1.7\%$ ). Thus, even with a minor change in number of repeat units, assembly and consequential physical properties are already greatly affected.



## 5.2. Film Casting and Surface Modification

Generally, the aforementioned molecular weight issues mentioned in fibers apply to films, with similar strategies employed. The Korley group reported the various factors which can contribute to the mechanical properties of polymer films. In all cases, similar polymers were synthesized – ABA triblock copolymers with a PDMS central block and peptidic flanking blocks (PZLL, Poly( $\beta$ -benzyl-L-aspartate) (PBLA) or PBLG) synthesized as prepolymers and then linked using a di- or tri-functional isocyanate molecule. The utilization of aromatic-based protecting groups resulted in highly controllable secondary structure content by modification of the chain length. Johnson *et al.* investigated this system using a diisocyanate linker to compare different peptidic blocks (specifically PBLA and PZLL with different lengths) (Figure 8).[137] Using PBLA<sub>5</sub> as the peptide sequence (predominantly  $\beta$ -sheet forming) and casting from a mixture with 5 wt% peptides resulted in a tensile modulus, strength and strain-at-break of 14.5 MPa, 2.5 MPa and 669.5 %, respectively. However, PBLA<sub>20</sub> instead, which has 13%  $\alpha$ -helical content, resulted in a drop in all these qualities (modulus of 9.26 MPa, strength of 0.8 MPa, strain-at-break of 217.2%). Increased peptide wt% increased the  $\alpha$ -helical content of the PBLA<sub>20</sub> films, but this increase in peptide concentration made films from both lengths of peptide more brittle with a strain-at-break reaching as low as 123.7% (PBLA<sub>20</sub> at 20 wt%). This extraordinary mechanical potential brought upon by  $\beta$ -sheet inclusion was not necessarily reflected once PZLL was introduced as the peptide unit, as the  $\alpha$ -helical forming counterparts (PZLL<sub>20</sub>) tended to outperform all the other combinations (at 5 wt%: modulus of 8.7 MPa, the strength of 5.2 MPa, strain-at-break of 821.9%). This inferiority can also be attributed to a lack of a truly fibrous  $\beta$ -sheet network compared to the use of PBLA.

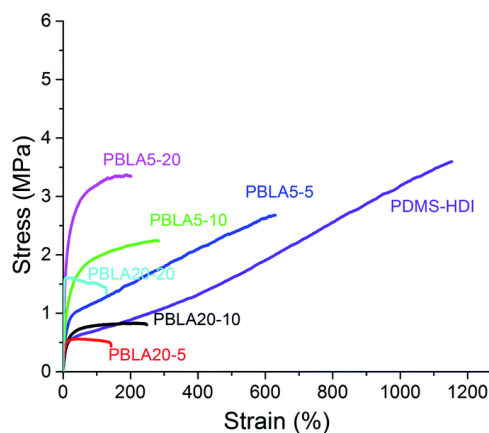


Figure 8: Tensile properties of PDMS-PBLA (polydimethylsiloxane-poly-L-benzyl aspartate) cast films. All polymers are notated as PBLA X-Y, where X refers to the chain length of the PBLA block, and Y refers to the weight percentage concentration of peptide in the film. PDMS- (hexamethylene diisocyanate) HDI refers to films cast from polymers with no PBLA content. Films formed from short-chain PBLAs, which formed  $\beta$ -sheets generally possessing greater tensile strength and extension at break than their PBLA<sub>20</sub> counterparts (with a lower  $\beta$ -sheet content). [137], Copyright 2014. Reproduced with permission from The Royal Society of Chemistry.

A technique exclusively available to film formation is the development of covalently crosslinked networks during solvent evaporation. Using PBLAs as the peptide sequence with the same system as devised by the Korley group, Matolyak *et al.* investigated the impact of using a di- or tri-functional isocyanate molecule.[138] Breakdown of the antiparallel and parallel  $\beta$ -sheet content within the films revealed in ATR-FTIR spectra (1620 – 1635  $\text{cm}^{-1}$  for antiparallel  $\beta$ -sheets, and 1635  $\text{cm}^{-1}$  – 1645  $\text{cm}^{-1}$  for parallel  $\beta$ -sheets) showed 100% parallel conformations when using the tri-isocyanate linker, while only 22-47% antiparallel  $\beta$ -sheet content was observed when using the

di-isocyanate linker. Typically, antiparallel  $\beta$ -sheet structures are more favored due to their higher stability. However, the reduced chain mobility offered by the tri-isocyanate linker forced parallel- $\beta$ -sheet formation instead and a reduction in fiber-like nanostructures (as confirmed by AFM).

Asides from conventional film synthesis techniques, the implementation of a polymerization-based synthetic method allows the unique use of grafting methods for polypeptide surface modification.[139] For surface initiated NCA ROP, surfaces need to be aminated such that nucleophilic end groups are available. Whitesell *et al.* investigated the use of an amine initiator with thiol groups for coupling to gold through thiolate-gold coupling.[140] In their work to develop helical structures from PLAla, they specifically spaced initiating molecules at distances larger than the helix diameter (9 Å), however it is possible that initiating sites closer together would cause spatial restriction, resulting in a  $\beta$ -sheet rich surface. Alternatively, polymerization of polypeptide macromonomers provides another avenue towards polypeptide surface modification. Electrochemical polymerization was employed by Yagci and coworkers to achieve this, driving the deposition of PLAla chains to the electrode surface, which was then functionalized at the surface for biosensing applications.[141, 142] Amino-functionalized thiophene was used to polymerize PLAla chains using NCA ROP.[141] A significant FTIR absorption peak at 1624  $\text{cm}^{-1}$  indicates  $\beta$ -sheet formation, supporting the theory that spatial constriction of such polypeptides can assist with increasing  $\beta$ -sheet content.[141, 142] To achieve similar structures using other synthetic polypeptide techniques, end group coupling to the surface is required which ultimately does not assure the spatial restriction that may be desired.

### 5.3. Polypeptide Based Gels

Hydrogels have been extensively researched for their relative ease of fabrication compared to other architectures. In most cases, the critical gelation condition is reached when polypeptides undergo intermolecular secondary structure conformations, resulting in the physical crosslinks necessary for gelation. A wide range of environmental conditions can trigger this secondary structure formation. This breadth can further be modified using of synthetic components including end groups or synthetic polymer which can be used as a (macro)initiator. Such components then modify the environmental sensitivity of the peptide component such as PEG which undergoes a dehydration effect upon heating, resulting in hydrophobic interactions causing tightened packing.[143] Most relevantly, increasing temperatures from chilled (*e.g.* 4 °C) to physiological (37 °C ) result in increased ordered structures for PLAla blocks, as shown by the Jeong group's PEG-PLAla system exhibited an increase in storage moduli from ~0.1 Pa to ~900 Pa.[144]

The Jeong group has further extensively studied the gelation properties of PAla blocks when used in copolymers with synthetic blocks. With the implementation of DL-alanine along with L-alanine NCA monomers, they were able to tune the ratio between stereoisomers without completely sacrificing the formation of secondary structures.[145-147] In one of these works, PAla-PLX-PAla triblock with different amounts of L- and D- stereoisomers were introduced to achieve this secondary structure control.[148] As the hydrogels were designed for biological studies, a thermal gelation temperature of 37 °C was targeted in a 10 wt% aqueous solution, but this required increasing the peptide chain length with an increase in the mixture of DL-alanine along with L-alanine. With only the L-stereoisomer, this gelation temperature could be achieved with a DP of approximately 5.2 (370 Da). With 40 mol% of racemic alanine NCA, this increases to a DP of 6.5 (460 Da) and jumps to 12.4 (880 Da) with 100% racemic alanine to achieve the desired

conformation. Secondary structure analysis revealed that the PLAla-based hydrogels had an  $\alpha$ -helical and  $\beta$ -sheet content of 27% and 43%, respectively, but with 40 mol% being racemic,  $\alpha$ -helical, and  $\beta$ -sheet content were found to change insignificantly (29% and 38%, respectively). However, the use of entirely racemic blocks yielded a significant rise in random coils (66%), and instead of the usual increase in  $\alpha$ -helical content associated with an increase in block length, a drop in both  $\alpha$ -helical and  $\beta$ -sheet content instead was observed (13% and 18% respectively). Interestingly, this had minimal effect mechanically as all hydrogels investigated held a storage modulus of 1600 Pa.

As expected, the presence of different blocks or functional end-groups can significantly impact secondary structure formation and the subsequent morphology of specific systems. The Li group's work into PEGLG-based gels extended into fabricating nanoribbons focused on  $\beta$ -sheet organogels and hydrogels based on alkyl initiators, which completely changed the packing of the polymers. During the formation of hydrogels, hexyl-, dodecyl- and hexadecyl-PEGLG<sub>11</sub> were all found to maintain a CGC of 2 wt%.[149] However, CD and FTIR spectroscopy showed their secondary structure content changed significantly, with CD showing changes in  $\alpha$ -helical and  $\beta$ -sheet content from 66% to 7% and 4 to 39%, respectively, with increasing alkyl chain size. TEM imaging still indicated nanoribbons within the fibrillar network, with widths in the range of 9-11 nm and heights of ~1 nm (found using AFM).

Organogels have been shown to form upon gelation of particular polypeptides in organic solvents. These are generally less popular, as their biological applications are severely restricted, but they are an important field of study for non-biological applications. Apart from the hydrogels mentioned above, the Li group has also observed the gelation characteristics of alkyl-terminated

PEGLG-based organogels with the polar aprotic solvent tetrahydrofuran (THF) as the medium.[150] The effect of increasing alkyl chain size was far more pronounced in this solvent with hexyl-, dodecyl- and hexadecyl-PEGLG<sub>7-8</sub> showing a steady decrease in CGC with increasing alkyl chain length (CGC is 5.0, 4.0 and 2.0 w/v% respectively). Interestingly, FTIR spectroscopy showed the converse trend in secondary structure content with  $\alpha$ -helical and  $\beta$ -sheet content from 19% to 26% and 60 to 36% with increasing alkyl chain size despite a similar mechanism to nanoribbon formation being proposed.

## 6. Applications

### 6.1. Drug/Payload Delivery

The method of drug delivery primarily depends on the morphology of the material, thus the greater sequence and subsequent morphological control of block copolymers/copolyptides is favored over their random counterparts. Interestingly, majority groups utilizing NCA ROP-based silk analogues have reported the drug delivery capabilities of polypeptide hydrogel systems.

In its simplest form, hydrogels form in aqueous media with the payload dissolved or suspended within to achieve encapsulation.[110, 151] As a hydrophobic block, PAla naturally associates with hydrophobic molecules and can be used for drug encapsulation and release. PAla is less hydrophobic than other amino acids, thus inducing a quicker release profile of drug molecules. The extensive study performed by Deming, Sofroniew, and coworkers looked at a range of different diblock copolypeptide hydrogels with a PLL<sub>ys180</sub> block and a hydrophobic block for their potential use in drug delivery.[152] For the release of cholesterol, PLL<sub>ys180</sub>-*b*-PLAla<sub>30</sub> was found to have one of the fastest release profiles of the hydrogels tested, with ~90% cumulative release achieved over around 6 d. In comparison, PLL<sub>ys180</sub>-*b*-PLL<sub>eu20</sub> and PLL<sub>ys180</sub>-*b*-PLPhe<sub>15</sub>, having more hydrophobic blocks, achieved ~70% and ~60% cumulative release over the same period.

The nanogels synthesized by the Jan group provide an alternative morphology for tuning drug release to hydrogels.[153] PLL<sub>60</sub>-*b*-PLThr<sub>15</sub> were contained within the discrete water phase of a water-in-oil emulsion and chemically crosslinked using genipin. The subsequent nanogels were found to show membranolytic activity against the Gram-negative *K. pneumoniae*. Furthermore, almost instantaneous apoptotic action (3-6 min) against cells treated with lipopolysaccharides instead of those without the liposaccharides (15-18 min) further reinforced the aforementioned electrostatic mechanism of the antibacterial action. TNF-Related Apoptosis-Inducing Ligand (TRAIL) – a protein responsible for inducing cell apoptosis primarily in tumor cells – was also encapsulated within these cells to further increase the therapeutic action of the system. The effect was pronounced in mice infected with *K. pneumoniae*, where a much greater survival rate (~67%) was obtained upon treatment with the TRAIL-encapsulated nanogels instead of treatment with TRAIL or the nanogel alone (~30% and ~10% survival rate, respectively).

## **6.2. Cell toxicity and antimicrobial behavior**

Generally, for NCA ROP-based antimicrobial polypeptides (AMPs), random copolypeptides of hydrophobic and cationic residues are well known to have high antimicrobial activity but also come with potentially high cytotoxicity resulting in the use of different architectures to restrict this cytotoxicity, leading to the use of  $\beta$ -sheet structures to allay this. PLL<sub>lys</sub> segments are known to have antibacterial properties due to electrostatic effects – an impact reported by the Li group on short oligopeptide-based antibacterial hydrogels mixed with sodium alginate (amino propanol modified PLGlu (PPLG)-*b*-PLL<sub>lys</sub>/sodium alginate (SA)). *Escherichia coli* (*E. coli*) was found to easily proliferate on PPLG<sub>5</sub>/SA hydrogels as those lacked the electrostatic repulsion required for any antibacterial properties. However, substituting the PPLG unit for a lysine residue (PPLG<sub>4</sub>-*b*-

PLLys<sub>1</sub>/SA) led to a decreased bacterial cell viability down to ~30%, with SEM revealing lesions and holes in the biofilm incubated with these hydrogels.

The Jan group expanded upon this, utilizing  $\beta$ -sheet fibril-based nanoribbons formed from DP 60 PLLys-*b*-PLThr polypeptides for anticancer applications.[154] With the PLThr blocks being responsible for the nanoribbon formation, PLLys created a “fuzzy” exterior. In PLLys<sub>60</sub> samples (i.e., lacking PLThr), membranolytic activity was the greatest against cancer cells, though similarly high activity was observed against other human cells (LL2, H1299, A549-Luc). Increasing the ratio to PLThr<sub>40</sub>-PLLys<sub>20</sub> resulted in decreased membranolytic activity in both cases and increased selectivity towards the cancer cells (LD<sub>50</sub> ~ 9  $\mu$ M for A549 cancerous cells vs. LD<sub>50</sub> ~ 14  $\mu$ M for BEAS-2B human cells). These results translated to positive *in vivo* results, where mouse models showed a significant decrease in tumor growth upon treatment with nanoparticles originating from PLThr<sub>20</sub>-*b*-PLLys<sub>40</sub>.

### 6.3. Tissue Engineering

Tissue engineering relies on mimicry of the natural fibrous scaffolds excreted by cells called the extracellular matrix (ECM), which provides cells a platform for cell attachment, movement, and proliferation.[155] This mimicry takes on multiple aspects naturally fulfilled by silk-like structures, including biodegradation, molecular and structural mimicry, and mechanical properties, essential for cell differentiation.[156, 157] Furthermore, having sufficient mechanical properties with prolonged stability prevents the polymer from being cleared away after insertion into the desired site and during the repair of the surrounding tissue. The ability to undergo environmentally sensitive crosslinking is necessary for hydrogels that form upon injection.[158] The aforementioned introduction of synthetic components . For thermogels, this requires preparing a thermally-sensitive solution at 10 – 20 °C with hydrogelation occurring upon injection into the



body at physiological temperatures (*i.e.*, 37 °C). The Jeong group has done extensive research on PLAla-based copolymer systems as injectable thermogels for tissue engineering.[144, 148, 159, 160] While there is naturally variation to their stiffness depending on the material, generally, storage moduli were found to be around 900 Pa or greater. Beyond injectability, cell signaling, and induced responses are vitally important to consider.

Bifunctional (macro)initiators have the side effect of introducing two N-termini which can be positively charged, thus introducing greater potential for ionic association. Park *et al* utilized hyaluronic acid as a polyanion to assist with the fibril formation and alignment of their PLAla-*b*-PLX (Pluronic 127)-*b*-PLAla triblock copolypeptides (Figure 9).[147] By aligning the fibrils, chondrocytes cultured on the scaffold showed better proliferation (from ~ 120% without hyaluronic acid to ~220% with 1 wt% hyaluronic acid, Figure 9a) as well as increased mRNA expression for type II collagen, which is required for articular cartilage formation. This scaffold drastically outperformed the Matrigel™ control. It should be noted that these promising results are not likely solely due to the fibril alignment, as hyaluronic acid itself would interact with chondrocyte surface receptors.[161] Nonetheless, the overall impact of  $\beta$ -sheet fibrils cannot be discounted, as biomarker (*i.e.* sulfonated glycosaminoglycan (sGAG)) production in the controls was, at most, 4 times lower than in all  $\beta$ -sheet fibril bearing samples, including those without hyaluronic acid. The alignment of these fibers, however, appears to be more important than their mechanical properties, as despite samples containing the highest amount of hyaluronic acid having the lowest stiffness (270-400 Pa compared to 1000-1600 Pa with no hyaluronic acid), sGAG production and mRNA expression was ~25% and ~50% greater. This translated into a loss of spherical morphology within the controls (revealed *via* LIVE/DEAD assay) – a loss which was not reflected in the polypeptide-bearing samples.

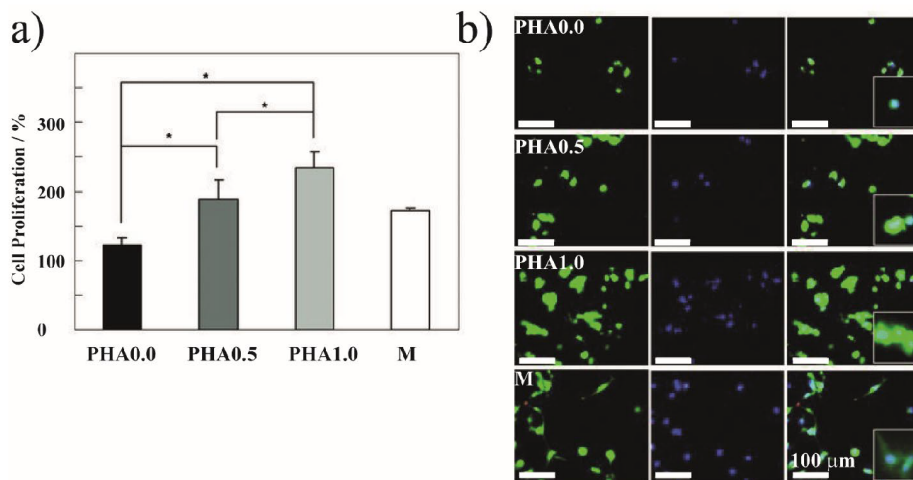


Figure 9: Effect of hyaluronic inclusion within PEG-b-PAla-based hydrogel on chondrocytes culture compared to Matrigel™ (M). a) Cell proliferation with increased hyaluronic acid content b) Cell morphology as observed using a LIVE/DEAD assay (green and red indicates living and dead cells, respectively) and nuclei staining using Hoechst 33342 (blue). The scale bar is 100 μm. [147], Copyright 2012. Reproduced with permission from John Wiley and Sons, License number: 5067660509443.

Cell signaling will naturally occur due to the peptidic nature of PAla, with manipulation of this block length dictating cell fate. Yeon *et al.* demonstrated the effect of manipulating PLAla block length (DP 8.7 – 34.9) of PEG<sub>113.5</sub>-b-PLAla hydrogels on biomarker expression (Figure 10).[162] Adipose-tissue-derived stem cells (ADSCs) dispersed and cultured over 7 days within the hydrogels were all found to maintain their spherical morphology in a LIVE/DEAD assay; after 14 days, cells cultured in PEG<sub>113.5</sub>-PLAla<sub>8.7</sub> hydrogels were found to lack sufficient adhesion and were washed away. Compared to a Matrigel™ control, the two-remaining peptide-based hydrogels

(PEG<sub>113.5</sub>-*b*-PLAAla<sub>15.5</sub> and PEG<sub>113.5</sub>-*b*-PLAAla<sub>34.9</sub>) promoted cell proliferation (PLAAla<sub>15.5</sub> cell proliferation of ~350%, PLAAla<sub>34.9</sub> ~450%, control ~300%). However, while the longest PLAAla block supported cell proliferation best, cells cultured in the PLAAla<sub>15.5</sub> block hydrogel produced the highest level of collagen II, a key protein for chondrogenesis, as mentioned above. As the storage moduli of all three hydrogels were similar, the drastic difference in biomarker expression is more directly related to the different PLAAla lengths causing different cell densities and triggering different signaling cues. Furthermore, *in vivo* injection of seeded PEG<sub>113.5</sub>-*b*-PLAAla<sub>15.5</sub> hydrogels and subsequent tissue staining around the remaining hydrogel revealed a clear presence of sulfated glucoaminoglycan (sGAG) – another biomarker for chondrogenesis.

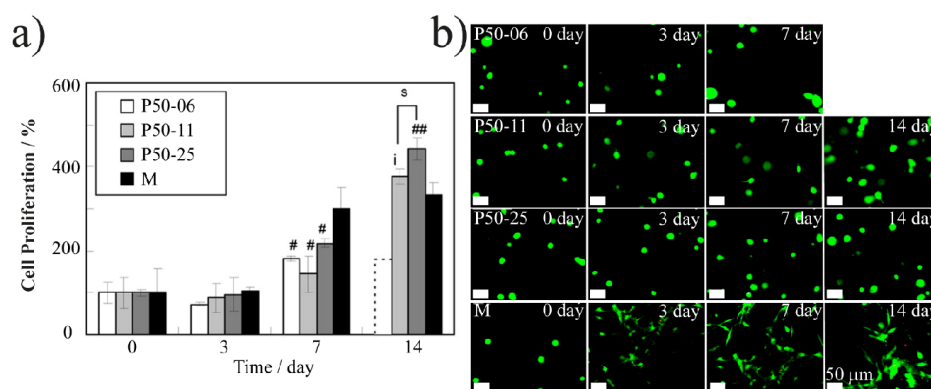


Figure 10: a) Cell proliferation of adipose-derived stem cells (ADSCs) over 14 days with different PLAAla block sizes; b) LIVE/DEAD assay (green and red indicates living and dead cells, respectively) revealing different morphologies after 14 days of culture.[163] The scale bar is 50 μm. [163], Copyright 2013. Adapted with permission from the American Chemical Society.

With the emergence of 3D printing, the use of shear-thinning hydrogels is gaining more and more importance. Murphy *et al.* has reported PNLC<sub>25</sub>-*co*-PLGlu<sub>45</sub>-*b*-poly(L-isoleucine) (PLIle)<sub>25</sub>

hydrogels for their potential as 3D printable materials, utilizing light-sensitive side-chain protecting groups to control chemical crosslinking.[109] Shear-thinning behavior was confirmed with a rheological strain sweep with the polypeptide hydrogels showing storage and loss moduli crossover at 80% strain. By ejecting the hydrogel through a moving syringe (through an 18-gauge nozzle), each layer could be printed onto glass petri dishes resulting in a 3D scaffold with a degree of complexity despite its mechanical softness (storage modulus of 350 Pa). Alkyne-terminated 4-arm PEG molecules were printed along with the hydrogel, allowing the 3D scaffold to be stabilized using UV deprotection of the PNLC residues and subsequent thiolene ‘click’ chemistry crosslinking. While this chemically stabilized the print, the printed structure lost its fibrillar nature.

#### **6.4. Further Applications**

##### 6.4.1 Amphiphilic Nanoparticle Dispersant

Aside from the polypeptide-specific functions of  $\beta$ -sheet fibrils, some groups have instead taken advantage of the amphiphilic nature of many of these copolymers to employ them as a dispersant for single-wall carbon nanotubes (SWCNT) in organic solvents. The general strategy for dispersion involves finding one component which can associate with the SWCNT while the other is favorable within the solvent. While the component that associates with the SWCNT is often the  $\beta$ -sheet fibril, this is not always the case. Tang *et al.*, for example, required a pyrenyl end group to enable an association with the SWCNTs.[164] As a result, the properties of the SWCNT can be utilized for other applications, such as with the PEG-PADLG/SWCNT organogel systems employed by the Wooley group.[165] Due to the photosensitive nature of the PADLG-PEG-PADLG assemblies (partially afforded by the modified side chains of the peptidic regions), patterning was induced *via* light irradiation under yellow-red light (532 and 785 nm wavelength lights were tested), achieving highly complex patterns and lettering. This gel phase was then further stabilized by removing the solvent through evaporation or reverted into the sol state *via*

sonication, giving a versatile patterning tool. Furthermore, the dispersed SWCNT resulted in a patterned film with a conductivity up to 130 S/m (based on SWCNT loading). The overall result is a conductive and rigid film resulting from the synergy of SWCNT and the  $\beta$ -sheet fibril network.

#### 6.4.2 Molecule Immobilization for Biosensing

Yagci and coworkers have reported using surface grafted PLAla blocks to immobilize peptides and enzymes for biosensing purposes.[141, 142] Thiophene-PLAla<sub>16</sub> synthesized using a thiophene functionalized initiator, yielding polypeptides which could be grafted-through without the need for further coupling. The thiophene end groups were electropolymerized and thus deposited onto glassy carbon electrodes. The sensing molecule was covalently coupled to the N-terminal amine *via* glutaraldehyde bonding, resulting in electrodes with different electrical resistances and subsequent different charge densities based on the target molecule concentration in solution. Upon conjugation of glucose oxidase, a linear relationship between charge density and glucose concentration (0.05mM - 1.0 mM) was observed (Figure 11).[141] Conversely, in the absence of PLAla, (*i.e.* only polythiophene), insufficient current density was obtained in the same range. While this is likely primarily due to the lack of binding sites for the covalent bonding of GOx, tests using a reduced density of PLAla chains exhibited the same issue, implying that the interaction between neighboring PLAla chains assists with inducing a response in charge density. Physical adsorption of glucose oxidase to the P(thiophene)-PLAla<sub>16</sub> surfaces did manage to yield sufficient response in the same range, but this response was not as sensitive. This technique was also successful for cocaine detection, with a covalently bonded cocaine aptamer registering a linear response in a 2.5 nM to 10 nM range for cocaine alone and 0.5-50  $\mu$ M when the cocaine metabolite benzoylecgonine was also present.[142]

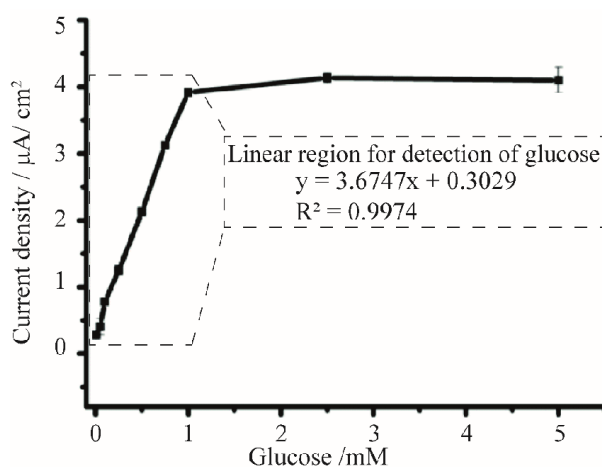


Figure 11: Calibration curves for sensing glucose by measuring the charge density of PLAla coated electrodes up to 5 mM. Inset: Linear biosensing region for glucose concentrations up to 1.0 mM. [141], Copyright 2014. Reproduced with permission from The Royal Society of Chemistry.

## 7. Conclusions and Future Perspectives

In the pursuit of bioinspired materials, the synthesis of silk-inspired polymers *via* synthetic chemical techniques has shown much promise in designing materials with superior mechanical properties and interesting biological applications. The breadth of study in the field still relies heavily on NCA ROP, although chemoenzymatic polymerization has also shown promise in synthesizing such polypeptides. These approaches utilize  $\beta$ -sheets within an amorphous matrix to afford structural mobility and take advantage of the structure-property relationship found in natural silk. Intriguingly, the biological application of these approaches is limited despite the success of silk in drug delivery, tissue engineering, and other bioapplications.

To unlock the future potential of the field, we have also reviewed works with poly(alanine blocks and with evidence of  $\beta$ -sheet fibrils for their facile implementation and thus introduction into more silk-inspired structures. Even with this expansion of scope, the potential for materials such as films and fibers has remained largely untapped. Works under these criteria show far greater potential in tissue engineering with evidence of degradation and cytocompatibility necessary for many bioapplications. However, few of these publications take full advantage of the mechanical potential afforded by such structures. Thus, the intersection between these two areas represents the next hurdle for the field – implementing tough materials in bioapplications. With the field of biomimicry remaining as popular as ever, using silk as a template for the inspiration of chemically synthesized materials remains exciting for the potential bioapplications that will ensue.

## **8. Acknowledgements**

N.J.C thanks The University of Melbourne for providing the Australian Government Research Training Program Scholarship (AGRTP) for providing funds for travel. This work is supported by grants DFG SCHE603/ 23-1. N.J.C, S.L., G.G.Q, and T.S. acknowledge funding from the German Academic Exchange Service (DAAD) through its thematic network Bayreuth-Melbourne Colloid/Polymer Network sponsored by the Federal Ministry of Education funds and Research (BMBF).

## 9. References

- [1] Balkenende DWR, Winkler SM, Messersmith PB. Marine-inspired polymers in medical adhesion. *European Polymer Journal*. 2019;116:134-43.
- [2] Wang J, Suhre MH, Scheibel T. A mussel polyphenol oxidase-like protein shows thiol-mediated antioxidant activity. *European Polymer Journal*. 2019;113:305-12.
- [3] Tadepalli S, Slocik JM, Gupta MK, Naik RR, Singamaneni S. Bio-Optics and Bio-Inspired Optical Materials. *Chemical Reviews*. 2017;117:12705-63.
- [4] Song B, Johansen VE, Sigmund O, Shin JH. Reproducing the hierarchy of disorder for Morpho-inspired, broad-angle color reflection. *Sci Rep*. 2017;7:46023-.
- [5] Fu Y, Yuan C, Bai X. Marine drag reduction of shark skin inspired riblet surfaces. *Biosurface and Biotribology*. 2017;3:11-24.
- [6] Bixler GD, Bhushan B. Shark skin inspired low-drag microstructured surfaces in closed channel flow. *Journal of Colloid and Interface Science*. 2013;393:384-96.
- [7] Rising A, Widhe M, Johansson J, Hedhammar M. Spider silk proteins: recent advances in recombinant production, structure–function relationships and biomedical applications. *Cellular and Molecular Life Sciences*. 2011;68:169-84.
- [8] Hardy JG, Römer LM, Scheibel TR. Polymeric materials based on silk proteins. *Polymer*. 2008;49:4309-27.
- [9] Hardy JG, Scheibel TR. Composite materials based on silk proteins. *Progress in Polymer Science*. 2010;35:1093-115.



- [10] Hakimi O, Knight DP, Vollrath F, Vадgama P. Spider and mulberry silkworm silks as compatible biomaterials. *Composites Part B: Engineering*. 2007;38:324-37.
- [11] Huang W, Ling S, Li C, Omenetto FG, Kaplan DL. Silkworm silk-based materials and devices generated using bio-nanotechnology. *Chemical Society Reviews*. 2018;47:6486-504.
- [12] Rising A, Johansson J. Toward spinning artificial spider silk. *Nature Chemical Biology*. 2015;11:309-15.
- [13] Keten S, Xu Z, Ihle B, Buehler MJ. Nanoconfinement controls stiffness, strength and mechanical toughness of  $\beta$ -sheet crystals in silk. *Nature Materials*. 2010;9:359-67.
- [14] Heim M, Keerl D, Scheibel T. *Spider Silk: From Soluble Protein to Extraordinary Fiber*. *Angewandte Chemie International Edition*. 2009;48:3584-96.
- [15] Köhler T, Vollrath F. Thread biomechanics in the two orb-weaving spiders *Araneus diadematus* (Araneae, Araneidae) and *Uloborus walckenaerius* (Araneae, Uloboridae). *Journal of Experimental Zoology*. 1995;271:1-17.
- [16] Allmeling C, Jokuszies A, Reimers K, Kall S, Vogt PM. Use of spider silk fibres as an innovative material in a biocompatible artificial nerve conduit. *Journal of cellular and molecular medicine*. 2006;10:770-7.
- [17] Gellynck K, Verdonk PC, Van Nimmen E, Almqvist KF, Gheysens T, Schoukens G, et al. Silkworm and spider silk scaffolds for chondrocyte support. *Journal of Materials Science: Materials in Medicine*. 2008;19:3399-409.

- [18] Chiarini A, Petrini P, Bozzini S, Dal Pra I, Armato U. Silk fibroin/poly (carbonate)-urethane as a substrate for cell growth: in vitro interactions with human cells. *Biomaterials*. 2003;24:789-99.
- [19] Lu Q, Zhang B, Li M, Zuo B, Kaplan DL, Huang Y, et al. Degradation Mechanism and Control of Silk Fibroin. *Biomacromolecules*. 2011;12:1080-6.
- [20] Horan RL, Antle K, Collette AL, Wang Y, Huang J, Moreau JE, et al. In vitro degradation of silk fibroin. *Biomaterials*. 2005;26:3385-93.
- [21] Saric M, Scheibel T. Engineering of silk proteins for materials applications. *Current Opinions in Biotechnology*. 2019;60:213-20.
- [22] Wang J, Scheibel T. Recombinant Production of Mussel Byssus Inspired Proteins. *Biotechnology Journal*. 2018;13:1800146.
- [23] Tokareva O, Michalczechen-Lacerda VA, Rech EL, Kaplan DL. Recombinant DNA production of spider silk proteins. *Microbial Biotechnology*. 2013;6:651-63.
- [24] Humenik M, Smith AM, Scheibel T. Recombinant Spider Silks—Biopolymers with Potential for Future Applications. *Polymers*. 2011;3:640.
- [25] Spiess K, Lammel A, Scheibel T. Recombinant Spider Silk Proteins for Applications in Biomaterials. *Macromolecular Bioscience*. 2010;10:998-1007.
- [26] Varnava KG, Sarojini V. Making Solid-Phase Peptide Synthesis Greener: A Review of the Literature. *Chemistry – An Asian Journal*. 2019;14:1088-97.

- [27] Amblard M, Fehrentz J-A, Martinez J, Subra G. Methods and protocols of modern solid phase peptide synthesis. *Molecular Biotechnology*. 2006;33:239-54.
- [28] He X, Fan J, Wooley KL. Stimuli-Triggered Sol–Gel Transitions of Polypeptides Derived from  $\alpha$ -Amino Acid N-Carboxyanhydride (NCA) Polymerizations. *Chemistry – An Asian Journal*. 2016;11:437-47.
- [29] Rasines Mazo A, Allison-Logan S, Karimi F, Chan NJ-A, Qiu W, Duan W, et al. Ring opening polymerization of  $\alpha$ -amino acids: advances in synthesis, architecture and applications of polypeptides and their hybrids. *Chemical Society Reviews*. 2020.
- [30] Huang J, Heise A. Stimuli responsive synthetic polypeptides derived from N-carboxyanhydride (NCA) polymerisation. *Chemical Society Reviews*. 2013;42:7373-90.
- [31] Deming TJ. Synthetic polypeptides for biomedical applications. *Progress in Polymer Science*. 2007;32:858-75.
- [32] Tsuchiya K, Numata K. Chemoenzymatic Synthesis of Polypeptides for Use as Functional and Structural Materials. *Macromolecular Bioscience*. 2017;17:1700177.
- [33] Numata K. Poly(amino acid)s/polypeptides as potential functional and structural materials. *Polymer Journal*. 2015;47:537-45.
- [34] Ganewatta MS, Wang Z, Tang C. Chemical syntheses of bioinspired and biomimetic polymers toward biobased materials. *Nature Reviews Chemistry*. 2021;5:753-72.
- [35] Sarkar A, Connor AJ, Koffas M, Zha RH. Chemical Synthesis of Silk-Mimetic Polymers. *Materials*. 2019;12:4086.

- [36] Katashima T, Malay AD, Numata K. Chemical modification and biosynthesis of silk-like polymers. *Current Opinion in Chemical Engineering*. 2019;24:61-8.
- [37] Craig CL. Evolution of arthropod silks. *Annual review of entomology*. 1997;42:231-67.
- [38] Rudall KM, Kenchington W. Arthropod Silks: The Problem of Fibrous Proteins in Animal Tissues. *Annual Review of Entomology*. 1971;16:73-96.
- [39] Vollrath F, Knight DP. Liquid crystalline spinning of spider silk. *Nature*. 2001;410:541-8.
- [40] Vehoff T, Glišović A, Schollmeyer H, Zippelius A, Salditt T. Mechanical properties of spider dragline silk: humidity, hysteresis, and relaxation. *Biophysical journal*. 2007;93:4425-32.
- [41] Yazawa K, Malay AD, Masunaga H, Norma-Rashid Y, Numata K. Simultaneous effect of strain rate and humidity on the structure and mechanical behavior of spider silk. *Communications Materials*. 2020;1:10.
- [42] Porter D, Vollrath F. Silk as a Biomimetic Ideal for Structural Polymers. *Advanced Materials*. 2009;21:487-92.
- [43] Iizuka E. The physico-chemical properties of silk fibers and the fiber spinning process. *Experientia*. 1983;39:449-54.
- [44] Heim M, Romer L, Scheibel T. Hierarchical structures made of proteins. The complex architecture of spider webs and their constituent silk proteins. *Chemical Society Reviews*. 2010;39:156-64.
- [45] Sutherland TD, Young JH, Weisman S, Hayashi CY, Merritt DJ. Insect Silk: One Name, Many Materials. *Annual Review of Entomology*. 2010;55:171-88.

- [46] Walker AA, Holland C, Sutherland TD. More than one way to spin a crystallite: multiple trajectories through liquid crystallinity to solid silk. *Proceedings of the Royal Society B: Biological Sciences*. 2015;282:20150259.
- [47] Shao Z, Vollrath F, Sirichaisit J, Young RJ. Analysis of spider silk in native and supercontracted states using Raman spectroscopy. *Polymer*. 1999;40:2493-500.
- [48] Dai B, Sargent CJ, Gui X, Liu C, Zhang F. Fibril Self-Assembly of Amyloid-Spider Silk Block Polypeptides. *Biomacromolecules*. 2019;20:2015-23.
- [49] Roche DB, Viet PD, Bakulina A, Hirsh L, Tosatto SCE, Kajava AV. Classification of  $\beta$ -hairpin repeat proteins. *Journal of Structural Biology*. 2018;201:130-8.
- [50] Addison B, Onofrei D, Stengel D, Blass B, Brenneman B, Ayon J, et al. Spider prey-wrapping silk is an  $\alpha$ -helical coiled-coil/ $\beta$ -sheet hybrid nanofiber. *Chemical Communications*. 2018;54:10746-9.
- [51] Sutherland TD, Trueman HE, Walker AA, Weisman S, Campbell PM, Dong Z, et al. Convergently-evolved structural anomalies in the coiled coil domains of insect silk proteins. *Journal of Structural Biology*. 2014;186:402-11.
- [52] Sutherland TD, Weisman S, Trueman HE, Sriskantha A, Trueman JWH, Haritos VS. Conservation of Essential Design Features in Coiled Coil Silks. *Molecular Biology and Evolution*. 2007;24:2424-32.
- [53] Bhattacharjee A, Bansal M. Collagen Structure: The Madras Triple Helix and the Current Scenario. *IUBMB Life*. 2005;57:161-72.

- [54] Perea GB, Riekel C, Guinea GV, Madurga R, Daza R, Burghammer M, et al. Identification and dynamics of polyglycine II nanocrystals in *Argiope trifasciata* flagelliform silk. *Sci Rep.* 2013;3:3061.
- [55] Jung D, Lee J, Park TY, Yang YJ, Cha HJ. Diverse silk and silk-like proteins derived from terrestrial and marine organisms and their applications. *Acta Biomaterialia.* 2021;136:56-71.
- [56] Borkner CB, Lentz S, Müller M, Fery A, Scheibel T. Ultrathin Spider Silk Films: Insights into Spider Silk Assembly on Surfaces. *ACS Applied Polymer Materials.* 2019;1:3366-74.
- [57] Zhou C-Z, Confalonieri F, Esnault C, Zivanovic Y, Jacquet M, Janin J, et al. The 62-kb upstream region of *Bombyx mori* fibroin heavy chain gene is clustered of repetitive elements and candidate matrix association regions. *Gene.* 2003;312:189-95.
- [58] Zhou C-Z, Confalonieri F, Jacquet M, Perasso R, Li Z-G, Janin J. Silk fibroin: Structural implications of a remarkable amino acid sequence. *Proteins: Structure, Function, and Bioinformatics.* 2001;44:119-22.
- [59] Tanaka K, Inoue S, Mizuno S. Hydrophobic interaction of P25, containing Asn-linked oligosaccharide chains, with the HL complex of silk fibroin produced by *Bombyx mori*. *Insect biochemistry and molecular biology.* 1999;29:269-76.
- [60] Asakura T, Suita K, Kameda T, Afonin S, Ulrich AS. Structural role of tyrosine in *Bombyx mori* silk fibroin, studied by solid-state NMR and molecular mechanics on a model peptide prepared as silk I and II. *Magnetic Resonance in Chemistry.* 2004;42:258-66.

- [61] Zafar MS, Belton DJ, Hanby B, Kaplan DL, Perry CC. Functional Material Features of *Bombyx mori* Silk Light versus Heavy Chain Proteins. *Biomacromolecules*. 2015;16:606-14.
- [62] Tanaka K, Kajiyama N, Ishikura K, Waga S, Kikuchi A, Ohtomo K, et al. Determination of the site of disulfide linkage between heavy and light chains of silk fibroin produced by *Bombyx mori*. *Biochimica et Biophysica Acta (BBA) - Protein Structure and Molecular Enzymology*. 1999;1432:92-103.
- [63] Brooks AE, Steinkraus HB, Nelson SR, Lewis RV. An Investigation of the Divergence of Major Ampullate Silk Fibers from *Nephila clavipes* and *Argiope aurantia*. *Biomacromolecules*. 2005;6:3095-9.
- [64] Saric M, Eisoldt L, Döring V, Scheibel T. Interplay of Different Major Ampullate Spidroins during Assembly and Implications for Fiber Mechanics. *Advanced Materials*. 2021;33:2006499.
- [65] Correa-Garhwal SM, Clarke TH, Janssen M, Crevecoeur L, McQuillan BN, Simpson AH, et al. Spidroins and Silk Fibers of Aquatic Spiders. *Sci Rep*. 2019;9:13656.
- [66] Xu M, Lewis RV. Structure of a protein superfiber: spider dragline silk. *Proceedings of the National Academy of Sciences*. 1990;87:7120-4.
- [67] Plaza GR, Pérez-Rigueiro J, Riekel C, Perea GB, Agulló-Rueda F, Burghammer M, et al. Relationship between microstructure and mechanical properties in spider silk fibers: identification of two regimes in the microstructural changes. *Soft Matter*. 2012;8:6015-26.
- [68] Grubb DT, Jelinski LW. Fiber Morphology of Spider Silk: The Effects of Tensile Deformation. *Macromolecules*. 1997;30:2860-7.

- [69] Riekel C, Bränden C, Craig C, Ferrero C, Heidelbach F, Müller M. Aspects of X-ray diffraction on single spider fibers. *International Journal of Biological Macromolecules*. 1999;24:179-86.
- [70] Winkler S, Kaplan DL. Molecular biology of spider silk. *Reviews in Molecular Biotechnology*. 2000;74:85-93.
- [71] Kümmerlen J, Van Beek J, Vollrath F, Meier B. Local structure in spider dragline silk investigated by two-dimensional spin-diffusion nuclear magnetic resonance. *Macromolecules*. 1996;29:2920-8.
- [72] Hijirida DH, Do KG, Michal C, Wong S, Zax D, Jelinski LW. <sup>13</sup>C NMR of *Nephila clavipes* major ampullate silk gland. *Biophysical Journal*. 1996;71:3442-7.
- [73] Liu Y, Sponner A, Porter D, Vollrath F. Proline and processing of spider silks. *Biomacromolecules*. 2008;9:116-21.
- [74] Holland GP, Jenkins JE, Creager MS, Lewis RV, Yarger JL. Quantifying the fraction of glycine and alanine in  $\beta$ -sheet and helical conformations in spider dragline silk using solid-state NMR. *Chemical communications*. 2008:5568-70.
- [75] Bauer J, Scheibel T. Conformational stability and interplay of helical N-and C-terminal domains with implications on major ampullate spidroin assembly. *Biomacromolecules*. 2017;18:835-45.
- [76] Deming TJ. Cobalt and Iron Initiators for the Controlled Polymerization of  $\alpha$ -Amino Acid-N-Carboxyanhydrides. *Macromolecules*. 1999;32:4500-2.



- [77] Deming TJ. Facile synthesis of block copolypeptides of defined architecture. *Nature*. 1997;390:386-9.
- [78] Deming TJ, Curtin SA. Chain Initiation Efficiency in Cobalt- and Nickel-Mediated Polypeptide Synthesis. *Journal of the American Chemical Society*. 2000;122:5710-7.
- [79] Chan NJ-A, Gu D, Tan S, Fu Q, Pattison TG, O'Connor AJ, et al. Spider-silk inspired polymeric networks by harnessing the mechanical potential of  $\beta$ -sheets through network guided assembly. *Nature Communications*. 2020;11:1630.
- [80] Rathore O, Sogah DY. Self-Assembly of  $\beta$ -Sheets into Nanostructures by Poly(alanine) Segments Incorporated in Multiblock Copolymers Inspired by Spider Silk. *Journal of the American Chemical Society*. 2001;123:5231-9.
- [81] Rathore O, Sogah DY. Nanostructure Formation through  $\beta$ -Sheet Self-Assembly in Silk-Based Materials. *Macromolecules*. 2001;34:1477-86.
- [82] Winningham MJ, Sogah DY. A Modular Approach to Polymer Architecture Control via Catenation of Prefabricated Biomolecular Segments: Polymers Containing Parallel  $\beta$ -Sheets Templated by a Phenoxathiin-Based Reverse Turn Mimic. *Macromolecules*. 1997;30:862-76.
- [83] Rathore O, Winningham MJ, Sogah DY. A novel silk-based segmented block copolymer containing GlyAlaGlyAla  $\beta$ -sheets templated by phenoxathiin. *Journal of Polymer Science Part A: Polymer Chemistry*. 2000;38:352-66.
- [84] Ayres L, Adams PHHM, Löwik DWPM, van Hest JCM.  $\beta$ -Sheet Side Chain Polymers Synthesized by Atom-Transfer Radical Polymerization. *Biomacromolecules*. 2005;6:825-31.

- [85] Smeenk JM, Schön P, Otten MBJ, Speller S, Stunnenberg HG, van Hest JCM. Fibril Formation by Triblock Copolymers of Silklike  $\beta$ -Sheet Polypeptides and Poly(ethylene glycol). *Macromolecules*. 2006;39:2989-97.
- [86] Vanhalle M, Corneillie S, Smet M, Van Puyvelde P, Goderis B. Poly (alanine): Structure and Stability of the D and L-Enantiomers. *Biomacromolecules*. 2016;17:183-91.
- [87] Iio T, Takahashi S. Regular Polypeptides of Glycine and L-Alanine (Special Issue on Polymer Chemistry, VIII). *Polymers*. 1971.
- [88] Iwakura Y, Uno K, Oya M. Polymerization of DL-alanine NCA and L-alanine NCA. *Journal of Polymer Science Part A-1: Polymer Chemistry*. 1967;5:2867-74.
- [89] Itoh K, Nakahara T, Shimanouchi T, Oya M, Uno K, Iwakura Y. Far-infrared spectra of polyalanines with  $\alpha$ -helical and  $\beta$ -form structures. *Biopolymers*. 1968;6:1759-66.
- [90] Iwakura Y, Uno K, Oya M. Polymerization of  $\alpha$ -amino acid N-carboxy anhydrides. III. Mechanism of polymerization of L- and DL-alanine NCA in acetonitrile. *Journal of Polymer Science Part A-1: Polymer Chemistry*. 1968;6:2165-77.
- [91] Liu H, Cheng Y, Chen J, Chang F, Wang J, Ding J, et al. Component effect of stem cell-loaded thermosensitive polypeptide hydrogels on cartilage repair. *Acta Biomaterialia*. 2018;73:103-11.
- [92] Jeong SY, Moon HJ, Park MH, Joo MK, Jeong B. Molecular captain: A light-sensitive linker molecule in poly(ethylene glycol)-poly(L-alanine)-poly(ethylene glycol) triblock copolymer

directs molecular nano-assembly, conformation, and sol-gel transition. *Journal of Polymer Science Part A: Polymer Chemistry*. 2012;50:3184-91.

[93] Lin J-Y, Lai P-L, Lin Y-K, Peng S, Lee L-Y, Chen C-N, et al. A poloxamer-polypeptide thermosensitive hydrogel as a cell scaffold and sustained release depot. *Polymer Chemistry*. 2016;7:2976-85.

[94] Sun Y, Deming TJ. Self-Healing Multiblock Copolypeptide Hydrogels via Polyion Complexation. *ACS Macro Letters*. 2019;8:553-7.

[95] Murphy R, Borase T, Payne C, O'Dwyer J, Cryan SA, Heise A. Hydrogels from amphiphilic star block copolypeptides. *RSC Advances*. 2016;6:23370-6.

[96] Thornton PD, Billah SMR, Cameron NR. Enzyme-Degradable Self-Assembled Hydrogels From Polyalanine-Modified Poly(ethylene glycol) Star Polymers. *Macromolecular Rapid Communications*. 2013;34:257-62.

[97] Jang JH, Choi YM, Choi YY, Joo MK, Park MH, Choi BG, et al. pH/temperature sensitive chitosan-g-(PA-PEG) aqueous solutions as new thermogelling systems. *Journal of Materials Chemistry*. 2011;21:5484-91.

[98] Yoshikawa HY, Rossetti FF, Kaufmann S, Kaindl T, Madsen J, Engel U, et al. Quantitative Evaluation of Mechanosensing of Cells on Dynamically Tunable Hydrogels. *Journal of the American Chemical Society*. 2011;133:1367-74.

[99] Kenney JM, Knight D, Wise MJ, Vollrath F. Amyloidogenic nature of spider silk. *European Journal of Biochemistry*. 2002;269:4159-63.

- [100] Numata K, Kaplan DL. Differences in Cytotoxicity of  $\beta$ -Sheet Peptides Originated from Silk and Amyloid  $\beta$ . *Macromolecular Bioscience*. 2011;11:60-4.
- [101] Humenik M, Scheibel T. Nanomaterial Building Blocks Based on Spider Silk–Oligonucleotide Conjugates. *ACS Nano*. 2014;8:1342-9.
- [102] Yarger JL, Cherry BR, van der Vaart A. Uncovering the structure–function relationship in spider silk. *Nature Reviews Materials*. 2018;3:18008.
- [103] Costantini S, Colonna G, Facchiano AM. Amino acid propensities for secondary structures are influenced by the protein structural class. *Biochemical and Biophysical Research Communications*. 2006;342:441-51.
- [104] Jang H, Hall CK, Zhou Y. Thermodynamics and stability of a beta-sheet complex: molecular dynamics simulations on simplified off-lattice protein models. *Protein Sci*. 2004;13:40-53.
- [105] Nova A, Keten S, Pugno NM, Redaelli A, Buehler MJ. Molecular and Nanostructural Mechanisms of Deformation, Strength and Toughness of Spider Silk Fibrils. *Nano Letters*. 2010;10:2626-34.
- [106] Humenik M, Magdeburg M, Scheibel T. Influence of repeat numbers on self-assembly rates of repetitive recombinant spider silk proteins. *Journal of Structural Biology*. 2014;186:431-7.
- [107] Fujiwara K, Toda H, Ikeguchi M. Dependence of  $\alpha$ -helical and  $\beta$ -sheet amino acid propensities on the overall protein fold type. *BMC Structural Biology*. 2012;12:18.
- [108] Sinaga A, Hatton TA, Tam KC. Hydrogen Bonded Assembly of Poly(acrylic acid)-block-poly(l-valine) in Dilute Solutions. *Macromolecules*. 2007;40:9064-73.

- [109] Murphy RD, Kimmins S, Hibbitts AJ, Heise A. 3D-extrusion printing of stable constructs composed of photoresponsive polypeptide hydrogels. *Polymer Chemistry*. 2019;10:4675-82.
- [110] Huang J, Hastings CL, Duffy GP, Kelly HM, Raeburn J, Adams DJ, et al. Supramolecular Hydrogels with Reverse Thermal Gelation Properties from (Oligo)tyrosine Containing Block Copolymers. *Biomacromolecules*. 2013;14:200-6.
- [111] Planellas M, Puiggali J. Synthesis and properties of poly (L-lactide)-b-poly (L-phenylalanine) hybrid copolymers. *International journal of molecular sciences*. 2014;15:13247-66.
- [112] Mayans E, Murase SK, Pérez-Madrigal MM, Cativiela C, Alemán C, Puiggali J. Hybrid Polypeptide/Poly lactide Copolymers with Short Phenylalanine Blocks. *Macromolecular Chemistry and Physics*. 2018;219:1800168.
- [113] Hou S-S, Fan N-S, Tseng Y-C, Jan J-S. Self-Assembly and Hydrogelation of Coil-Sheet Poly(l-lysine)-block-poly(l-threonine) Block Copolypeptides. *Macromolecules*. 2018;51:8054-63.
- [114] Rösler A, Klok H-A, Hamley IW, Castelletto V, Mykhaylyk OO. Nanoscale structure of poly (ethylene glycol) hybrid block copolymers containing amphiphilic  $\beta$ -strand peptide sequences. *Biomacromolecules*. 2003;4:859-63.
- [115] Eisenberg D. Three-dimensional structure of membrane and surface proteins. *Annual Review of Biochemistry*. 1984;53:595-623.
- [116] Charton M, Charton BI. The structural dependence of amino acid hydrophobicity parameters. *Journal of Theoretical Biology*. 1982;99:629-44.

- [117] Kyte J, Doolittle RF. A simple method for displaying the hydropathic character of a protein. *Journal of Molecular Biology*. 1982;157:105-32.
- [118] Wolfenden R, Andersson L, Cullis PM, Southgate CCB. Affinities of amino acid side chains for solvent water. *Biochemistry*. 1981;20:849-55.
- [119] Jiang H, Duan L, Ren X, Gao G. Hydrophobic association hydrogels with excellent mechanical and self-healing properties. *European Polymer Journal*. 2019;112:660-9.
- [120] Tan S, Chan NJ-A, Collins J, Fu Q, Qiao GG. CHAPTER 13 New Approaches Towards the Design of Tough Amphiphilic Polymeric Co-networks. *Amphiphilic Polymer Co-networks: Synthesis, Properties, Modelling and Applications: The Royal Society of Chemistry*; 2020. p. 277-308.
- [121] Stulz J, Müller D, Hull WE, Kricheldorf HR. Secondary structure of peptides, 10. FT-IR and <sup>13</sup>C NMR CP/MAS study on tacticity and secondary structure of poly(D,L-leucine)s. *Die Makromolekulare Chemie*. 1983;184:1311-22.
- [122] Holowka EP, Pochan DJ, Deming TJ. Charged Polypeptide Vesicles with Controllable Diameter. *Journal of the American Chemical Society*. 2005;127:12423-8.
- [123] Zhang S, Alvarez DJ, Sofroniew MV, Deming TJ. Design and synthesis of nonionic copolypeptide hydrogels with reversible thermoresponsive and tunable physical properties. *Biomacromolecules*. 2015;16:1331-40.
- [124] Breedveld V, Nowak AP, Sato J, Deming TJ, Pine DJ. Rheology of Block Copolypeptide Solutions: Hydrogels with Tunable Properties. *Macromolecules*. 2004;37:3943-53.

- [125] Hu Y-Y, Yusufoglu Y, Kanapathipillai M, Yang C-Y, Wu Y, Thiyagarajan P, et al. Self-assembled calcium phosphate nanocomposites using block copolypeptide templates. *Soft Matter*. 2009;5:4311-20.
- [126] Higuchi M, Inoue T, Miyoshi H, Kawaguchi M. pH-Induced Reversible Conformational and Morphological Regulation of Poly-leucine Grafted Polyallylamine Assembly in Solution. *Langmuir*. 2005;21:11462-7.
- [127] Grigsby JJ, Blanch HW, Prausnitz JM. Effect of secondary structure on the potential of mean force for poly-L-lysine in the  $\alpha$ -helix and  $\beta$ -sheet conformations. *Biophysical Chemistry*. 2002;99:107-16.
- [128] Fulara A, Dzwolak W. Bifurcated Hydrogen Bonds Stabilize Fibrils of Poly(L-glutamic) Acid. *The Journal of Physical Chemistry B*. 2010;114:8278-83.
- [129] Hernik A, Puławski W, Fedorczyk B, Tymecka D, Misicka A, Filipek S, et al. Amyloidogenic Properties of Short  $\alpha$ -L-Glutamic Acid Oligomers. *Langmuir*. 2015;31:10500-7.
- [130] Papadopoulos P, Floudas G, Klok HA, Schnell I, Pakula T. Self-Assembly and Dynamics of Poly( $\gamma$ -benzyl-L-glutamate) Peptides. *Biomacromolecules*. 2004;5:81-91.
- [131] Ibarboure E, Papon E, Rodríguez-Hernández J. Nanostructured thermotropic PBLG–PDMS–PBLG block copolymers. *Polymer*. 2007;48:3717-25.
- [132] Ibarboure E, Rodríguez-Hernández J. Supramolecular structures from self-assembled poly( $\gamma$ -benzyl-L-glutamate)–polydimethylsiloxane–poly( $\gamma$ -benzyl-L-glutamate) triblock copolypeptides in thin films. *European Polymer Journal*. 2010;46:891-9.

- [133] Shen J, Chen C, Fu W, Shi L, Li Z. Conformation-specific Self-assembly of Thermo-responsive Poly(ethylene glycol)-b-polypeptide Diblock Copolymer. *Langmuir*. 2013;29:6271-8.
- [134] Zhang S, Fu W, Li Z. Supramolecular hydrogels assembled from nonionic poly(ethylene glycol)-b-polypeptide diblocks containing OEGylated poly-L-glutamate. *Polymer Chemistry*. 2014;5:3346-51.
- [135] Shi S-Y, He Y-G, Chen W-W, Liu N, Zhu Y-Y, Ding Y-S, et al. Polypeptide-b-Poly(Phenyl Isocyanide) Hybrid Rod-Rod Copolymers: One-Pot Synthesis, Self-Assembly, and Cell Imaging. *Macromolecular Rapid Communications*. 2015;36:1511-20.
- [136] Zou J, Zhang F, Chen Y, Raymond JE, Zhang S, Fan J, et al. Responsive organogels formed by supramolecular self assembly of PEG-block-allyl-functionalized racemic polypeptides into  $\beta$ -sheet-driven polymeric ribbons. *Soft Matter*. 2013;9:5951-8.
- [137] Johnson JC, Wanasekara ND, Korley LTJ. Influence of secondary structure and hydrogen-bonding arrangement on the mechanical properties of peptidic-polyurea hybrids. *Journal of Materials Chemistry B*. 2014;2:2554-61.
- [138] Matolyak L, Keum J, Korley LTJ. Molecular Design: Network Architecture and Its Impact on the Organization and Mechanics of Peptide-Polyurea Hybrids. *Biomacromolecules*. 2016;17:3931-9.
- [139] Wibowo SH, Sulistio A, Wong EHH, Blencowe A, Qiao GG. Polypeptide films via N-carboxyanhydride ring-opening polymerization (NCA-ROP): past, present and future. *Chemical Communications*. 2014;50:4971-88.



- [140] Whitesell JK, Chang HK. Directionally aligned helical peptides on surfaces. *Science*. 1993;261:73-6.
- [141] Akbulut H, Yavuz M, Guler E, Demirkol DO, Endo T, Yamada S, et al. Electrochemical deposition of polypeptides: bio-based covering materials for surface design. *Polymer Chemistry*. 2014;5:3929-36.
- [142] Bozokalfa G, Akbulut H, Demir B, Guler E, Gumus ZP, Odaci Demirkol D, et al. Polypeptide Functional Surface for the Aptamer Immobilization: Electrochemical Cocaine Biosensing. *Analytical Chemistry*. 2016;88:4161-7.
- [143] Park MH, Yu Y, Moon HJ, Ko du Y, Kim HS, Lee H, et al. 3D culture of tonsil-derived mesenchymal stem cells in poly(ethylene glycol)-poly(L-alanine-co-L-phenyl alanine) thermogel. *Advanced Healthcare Materials*. 2014;3:1782-91.
- [144] Yun EJ, Yon B, Joo MK, Jeong B. Cell Therapy for Skin Wound Using Fibroblast Encapsulated Poly(ethylene glycol)-poly(L-alanine) Thermogel. *Biomacromolecules*. 2012;13:1106-11.
- [145] Kim JY, Park MH, Joo MK, Lee SY, Jeong B. End Groups Adjusting the Molecular Nano-Assembly Pattern and Thermal Gelation of Polypeptide Block Copolymer Aqueous Solution. *Macromolecules*. 2009;42:3147-51.
- [146] Choi BG, Park MH, Cho S-H, Joo MK, Oh HJ, Kim EH, et al. Thermal gelling polyalanine-ploxamine-polyalanine aqueous solution for chondrocytes 3D culture: Initial concentration effect. *Soft Matter*. 2011;7:456-62.

- [147] Park MH, Choi BG, Jeong B. Complexation-Induced Biomimetic Long Range Fibrous Orientation in a Rigid-Flexible Block Copolymer Thermogel. *Advanced Functional Materials*. 2012;22:5118-25.
- [148] Choi BG, Park MH, Cho SH, Joo MK, Oh HJ, Kim EH, et al. In situ thermal gelling polypeptide for chondrocytes 3D culture. *Biomaterials*. 2010;31:9266-72.
- [149] Chen C, Wu D, Fu W, Li Z. Peptide Hydrogels Assembled from Nonionic Alkyl-polypeptide Amphiphiles Prepared by Ring-Opening Polymerization. *Biomacromolecules*. 2013;14:2494-8.
- [150] Chen C, Wu D, Fu W, Li Z. Tunable Organogelator from Alkyl-Polypeptide Diblock Prepared by Ring-Opening Polymerization. *Australian Journal of Chemistry*. 2014;67:59-65.
- [151] Fan J, Li R, Wang H, He X, Nguyen TP, Letteri RA, et al. Multi-responsive polypeptide hydrogels derived from N-carboxyanhydride terpolymerizations for delivery of nonsteroidal anti-inflammatory drugs. *Organic & Biomolecular Chemistry*. 2017;15:5145-54.
- [152] Zhang S, Anderson MA, Ao Y, Khakh BS, Fan J, Deming TJ, et al. Tunable diblock copolypeptide hydrogel depots for local delivery of hydrophobic molecules in healthy and injured central nervous system. *Biomaterials*. 2014;35:1989-2000.
- [153] Chen Y-F, Chen G-Y, Chang C-H, Su Y-C, Chen Y-C, Jiang Y-s, et al. TRAIL encapsulated to polypeptide-crosslinked nanogel exhibits increased anti-inflammatory activities in Klebsiella pneumoniae-induced sepsis treatment. *Materials Science and Engineering: C*. 2019;102:85-95.

- [154] Chen Y-F, Shiau A-L, Chang S-J, Fan N-S, Wang C-T, Wu C-L, et al. One-dimensional poly(L-lysine)-block-poly(L-threonine) assemblies exhibit potent anticancer activity by enhancing membranolysis. *Acta Biomaterialia*. 2017;55:283-95.
- [155] MacPhee CE, Woolfson DN. Engineered and designed peptide-based fibrous biomaterials. *Current Opinion in Solid State and Materials Science*. 2004;8:141-9.
- [156] Engler AJ, Sen S, Sweeney HL, Discher DE. Matrix Elasticity Directs Stem Cell Lineage Specification. *Cell*. 2006;126:677-89.
- [157] Hiew VV, Simat SFB, Teoh PL. The Advancement of Biomaterials in Regulating Stem Cell Fate. *Stem Cell Reviews and Reports*. 2018;14:43-57.
- [158] Liu M, Zeng X, Ma C, Yi H, Ali Z, Mou X, et al. Injectable hydrogels for cartilage and bone tissue engineering. *Bone Research*. 2017;5:17014.
- [159] Kang EY, Yeon B, Moon HJ, Jeong B. PEG-l-PAF and PEG-d-PAF: Comparative Study on Thermogelation and Biodegradation. *Macromolecules*. 2012;45:2007-13.
- [160] Shinde UP, Joo MK, Moon HJ, Jeong B. Sol-gel transition of PEG-PAF aqueous solution and its application for hGH sustained release. *Journal of Materials Chemistry*. 2012;22:6072-9.
- [161] Chow G, Knudson CB, Homandberg G, Knudson W. Increased expression of CD44 in bovine articular chondrocytes by catabolic cellular mediators. *Journal of Biological Chemistry*. 1995;270:27734-41.

- [162] Yeon B, Park MH, Moon HJ, Kim S-J, Cheon YW, Jeong B. 3D Culture of Adipose-Tissue-Derived Stem Cells Mainly Leads to Chondrogenesis in Poly(ethylene glycol)-Poly(L-alanine) Diblock Copolymer Thermogel. *Biomacromolecules*. 2013;14:3256-66.
- [163] Joo MK, Ko DY, Jeong SJ, Park MH, Shinde UP, Jeong B. Incorporation of D-alanine into poly(ethylene glycol) and L-poly(alanine-co-phenylalanine) block copolymers affects their nanoassemblies and enzymatic degradation. *Soft Matter*. 2013;9:8014-22.
- [164] Tang H, Zhang D. Solid state self-assembly of the single-walled carbon nanotubes and poly( $\gamma$ -benzyl-L-glutamate)s with different conformations. *Journal of Polymer Science Part A: Polymer Chemistry*. 2013;51:4489-97.
- [165] He X, Fan J, Zou J, Wooley KL. Reversible photo-patterning of soft conductive materials via spatially-defined supramolecular assembly. *Chemical Communications*. 2016;52:8455-8.
- [166] Katakai R, Oya M, Iwakura Y. Synthesis and conformational study of sequential polypeptides, (L-Ala-L-Val-Gly)<sub>n</sub> and (L-Val-L-Ala-Gly)<sub>n</sub>. *Biopolymers: Original Research on Biomolecules*. 1975;14:1315-26.
- [167] Kim KY, Kōmoto T, Katakai R, Ōya M, Kawai T. Growth mechanism of crystals of glycine-L-alanine copolymer in the course of polymerization. *Die Makromolekulare Chemie*. 1975;176:373-89.
- [168] Hachisu M, Ohkawa K, Yamamoto H. Preparation of Silk-Like Fibers Designed by Self-Assembled Ionic Polypeptides. *Macromolecular Bioscience*. 2003;3:92-9.

- [169] Dong C-M, Sun X-L, Faucher KM, Apkarian RP, Chaikof EL. Synthesis and Characterization of Glycopolymer-Polypeptide Triblock Copolymers. *Biomacromolecules*. 2004;5:224-31.
- [170] Huang H, Hu J, Zhu Y. Shape-Memory Biopolymers Based on  $\beta$ -Sheet Structures of Polyalanine Segments Inspired by Spider Silks. *Macromolecular Bioscience*. 2013;13:161-6.
- [171] Studenovská H, Vodička P, Proks V, Hlučilová J, Motlík J, Rypáček F. Synthetic poly(amino acid) hydrogels with incorporated cell-adhesion peptides for tissue engineering. *Journal of Tissue Engineering and Regenerative Medicine*. 2010;4:454-63.
- [172] Choi YY, Jang JH, Park MH, Choi BG, Chi B, Jeong B. Block length affects secondary structure, nanoassembly and thermosensitivity of poly(ethylene glycol)-poly(L-alanine) block copolymers. *Journal of Materials Chemistry*. 2010;20:3416-21.
- [173] Moon HJ, Choi BG, Park MH, Joo MK, Jeong B. Enzymatically Degradable Thermogelling Poly(alanine-co-leucine)-poloxamer-poly(alanine-co-leucine). *Biomacromolecules*. 2011;12:1234-42.
- [174] Park SH, Choi BG, Moon HJ, Cho S-H, Jeong B. Block sequence affects thermosensitivity and nano-assembly: PEG-l-PA-dl-PA and PEG-dl-PA-l-PA block copolymers. *Soft Matter*. 2011;7:6515-21.
- [175] Sedlačík T, Studenovská H, Rypáček F. Enzymatic degradation of the hydrogels based on synthetic poly( $\alpha$ -amino acid)s. *Journal of Materials Science: Materials in Medicine*. 2011;22:781.

- [176] Habraken GJM, Wilsens KHRM, Koning CE, Heise A. Optimization of N-carboxyanhydride (NCA) polymerization by variation of reaction temperature and pressure. *Polymer Chemistry*. 2011;2:1322-30.
- [177] Jan J-S, Chen P-S, Hsieh P-L, Chen B-Y. Silicification of Genipin-Cross-Linked Polypeptide Hydrogels Toward Biohybrid Materials and Mesoporous Oxides. *ACS Applied Materials & Interfaces*. 2012;4:6865-74.
- [178] Kang EY, Moon HJ, Joo MK, Jeong B. Thermogelling Chitosan-g-(PAF-PEG) Aqueous Solution As an Injectable Scaffold. *Biomacromolecules*. 2012;13:1750-7.
- [179] Song A, Rane AA, Christman KL. Antibacterial and cell-adhesive polypeptide and poly(ethylene glycol) hydrogel as a potential scaffold for wound healing. *Acta Biomater*. 2012;8:41-50.
- [180] Ling J, Peng H, Shen Z. Deprotonation reaction of  $\alpha$ -amino acid N-carboxyanhydride at 4-CH position by yttrium tris[bis(trimethylsilyl)amide]. *Journal of Polymer Science Part A: Polymer Chemistry*. 2012;50:3743-9.
- [181] Peng H, Ling J, Zhu Y, You L, Shen Z. Polymerization of  $\alpha$ -amino acid N-carboxyanhydrides catalyzed by rare earth tris(borohydride) complexes: Mechanism and hydroxy-endcapped polypeptides. *Journal of Polymer Science Part A: Polymer Chemistry*. 2012;50:3016-29.
- [182] Cao H, Yao J, Shao Z. Synthesis of poly ( $\gamma$ -benzyl-L-glutamate) with well-defined terminal structures and its block polypeptides with alanine, leucine and phenylalanine. *Polymer International*. 2012;61:774-9.

- [183] Chiang P-R, Lin T-Y, Tsai H-C, Chen H-L, Liu S-Y, Chen F-R, et al. Thermosensitive Hydrogel from Oligopeptide-Containing Amphiphilic Block Copolymer: Effect of Peptide Functional Group on Self-Assembly and Gelation Behavior. *Langmuir*. 2013;29:15981-91.
- [184] Hamley IW, Dehsorkhi A, Castelletto V, Seitsonen J, Ruokolainen J, Iatrou H. Self-assembly of a model amphiphilic oligopeptide incorporating an arginine headgroup. *Soft Matter*. 2013;9:4794-801.
- [185] Joo JH, Ko DY, Moon HJ, Shinde UP, Park MH, Jeong B. Ion and Temperature Sensitive Polypeptide Block Copolymer. *Biomacromolecules*. 2014;15:3664-70.
- [186] Kye EJ, Kim S-J, Park MH, Moon HJ, Ryu KH, Jeong B. Differentiation of Tonsil-Tissue-Derived Mesenchymal Stem Cells Controlled by Surface-Functionalized Microspheres in PEG-Polypeptide Thermogels. *Biomacromolecules*. 2014;15:2180-7.
- [187] Fagerland J, Finne-Wistrand A, Numata K. Short One-Pot Chemo-Enzymatic Synthesis of l-Lysine and l-Alanine Diblock Co-Oligopeptides. *Biomacromolecules*. 2014;15:735-43.
- [188] Guo Z, Tian H, Lin L, Chen J, He C, Tang Z, et al. Hydrophobic Polyalanine Modified Hyperbranched Polyethylenimine as High Efficient pDNA and siRNA Carrier. *Macromolecular Bioscience*. 2014;14:1406-14.
- [189] Peng H, Chen W-l, Kong J, Shen Z-q, Ling J. Synthesis of  $\alpha$ -hydroxy- $\omega$ -aminotelechelic polypeptide from  $\alpha$ -amino acid N-carboxyanhydrides catalyzed by alkali-metal borohydrides. *Chinese Journal of Polymer Science*. 2014;32:743-50.

- [190] Kim S-J, Park MH, Moon HJ, Park JH, Ko DY, Jeong B. Polypeptide Thermogels as a Three Dimensional Culture Scaffold for Hepatogenic Differentiation of Human Tonsil-Derived Mesenchymal Stem Cells. *ACS Applied Materials & Interfaces*. 2014;6:17034-43.
- [191] Lai J, Fu W, Zhu L, Guo R, Liang D, Li Z, et al. Fibril Aggregates Formed by a Glatiramer-Mimicking Random Copolymer of Amino Acids. *Langmuir*. 2014;30:7221-6.
- [192] Hamley IW, Kirkham S, Dehsorkhi A, Castelletto V, Adameik J, Mezzenga R, et al. Self-Assembly of a Model Peptide Incorporating a Hexa-Histidine Sequence Attached to an Oligo-Alanine Sequence, and Binding to Gold NTA/Nickel Nanoparticles. *Biomacromolecules*. 2014;15:3412-20.
- [193] Shinde UP, Moon HJ, Ko DY, Jung BK, Jeong B. Control of rhGH Release Profile from PEG-PAF Thermogel. *Biomacromolecules*. 2015;16:1461-9.
- [194] Yu L, Fu W, Li Z. Tuning the phase transition temperature of thermal-responsive OEGylated poly-l-glutamate via random copolymerization with l-alanine. *Soft Matter*. 2015;11:545-50.
- [195] Popescu M-T, Lontos G, Avgeropoulos A, Tsitsilianis C. Stimuli responsive fibrous hydrogels from hierarchical self-assembly of a triblock copolypeptide. *Soft Matter*. 2015;11:331-42.
- [196] Ageitos JM, Yazawa K, Tateishi A, Tsuchiya K, Numata K. The Benzyl Ester Group of Amino Acid Monomers Enhances Substrate Affinity and Broadens the Substrate Specificity of the Enzyme Catalyst in Chemoenzymatic Copolymerization. *Biomacromolecules*. 2016;17:314-23.



- [197] Popescu M-T, Lontos G, Avgeropoulos A, Voulgari E, Avgoustakis K, Tsitsilianis C. Injectable Hydrogel: Amplifying the pH Sensitivity of a Triblock Copolypeptide by Conjugating the N-Termini via Dynamic Covalent Bonding. *ACS Applied Materials & Interfaces*. 2016;8:17539-48.
- [198] Peng S, Lin J-Y, Cheng M-H, Wu C-W, Chu IM. A cell-compatible PEO-PPO-PEO (Pluronic®)-based hydrogel stabilized through secondary structures. *Materials Science and Engineering: C*. 2016;69:421-8.
- [199] Wei L, Chen J, Zhao S, Ding J, Chen X. Thermo-sensitive polypeptide hydrogel for locally sequential delivery of two-pronged antitumor drugs. *Acta Biomaterialia*. 2017;58:44-53.
- [200] Skoulas D, Stavroulaki D, Santorinaios K, Iatrou H. Synthesis of Hybrid-Polypeptides m-PEO-b-poly (His-co-Gly) and m-PEO-b-poly (His-co-Ala) and Study of Their Structure and Aggregation. Influence of Hydrophobic Copolypeptides on the Properties of Poly (L-histidine). *Polymers*. 2017;9:564.
- [201] Zhang Y, Song H, Zhang H, Huang P, Liu J, Chu L, et al. Fine tuning the assembly and gel behaviors of PEG ylated polypeptide conjugates by the copolymerization of l-alanine and  $\gamma$ -benzyl-l-glutamate N-carboxyanhydrides. *Journal of Polymer Science Part A: Polymer Chemistry*. 2017;55:1512-23.
- [202] Lin H-C, Chen C-Y, Kao C-W, Wu S-T, Chen C-L, Shen C-R, et al. In situ gelling-polypeptide hydrogel systems for the subcutaneous transplantation of MIN6 cells. *Journal of Polymer Research*. 2020;27:64.

- [203] Peng S, Wu CW, Lin JY, Yang CY, Cheng MH, Chu IM. Promoting chondrocyte cell clustering through tuning of a poly(ethylene glycol)-poly(peptide) thermosensitive hydrogel with distinctive microarchitecture. *Materials Science and Engineering C: Materials for Biological Applications*. 2017;76:181-9.
- [204] Tinajero-Díaz E, Martínez de Ilarduya A, Muñoz-Guerra S. Block and Graft Copolymers Made of 16-Membered Macrolactones and L-Alanine: A Comparative Study. *Macromolecular Chemistry and Physics*. 2019;220:1900214.
- [205] Lin H-C, Anggelia MR, Cheng C-C, Ku K-L, Cheng H-Y, Wen C-J, et al. A Mixed Thermosensitive Hydrogel System for Sustained Delivery of Tacrolimus for Immunosuppressive Therapy. *Pharmaceutics*. 2019;11:413.
- [206] Tsuchiya K, Numata K. Facile terminal functionalization of peptides by protease-catalyzed chemoenzymatic polymerization toward synthesis of polymeric architectures consisting of peptides. *Polymer Chemistry*. 2020;11:560-7.
- [207] Devarayan K, Nakagami S, Suzuki S, Yuki I, Ohkawa K. Electrospinning and Post-Spun Chain Conformations of Synthetic, Hydrophobic Poly ( $\alpha$ -amino acid) s. *Polymers*. 2020;12:327.
- [208] Ageitos JM, Baker PJ, Sugahara M, Numata K. Proteinase K-Catalyzed Synthesis of Linear and Star Oligo(L-phenylalanine) Conjugates. *Biomacromolecules*. 2013;14:3635.
- [209] Chen K-J, Chen H-L, Tang C-C, Wu H-H, Jan J-S. Synthesis of silica/polypeptide hybrid nanomaterials and mesoporous silica by molecular replication of sheet-like polypeptide complexes through biomimetic mineralization. *Journal of Colloid and Interface Science*. 2019;542:243-52.

- [210] Centore R, Totsingan F, Amason A-C, Lyons S, Zha RH, Gross RA. Self-Assembly-Assisted Kinetically Controlled Papain-Catalyzed Formation of mPEG-b-Phe(Leu)<sub>x</sub>. *Biomacromolecules*. 2020;21:493-507.
- [211] Wang J, Lu H, Kamat R, Pingali SV, Urban VS, Cheng J, et al. Supramolecular Polymerization from Polypeptide-Grafted Comb Polymers. *Journal of the American Chemical Society*. 2011;133:12906-9.
- [212] Perry SL, Leon L, Hoffmann KQ, Kade MJ, Priftis D, Black KA, et al. Chirality-selected phase behaviour in ionic polypeptide complexes. *Nature Communications*. 2015;6:6052.
- [213] Matolyak LE, Thompson CB, Li B, Keum JK, Cowen JE, Tomazin RS, et al. Secondary-Structure-Mediated Hierarchy and Mechanics in Polyurea–Peptide Hybrids. *Biomacromolecules*. 2018;19:3445-55.
- [214] Naik SS, Savin DA. Poly(Z-lysine)-Based Organogels: Effect of Interfacial Frustration on Gel Strength. *Macromolecules*. 2009;42:7114-21.
- [215] You Y, Chen Y, Hua C, Dong C-M. Synthesis and thermoreversible gelation of dendron-like polypeptide/linear poly( $\epsilon$ -caprolactone)/dendron-like polypeptide triblock copolymers. *Journal of Polymer Science Part A: Polymer Chemistry*. 2010;48:709-18.
- [216] Fan J, Zou J, He X, Zhang F, Zhang S, Raymond JE, et al. Tunable mechano-responsive organogels by ring-opening copolymerizations of N-carboxyanhydrides. *Chemical Science*. 2014;5:141-50.

- [217] He X, Fan J, Zhang F, Li R, Pollack KA, Raymond JE, et al. Multi-responsive hydrogels derived from the self-assembly of tethered allyl-functionalized racemic oligopeptides. *Journal of Materials Chemistry B*. 2014;2:8123-30.
- [218] Zou J, He X, Fan J, Raymond JE, Wooley KL. Supramolecularly Knitted Tethered Oligopeptide/Single-Walled Carbon Nanotube Organogels. *Chemistry – A European Journal*. 2014;20:8842-7.
- [219] Shen Y, Zhang S, Wan Y, Fu W, Li Z. Hydrogels assembled from star-shaped polypeptides with a dendrimer as the core. *Soft Matter*. 2015;11:2945-51.
- [220] Wan Y, Wang Z, Sun J, Li Z. Extremely Stable Supramolecular Hydrogels Assembled from Nonionic Peptide Amphiphiles. *Langmuir*. 2016;32:7512-8.
- [221] Wan Y, Liu L, Yuan S, Sun J, Li Z. pH-Responsive Peptide Supramolecular Hydrogels with Antibacterial Activity. *Langmuir*. 2017;33:3234-40.
- [222] Liu R, Shi Z, Sun J, Li Z. Enzyme responsive supramolecular hydrogels assembled from nonionic peptide amphiphiles. *Science China Chemistry*. 2018;61:1314-9.

**Appendix A: Overview of different  $\beta$ -sheet forming polypeptides, synthetic methods, and architectures for silk mimicry with the respective natural construct used as a blueprint and characterization methods**

Peptidic component <sup>[a]</sup>	Structure Ref. <sup>[b]</sup>	Other peptides/ polymers/ materials	Natural Blueprint	Polymerization Method	Morphology	Secondary Structure Composition	Ref.
PLAla	D1	None	None, compared against silk fibroin	NCA ROP	Films	Exact not specified Identification of secondary structure with FIR spectra bands	[89]
PLAla- <i>r</i> -PDAla	D2						
PLAla- <i>r</i> -poly(glycine) (PGly)	D3						
PLAla	D1	None	Silkworm Silk fibroin	Solid-phase synthesis and NCA ROP	None shown	Higher $\alpha$ -helical content in polymers in which glycine is in the <i>i</i> -th and the ( <i>i</i> +3) residue positions  Higher $\beta$ -sheet content in polymers in which glycine is in the <i>i</i> -th residue positions ( <i>i</i> +2) and ( <i>i</i> +4)  The less repeat units the less stable the $\alpha$ -helices.	[87]
P(PLAla <sub>2</sub> -Gly)	D4						
P(PLAla <sub>3</sub> -Gly)	D5						
P(LAla-PGly <sub>2</sub> )	D6						
Poly(DL-glutamic acid) (PDLGlu)- <i>b</i> -PLAla- <i>b</i> -PDLGlu	D7						
PDLGlu- <i>b</i> -P(PLAla <sub>2</sub> -Gly)- <i>b</i> -PDLGlu	D8						
PDLGlu- <i>b</i> -P(PLAla <sub>3</sub> -Gly)- <i>b</i> -PDLGlu	D9						

PDLGlu- <i>b</i> -P(LAla-PGly <sub>2</sub> )- <i>b</i> -PDLGlu	D10						
P(LAla-LVal-Gly)	D11	None	Silk fibroin	NCA ROP	None shown	Decreased by treatment with dichloroacetic acid from predominantly $\beta$ -form to $\alpha$ -helical form Alternation of the simple tripeptide sequence change the conformation of the peptide	[166]
P(LVal-LAla-Gly)	D12						
PLAla- <i>r</i> -PGly	D3	None	No mention	NCA ROP	Spherical aggregates		[167]
PLLys/PLGlu	D13/D14	None	Silk structure	NCA ROP	Fibers	Exact not specified  Increase of glycine content increase the cross- $\beta$ structure	[168]
PLAla	D1	Poly(2-acryloyloxy ethyl-lactoside)	Spider silk	Sequential ATRP and NCA ROP	Spherical aggregates	Ratio of $\alpha$ -helix/ $\beta$ -sheet secondary structure increased for PLAla end blocks with increased block length	[169]
PLAla	D1	Poly ( $\epsilon$ -caprolactone) (PCL)	Spider silk	NCA ROP	Film	Exact not specified Predominant antiparallel $\beta$ -sheet, less content of random coil conformation	[170]
P((Gly-LAla-Gly-LAla)- <i>b</i> -PEG- <i>b</i> -(LAla-Gly-LAla-Gly))	D15	PEG	Nephila clavipes and	Step-growth polymerization	Films	Solution synthesis led to antiparallel stacking of $\beta$ -sheets - higher $\beta$ -	[80-83]

P(PLAAla- <i>b</i> -PEG- <i>b</i> -PLAAla)	D16		Bombyx mori			sheet content compared to other conformations	
						Interfacial polymerization led to lower $\beta$ -sheet content and an increase in random coil proportion	

<sup>[a]</sup> Polypeptides of repetitive amino acid sequences are indicated using the appropriate abbreviation

<sup>[b]</sup> Polymer structure can be found in Appendix D under the corresponding code.

## Appendix B: Overview of different poly(alanine)-based polymers, secondary structure, and other applicable properties

Peptide-bearing copolymer	Structure Ref. <sup>[a]</sup>	Morphology	Secondary Structure Composition	Mechanical Properties	Other materials and Applicable Properties	Ref.
PLAAla- <i>r</i> - poly(DL-alanine) (PDLAla)- <i>b</i> -PLX- <i>b</i> -PLAAla- <i>r</i> -PDLAla (end-capped with alkyl end group)	D17	Hydrogel	Not specified Predominant $\beta$ -sheet, increase with alkyl chain size	Storage Moduli (50 °C): ~200-1000 Pa Increase with alkyl chain size	Thermally induced gelation	[145]
PLAAla- <i>r</i> -PDLAla- <i>b</i> -PLX- <i>b</i> -PLAAla- <i>r</i> -PDLAla	D18	Hydrogel	Depending on ratio of L-:DL- stereoisomer, (increasing DL increases random coils) $\beta$ -sheet (18-43%), $\alpha$ -helix (13-29%) random coil (20-66%), others (3-12%)	Storage Moduli (37 °C after 100 min): ~1600-700 Pa Overall decrease with increasing DL	Morphological control in 2D and 3D chondrocyte cell cultures  <i>In vivo</i> injection and native cell biomarker expression	[148]
Poly [N5-(2-hydroxyethyl)-L-glutamine] (PHLG)- <i>r</i> -PLAAla- <i>r</i> -Poly(L-lysine-g-methylacrylate) (PMLL)	D19	Hydrogel (crosslinked through methacrylate side chains)	No analysis	None shown	Chemically crosslinked with (Hydroxyethyl)methacrylate (HEMA)  Porcine mesenchymal stem cells (MSC) culture on surface with cell adhesive motifs	[171]
PLAAla	D1	Hydrogel	Decreased $\beta$ -sheet and increased $\alpha$ -helix with	Storage Moduli (40 °C): ~10-1000 Pa	Thermally induced gelation	[172]
PEG- <i>b</i> -PLAAla	D20					



<b>PEG-<i>b</i>-PDLAAla</b>	D21		<p>increased PEG length</p> <p><math>\beta</math>-sheet (36-74%), <math>\alpha</math>-helix (4-42%) random coil (5-24%), others (5-17%)</p> <p>(Except for PDLAAla containing hydrogels which is majority random coils)</p>	Increase with increasing PEG length		
<b>chitosan-<i>g</i>-(PLAAla-<i>b</i>-PEG)</b>	D22	Hydrogel	<p>Non-specific, significant <math>\beta</math>-sheet and <math>\alpha</math>-helical content, with <math>\alpha</math>-helical content increasing with temperature and decreasing with pH</p>	<p>Storage Moduli (37°C): 43-396 Pa</p> <p>Increase with decreasing pH</p>	Thermally induced gelation	[97]
<b>PLAAla-<i>r</i>-PLLeu-<i>b</i>-PLX-<i>b</i>-PLAAla-<i>r</i>-PLLeu</b>	D23	Hydrogel	<p>Increased <math>\beta</math>-sheet and decreased <math>\alpha</math>-helix with</p> <p><math>\beta</math>-sheet (31-42%), <math>\alpha</math>-helix (37-48%), random coil (21-22%)</p>	<p>Storage Moduli (37°C): 380 Pa</p>	<p>Thermally induced gelation</p> <p>~50-95% mass loss over six days in proteinase K, elastase and MMP-12</p> <p><i>In vivo</i> injection, long term dissolution</p> <p>FITC-labeled bovine serum albumin (BSA) zeroth-order</p>	[173]

					kinetics release over sustained period	
<b>PEG-<i>b</i>-PLAAla-<i>b</i>-PDLAAla</b>	D24	Hydrogel	Unspecified, but significant proportions of both $\alpha$ -helices and $\beta$ -sheets	Storage Moduli (40 °C): PEG- <i>b</i> -PLAAla- <i>b</i> -PDLAAla: ~300 Pa  PEG- <i>b</i> -PDLAAla- <i>b</i> -PLAAla: ~1000 Pa	None shown	[174]
<b>PEG-<i>b</i>-PDLAAla-<i>b</i>-PLAAla</b>	D25					
<b>PHLG-<i>r</i>-PLAAla-<i>r</i>-PMLL</b>	D19	Hydrogel (crosslinked through methacrylate side chains)	No analysis performed	Not stated	>50% mass loss over six days in elastase	[175]
<b>PLAAla-<i>r</i>-PDLAAla-<i>b</i>-PLX-<i>b</i>-PLAAla-<i>r</i>-PDLAAla</b>	D18	Hydrogel	Increased $\beta$ -sheet with increased concentration $\beta$ -sheet (37-47%), $\alpha$ -helix (22-25%), random coil (20-24%), others (9-18%)	Storage Moduli (37 °C): ~100-6000 Pa  Increase with concentration	Thermally induced gelation  3D chondrocyte cell culture  Cell biomarker expression	[146]
<b>PLAAla</b>	D1	None	Unspecified, significant $\alpha$ -helix and $\beta$ -sheet	N/A	None shown	[176]
<b>PBLG-<i>b</i>-PLAAla</b>	D26					
<b>PBLG-<i>b</i>-PLAAla-<i>b</i>-PZLL</b>	D27					

<b>PBLG-<i>b</i>-PLAla-<i>b</i>-PZLL-<i>b</i>-PBLA</b>	D28					
<b>PBLG-<i>b</i>-PZLL-<i>b</i>-PLAla</b>	D29					
<b>PLlys-<i>b</i>-PLAla</b>	D30	Hydrogel (genipin crosslinking)	In all cases, predominantly random coil	Compressive Strength: 30-120 kPa  Increase with overall polypeptide length	Biosilification ( <i>via</i> calcination)  Morphological control of 3T3 fibroblast cell culture on surface	[177]
<b>PEG-<i>b</i>-PLAla-Abz(azobenzene)-<i>b</i>-PLAla-<i>b</i>-PEG</b>	D31	Hydrogel	Under UV light: $\beta$ -sheet (40.8%), $\alpha$ -helix (7.0%), random coil (46.4%), others (5.8%)  Under visible light: $\beta$ -sheet (44.1%), $\alpha$ -helix (8.2%), random coil (40.5%), others (7.2%)	Storage Moduli (37°C): ~1000-1500 Pa  Higher under UV	Thermally induced gelation	[92]
<b>chitosan-<i>g</i>-(PLAla-<i>r</i>-PLPhe-<i>b</i>-PEG)</b>	D32	Hydrogel	Not broken down, primarily $\alpha$ -helix	Storage Moduli (37°C): 128 Pa	Thermally induced gelation  <i>In vivo</i> injection, long term dissolution  Histologically compatible	[178]

<b>PEG-<i>b</i>-PLAla-<i>r</i>-PLPhe</b>	D33	Hydrogel	Not broken down, primarily $\alpha$ -helix	Storage Moduli (37°C): ~150 Pa	Thermally induced gelation  <i>In vivo</i> injection, long term dissolution for L-isomer only	[159]
<b>PEG-<i>b</i>-PDAla-<i>r</i>-PDPhe</b>	D34				Histologically compatible L-isomer, irritation with D-isomer	
<b>PEG-<i>b</i>-PLAla-<i>r</i>-PLPhe</b>	D33	Hydrogel	$\beta$ -sheet (46%), $\alpha$ -helix (28%), random coil (26%)	Storage Moduli (37°C): ~150 Pa	Thermally induced gelation  <i>In vivo</i> injection, long term dissolution  Marginal inflammatory response  Human growth hormone (hGH) zeroth-order kinetics release over sustained period	[160]
<b>PLLys</b>	D13	Hydrogel	No analysis performed	Storage Moduli: 1400 Pa	3T3 fibroblast cell culture on surface with increased mitochondrial activity	[179]
<b>PLAla-<i>r</i>-PLLys</b>	D35	(chemical crosslinking via 6-arm PEG-ASG (NHS groups))			Inhibition against <i>E. coli</i> and <i>S. aureus</i>	
<b>PLAla</b> <b>PDAla</b>	D1	None	<u>L-enantiomer</u> Predominantly $\alpha$ -helix <u>D-enantiomer</u> Predominantly $\beta$ -sheet Predominantly $\alpha$ -helix in	N/A	None shown	[86]

			hexafluoroisopropanol (HFIP)			
<b>PEG-<i>b</i>-PLAAla</b>	D20	Hydrogel	$\beta$ -sheet (65%), $\alpha$ -helix (17%), random coil (14%), others (4%)	Storage Moduli (37°C): 600 Pa	Thermally induced gelation  Fibroblast cell culture within hydrogel with altered mRNA expression for collagen type I and II  <i>In vivo</i> wound healing	[144]
<b>PLAAla</b>	D1	None	No secondary structure analysis performed	N/A	None Shown	[180, 181]
<b>PBLG-<i>b</i>-PLAAla</b>	D26					
<b>PLAAla-<i>r</i>-PDLAAla-<i>b</i>-PLX-<i>b</i>-PLAAla-<i>r</i>-PDLAAla</b>	D18	Hydrogel	Predominantly $\beta$ -sheet	Storage Moduli: 270-1600 Pa  Increase with decreasing hyaluronic acid concentration	Fibril alignment upon inclusion of hyaluronic acid  Chondrocyte cell culture within hydrogel  Biomarker and mRNA expression for collagen type I and II	[147]
<b>PBLG-<i>b</i>-PLAAla</b>	D26	None	No analysis performed	N/A	None shown	[182]
<b>PLAAla</b>	D1	Film	Predominantly $\beta$ -sheet	Storage Modulus: ~400-1000 kPa  Increase with decreasing PLAAla length	PCL and hexamethylene diisocyanate (HDI) linkers  Strong tensile hysteresis	[170]

<b>PEG-<i>b</i>-PLAla-<i>r</i>-PDAla-<i>b</i>-PLPhe</b>	D36	Hydrogel	Predominantly $\beta$ -sheet with increasing $\alpha$ -helix content with increasing D-enantiomer	Storage Modulus (37°C): ~0.1-500 Pa  Higher with only single stereoisomer	Thermally induced gelation  Degraded polymer size over three days in elastase	[163]
<b>4-arm PEG-<i>b</i>-PLAla</b>	D37	Hydrogel	Predominantly $\alpha$ -helix for DP 5, an increase of $\beta$ -sheet content with arm length DP 10	Storage Modulus: ~10 kPa	Degradation over 18 h by elastase  FITC-labeled albumin release sustained with elastase	[96]
<b>PLAla-<i>r</i>-PBLA-<i>r</i>-PLPhe-<i>b</i>-PLX-<i>b</i>-PLAla-<i>r</i>-PBLA-<i>r</i>-PLPhe</b>  <b>PLAla-<i>r</i>-poly(L-aspartic acid) (PLAsp)-<i>r</i>-PLPhe-<i>b</i>-PLX-<i>b</i>-PLAla-<i>r</i>-PLAsp-<i>r</i>-PLPhe</b>	D38  D39	Hydrogel	Increase in $\beta$ -sheet and decrease of $\alpha$ -helix with increase temperature and deprotection of benzyl group on PLAsp  $\beta$ -sheet (4-45%), $\alpha$ -helix (~10-58%), random coil (~38-50%)	Storage Modulus (50°C): ~0-600 Pa  Increase with PBLA deprotection	Thermally induced gelation  Low cytotoxicity to human retinal pigment epithelial cells	[183]
<b>Poly(L-arginine) (PLArg)-<i>b</i>-PLAla</b>	D40	Hydrogel	Predominantly $\beta$ -sheet	None shown	None shown	[184]
<b>P(PLAla-<i>b</i>-PEG-<i>b</i>-PLAla-<i>b</i>-EDTA)</b>	D41	Hydrogel	Predominantly $\alpha$ -helix	Storage Modulus (37°C): 28-110 Pa	Thermally induced gelation	[185]

				Increase with decreasing ion binding affinity	Cu <sup>2+</sup> , Zn <sup>2+</sup> and Ca <sup>2+</sup> binding to anionic ethylenediamine tetraacetic acid (EDTA)	
<b>PEG-<i>b</i>-PLAla</b>	D20	Hydrogel	None	Storage Modulus (37°C): ~400 Pa	Incorporation of functionalized polystyrene microspheres  Thermally induced gelation  Morphological and cell differentiation control of tonsil-tissue-derived mesenchymal stem cells (TSMCs) cultured in hydrogels	[186]
<b>PLLys-<i>b</i>-PLAla</b>	D30	Hydrogel	None performed	Storage Modulus: 10-50 Pa  Increase with longer alanine peptides and lower cholesterol loading	Sustained cholesterol and temozolomide release  <i>In vivo</i> injection, biomarker increase with tamoxifen release	[152]
<b>PLLys-<i>b</i>-PLAla-<i>r</i>-PLLeu</b>	D42					
<b>PLLys-<i>b</i>-PLLeu</b>	D43					
<b>PLLys-<i>b</i>-PLPhe</b>						
<b>PLAla</b>	D1	Films	None performed	N/A	Human mesenchymal stem cells cultured on crystals and films	[187]
<b>PLLys</b>	D13					
<b>PLLys-<i>b</i>-PLAla</b>	D30					

<b>Polyethyleneimine (PEI)-g-PLAAla</b>	D44	Nanostructures	None performed	N/A	DNA transfection into HeLa, 293T, A549 and CHO cell lines	[188]
<b>P(thiophene)-g-PLAAla-glucose oxidase</b>	D45	Surface/Film	None performed	None shown	Glucose sensing at range of 0.01-0.1 mM  Moderate antimicrobial activity against <i>E. coli</i> and <i>S. aureus</i>	[141]
<b>PLAAla</b>	D1	None	None	N/A	None shown	[189]
<b>PEG-b-PLAAla</b>	D20	Hydrogel	Predominantly $\beta$ -sheet	Storage Modulus (37°C): 700-100 Pa	Thermally induced gelation  Tonsil-Derived Mesenchymal Stromal Cells (TMSC) culture within hydrogels and differentiation with hepatogenic growth factors	[190]
<b>PLGlu-<i>r</i>-PLLys-<i>r</i>-PLAAla-<i>r</i>-PLTyr</b>	D46	Nanostructures	Increase in $\beta$ -strands and decrease in $\alpha$ -helix with increase in temperature  $\beta$ -strand (9.2-29.4%), $\beta$ -turn (18.4-21.5%) $\alpha$ -helix (15.2-37.8%), random coil (32.7-33.6%)	N/A	None-shown	[191]
<b>PLAAla-b-poly(L-histidine) (PLHis)</b>	D47	Nanostructures	Majority $\beta$ -sheet	N/A	Histidine tagging to gold nanoparticles	[192]



<b>PEG-<i>b</i>-PLAAla-<i>r</i>-PLPhe</b>	D33	Hydrogel	Decreased $\beta$ -sheet and increased $\alpha$ -helices with increase in overall polymer size $\beta$ -sheet (29-36%), $\alpha$ -helix (34-48%), random coil (20-22%), others (1-10%)	Storage Modulus (37°C): 135-240 Pa (37°C) Increase with overall increase in polymer length	Thermally induced gelation  <i>In vivo</i> injection loaded with native cells  rhGH (recombinant human growth hormone) release sustained <i>in vitro</i> and <i>in vivo</i>	[193]
<b>PEG<sub>2</sub>LG-<i>r</i>-PLAAla</b>	D48	Hydrogel	Predominantly $\alpha$ -helical	Storage Modulus: 115-3600 Pa  Increase with increased PEG size and decreased PEG <sub>2</sub> LG length	Tunable thermally induced gelation	[194]
<b>PEG-<i>b</i>-PEG<sub>2</sub>LG-<i>r</i>-PLAAla</b>	D49					
<b>PEG<sub>2</sub>DLG-<i>b</i>-PLLeu</b>	D50	Hydrogels (Other polypeptides investigated in study, but focused on those presented)	Decrease in $\alpha$ -helix with increase in temperature for PEG <sub>2</sub> DLG- <i>b</i> -PEG <sub>2</sub> LG- <i>r</i> -PLLeu	Storage Modulus (40°C): ~50-1000 Pa  Increase with increased PEG <sub>2</sub> LG- <i>r</i> -PLLeu size	Thermally induced gelation  Sustained release of chicken egg white lysozyme  MSC cell compatibility	[123]
<b>PEG<sub>2</sub>DLG-<i>b</i>-PEG<sub>2</sub>LG-<i>r</i>-PLLeu</b>	D51					
<b>PEG<sub>2</sub>DLG-<i>b</i>-PEG<sub>1</sub>LG-<i>r</i>-PEG<sub>2</sub>LG-<i>r</i>-PLLeu</b>	D52					
<b>PEG<sub>2</sub>DLG-<i>b</i>-PEG<sub>2</sub>LG-<i>r</i>-PLAAla</b>	D53					
<b>PLAAla-<i>b</i>-PLGlu-C6-PLGlu-<i>b</i>-PLAAla<sup>[b]</sup></b>	D54	Hydrogel	Predominantly $\beta$ -sheet at pH 7.4	Storage Modulus:	Thermally induced gelation (cooling)	[195]

			Predominantly $\alpha$ -helix at pH 4	~40-120 kPa Increase at pH 7.4 and PBS 0.15 M NaCl	pH sensitive gelation (pH 7.4 from 4)	
<b>8-arm PZLL-<i>b</i>-PLAla</b>	D55	Attempted Hydrogel (other residues found greater success)	Predominantly random coil	N/A	No gelation compared to other hydrophobic residues (valine, tyrosine, and phenylalanine)	[95]
<b>PLAla-O-R<sup>[c]</sup></b>	D56	None	Predominantly $\beta$ -sheets	N/A	Thermal degradation	[196]
<b>PGly-O-R</b>	D57					
<b>PLAla-<i>r</i>-PGly</b>	D58					
<b>PLLys-<i>b</i>-PLAla-<i>b</i>-PLX-<i>b</i>-PLAla-<i>b</i>-PLLys</b>	D59	Hydrogel	Increase in $\beta$ -sheet and decrease in $\alpha$ -helix with increased temperature  $\beta$ -sheet (2-4%), $\alpha$ -helix (58-61%), other (37-38%)	Storage Modulus (40 °C): ~8 Pa	Thermally induced gelation  2D and 3D MC3T3-E1 cell culture  32% mass loss over seven days in elastase  BSA-FITC release with zeroth-order kinetics over ~180 h	[93]
<b>P(thiophene)-<i>g</i>-PLAla-aptamer</b>	D45	Surface	None shown	None shown	Cocaine sensing at range of 2.5-10 nM  Benzoylecgonine sensing at range of 0.5-50 $\mu$ M	[142]

<b>Bzl-PLAla-<i>b</i>-PLGlu-C6-PLGlu-<i>b</i>-PLAla-Bzl<sup>[b]</sup></b>	D60	Hydrogel	Predominantly $\beta$ -sheet	Storage Moduli: ~10-200 kPa  Increase at pH 4 and PBS 0.15 M NaCl	Thermally induced gelation (cooling)  pH sensitive gelation (pH 4.0 from 6.5)  Embedded with PCL-PEG-P2VP-PEG-PCL vesicles  Sustained release of calcein  A549 cell viability	[197]
<b>PLAla-<i>b</i>-PLX-<i>b</i>-PLAla</b>	D61	Hydrogel	Increasing $\alpha$ -helical content with alanine length	Storage Moduli: ~100-1000 kPa  Increase with lower $\alpha$ -helical content	Thermally induced gelation  Chondrocyte cultured within hydrogels  <i>In vivo</i> injection	[198]
<b>PEG-<i>b</i>-PLAla-<i>r</i>-PLPhe</b>	D33	Hydrogel	No analysis performed	Storage Modulus (40 °C): ~300 Pa	Thermally induced gelation  Doxorubicin (DOX) and Combretastatin A4 (CA4) combined and sustained release  58.8-92.2% mass loss over 28 days in PBS pH 7.4 and elastase  <i>In vivo</i> injection and tumor treatment	[199]

<b>PEG-<i>b</i>-PLAAla</b>	D20	Hydrogel	Predominantly $\alpha$ -helical	Storage Modulus (37°C): ~600-1000 Pa  Concentration adjusted to achieve range	Thermally induced gelation  Morphological control of Adipose-tissue-derived stem cells (ADSC) cultured in hydrogels  Biomarkers for neurogenesis and myogenesis observed during culture  <i>In vivo</i> injection  Histological compatibility	[162]
<b>PEG-<i>b</i>-PLHis-<i>r</i>-PLAAla</b>	D62	Nanostructures	Primarily $\alpha$ -helix and random coil	N/A	None shown	[200]
<b>PEG-<i>b</i>-PLAAla</b>  <b>PEG-<i>b</i>-PLAAla-<i>r</i>-PBLG</b>	D20  D63	Hydrogels	Highly dependent on ratios and length	Storage modulus (40 °C): 100-600 Pa  Increase with overall increase in polypeptide block length	Sustained nanosilver release with subsequent antibacterial activity against <i>S. aureus</i> and <i>B. subtilis</i>	[201]
<b>PEG-<i>b</i>-PLAAla-<i>r</i>-PGly-<i>r</i>-PLIle</b>	D64	Hydrogels	Primarily $\beta$ -sheet	Not shown	Thermally induced gelation  ~50% mass loss over 10 days in Tris-HCl 0.05 M, pH 8.0	[151]

					30-90% mass loss over four days in proteinase K and MMP-2	
					Sustained release of naproxen	
<b>PEG-<i>b</i>-PLA<sub>12</sub></b>	D20	Hydrogel	Not analyzed	Storage modulus (40 °C): ~1.5 Pa	Thermally induced gelation  ~15% mass loss over 7 days in PBS  ~75% mass loss over 10 days in elastase  2D and 3D culture of MIN6 cells  Sustained release of BSA  <i>In vivo</i> injection, mild inflammation	[202]
<b>PEG-<i>b</i>-PLA<sub>12</sub></b>	D20	Hydrogel	Increase in antiparallel $\beta$ -sheets with lower PLA <sub>12</sub> DP (except for DP ~10 which has lower $\beta$ -sheet content than DP ~13)  antiparallel $\beta$ -sheet (23.5-43.3%), parallel $\beta$ -sheet	Storage modulus (40 °C): 63-844 Pa  Increase with increase PLA <sub>12</sub> length	Thermally induced gelation  Chondrocyte culture and resultant clustering within hydrogel with glycosaminoglycans (GAGs) and collagen	[203]

			(11.5-12.6%), $\alpha$ -helix (18.5-22.2%), random coil (40.7-42.6%)			
<b>PLAla-<i>b</i>-PEG-<i>b</i>-PLAla</b>	D65	Hydrogel	No analysis performed	Storage modulus (37 °C): 138-579 Pa	Thermally induced gelation	[91]
<b>PLAla-<i>r</i>-PLPhe-<i>b</i>-PEG-<i>b</i>-PLAla-<i>r</i>-PLPhe</b>	D66			Increase with increasing PLPhe length	Bone marrow mesenchymal stem cell culture within hydrogel  <i>In vivo</i> injection in osteochondral defects with increased GAGs and collagen type II expression	
<b>(Polypentdecylactone) PPDL-<i>b</i>-PLAla</b>	D67	Nanostructures	Significant $\alpha$ -helix and $\beta$ -sheets	N/A	None shown	[204]
<b>(Polyglobalide) PGI-<i>g</i>-PLAla</b>	D68					
<b>PLLys-<i>b</i>-PLAla-<i>b</i>-PLX-<i>b</i>-PLAla-<i>b</i>-PLLys</b>	D59	Hydrogel	Based on [93]  Increase in $\beta$ -sheet and decrease in $\alpha$ -helix with increased temperature  $\beta$ -sheet (2-4%), $\alpha$ -helix (58-61%), other (37-38%)	Not shown	Thermally induced gelation  293T cell culture within hydrogel  ~55-82% mass loss over 14 days in PBS and elastase  <i>In vivo</i> injection and sustained release of Tacrolimus	[205]
<b>Poly(Sulfoxide methanoinine)</b>	D69	Hydrogel	Predominantly random coil,	Storage modulus:	Polypeptide mixtures to form hydrogel	[94]

<b>(POLM)-<i>r</i>-PLAla-<i>b</i>-PLLys</b>			significant $\beta$ -sheet, increases with the number of blocks	~3-3000 Pa	Self-healing	
<b>POLM-<i>r</i>-PLAla-<i>b</i>-PLLys-<i>b</i>-POLM-<i>r</i>-PLAla</b>	D70			Increase with number of ionic blocks per polypeptide		
<b>POLM-<i>r</i>-PLAla-<i>b</i>-PLLys-<i>b</i>-POLM-<i>r</i>-PLAla-<i>b</i>-PLLys-<i>b</i>-POLM-<i>r</i>-PLAla</b>	D71					
<b>POLM-<i>r</i>-PLAla-<i>b</i>-PLGlu</b>	D72					
<b>POLM-<i>r</i>-PLAla-<i>b</i>-PLGlu-<i>b</i>-POLM-<i>r</i>-PLAla</b>	D73					
<b>POLM-<i>r</i>-PLAla-<i>b</i>-PLGlu-<i>b</i>-POLM-<i>r</i>-PLAla-<i>b</i>-PLGlu-<i>r</i>-POLM-<i>r</i>-PLAla</b>	D74					
<b>PLAla</b>	D1	None shown	Predominantly random coil	N/A	None shown	[206]
<b>C12-<i>b</i>-PLAla</b>	D75					
<b>Poly(N-isopropylacrylamide) (PNIPAM)-<i>b</i>-PLAla</b>	D76					
<b>PLAla</b>	D1	Fiber (electrospun mat)	Predominantly $\alpha$ -helix	Not shown	None shown	[207]

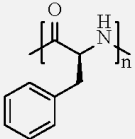
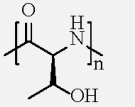
<sup>[a]</sup> Polymer structure can be found in Appendix D under the corresponding code.

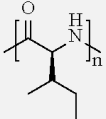
<sup>[b]</sup> CX represents an alkane chain where X is the number of carbons in the alkane chain

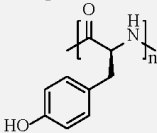
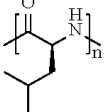
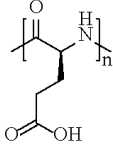
<sup>[c]</sup> R Represents a short chain alkane or a benzyl group.

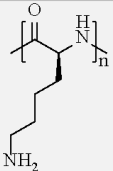
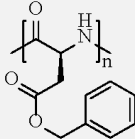
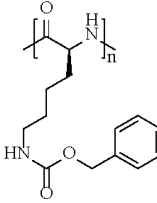


### Appendix C: Overview of different $\beta$ -sheet fibril forming copolymers, synthesis methods and morphologies with mechanical and other applicable properties

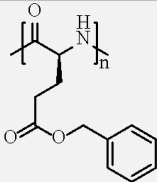
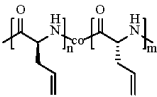
$\beta$ -sheet Forming Peptide	Other peptides/ polymers/ materials	Morphologies	Fibril Dimension	Mechanical Properties	Applicable Properties	Ref.
<b>PLPhe</b> 	Poly(L-lactic acid)	Nanostructures	Fibril width not stated	N/A	None shown	[111, 112]
	None	Hydrogel	Fibril width not stated	None shown	HEK 293 cells cultured in polymer solutions	[208]
<b>PLThr</b> 	PLLys	Nanostructures	Fibril width not stated	N/A	Low cytotoxicity to BEAS-2B and BES-6 human cell lines cultured in polymer solutions  Greater cytotoxicity to A549 and HEPG2 cancer cell lines cultured in polymer solutions  Low haemolytic activity  <i>In vivo</i> reduction of tumor growth	[154]
		Nanogels	Fibril width not stated	N/A	Toxicity towards <i>K. pneumoniae</i>  <i>In vivo</i> tumor necrosis factor (TNF)-related	[153]

					apoptosis-inducing ligands (TRAIL) release and action against towards <i>K. pneumoniae</i>	
		Hydrogel	Fibril width not stated	Storage Modulus: ~40-200 Pa  Increase with increasing PLThr length	None shown	[113]
	PLLys, PLGlu (separate polymer)	Films	Fibril width not stated	None shown	Biosilification (via calcination)	[209]
<b>PLIle</b> 	PLGlu, PNBLC, 4-arm PEG	Hydrogel	Fibril width not stated	Storage modulus: 350 Pa	3D printable and crosslinkable  Dermal fibroblast cell cultured within hydrogel	[109]
	PEG, PLAla (also likely contributes to $\beta$ -sheet), PGly	Hydrogel	13.3 nm	Not shown	Thermally induced gelation  ~50% mass loss over 10 days in Tris-HCl 0.05 M, pH 8.0  30-90% mass loss over four days in proteinase K and MMP-2  Sustained release of naproxen	[151]

<b>PLTyr</b> 	PEG	Hydrogel	Fibril width not stated	Storage Modulus (60 °C): ~125-200 Pa  Increase with increase in temperature	Thermally induced gelation  ~5-20% mass loss over 9 days in Krebs buffer (concentration dependent)  Fast degradation in chymotrypsin  Sustained release of desferrioxamine (DFO)	[110]
<b>PLLeu</b> 	PEG (mixture with and without PEG)	Nanostructures	Fibril width calculated (formed between spherical formations)	N/A	Not shown	[210]
	Poly(allylamine) (PLLeu branched from backbone)	Nanostructures	4.8 nm width	N/A	None shown	[126]
<b>PLGlu</b> 	Poly(norbornene) (grafted from backbone), Gold Nanoparticles (grafted from nanoparticles)	Nanostructures	Not stated	N/A	Grafted from gold nanoparticles	[211]
<b>PLLys</b>	PLLeu	Hydrogel	~ 3 nm from SAXS	Not shown	Hydroxyapatite nanocomposite inclusion	[125]

						
<b>PLLys + PLGlu + PDLys + PDGlu</b>	None	Nanostructures	Fibril width not stated	N/A	None shown	[212]
<b>PBLA</b> 	PDMS, difunctionalised and trifunctionalised isocyanates	Film	Fibril width not stated	<u>Tensile</u> Moduli: 9.8-72.5 MPa Elongation at Break: 52.1-285.0 % Toughness: 0.81-6.47 MJ/m <sup>3</sup>  Overall modulus, extension at break and toughness increase with decreased covalent crosslinking and increased PDMS content	Strong tensile hysteresis	[138]
<b>PZLL</b> 	PEG, difunctionalised and trifunctionalised isocyanates	Film	Fibril width not stated	<u>Tensile (only those with β-sheet)</u> Moduli: 58-96 MPa Strength: 3-8 MPa Elongation at Break: 46-366 % Toughness: 1.3-21.1 MJ/m <sup>3</sup>	None shown	[213]

				Overall modulus, extension at break and toughness increase with decreased PEG content		
	Poly(p-phenylene oxide) (PPO) or polyhedral oligomeric silsesquioxane (POSS)	Organogel (THF, Chloroform)	Fibril width not stated	Storage Modulus: 9-348 Pa  Increase with overall PZLL length	None shown	[214]
<b>PBLA + PZLL</b>	PDMS, difunctionalised and trifunctionalised isocyanates	Film	Fibril width not stated	<u>Tensile (only those without significant <math>\alpha</math>-helix):</u> Moduli: 8.6-43.8 MPa Strength: 1.6-3.4 MPa Elongation at Break: 202.5-669.5 % Toughness: 4.8-12.7 MJ/m <sup>3</sup>  Overall modulus and strength increase with increased PDMS content, overall extension at break and toughness increase with lower PBLA or higher PZLL content	None shown	[137]
<b>PBLG</b>	Pyrenyl endgroup, SWCNT	Nanostructures	50 nm width after coating with SWCNT	N/A	Dispersant for SWCNT	[164]

 <p>(Note: secondary structures focusing on short length)</p>						
	PCL (combination of dendron and linear, though linear promotes greatest $\beta$ -sheet formation)	Organogel (toluene)	20 nm, 13 nm (SAXS)	None shown	Thermally induced gelation	[215]
	PDMS	Nanostructures	~12 nm (10 nm in SAXS)	N/A	None shown	[131]
		Films	4-9 nm	N/A	None shown	[132]
	PEG, PGly	Organogel (DMF)	10.4-14.5 nm	Storage Modulus: 3.0-11.6 kPa  Overall increase with increasing PGly content	Reversible gelation by sonication	[216]
<p><b>PADLG</b></p> 	PEG	Organogel (DMF, DMSO, Methanol)	10-18 nm width 2.5 nm height	Storage Modulus: 20.7 kPa  <u>Compressive Modulus: 25 kPa</u>	Thermally induced gelation  Reversible gelation by sonication	[136]

				Strength: >200 Pa Compression at break: >1.1%		
		Hydrogel	Not stated	Storage Modulus: ~4 kPa	Thermally induced gelation  Reversible gelation by sonication  ~90 wt% mass loss over 2-4 days in trypsin and proteinase  ~80 wt% mass loss over 14 days in Tris HCl pH 8.0	[217]
	PEG, SWCNT (dispersed)	Organogel (DMF)	3.2-8.8 nm width	Storage Modulus: ~400 kPa	Reversible gelation by sonication  Dispersant for SWCNT	[218]
		Organogel (DMF), Film	2.4 – 18.9 nm width	Storage Modulus: 5-20 kPa  Increase with increasing concentration	Reversible gelation by sonication  Film formation upon light-induced crosslinking and drying  Conductive upon SWCNT loading	[165]
<b>PEGLG</b>	PEG	Hydrogel	7.5–14 width 1.5-2.1 nm height	Storage Modulus (30 °C): ~60 Pa	Thermally modifiable storage modulus	[134]

						
	8- and 32- arm core (core first initiation)	Hydrogel	16-23 nm width, 1.1 nm high	Storage Modulus: 24-3350 Pa  Increase with increasing star number and peptide length	None shown	[219]
	Alkyl endgroup	Hydrogel	9-13 nm width, 1 nm high	Storage Modulus: ~1-1000 Pa  Increase with increasing alkyl end group chain length	None shown	[149]
	PEG	Nanostructures	30-70 nm width	N/A	None shown	[133]
	Alkyl endgroup	Organogel (THF, chloroform, dichloromethane (DCM))	8-17 nm width	Not shown	None shown	[150]
<b>Modified PLGlu</b> 	Alkyl endgroup	Hydrogel	4.5 nm width	Storage Modulus: ~20-20,000 Pa  Increase with increasing sidechain length	None shown	[220]



$R = \left\{ \begin{array}{l} \text{---OH} \\ \text{---OH} \\ \text{---O---OH} \\ \text{---OH} \\ \text{---OH} \end{array} \right.$						
$R = \text{---OH}$	PLlys, Sodium alginate (separate polymer)	Hydrogel	Fibril width not stated	Storage Modulus: ~0-1000 Pa  Increase with decrease in PLLys units and upon inclusion of sodium alginate	pH induced gelation (alkali)  Antimicrobial activity against <i>E. coli</i>	[221]
$R = \text{---OH}$	PLTyr (Also contributing to $\beta$ -sheet)	Hydrogel, Nanogel	6-9 nm width, ~7 nm height	Storage Modulus: 100-656 Pa  Increase with overall decrease in length	Further crosslinking with horseradish peroxidase crosslinking	[222]

## Appendix D: Chemical Structure of Polymers Presented

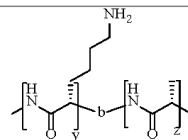
Table Ref.	Polymer	Chemical Structure
D1	PLAla	
D2	PLAla- <i>r</i> -PDAla	
D3	PLAla- <i>r</i> -PGly	
D4	P(PLAla <sub>2</sub> -Gly)	
D5	P(PLAla <sub>3</sub> -Gly)	
D6	P(LAla-PGly <sub>2</sub> )	
D7	PDLGlu- <i>b</i> -PLAla- <i>b</i> -PDLGlu	
D8	PDLGlu- <i>b</i> -P(PLAla <sub>2</sub> -Gly)- <i>b</i> -PDLGlu	
D9	PDLGlu- <i>b</i> -P(PLAla <sub>3</sub> -Gly)- <i>b</i> -PDLGlu	

<b>D10</b>	PDLGlu- <i>b</i> -P(LAla-PGly <sub>2</sub> )- <i>b</i> -PDLGlu	
<b>D11</b>	P(LAla-LVal-Gly)	
<b>D12</b>	P(LVal-LAla-Gly)	
<b>D13</b>	PLLys	
<b>D14</b>	PLGlu	
<b>D15</b>	P((Gly-LAla-Gly-LAla)- <i>b</i> -PEG- <i>b</i> -(LAla-Gly-LAla-Gly))	
<b>D16</b>	P(PLAla- <i>b</i> -PEG- <i>b</i> -PLAla)	
<b>D17</b>	PLAla- <i>r</i> -PDLAla- <i>b</i> -PLX- <i>b</i> -PLAla- <i>r</i> -PDLAla (end-capped with alkyl end group)	

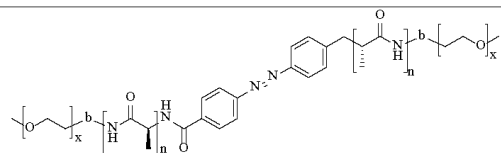
<b>D18</b> PLAla- <i>r</i> -PDLAla- <i>b</i> -PLX- <i>b</i> -PLAla- <i>r</i> -PDLAla	
<b>D19</b> PHLG- <i>r</i> -PLAla- <i>r</i> -PMLL	
<b>D20</b> PEG- <i>b</i> -PLAla	
<b>D21</b> PEG- <i>b</i> -PDLAla	
<b>D22</b> chitosan- <i>g</i> -(PLAla- <i>b</i> -PEG)	
<b>D23</b> PLAla- <i>r</i> -PLLeu- <i>b</i> -PLX- <i>b</i> -PLAla- <i>r</i> -PLLeu	

<b>D24</b>	PEG- <i>b</i> -PLAla- <i>b</i> -PDLAla	
<b>D25</b>	PEG- <i>b</i> -PDLAla- <i>b</i> -PLAla	
<b>D26</b>	PBLG- <i>b</i> -PLAla	
<b>D27</b>	PBLG- <i>b</i> -PLAla- <i>b</i> -PZLL	
<b>D28</b>	PBLG- <i>b</i> -PLAla- <i>b</i> -PZLL- <i>b</i> -PBLA	
<b>D29</b>	PBLG- <i>b</i> -PZLL- <i>b</i> -PLAla	

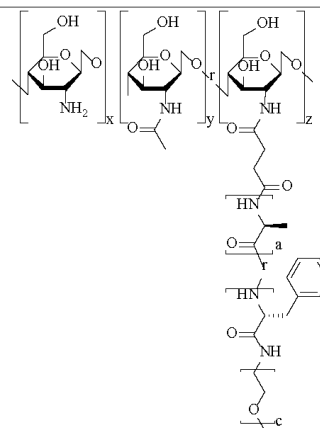
D30 PLLys-*b*-PLAla



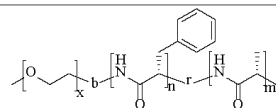
D31 PEG-*b*-PLAla-Abz(azobenzene)-*b*-PLAla-*b*-PEG



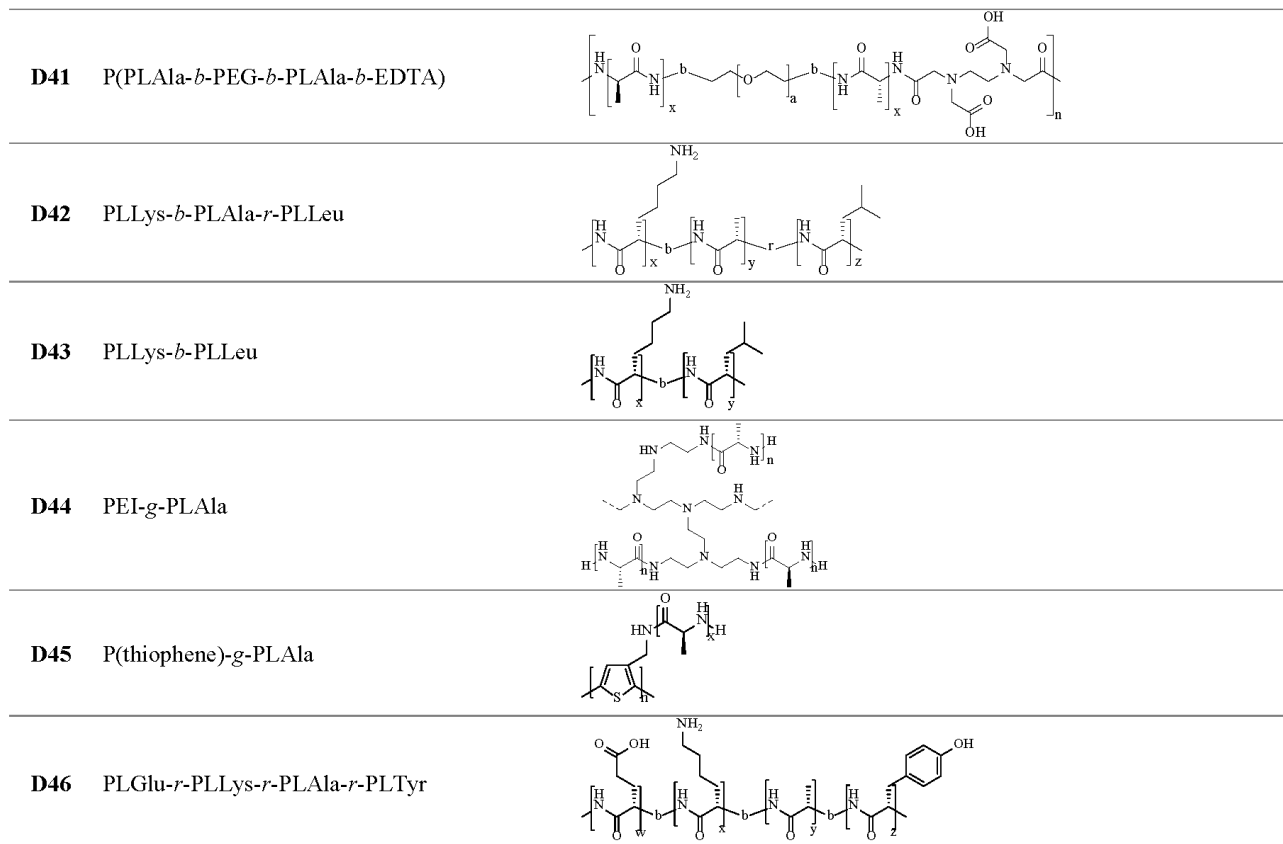
D32 chitosan-*g*-(PLAla-*r*-PLPhe-*b*-PEG)



D33 PEG-*b*-PLAla-*r*-PLPhe



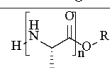
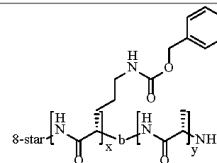
<b>D34</b>	PEG- <i>b</i> -PDAla- <i>r</i> -PDPhe	
<b>D35</b>	PLAla- <i>r</i> -PLLys	
<b>D36</b>	PEG- <i>b</i> -PLAla- <i>r</i> -PDAla- <i>b</i> -PLPhe	
<b>D37</b>	4-arm PEG- <i>b</i> -PLAla	
<b>D38</b>	PLAla- <i>r</i> -PBLA- <i>r</i> -PLPhe- <i>b</i> -PLX- <i>b</i> -PLAla- <i>r</i> -PBLA- <i>r</i> -PLPhe	
<b>D39</b>	PLAla- <i>r</i> -PLAsp- <i>r</i> -PLPhe- <i>b</i> -PLX- <i>b</i> -PLAla- <i>r</i> -PLAsp- <i>r</i> -PLPhe	
<b>D40</b>	PLArg- <i>b</i> -PLAla	



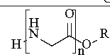
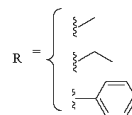


<b>D47</b>	PLAla- <i>b</i> -PLHis	
<b>D48</b>	PEG <sub>2</sub> LG- <i>r</i> -PLAla	
<b>D49</b>	PEG- <i>b</i> -PEG <sub>2</sub> LG- <i>r</i> -PLAla	
<b>D50</b>	PEG <sub>2</sub> DLG- <i>b</i> -PLLeu	
<b>D51</b>	PEG <sub>2</sub> DLG- <i>b</i> -PEG <sub>2</sub> LG- <i>r</i> -PLLeu	
<b>D52</b>	PEG <sub>2</sub> DLG- <i>b</i> -PEG <sub>1</sub> LG- <i>r</i> -PEG <sub>2</sub> LG- <i>r</i> -PLLeu	
<b>D53</b>	PEG <sub>2</sub> DLG- <i>b</i> -PEG <sub>2</sub> LG- <i>r</i> -PLAla	
<b>D54</b>	PLAla- <i>b</i> -PLGlu-C6-PLGlu- <i>b</i> -PLAla	

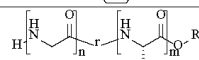
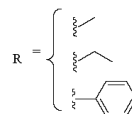
**D55** 8-arm PZLL-*b*-PLAla



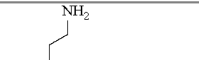
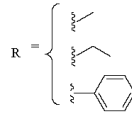
**D56** PLAla-O-R



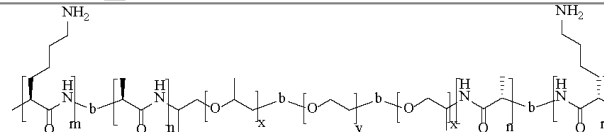
**D57** PLGly-O-R



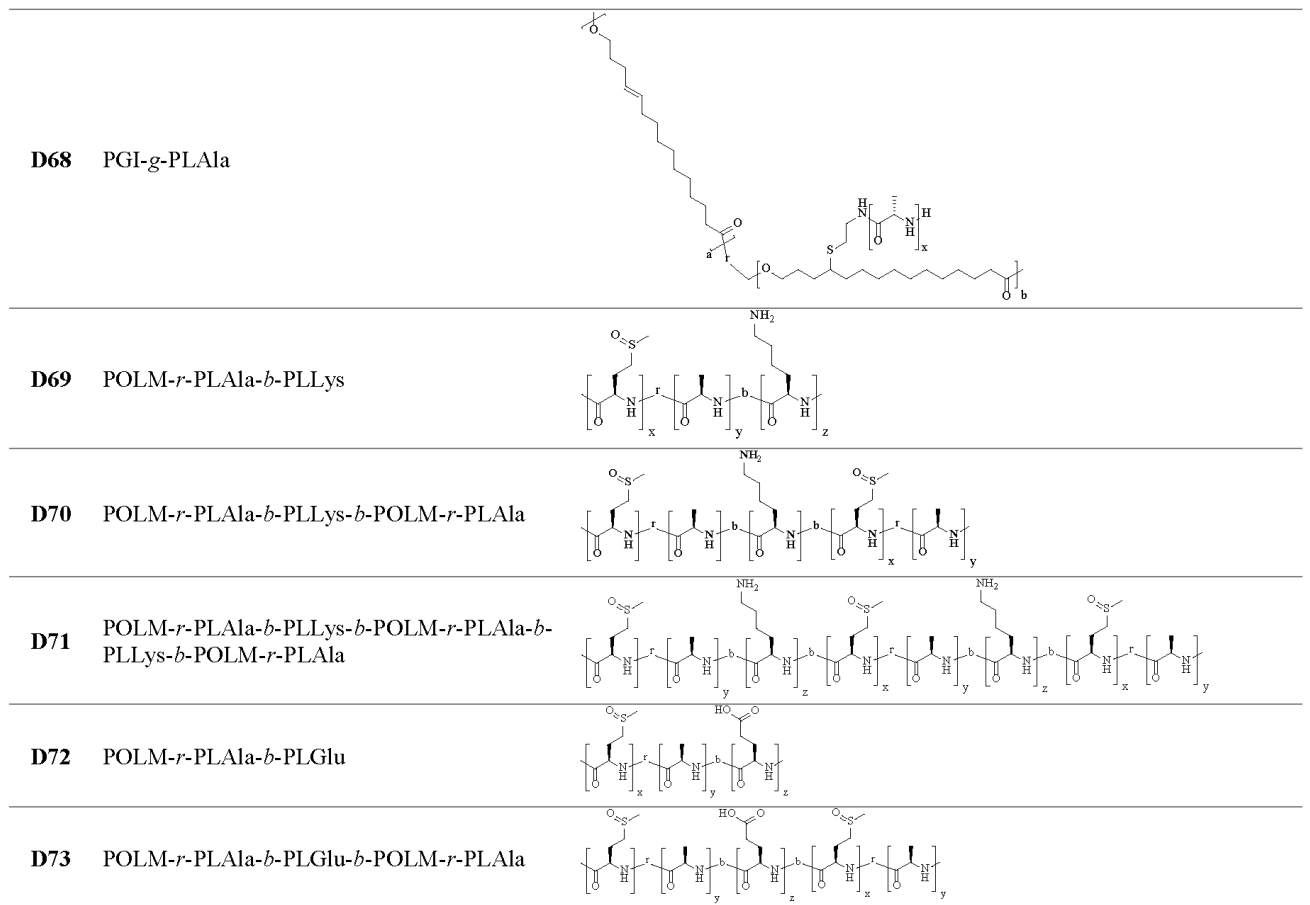
**D58** PLAla-r-PGly-O-R



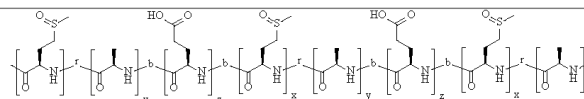
**D59** PLLys-*b*-PLAla-*b*-PLX-*b*-PLAla-*b*-PLLys



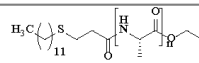
<b>D60</b>	Bzl-PLAla- <i>b</i> -PLGlu-C6-PLGlu- <i>b</i> -PLAla-Bzl	
<b>D61</b>	PLAla- <i>b</i> -PLX- <i>b</i> -PLAla	
<b>D62</b>	PEG- <i>b</i> -PLHis- <i>r</i> -PLAla	
<b>D63</b>	PEG- <i>b</i> -PLAla- <i>r</i> -PBLG	
<b>D64</b>	PEG- <i>b</i> -PLAla- <i>r</i> -PGly- <i>r</i> -PLIle	
<b>D65</b>	PLAla- <i>b</i> -PEG- <i>b</i> -PLAla	
<b>D66</b>	PLAla- <i>r</i> -PLPhe- <i>b</i> -PEG- <i>b</i> -PLAla- <i>r</i> -PLPhe	
<b>D67</b>	PPDL- <i>b</i> -PLAla	



**D74** POLM-*r*-PLAla-*b*-PLGlu-*b*-POLM-*r*-PLAla-*b*-  
PLGlu-*r*-POLM-*r*-PLAla



**D75** C12-*b*-PLAla



**D76** PNIPAM-*b*-PLAla

